AD 265 569

621-2
XEROX

VERTOL DIVISION
BOEING

Best
Available
Copy

VERTODYNE FAN-IN-WING VTOL AIRCRAFT

FINAL SUMMARY REPORT

PREPARED BY: E. Brogan
G. Casey
B. Engel
C. Fay
J. Gaffney
R. Hooper
H. Wahl

CHECKED BY: R. Hooper
J. Mallen
A. Petach

APPROVED BY: W. Z. Stepniewski

DATE: 15 July 1961

REPORT NO. R-254

MODEL: Vertodyne Semi-Span Model

CONTRACT NO. NONR 2364(00)

ABSTRACT

This report summarizes and supercedes three previous reports on the Vertodyne fan-in-wing concept (Report R-158, of varying dates and titles). The Vertodyne concept has been studied in a series of static and forward speed tests to determine the characteristics of the wing-submerged ducted fan. This has been accomplished under contract to the Office of Naval Research and with the assistance of the U.S. Army Transportation Research and Engineering Command.

Tests were performed at the laboratory and wind tunnel facilities of the University of Detroit. Instrumentation measured fan thrust and torque, wing pressures, and forces and moments. Data are presented in both raw and non-dimensional form for a range of static and forward flight conditions.

Results obtained under static conditions and in the wind tunnel (simulating forward flight) are discussed and correlated with those of several other investigators. The report concludes with recommendations for further study.

TABLE OF CONTENTS

		PAGE NO.
	ABSTRACT	i
	TABLE OF CONTENTS	ii
	LIST OF FIGURES	iii
	LIST OF TABLES	x
	LIST OF SYMBOLS	xi
I.	INTRODUCTION	1
II.	SUMMARY	3
III.	DESCRIPTION OF PROGRAM	5
	A. General	5
	B. Description of Model and Instrumentation	5
	C. Test Program and Procedure	22
IV.	REVIEW OF VERTODYNE TEST RESULTS	25
	A. General	25
	B. Phase I - Static Test Phase	25
	C. Phase II - Forward Flight Test Phase	55
	D. Nondimensional presentation of Phase I and Phase II data	76
V.	THEORY AND DATA CORRELATION FOR WING-SUBMERGED DUCTED FAN CONFIGURATIONS	91
	A. General	91
	B. Static Correlation	91
	C. Forward Flight Correlation	91
	D. Static Theory	95
VI.	CONCLUSIONS	135
VII.	RECOMMENDATIONS	137
VIII.	REFERENCES	139
IX.	APPENDICES	A-1
	A. Wind Tunnel Program and Log of Test Runs	A-1
	B. Wind Tunnel Balance System Data Plots	B-1
	C. Nondimensional Plots of Phase I and Phase II data	C-1

LIST OF FIGURES

FIGURE NO.		PAGE NO.
1.	Vertodyne Model, Top View, Looking Upstream	7
2.	Vertodyne Model, Bottom View, Looking Downstream	7
3.	Section Through Wing at Fan Centerline	8
4.	Vertodyne Plan View Dimensions	9
5.	Diagram of Forces and Moments Recorded during Wind Tunnel Tests	11
6.	Wing Surface Pressure Pickup Locations	12
7.	Shroud Surface Pickup Locations	13
8.	Vertodyne Model Wing Opened, Showing Wing Pressure Pickups	14
9.	Fan Inlet Shroud with Pressure Pickups	14
10.	Static Test Installation	15
11.	Sketch of Model in Wind Tunnel	16
12.	Schematic Diagram of Vertodyne Model Installation and Instrumentation	17
13.	Sketch of Vertodyne Wind Tunnel, including Instrumentation	18
14.	Sketch of Vertodyne Static Test Installation	19
15.	Sketch of Lift and Torque Flexures Installation	21
16.	Forces Acting on Torque Flexures	21
17.	Summary Plot, Fan Static Thrust Vs $\emptyset_{Root}$	26

TOTAL MODEL DATA - MODEL STATIC

18.	Total Model Thrust vs Fan RPM	27
19.	Total Model Thrust vs h/D	29
20.	Total Model T/T_∞ vs h/D	30

LIST OF FIGURES (Continued)

FIGURE NO.		PAGE NO.
21.	Total Model (T/HP) vs h/D	32
22.	Total Model (T/HP)/(T/HP)∞ vs Height (h/D), In Ground Effect	33

WING AND FAN SHROUD SURFACE PRESSURES (MODEL STATIC)

23.	Inboard Wing Pressures, Medium Pitch Fan, Model Static with Ground Effect	34
24.	Fan Center Wing Pressures, Medium Pitch Fan, Model Static with Ground Effect	35
25.	Outboard Wing Pressures, Medium Pitch Fan, Model Static with Ground Effect	36
26.	Shroud Pressures, Medium Pitch Fan, Model Static with Ground Effect	37
27.	High Pitch Fan, Inboard Pressure Station	38
28.	High Pitch Fan, Center Pressure Station	39
29.	High Pitch Fan, Outboard Pressure Station	40

FAN STATIC, OUT OF GROUND EFFECT

30.	Fan Static Thrust vs Fan RPM	43
31.	Fan Static Thrust vs Incidence Angle	44
32.	Fan Power from Torque Flexures vs Fan RPM	45
33.	Torque and Horsepower vs RPM (No Fan)	46
34.	Thrust Per Horsepower vs RPM	47
35.	Thrust Per Horsepower vs Incidence Angle	48
36.	Center of Pressure vs Fan RPM	49

LIST OF FIGURES (Continued)

FIGURE NO.		PAGE NO.
	FAN STATIC, SHOWING GROUND EFFECT	
37.	Fan Static Thrust vs h/D	51
38.	Fan Static Thrust ($T/T\infty$) vs Height (h/D)	52
39.	Horsepower vs h/D	53
40.	Center of Pressure vs h/D	54
	TOTAL MODEL IN FORWARD FLIGHT	
41.	Total Model Thrust Per Horsepower vs Forward Speed	56
42.	Total Model L/D vs Forward Speed, 3 Fans, $\alpha = 0^\circ$	57
43.	Total Model L/D vs Forward Speed, 3 Fans, $\alpha = +10^\circ$	58
44.	Total Model L/D vs Forward Speed, 2 Fans, $\alpha = -10^\circ$	59
45.	Outboard Wing Pressures, Hole Covered, 100 MPH	61
46.	Fan Center Wing Pressures, Medium Pitch Fan, 10,000 RPM, 100 MPH	62
47.	Fan Center Wing Pressures, Locked Rotor, 100 MPH	64
48.	Fan Center Wing Pressure, High Pitch Fan, 9,060 RPM, 100 MPH	65
49.	Outboard Wing Pressure, Hole Covered, 60 MPH	66
50.	Fan Center Wing Pressure, Medium Pitch Fan, 10,000 RPM, 100 MPH	67
51.	Fan Center Wing Pressure, Medium Pitch Fan 10,000 RPM, 40 MPH	68
52.	Fan Center Wing Pressure, High Pitch Fan, 9,060 RPM, 100 MPH	69
53.	Fan Shroud Pressure, Medium Pitch Fan, 10,000 RPM, 60 MPH	70

LIST OF FIGURES (Continued)

FIGURE NO.		PAGE NO.
54.	Fan Shroud Pressure, High Pitch Fan, 9,060 RPM, 100 MPH	71
55.	Fan Center Wing Pressure, Medium Pitch Fan, 10,000 RPM, 100 MPH, 40° Fan Exit Elbow	72
56.	Fan Center Wing Pressure, Medium Pitch Fan, 10,000 RPM, 60 MPH, 40° Fan Exit Elbow	73
57.	Fan Center Wing Pressure, Medium Pitch Fan, 10,000 RPM, 80 MPH, 20° Wing Flap	74
58.	Fan Center Wing Pressure, Medium Pitch Fan, 10,000 RPM, 80 MPH	75
59.	Fan Center Wing Pressure, High Pitch Fan, 9,060 RPM, 60 MPH	77
60,	Fan Center Wing Pressure, High Pitch Fan, 9,060 RPM, 100 MPH, 20° Wing Flap	78
61.	Fan Center Wing Pressure, High Pitch Fan, 9,060 RPM, 120 MPH	79
62.	Fan Center Wing Pressure, High Pitch Fan, 9,060 RPM, 100 MPH, 40° Fan Exit Elbow	80

FAN FORWARD FLIGHT

63.	Fan Thrust vs Forward Speed, Low Pitch Fan	81
64.	Fan Thrust vs Forward Speed, Medium Pitch Fan	82
65.	Fan Thrust vs Forward Speed, High Pitch Fan	83
66.	Summary Fan Thrust vs Forward Speed $\alpha = 0^{\circ}$	84
67.	Fan Horsepower vs Forward Speed, Low Pitch Fan	85
68.	Fan Horsepower vs Forward Speed, Medium Pitch Fan	86
69.	Center of Pressure vs Forward Speed, Low Pitch Fan	87

LIST OF FIGURES (Continued)

FIGURE NO.		PAGE
70.	Center of Pressure vs Forward Speed, Medium Pitch Fan	88
71.	Center of Pressure vs Forward Speed, High Pitch Fan	89
	STATIC CORRELATION	
72.	Lift Per Horsepower vs Disc Loading (Vertol)	96
73.	Lift Per Horsepower vs Disc Loading (G-E)	97
74.	Lift Per Horsepower vs Disc Loading (M.I.T./Moser)	98
75.	Lift Per Horsepower vs Disc Loading (M.I.T./Moser-Ducted Fan)	99
76.	Lift Per Horsepower vs Disc Loading (Hiller-Ducted Fan)	100
77.	Lift Per Horsepower vs Disc Loading (Grumman-Ducted Fan)	101
78.	Lift Per Horsepower vs Disc Loading (Correlated Data)	102
79.	Figure of Merit vs C_T/σ (Vertol)	103
80.	Figure of Merit vs C_T/σ (C-E)	104
81.	Figure of Merit vs C_T/σ (M.I.T./Moser)	105
82.	Figure of Merit vs C_T/σ (M.I.T./Moser-Ducted Fan)	106
83.	Figure of Merit vs C_T/σ (Hiller-Ducted Fan)	107
84.	Figure of Merit vs C_T/σ (Correlated Data)	108
	FORWARD FLIGHT CORRELATION	
85.	Lift Ratio vs Dynamic Pressure (Vertol)	109
86.	Lift Ratio vs Dynamic Pressure (GE-NASA)	110
87.	Lift Ratio vs Dynamic Pressure (M.I.T./Moser)	111
88.	Lift Ratio vs Dynamic Pressure (M.I.T./Duvivier)	112
89.	Lift Ratio vs Dynamic Pressure (Canadian)	113
90.	Lift Ratio vs Dynamic Pressure (Correlated Data)	114
91.	Lift Ratio vs Dynamic Pressure/Static Factor (Vertol)	115
92.	Lift Ratio vs Dynamic Pressure/Static Factor (GE-NASA)	116

<u>LIST OF FIGURES</u> (Continued)

FIGURE NO.		PAGE NO.
93.	Lift Ratio vs Dynamic Pressure/Static Factor (M.I.T./Moser)	117
94.	Lift Ratio vs Dynamic Pressure/Static Factor (M.I.T./Duvivier)	118
95.	Lift Ratio vs Dynamic Pressure/Static Factor (Canadian)	119
96.	Lift Ratio vs Dynamic Pressure/Static Factor (Correlated Data)	120
97.	Lift Ratio vs Dynamic Pressure/Static Factor (Correlated Data)	121
98.	Lift Ratio vs Dynamic Pressure/Static Factor (Correlated Data)	122
	STATIC THEORY	
99.	Streamline Flow Pattern	123
100.	G-E Fan Effective Area Coefficient	130
101.	Pressure Distribution Near Fan	131
102.	Static Thrust Distribution	132
103.	Representative Values of K	133
APPENDICES		
B-1	Basic Wing Data	B-4
B-2	Basic Wing with Duct Open	B-5
B-3	Low Pitch Fan Data	B-6
B-4	Medium Pitch Fan Data	B-7
B-5	Medium Pitch Fan Data with 20° Exit Duct	B-8
B-6	Medium Pitch Fan Data with 40° Exit Duct	B-9
B-7	High Pitch Fan Data	B-10
B-8	High Pitch Fan Data with 40° Exit Duct	B-11

LIST OF FIGURES (Continued)

FIGURE NO.		PAGE NO.
C-1	Model Static C_T and C_P vs ϕ_R	C-2
C-2	Model C_L vs μ^2	C-3
C-3	Model C_D vs μ^2	C-4
C-4	Model C_M vs μ^2	C-5
C-5	Model C_P vs μ^2	C-6
C-6	Location of Model Center of Pressure vs μ^2 ; ϕ_R = 55.9	C-7
C-7	Location of Model Center of Pressure vs μ^2 ; ϕ_R = 39.7	C-8
C-8	Fan C_L vs μ^2	C-9
C-9	Fan C_D vs μ^2	C-10
C-10	Model Lift and Fan Thrust per Horsepower vs μ^2; ϕ_R = 39.7	C-11

LIST OF TABLES

TABLE NO.		PAGE NO.
I	DATA SUMMARY	5
II	CHORDWISE LOCATIONS OF PRESSURE PICKUPS IN PERCENT OF CHORD LENGTH	12
III	EFFECT OF GROUND PROXIMITY ON TESTED FAN CONDITIONS	28
IV	EFFECT OF INCREASED GROUND PROXIMITY ON TESTED FAN CONDITIONS	31
V	FAN SHROUD INLET RADIUS DATA	42
VI	SUMMARY OF GROUND EFFECT DATA	52
VII	SUMMARY OF STATIC PARAMETERS	93

LIST OF SYMBOLS
(Reference Areas)

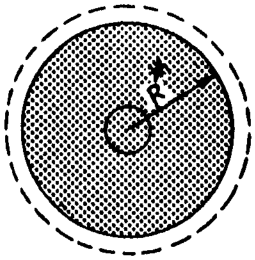

A* (Fan* Area) (Excluding Bellmouth)

R* (Fan* Radius) (Excluding Bellmouth)

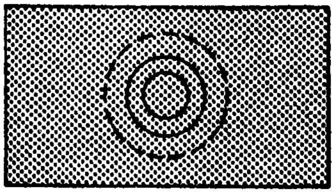

S (Wing Area)

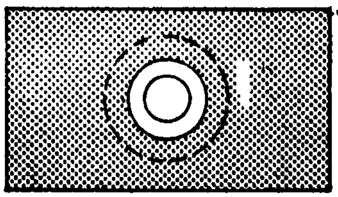

$A_s = S - A^*$ (Shroud Area)

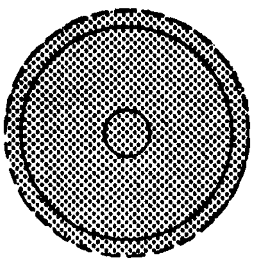

A (Fan Area) (Including Bellmouth)

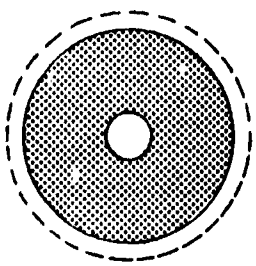

A_{Fan} (Fan Annular Area) (Excluding Bellmouth and Hub)

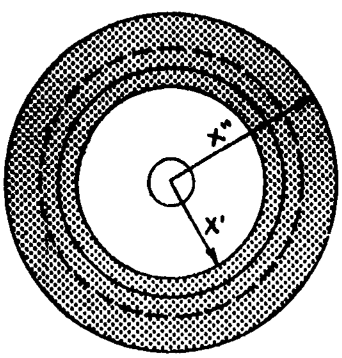

(Static Theory Radius)

$$X' = R\sqrt{K}$$

$$X'' = \sqrt{\frac{S}{\pi}}$$

LIST OF SYMBOLS

SYMBOL	
A	Fan area including hub and bellmouth, square feet.
A^*	Fan* area, including hub, square feet.
A_{Fan}	Fan annulus cross-sectional area, square feet.
A_s	Shroud area, square feet ($A_s = S - A^*$)
A_{s_x}	Shroud area enclosed at any radius x, square feet
c	Force in chordwise direction, pounds
C	Wing chord length, feet
C_D	Forward flight drag coefficient; $C_D = \frac{D}{1/2 \rho V_o^2 S}$
C_D'	Forward flight drag coefficient due to fan thrust; $C_D' = \frac{T \sin}{1/2 \rho V_o^2 S}$
C_F	Effective area coefficient used by G-E (See Figure 100)
$C_{1_{max}}$	Maximum wing lift coefficient, maximum value of C_L.
C_L	Forward flight lift coefficient; $C_L = \frac{L}{1/2 \rho V_o^2 S}$
C_L'	Forward flight lift coefficient due to fan thrust; $C_L' = \frac{T \cos \alpha}{1/2 \rho V_o^2 S}$
C_{L_t}	Forward flight lift coefficient based on fan rotor tip speed; $C_{L_t} = \frac{L}{1/2 \rho V_T^2 S}$

SYMBOL	
C_M	Forward flight pitching moment coefficient: $$C_M = \frac{M}{1/2 \rho V_o^2 SC}$$
C_P	Fan power coefficient; $$C_P = \frac{HP}{\rho \pi R^2 V_T^3}$$
C.P.	Center of pressure forward of fan center, inches or percent of fan radius
C_T	Static thrust coefficient; $$C_T = \frac{T}{\rho \pi R^2 V_T^2}$$
C_{t_o}	Total lift coefficient at V = 0 $$C_{t_o} = \frac{L_o}{\rho A^* V_T^2}$$
D	Drag force, pounds
D	Fan diameter, feet
f	Total force on a fan shroud flexure, pounds
h	Fan or model height above ground; feet
HP	Horsepower
HP_∞	Horsepower, out of ground effect
K	Shroud shape factor, as defined by the Hovering Theory, Equation V14.
L	Lifting force, pounds
L/D	Ratio of lift force to drag force
L_o	Lifting force when V = 0, pounds

LIST OF SYMBOLS (Continued

SYMBOL	
L/L_o	Lift ratio
L_p	Lifting force of the fan*, excluding the Bellmouth induced lift, pounds.
L_s	Lifting force of shroud, pounds.
L.E.	Wing leading edge
M	Figure of merit

$$M = \frac{L_o}{HP\ 53.66} \sqrt{\frac{L_o}{A_{fan}}}$$

MPH	Speed, miles per hour
P	$P = (P_a - P_s)$ when $x > R$, pressure, pounds per square foot
P_a	Ambient static pressure, pounds per square foot
P_o	Average pressure in the area A*, pounds per square foot.
P_s	Static pressure on the shroud, pounds per square foot.
P	Differential pressure referred to ambient static pressure, inches of water.
psi	Pounds per square inch.
q	Tunnel dynamic pressure, pounds per square foot ($q = 1/2 \rho V^2$)
q'	Free stream dynamic pressure; inches of water
Q	Fan torque, pound-feet
r	Fan blading radial station, inches
r'	Radius from fan to torque flexure, inches
R^*	Fan* radius, inches
R'	Fan shroud inlet radius
R'/D	Fan shroud inlet radius to fan diameter ratio

LIST OF SYMBOLS (Continued)

SYMBOL	
RPM	Revolutions per minute
s	Spanwise force, inboard direction positive; pounds
S	Semi-span wing area, square feet
SF	Static factor $SF = \frac{L_o C_{t_o} M^2}{S}$
t	Moments on fan shroud flexures, positive counterclockwise, foot pounds.
T_∞	Thrust, pounds
T	Fan axial thrust out of ground effect, pounds.
u	Velocity over the shroud, feet per second
u_o	$u_o = u$ @ $x = R$, velocity, feet per second
U	Velocity through the fan* feet per second
V	Free stream velocity, miles per hour
V_o	Free stream velocity, feet per second
V_T	Fan blade tip speed, feet per second
x	Perpendicular distance from the fan axis of rotation, feet.
x'	Perpendicular distance from the fan axis of rotation where $x' = R\sqrt{K}$
x''	Perpendicular distance from the fan axis of rotation where $x'' = \sqrt{\frac{S}{\pi}}$
α	Wing angle of attack, degrees
ΔKE	Change in Kinetic energy, foot - pounds per second
∞	Infinity (or out of ground effect)
δ_{FF}	Fan exit elbow turning angle, degrees
δ_{f_w}	Wing flap deflection angle, degrees

LIST OF SYMBOLS (Continued)

SYMBOL	
ρ	Mass density of air, slugs per cubic foot
ψ	Stream function, velocity direction
μ	Tip speed to forward speed ratio
$\beta_{.75}$	Blade angle at .75 radius (see Reference 11)
ϕ	Velocity potential, lines of equal velocity
θ	Fan blading incidence angle, degrees
θ_o	Blade angle (see Reference 12)
θ_R	Fan blading root incidence angle, degrees

PART 1

INTRODUCTION

I. INTRODUCTION

The Vertodyne concept has been proposed as a possible means of obtaining VTOL flight characteristics within an airframe possessing high speed forward flight capability. A wing-submerged ducted lift fan is used to provide lift in hover and in transition flight. When adequate forward speed has been attained the lift fan can be stopped and the duct openings in the wing closed allowing flight as a conventional fixed wing aircraft.

The basic fan-in-wing concept has been evaluated by several agencies and presented in References 3 to 13, inclusive. Favorable results are reported in these studies. Of particular interest is the basic propulsion system study conducted by General Electric (Ref. 2), under sponsorship of the USATRECOM. The results obtained in these studies show substantially good agreement with the Vertodyne results.

Vertol has conducted extensive analytical investigations in this field, both privately and in connection with government contracts. The Vertodyne configuration is one of the most promising concepts for transport and observation-liaison type VTOL aircraft. Reference 1, reporting the results of a VTOL aircraft comparative study performed under contract to the Office of Naval Research, indicates the Vertodyne concept to be promising for the 400 MPH cruise regime.

The Vertodyne program was initiated to explore the flight problems in the transition range. Transition is defined as the low speed forward flight range in which the basic lift of the wing must be augmented by the thrust and induced lift created by the fan. The problems of ducted fan design had been treated analytically and experimentally by numerous investigators. However, the problems associated with the fan-in-wing combination had received only limited experimental investigation, as reported in References 3 to 6, inclusive. At the time Vertol began studies in preparation for the subject contract, the possibility of establishing an analytical approach to the Vertodyne problem appeared remote. An extensive wind tunnel program was proposed to establish basic empirical information for definition and solution of the transition problems. In addition, an investigation of the hovering characteristics both in and out of ground effect was proposed.

During wing tunnel tests, force and moment data were obtained from the tunnel balance system. Direct force measurements were made on the model in the static tests. The fan shroud was attached to the wing by strain gaged flexures which allowed measurement of fan thrust and torque. In addition to the force and moment measuring devices, the wing was provided with extensive surface pressure instrumentation to allow study of surface pressure distribution.

PART II

SUMMARY

II. SUMMARY

The Vertodyne Test Program was conducted by Boeing-Vertol at Morton, Pennsylvania, under Contract NONR 2364(00), to determine the static and transition flight characteristics of a wing-submerged ducted lift fan. Static tests were performed in the Laboratory of the University of Detroit Wind Tunnel. Tests were conducted in ground effect at various heights, and out of ground effect. Forward flight tests were conducted in the seven foot by ten foot wind tunnel of the University of Detroit.

A semi-span reflection plate type model suitable for testing in a seven foot by ten foot wind tunnel was designed. A mechanically driven ducted fan was used, with all drive components contained within the basic wing contour. Three interchangeable fan impellors, high pitch ($\phi_R = 55.9^{\circ}$), medium pitch ($\phi_R = 39.7^{\circ}$), low pitch ($\phi_R = 25.0^{\circ}$) provided variation in fan thrust.

The test set-up was provided with instrumentation which measured forces and moments on the model support and thrust and torque on the fan shroud. Wing surface pressure pickups provided data for a study of surface pressure distributions.

The results of the Vertodyne Test Program are presented to facilitate their application to future studies and designs and to permit comparison with other investigations. Basic knowledge of the flight characteristics of the Vertodyne configuration has been gained indicating the direction in which further research is necessary.

The most significant results of the Vertodyne study are:

1. The determination of the basic forward flight parameters covering lift, drag, pitching moment and fan power.

2. The determination of the static out-of-ground-effect thrust and power characteristics, and the changes occuring in-ground effect.

3. The presentation of surface pressure surveys to illustrate the wing surface flow characteristics, and to show the origin of the forces and moments acting on the wing.

PART III

DESCRIPTION OF PROGRAM

III. DESCRIPTION OF PROGRAM

A. GENERAL

The Vertodyne Model Test Program was conducted in two phases by The University of Detroit as established by Boeing-Vertol under Contract NONR 2364(00). The forward flight phase was performed in The University of Detroit seven foot by ten foot subsonic wind tunnel during February, March and April, 1958. The major portion of the static test phase was conducted out of the tunnel in The University of Detroit's Aeronautical Laboratory in August, 1958. However, some static fan performance was investigated in the tunnel by operating each fan, with rotor blade root incidence angles of 25.0°, 39.7° and 55.9°, at various rotational speeds.

B. DESCRIPTION OF MODEL AND INSTRUMENTATION

1. Basic Model

The Vertodyne model arrangement consisted of the right half of a wing with an aspect ratio of 3.27, composed of a rectangular center section and tapered outer panel, both of NACA 644-221 airfoil section, (see Figures 1, 2 and 3). The ducted fan was contained within the center section. Three fans, each with a different fixed incidence angle, in combination with fan rotational speed, provided variations in fan thrust. NACA Series 65 compressor blading was used in the 52% solidity angle stage fan rotor. Variable incidence angle blading was not employed because of the high cost involved, instead three separate fan impellors with root pitch angles of 25.0°, 39.7° and 55.9° were used. No stator was provided because of the axial depth limitation imposed by the thickness of the wing. The same blading, including twist distribution, was provided for each of the three fans, with the design point, a disc loading of two hundred pounds per square foot, to be met by the fan with the highest incidence angle. The wing was provided with a twenty-five per cent chord flap at the trailing edge. Fan exit elbows of 20° and 40° bend angle, although not suitable for practical applications, were tested to obtain a basis for comparison for more practical systems leading to the use of the fan for forward propulsion. Physical dimensions are summarized in Table I and Figure 4.

TABLE I - DATA SUMMARY

FAN PHYSICAL DATA

Component	Dimensional Value
Diameter of Fan	12"
Hub Radius	3.6"
Outside Radius	6.0"
Number of Blades	13
Fan Speed	10,000 RPM
Maximum Disc Loading	200 lb/ft.^{2}
Semi-Span Area (Incl. Disc)	5.5 ft.^{2}
Fan Disc Area	.785 ft.^{2}

TABLE I - DATA SUMMARY (Continued)

FAN BLADE DATA

Station (% Radius)	Radius (In.)	Air Foil NACA	Pitch (deg.)	Chord (In.)	Twist Distribution (deg.)
60.0	3.60	65-(15) 10	55.9	1.885	0
73.3	4.40	65-(9.3) 10	46.5	1.885	-9.4
86.7	5.20	65-(6.7) 10	42.0	1.885	-13.9
100.0	6.00	65-(5.5) 10	38.3	1.885	-17.6

2. Model Drive System

The model was powered by a 3 phase, 4 pole variable frequency electric motor, developing approximately 40 HP at 10,000 RPM. The motor was obtained on a loan basis from David Taylor Model Basin. The motor was powered by the variable frequency motor-generator set of the University of Detroit Wind Tunnel facility.

A Berkely 7350 Universal EPUT Meter measured the rotational speed of the model motor. This electronic counter had an accuracy in this particular application of ± 30 RPM.

There were three iron-constantan thermocouples in the model motor which were connected to three temperature indicators. These thermocouples determined the temperature at the hottest points of the motor coils. The motor was cooled by water which passed through a water jacket surrounding the motor. Water was pumped from a water main to the motor jacket by a Worthington turbine pump at pressures varying from 40 psi with the low pitch fan to 80 psi with the high pitch fan. The water jacket was drained directly to a sink.

The motor to fan drive passed through a 90° angle drive transmission located behind the fan hub and within the wing contour. This was accomplished by a set of spiral bevel gears having a ratio of 1:1. The gears were supported in anti-friction bearings and were totally enclosed in a steel case. The gears and bearings were lubricated and cooled by both oil spray under pressure and splash lubrication. The oil was fed to the spray nozzles at 30 psi by a feed pump and supplied by a tank filled with ten gallons of MIL 1065 oil. The oil in the gear box was removed by a sump pump which then returned it to the oil tank. Both oil pumps were Tuthill internal gear type. Oil temperature was measured in a temperature well located in the line between the sump pump and the oil tank.

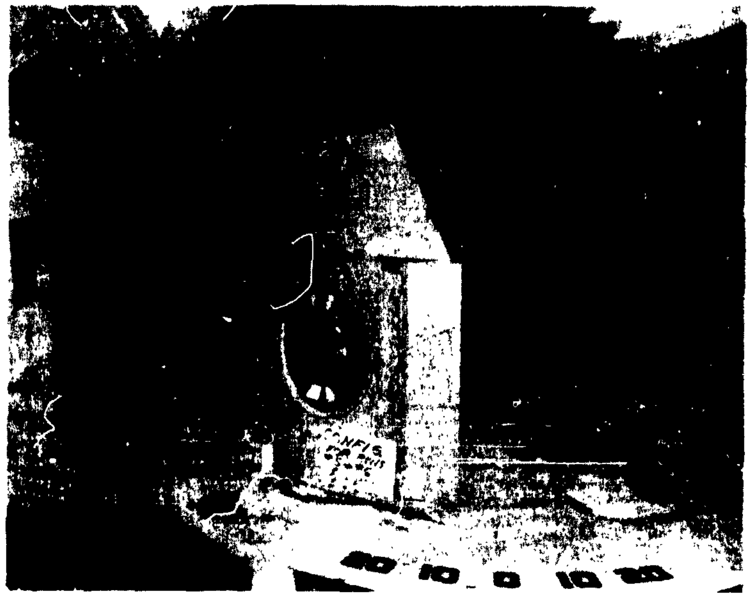

FIGURE 1

VERTODYNE MODEL, TOP VIEW, LOOKING UPSTREAM

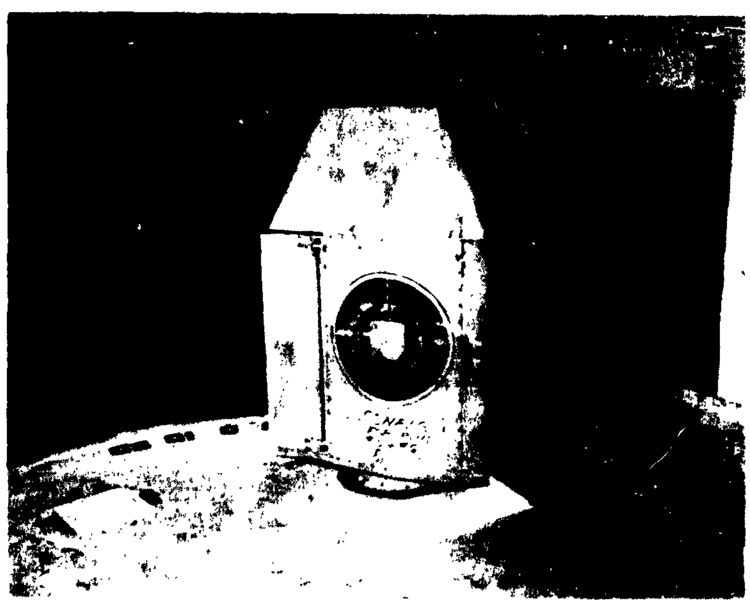

FIGURE 2

VERTODYNE MODEL, BOTTOM VIEW, LOOKING DOWNSTREAM

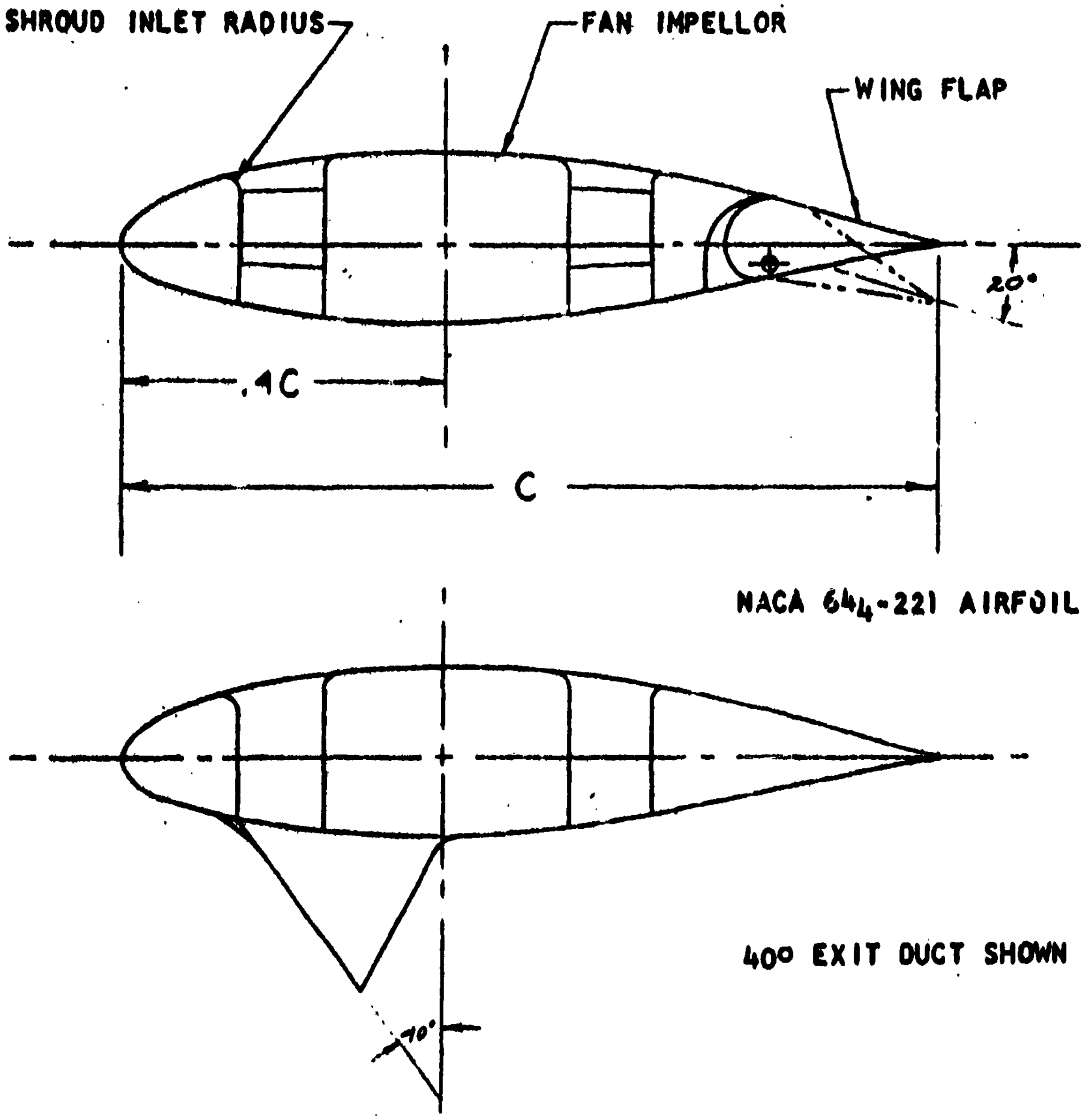

FIGURE 3

SECTION THROUGH WING AT FAN CENTER LINE

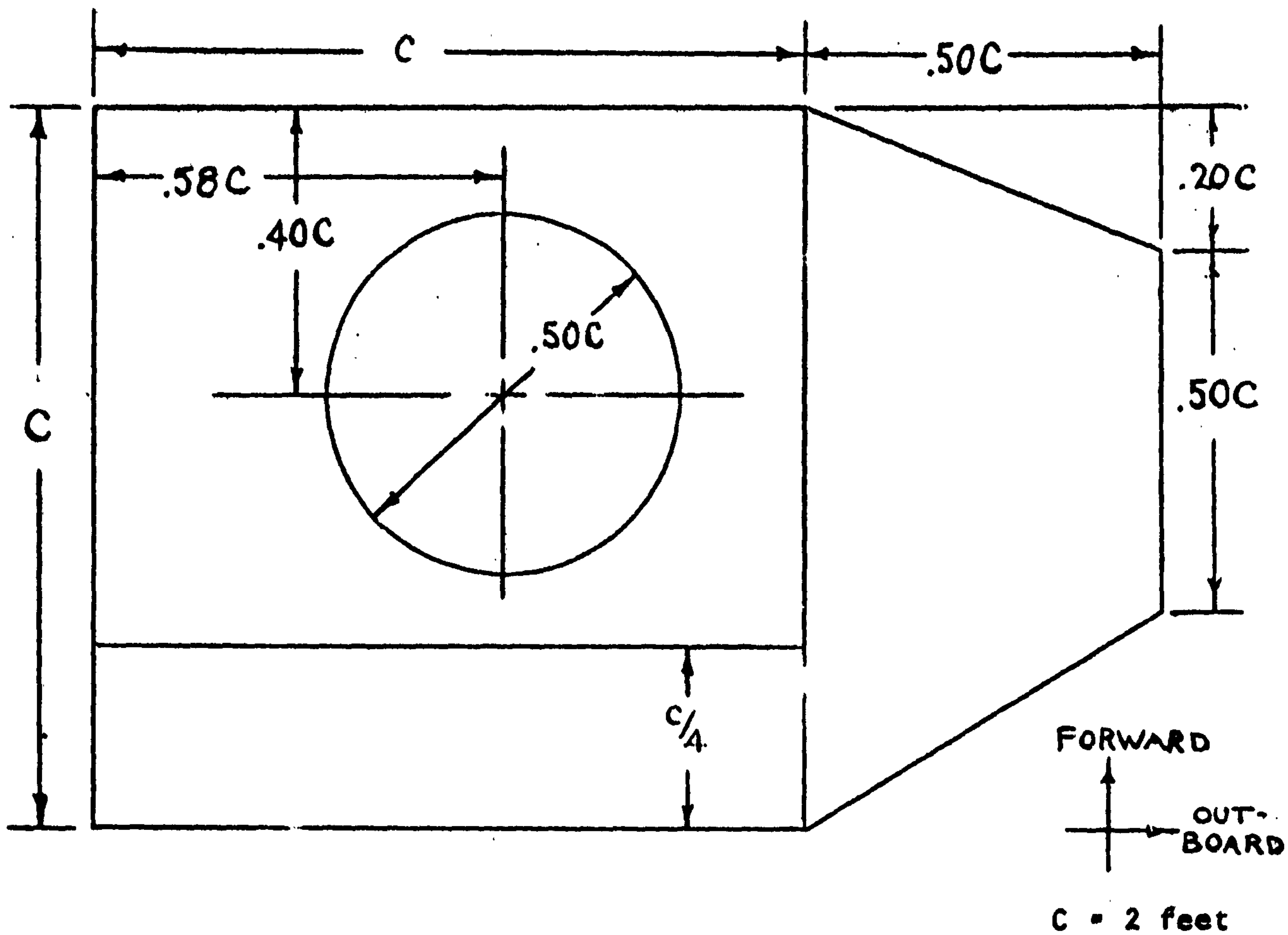

FIGURE 4

VERTODYNE PLAN VIEW DIMENSIONS

3. Angle of Attack System

The angle of attack of the model (see Figure 5) was varied by an Airborne Accessories electric-linear actuator. A slide wire null balance bridge circuit was used as an angle of attack indicator. The model was locked in place by a Hannifin hydraulic (oil) cylinder and pressure was applied by a hand hydraulic pump.

4. Model Data System

Pressure pickups were installed in the shroud and ring assembly, wing leading edge, wing tip, upper and lower wing surfaces, and wing flap (see Figures 6 and 7). These pickups consisted of stainless steel tubes imbedded in the model. Tempaflex tubing was used to connect the pressure pickups to a 100 tube manometer bank. Figures 8 and 9 show pressure pickup installations. Figure 10 shows the fan components mounted in the fan shroud of the Static Test Installation. See Table II for fan shroud inlet radius data.

5. General Installation

Figures 11, 12 and 13 illustrate the arrangements of the model, power, lubrication, cooling, control and instrumentation systems for the wind tunnel tests.

6. Ground Plane

The ground plane used in the ground proximity tests consisted of a four foot square piece of plywood supported in a steel framework. The framework was constructed so that the center of the ground plane coincided with the center of the ducted fan. The ground plane could be moved so as to be any desired distance from the model, to a minimum of 0.3 fan diameter (3.6 inches).

7. Lift Measuring Device for Static Tests

The model was mounted on a table which in turn was mounted on a set of steel casters. The casters rested on steel plates to reduce frictional drag due to the roughness of the Laboratory concrete floor. A Chatillon spring scale (one hundred pounds capacity) was attached to the table to register total model lift (see Figure 14). This setup was calibrated with dead weights and found to be accurate to within one-half pound up to one hundred pound thrust.

8. Power Measurements

The power used by the model motor was determined from a fan torque strain gage system and fan RPM. A wattmeter and motor calibration were used to substantiate the power determined from torque and RPM.

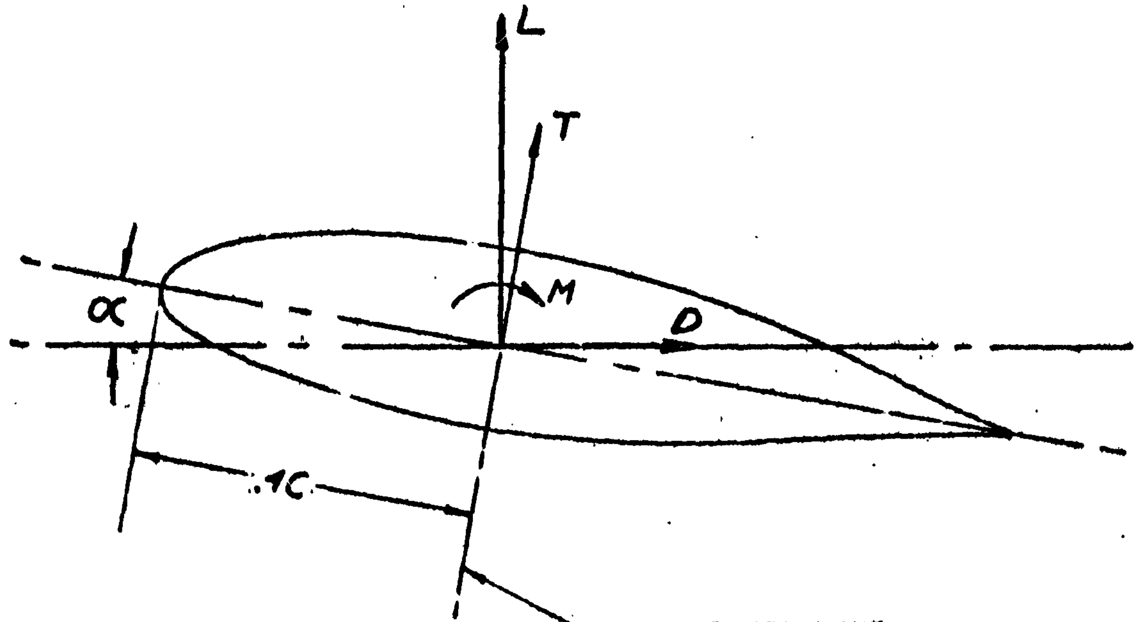

FIGURE 5

DIAGRAM OF FORCES AND MOMENTS RECORDED DURING WIND TUNNEL TESTS

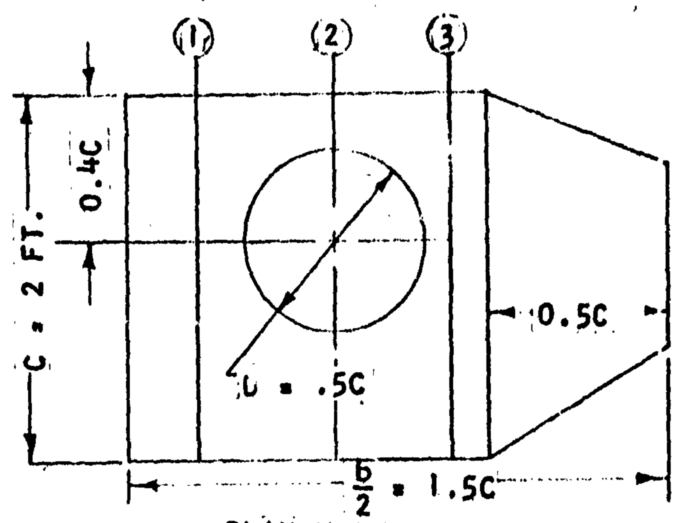

PLAN VIEW
(NOT TO SCALE)

WING STATIONS OF CHORDWISE PRESSURE STATIONS:

INBOARD PRESSURE STATION (1) 0.25C

FAN CENTER PRESSURE STATION (2) 0.58C

OUTBOARD PRESSURE STATION (3) 0.97C

TABLE II - CHORDWISE LOCATIONS OF PRESSURE PICKUPS IN PERCENT OF CHORD LENGTH

INBOARD	FAN CENTER	OUTBOARD
2.5	1.25	2.5
5.0	2.5	5.0
9.8	5.0	9.8
20.2	9.8	20.2
40.0	71.0	40.0
60.3	78.0	60.3
78.0	90.0	78.0
	95.0	

FIGURE 6

WING SURFACE PRESSURE PICKUP LOCATIONS

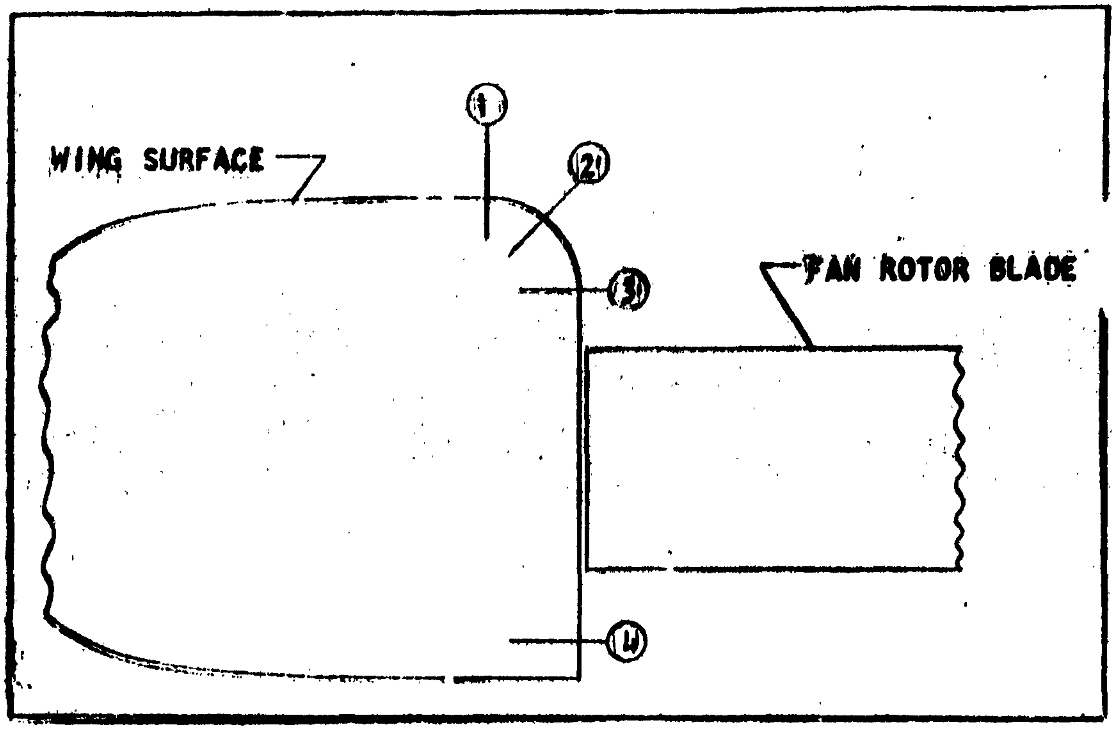

VIEW THROUGH FAN ANNULUS (NOT TO SCALE)

FAN SHROUD FLOW-WISE PRESSURE STATIONS

1. At Tangency Line Of Upper Wing Surface and Inlet Radius
2. 45° Through Inlet Radius
3. At Tangency Line of Inlet Radius and Shroud Diameter
4. 0.25 Inch Upstream of Annulus Exit

Peripheral Azimuth Locations of Pressure Pickups
(0° At Leading Edge, Clockwise From Above)

0°, 22.5°, 67.5°, 112.5°, 157.5°, 202.5°, 247.5°, 292.5°, 337.5°

Cautionary Note: Static Test Data are Presented as in Azimuth Description Above, but Forward Flight Data are Presented According to Conventional Helicopter Rotor Azimuth Locations, i.e., 0° at Trailing Edge, Positive in Direction of Rotation.

FIGURE 7

SHROUD SURFACE PICKUP LOCATIONS

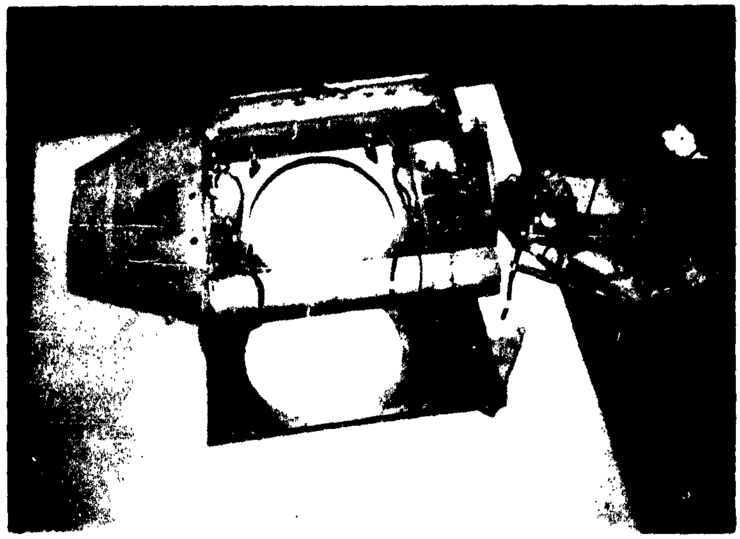

FIGURE 8

VERTODYNE MODEL WING OPENED, SHOWING WING PRESSURE PICKUPS

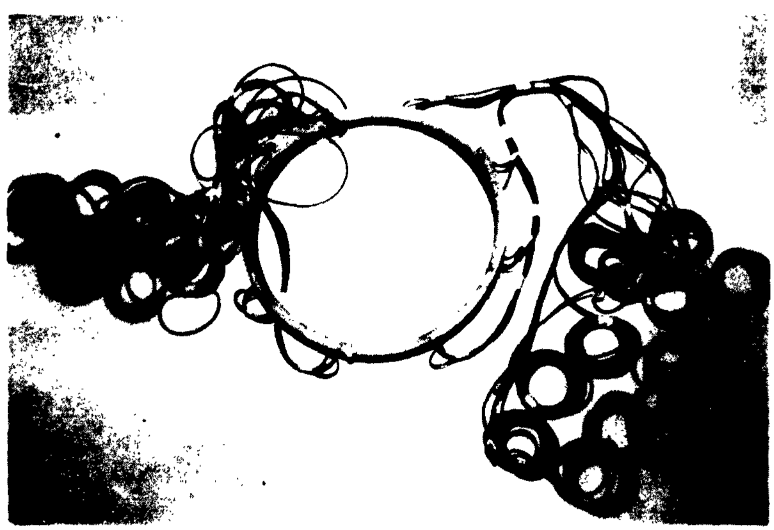

FIGURE 9

FAN INLET SHROUD WITH PRESSURE PICKUPS

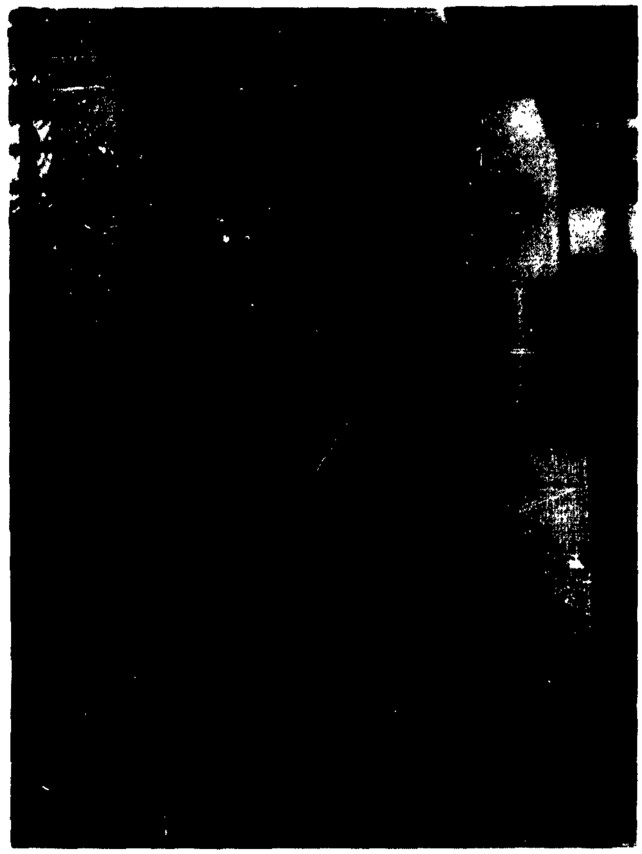

FIGURE 10

STATIC TEST INSTALLATION

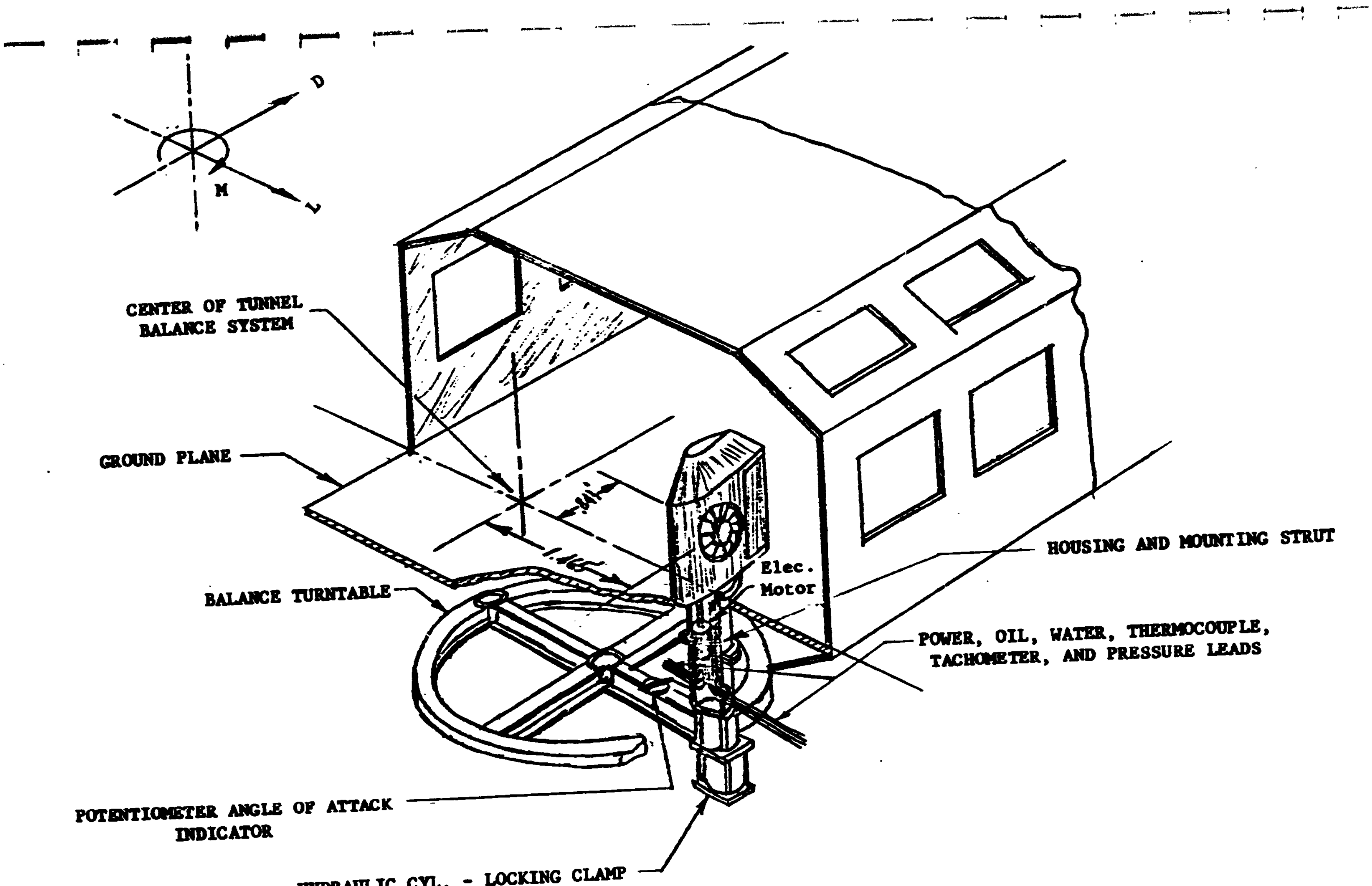

FIGURE 11

SKETCH OF MODEL IN WIND TUNNEL

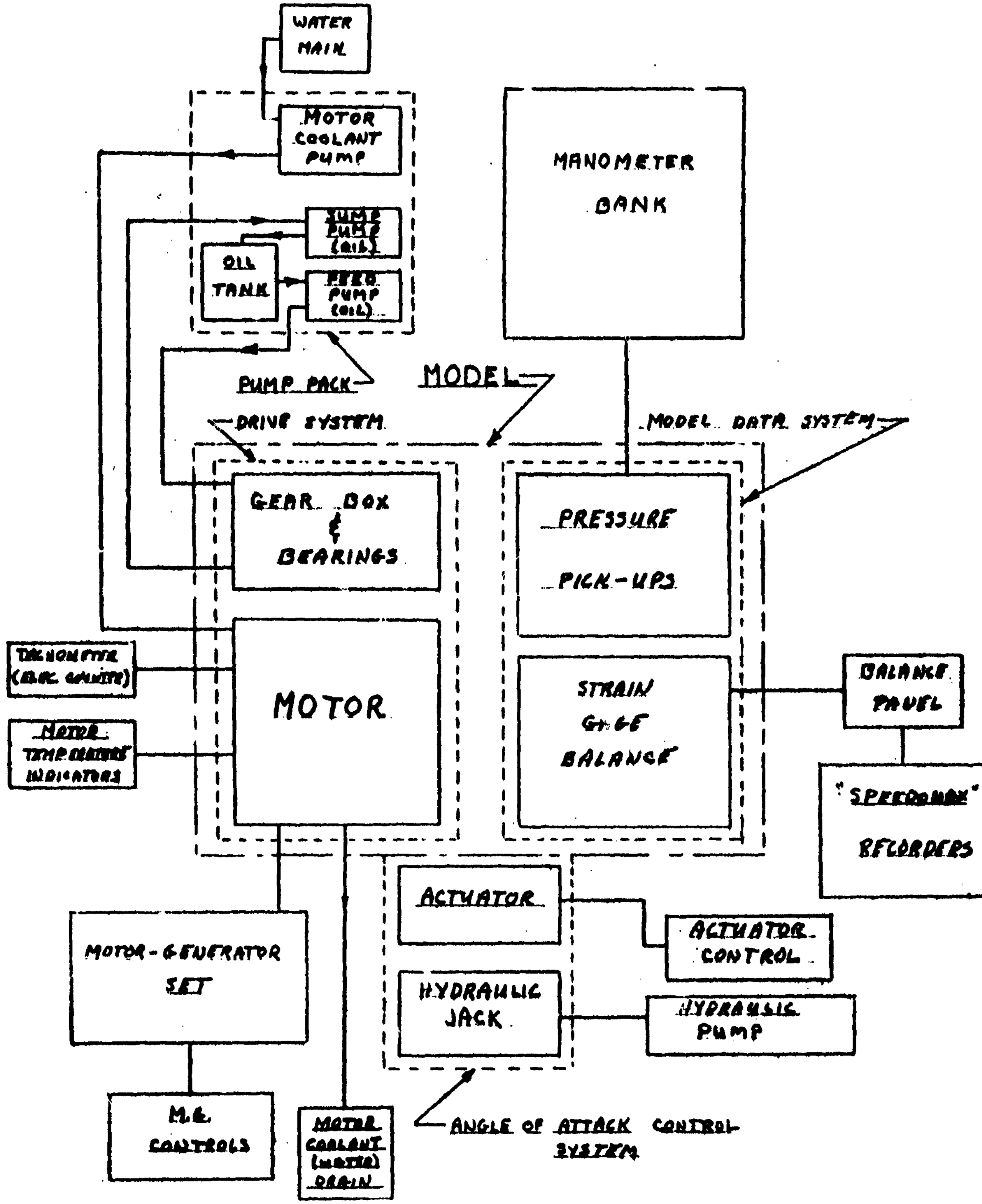

FIGURE 12

SCHEMATIC DIAGRAM OF VERTODYNE MODEL INSTALLATION AND INSTRUMENTATION

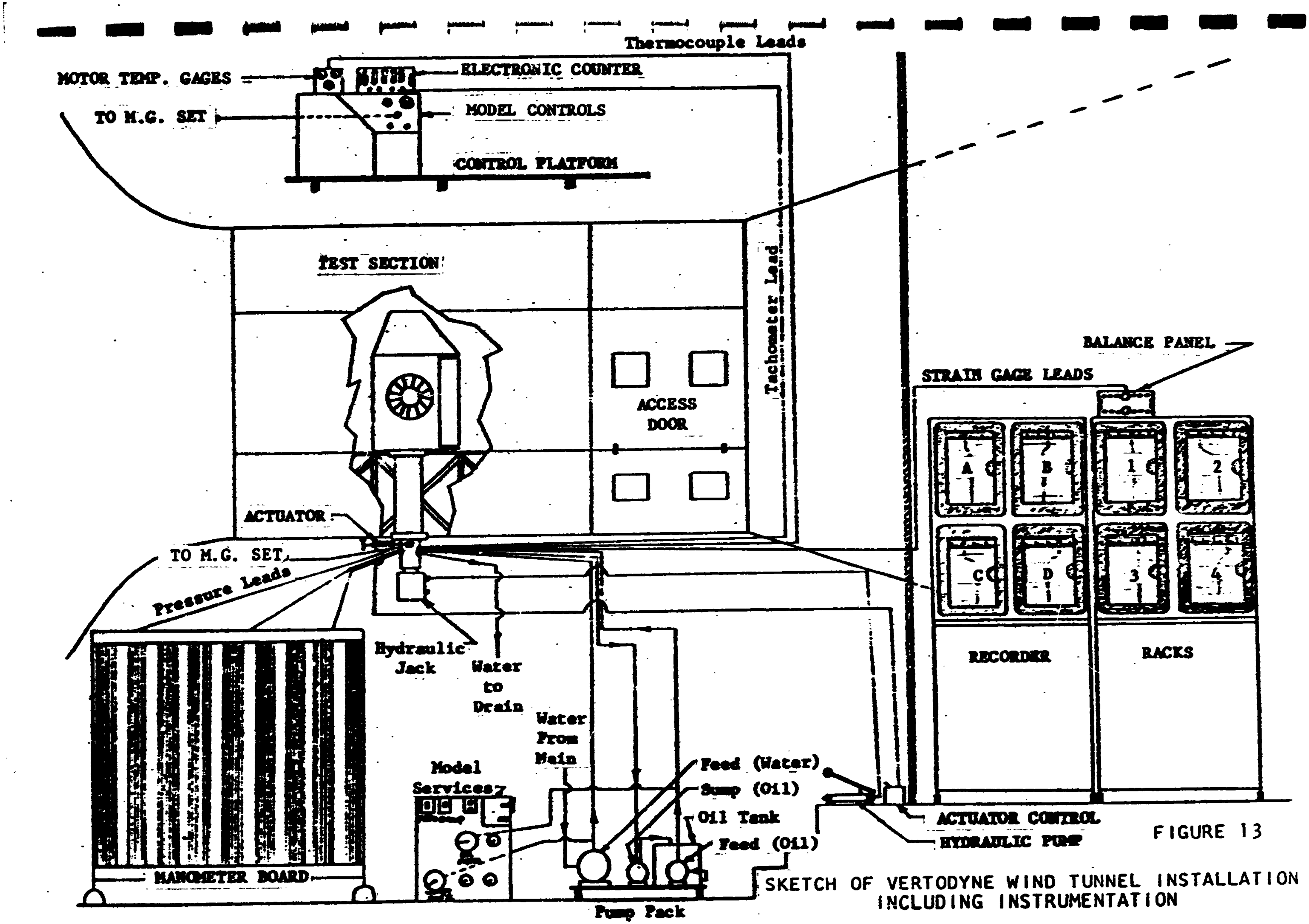

FIGURE 13

SKETCH OF VERTODYNE WIND TUNNEL INSTALLATION INCLUDING INSTRUMENTATION

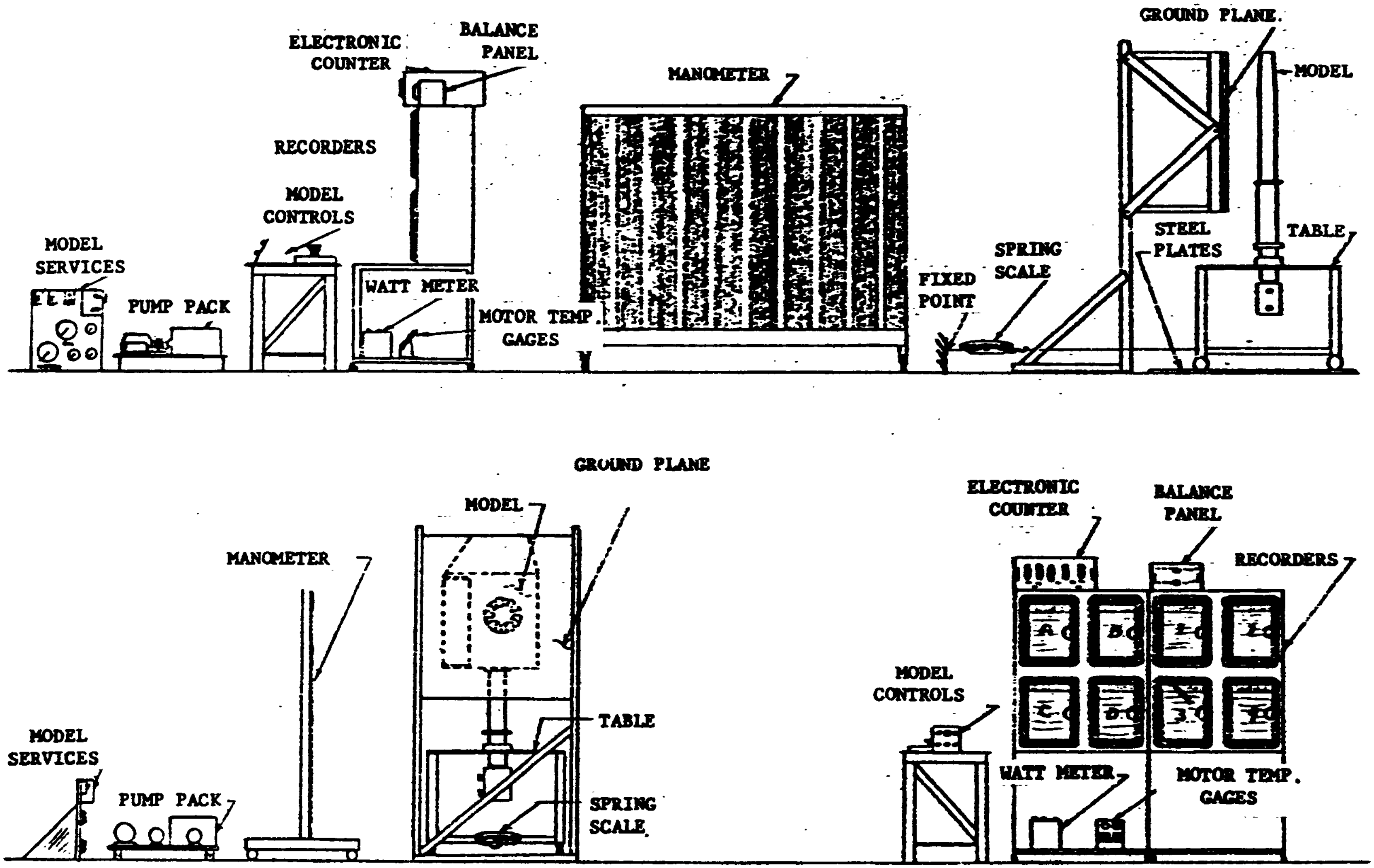

FIGURE 14

SKETCH OF VERTODYNE STATIC TEST INSTALLATION

9. Vertodyne Balance System

The balance system used in the Vertodyne Model was designed primarily to measure fan lift and fan torque. A total of eight strain gaged flexures were used, four in each system. Each flexure was designed to measure axial load with a minimum of sensitivity to other loads.

To measure torque, the fan, transmission, and fan shroud assembly were supported by four strain gaged flexures. These flexures were arranged with their sensitive axis tangential to the fan periphery in the plane perpendicular to the fan's rotational axis. The strain gaged flexures were attached to a rigid intermediate ring around the shroud assembly. Figures 15 and 16 show the location of the strain gaged flexures, and the forces acting on the torque flexures.

To measure lift, the intermediate ring was supported by the other four strain gaged flexures. These strain gaged flexures were arranged with their sensitive axis parallel to the fan thrust axis. In this case the strain gaged flexures were attached to the wing main structure.

In both the lift and torque systems the four flexures were arranged at 90 degree intervals about the fan.

Each of the eight strain gaged flexures contained a 4-arm bending bridge utilizing Baldwin SR-4 strain gages, type AB-7, with a gage resistance of approximately 120 ohms. All eight bridges were powered by a common gage power battery. Balancing was accomplished by using a Type 12-200 Balance Panel. This balance panel also supplied a short calibration of each bridge for periodic checks of circuit sensitivity. Each bridge output was individually recorded on one of eight Leeds & Northrup Speedomax Recorders of the Strip Chart type.

Lift was determined as the sum of the average strain gage readings at flexures A, B, C and D. Torque was obtained as a sum of the average strain gage readings at flexures 1, 2, 3 and 4, and pitching moment was computed from the reaction values at flexures A and B compared to the values at C and D. The torque absorbed by the fan is less than the torque delivered to the gear box by the motor by the amount of the transmission torque loss. This loss is usually between one-half and one per cent of the transmitted torque per gear mesh. Therefore, the fan torque may be expected to be slightly less than the indicated torque by the amount of this gear loss.

By writing equations summing the forces which act on the four flexures, it may be seen that chordwise and spanwise forces cancel out, so that the average of the torque measured by each of the flexures is the fan torque plus the transmission loss torque. It should be remembered that the fan shroud, where the flexures are situated, offers the only torque restraint. The torque is transmitted from the transmission through the support struts to the shroud ring.

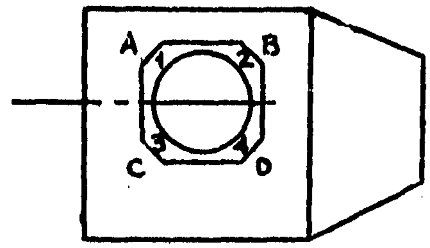

FIGURE 15

SKETCH OF LIFT AND TORQUE FLEXURES INSTALLATION

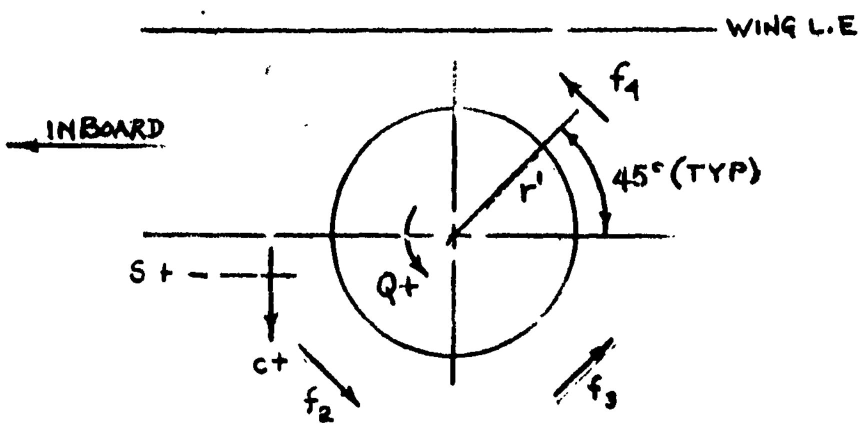

FIGURE 16

FORCES ACTING ON TORQUE FLEXURES

Knowing the magnitude of the forces in each flexure (1 to 4, inclusive), chordwise and spanwise components, as well as the torque value, can be obtained:

$$c = .707\,(f_1 + f_2 - f_3 - f_4)$$

$$s = .707\,(f_1 - f_2 - f_3 + f_4)$$

$$Q = t_r'$$

$$= (f_1 + f_2 + f_3 + f_4)\,r'$$

where c = Chordwise forces, positive toward trailing edge,

s = Spanwise forces, positive in inboard sense,

t = Torque forces, positive counterclockwise,

Q = Torque

f = Total force on a given flexure, denoted by subscripts,

r' = Radius from center of rotation to flexure.

Since static load calibrations of pure torque application were performed, a valid determination of torque was obtained by entering the respective static calibration curve with the test trace deflection value for each flexure and averaging the indicated total torque from each calibration, at a given operating condition. One fallacy could have existed with this system due to physical limitations of the flexure design. That was interaction between the lift and torque forces. This question was eliminated by obtaining interaction results during the static calibrations and correcting for them. It was found that torque did not affect the lift or thrust gages but that thrust did result in interaction in the torque gages.

C. TEST PROGRAM AND PROCEDURE

The Vertodyne Model Test Program consisted of a static test and a forward flight phase. The model performance in forward flight was investigated by using two of the three fan rotors at the design rotational speed of 10,000 RPM and the third, ($\phi_R = 55.9°$) at 9060 RPM because of excessive motor heat at higher powers. Wing angle of attack, air speed, wing flap position, and fan exit duct turning angle were also varied to study the model performance. The low pitch fan, with a root incidence angle of 25°, was accidentally destroyed in the wind tunnel. Fortunately, a sufficient investigation of the low pitch fan configuration had been conducted prior to this mishap to determine the most forward location of the model apparent center of pressure associated with airspeed variation.

During the model static ground effect tests, it was intended that, as in the forward flight tests, each of the three fans be tested. However, the replacement fan for the one destroyed in the wind tunnel was itself destroyed at the fan manufacturer's test facility during acceptance tests prior to delivery. This incident occurred two work days before the scheduled start of the static test phase. The other equipment had already been delivered to the University of Detroit and the test facility scheduled, so it was decided to proceed with testing. As an alternative to using the low pitch fan, the medium pitch fan was operated (in addition to its design speed of 10,000 RPM) at 6,000 RPM, to approximate the disc loading of the low pitch fan. Therefore, the fan configurations tested in the ground proximity test were:

1. Medium pitch fan, root incidence angle 39.7°, @ 6,000 RPM
2. Medium pitch fan, root incidence angle 39.7°, @ 10,000 RPM
3. High pitch fan, root incidence angle 55.9°, @ 9,060 RPM

PART IV

REVIEW OF VERTODYNE TEST RESULTS

IV. REVIEW OF VERTODYNE TEST RESULTS

A. GENERAL

The results of the subject testing are presented graphically in Figures 17 to 71. The data have been divided into the static and powered flight phases for (1) the total model (2) the wing and fan shroud surfaces and (3) the fan. Each of the three major categories within their respective test phase include the following effects of model operation:

1. Static tests; model out of ground effect.

2. Static tests; with effect of ground proximity.

3. Forward flight tests; model out of ground effect.

The performance of the fan pertains to the thrust, power, pitching moment and longitudinal center of pressure data of the fan rotor and shroud assembly alone (fan), and was determined from the lift and torque flexures of this assembly.

The performance of the total model pertains to the lift, drag, pitching moment, and longitudinal center of pressure of the complete model, and was determined from the wind tunnel balance system in the forward flight test and from the force measuring system of the complete model in the static tests. The power was determined from loads on the fan assembly torque flexures and fan rotational speed, and was checked with a wattmeter and a motor calibration.

In addition to Figures 17 to 71, data for the total model in forward flight are presented in Appendix B. These data, plotted as pitching moment, drag, and lift coefficients versus wing angle of attack, were prepared by the University of Detroit from the tunnel balance system readings.

B. PHASE I - STATIC TEST PHASE

1. Total Model Static Tests (Out of Ground Effect)

The static performance of the total model out of ground effect is summarized in Figure 18. It will be recalled that total model lift or thrust is that measured for the complete model, as opposed to the thrust of the fan, which includes only a portion of the lift induced on the wing upper surface due to fan operation. That portion refers to the fan inlet shroud and is measurable by the fan lift flexures.

Figure 18 compares the model static thrust versus fan speed measured in the tunnel by the Tunnel Balance System to that measured outside of the tunnel by a spring scale. No comparison is possible for the low pitch fan because none was available for the static tests. For the medium and high pitch fans it is apparent from Figure 18 that the total model thrust at 10,000 RPM was consistently higher in the tests outside of the tunnel. This difference is attributed to the tunnel wall effects.

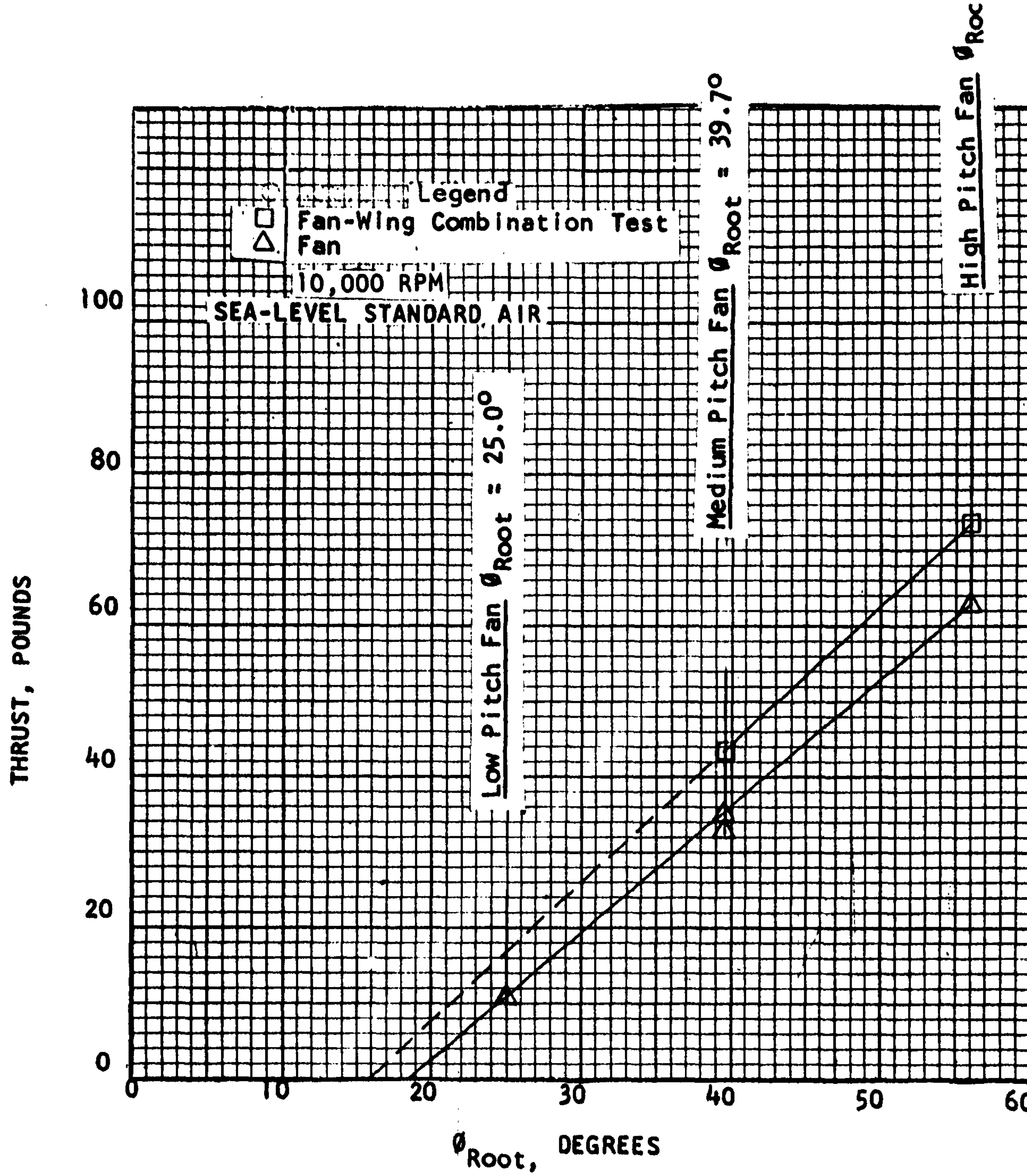

FIGURE 17

SUMMARY PLOT, FAN STATIC THRUST VS. $\emptyset_{Root}$

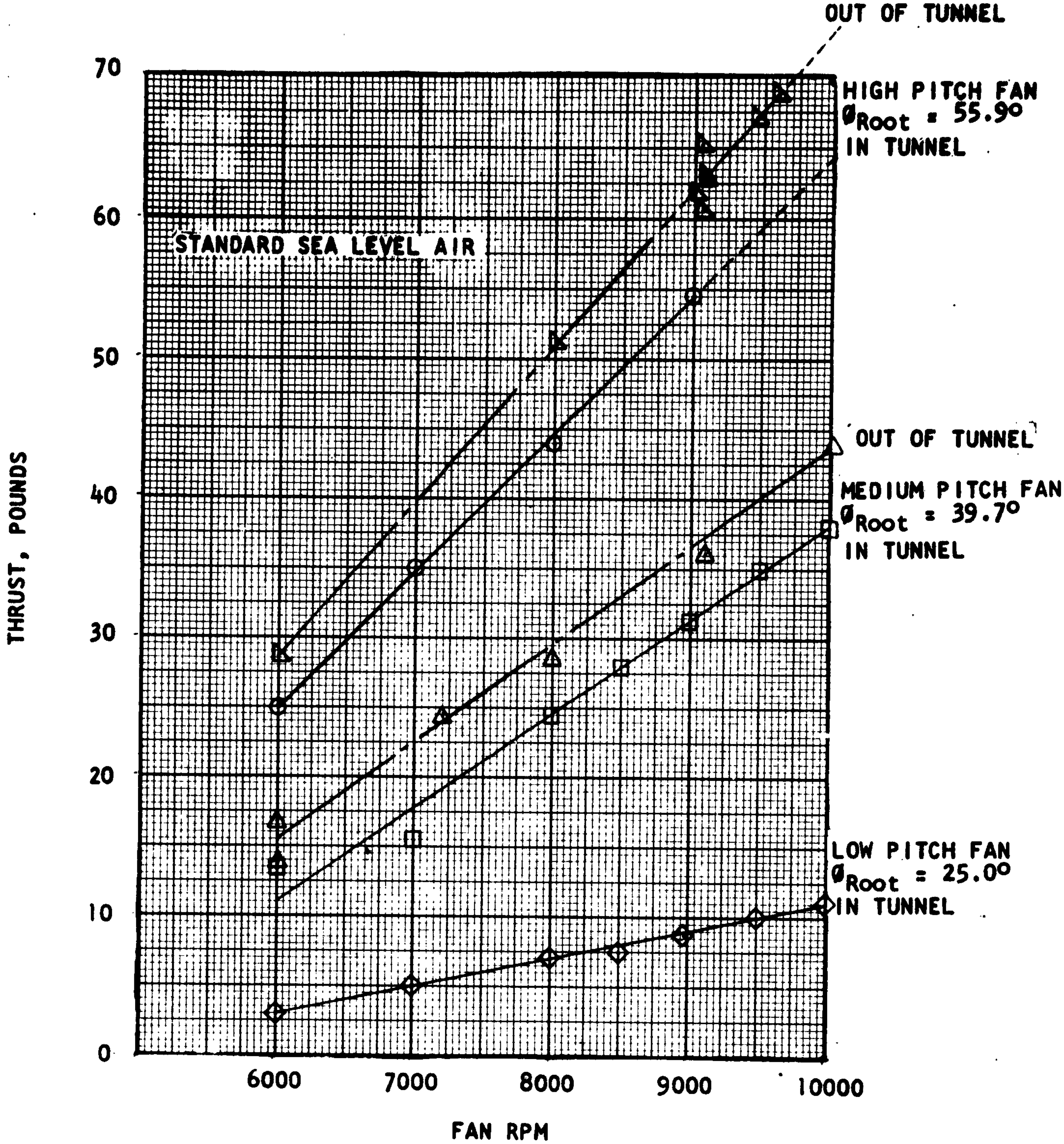

FIGURE 18

TOTAL MODEL THRUST VS. FAN RPM

2. Total Model Static Tests (Effect of Ground Proximity)

In ground effect, the relative thrust increase at constant fan speed was not so great for the total model as for the fan. However, the absolute magnitudes were greater for the total model than for the fan, due to the lift induced on the upper wing surface, even at close ground proximity. It should be pointed out, however, that the negative pressures on the upper wing surface became less negative with approaching ground proximity. This fact explains why the total model thrust approaches that of the fan plus shroud thrust at close ground proximity.

Table III shows the effect of ground proximity for the three fan conditions tested in terms of the ratio of thrust in ground effect to thrust out of ground effect.

The total model thrust per horsepower decreased with increased ground proximity as indicated by Table IV. This is attributed to the same decrease in induced lift. The thrust to horsepower ratio of the fan is 1.00 from a ground height to diameter ratio of infinity down to 0.5, whereas, for the three fan conditions tested, the total model thrust to horsepower ratio decreased as follows based on the reference value at $h/D = \infty$.

TABLE III - EFFECT OF GROUND PROXIMITY ON TOTAL MODEL $\left(\frac{T}{T_\infty}\right)$

Nomenclature ⁄ h/D		2	1	.5
Medium Pitch Fan Ø root = 39.7° 6000 RPM	1.00	1.06	1.11	1.15
Medium Pitch Fan Ø root = 39.7° 10,000 RPM	1.00	1.07	1.15	1.25
High Pitch Fan Ø root = 55.9° 9060 RPM	1.00	1.00	1.02	1.08
Note: See Figures 19 and 20				

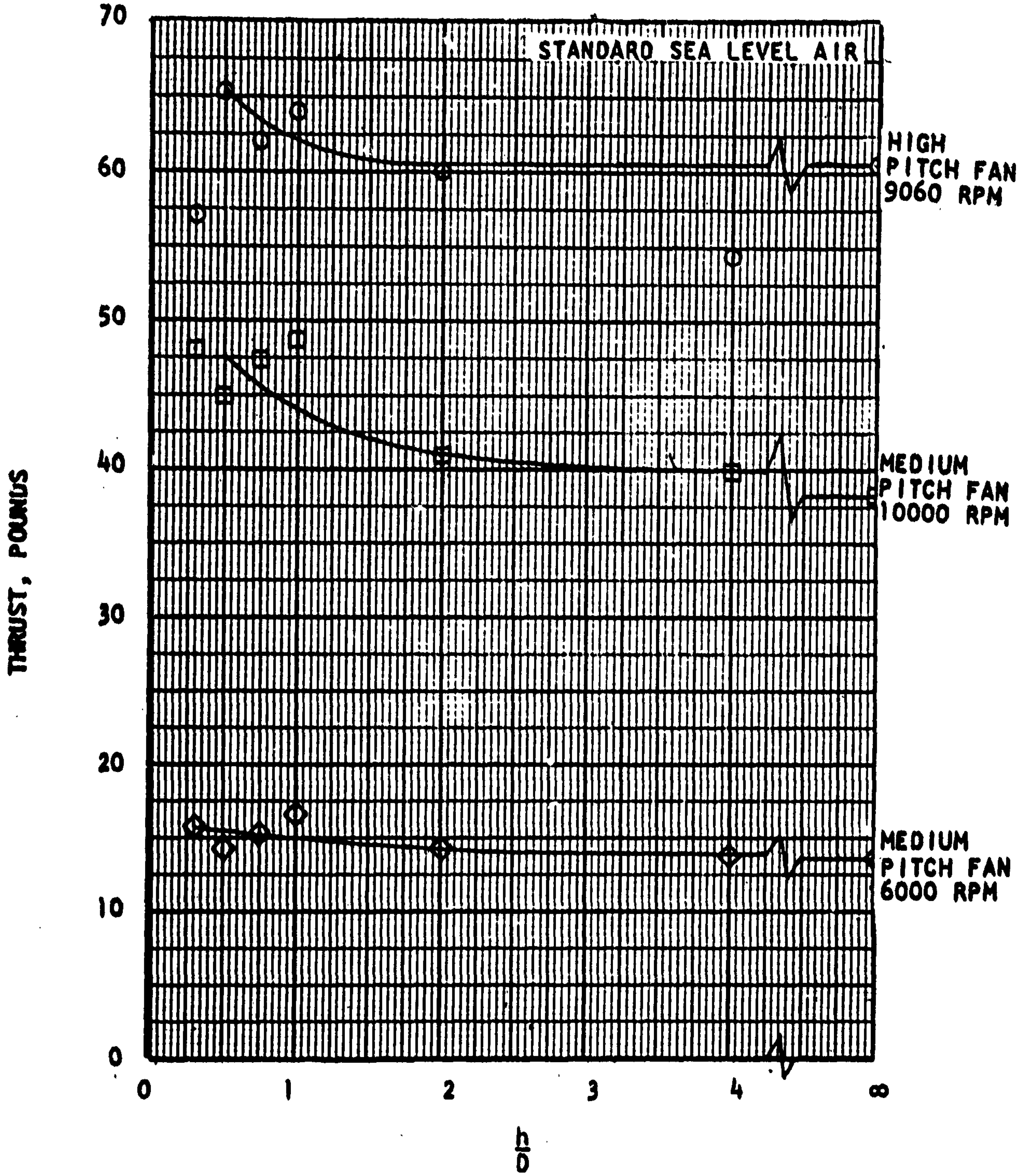

FIGURE 19

TOTAL MODEL THRUST VS. h/D

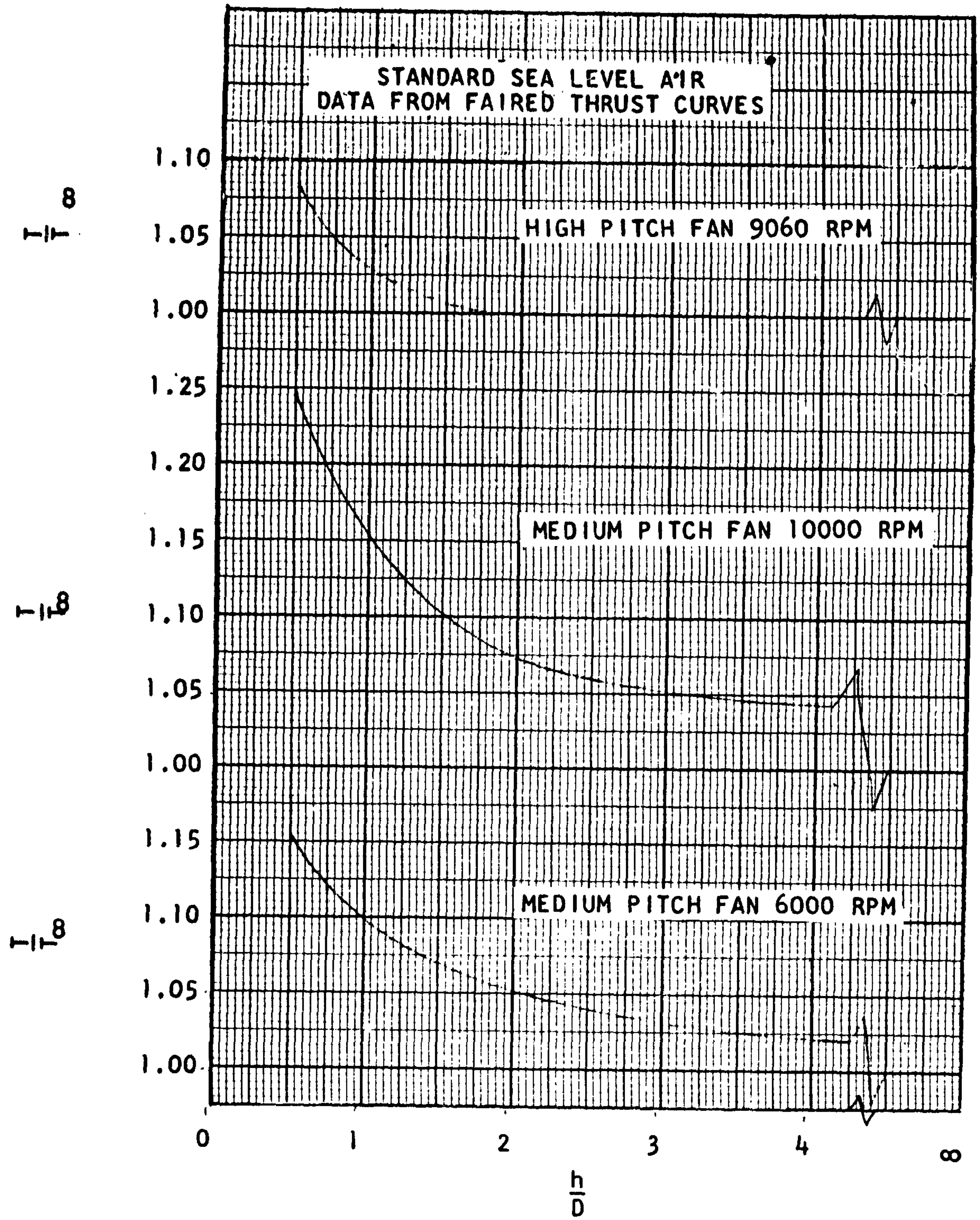

FIGURE 20

TOTAL MODEL T/T∞ VS. h/D

TABLE IV. - EFFECTS OF INCREASED GROUND PROXIMITY ON TOTAL MODEL $\frac{(T/HP)}{(T_\infty/HP_\infty)}$

Nomenclature / h/D	∞	2	1	.5
Medium Pitch Fan Ø root = 39.7° 6000 RPM	1.00	.90	.85	.80
Medium Pitch Fan Ø root = 39.7° 10,000 RPM	1.00	.94	.93	.92
High Pitch Fan Ø root = 55.9° 9060 RPM	1.00	.97	.96	.95
Note: See Figures 21 and 22				

3. Wing and Fan Shroud Surface Pressures (Model Static, Including Ground Effect

A considerable amount of wing and fan shroud surface pressure data were obtained during the subject tests (see Figures 23 to 29). The chordwise distribution of wing surface pressures was determined at three spanwise stations, one inboard of the fan, one through the fan centerline, and one outboard of the fan in the wing main panel. In addition, fan shroud pressure data were obtained at four stations.

With the model out of ground effect, the significant information was the negative pressures experienced over the wing upper surface. This negative pressure accounts for the total model lift exceeding the fan and shroud thrust in the static condition.

Regarding ground effect, it should be noticed that no negative pressures were experienced on the wing lower surface at or above h/D = 0.5. At h/D = 0.3, with the medium pitch fan at Ø root = 39.7° and 10,000 RPM, a localized negative pressure of 0.15 inches of water was experienced at 2.5% chord at the inboard pressure station. No other negative pressures were found on the lower surface with the medium pitch fan, from h/D = ∞ to h/D = 0.3.

Regarding upper surface pressures as affected by ground effect, the inboard station experienced increasingly negative pressures with increased proximity to the ground, whereas the fan centerline and outboard stations showed decreased negative pressure with increased proximity to the ground. A note of caution is required here. In the wind tunnel, the Vertodyne model was operated as a reflection plate model. However, during the static tests outside of the tunnel, no attempt was made either to simulate a fuselage or to provide a reflection wall for the sake of symmetry. Therefore, the surface pressure results must be considered in light of the fact that in actual cases in which the wing would be attached to a fuselage, those surface pressures could be different.

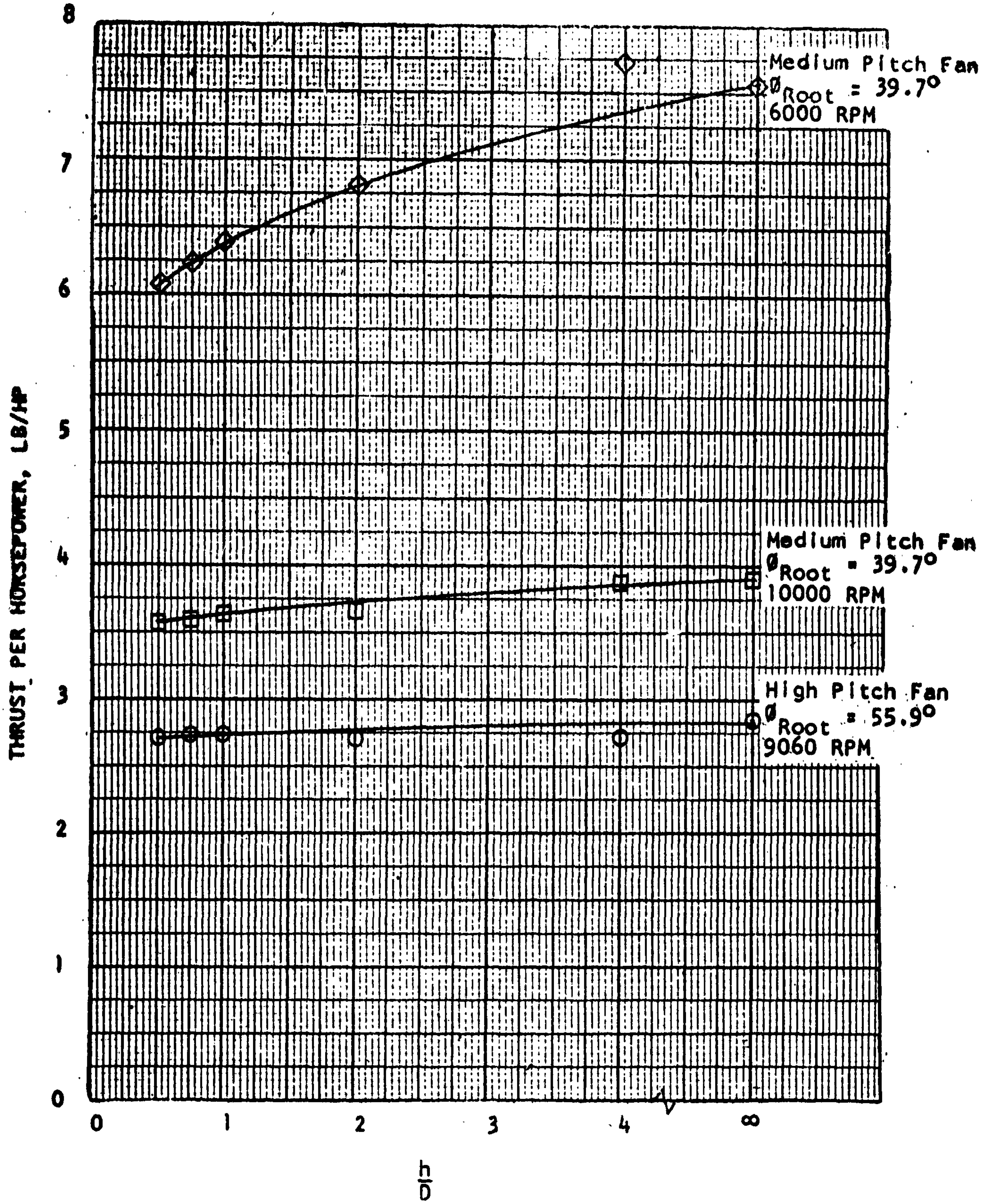

FIGURE 21

TOTAL MODEL (T/HP) VS. h/D

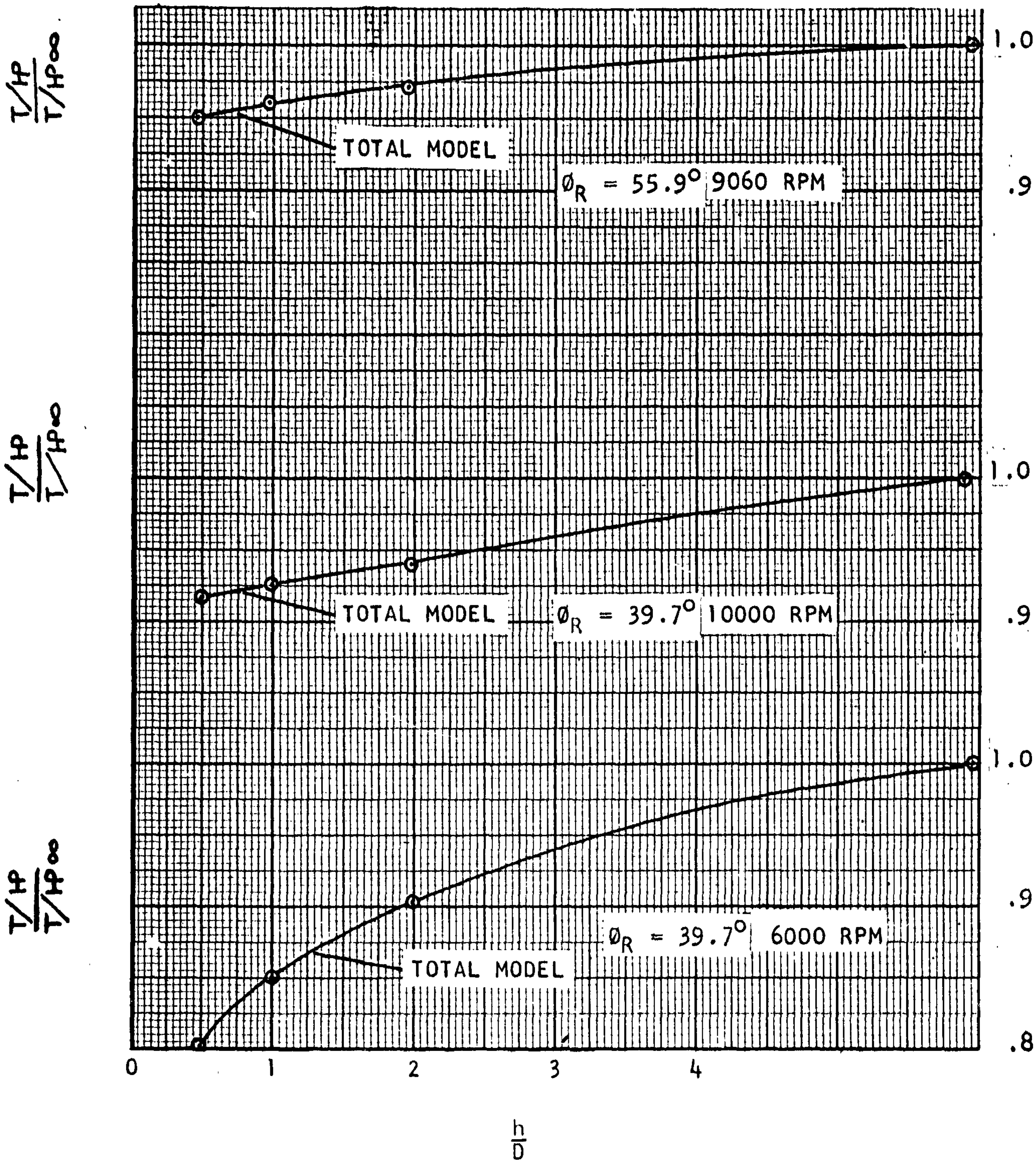

FIGURE 22

TOTAL MODEL $(T/HP)/(T/HP)_\infty$ VS HEIGHT (h/D), IN GROUND EFFECT

PRESSURES NOT INDICATED ARE ZERO
PRESSURES ARE IN RELATION TO AMBIENT STATIC PRESSURE
MEDIUM PITCH FAN   10000 RPM   Ø root = 39.7°

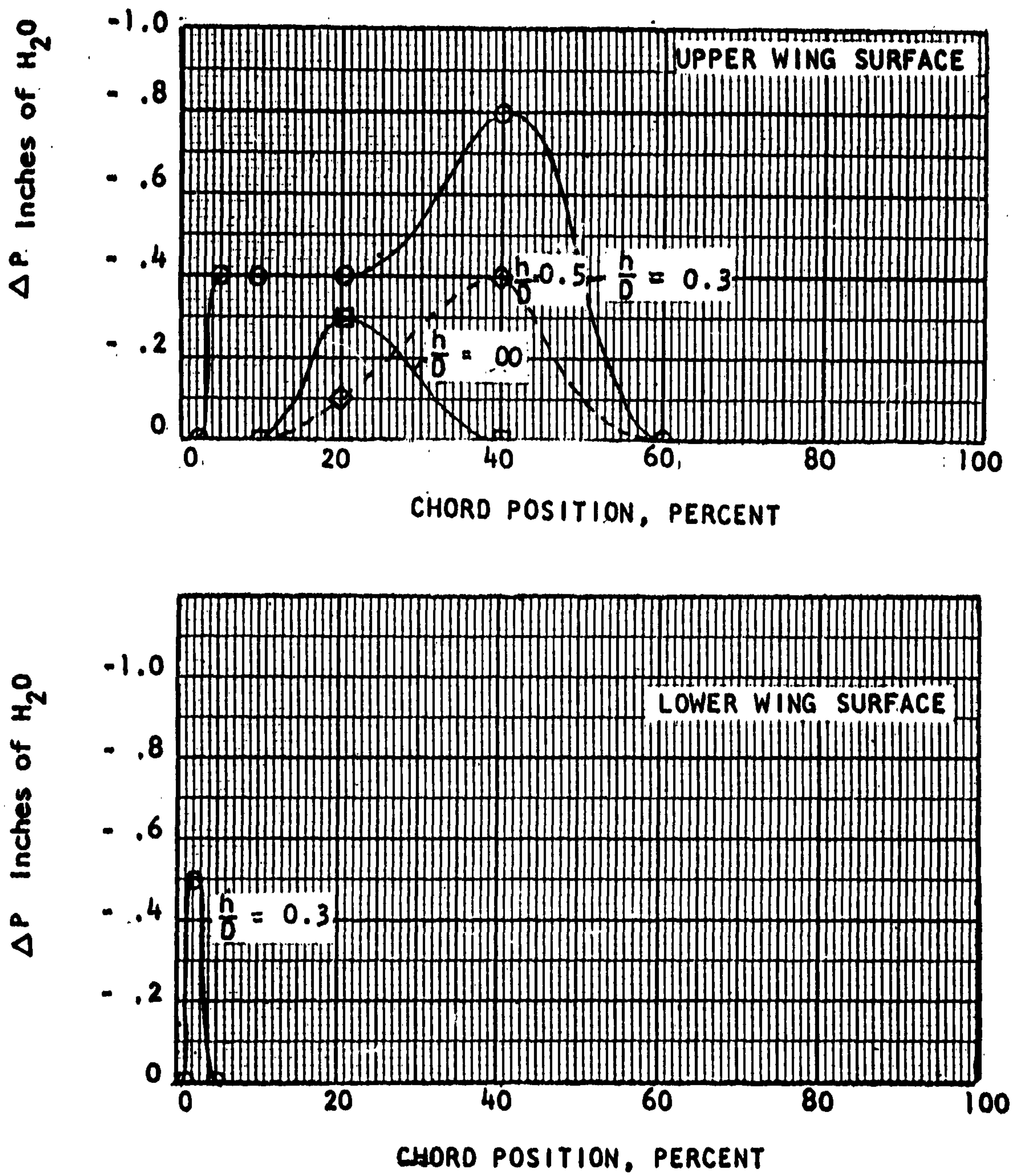

FIGURE 23

INBOARD WING PRESSURES, MEDIUM PITCH FAN,
MODEL STATIC WITH GROUND EFFECT

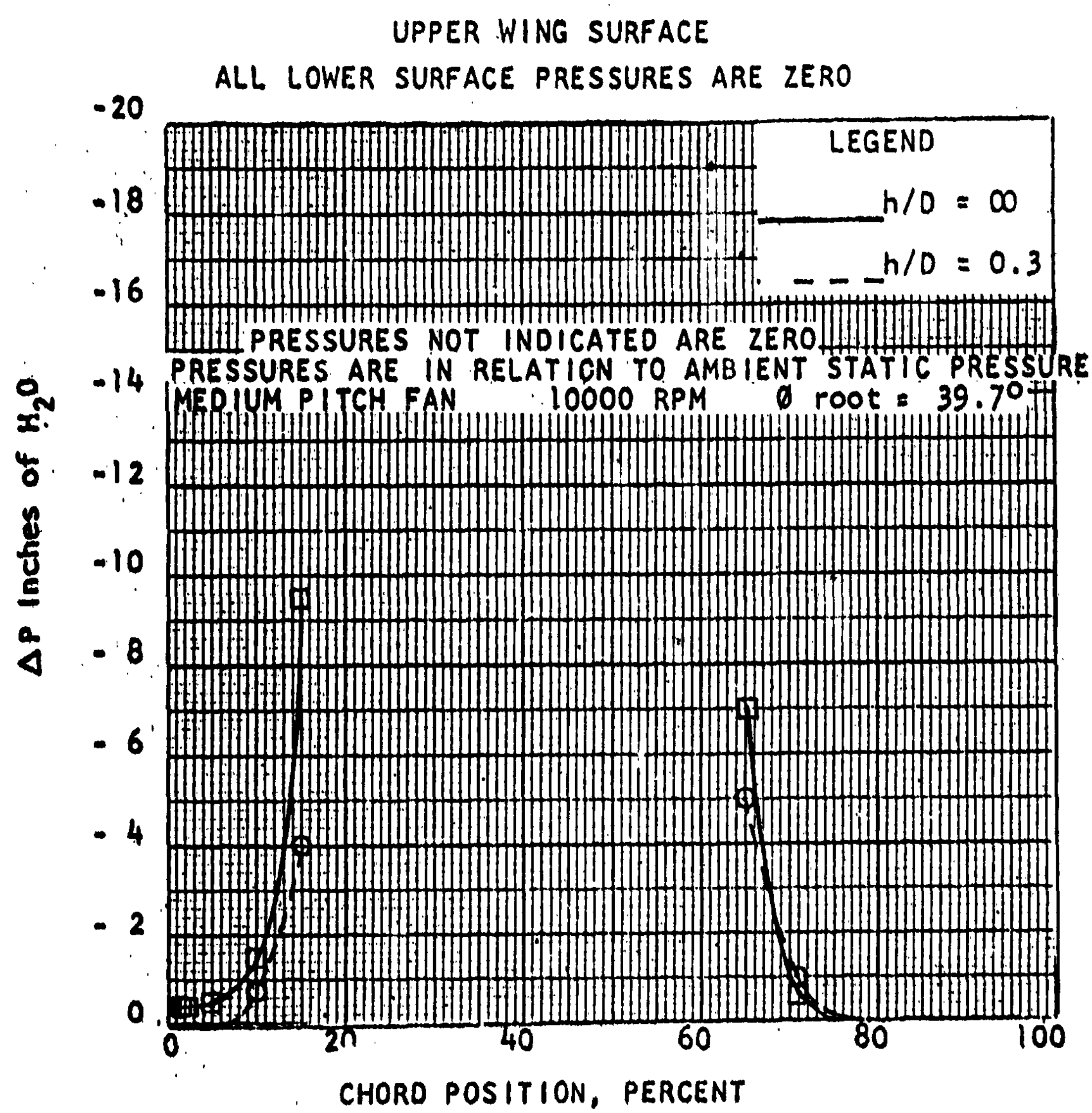

FIGURE 24

FAN CENTER WING PRESSURES, MEDIUM PITCH FAN, MODEL STATIC WITH GROUND EFFECT

MEDIUM PITCH FAN 10000 RPM Ø root = 39.7°

PRESSURES NOT INDICATED ARE ZERO
PRESSURES ARE IN RELATION TO AMBIENT STATIC PRESSURE.

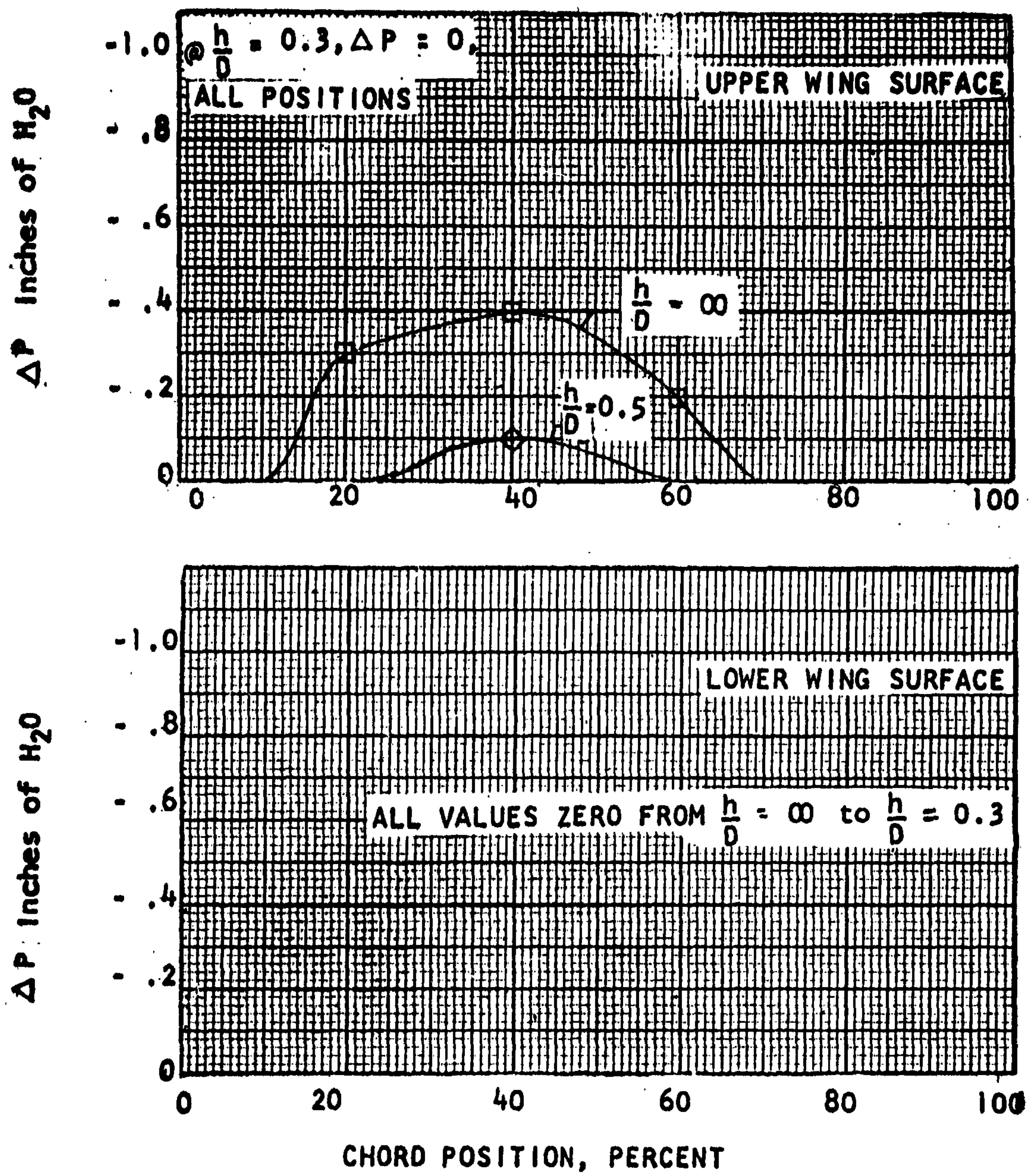

FIGURE 25

OUTBOARD WING PRESSURES, MEDIUM PITCH FAN, MODEL STATIC WITH GROUND EFFECT

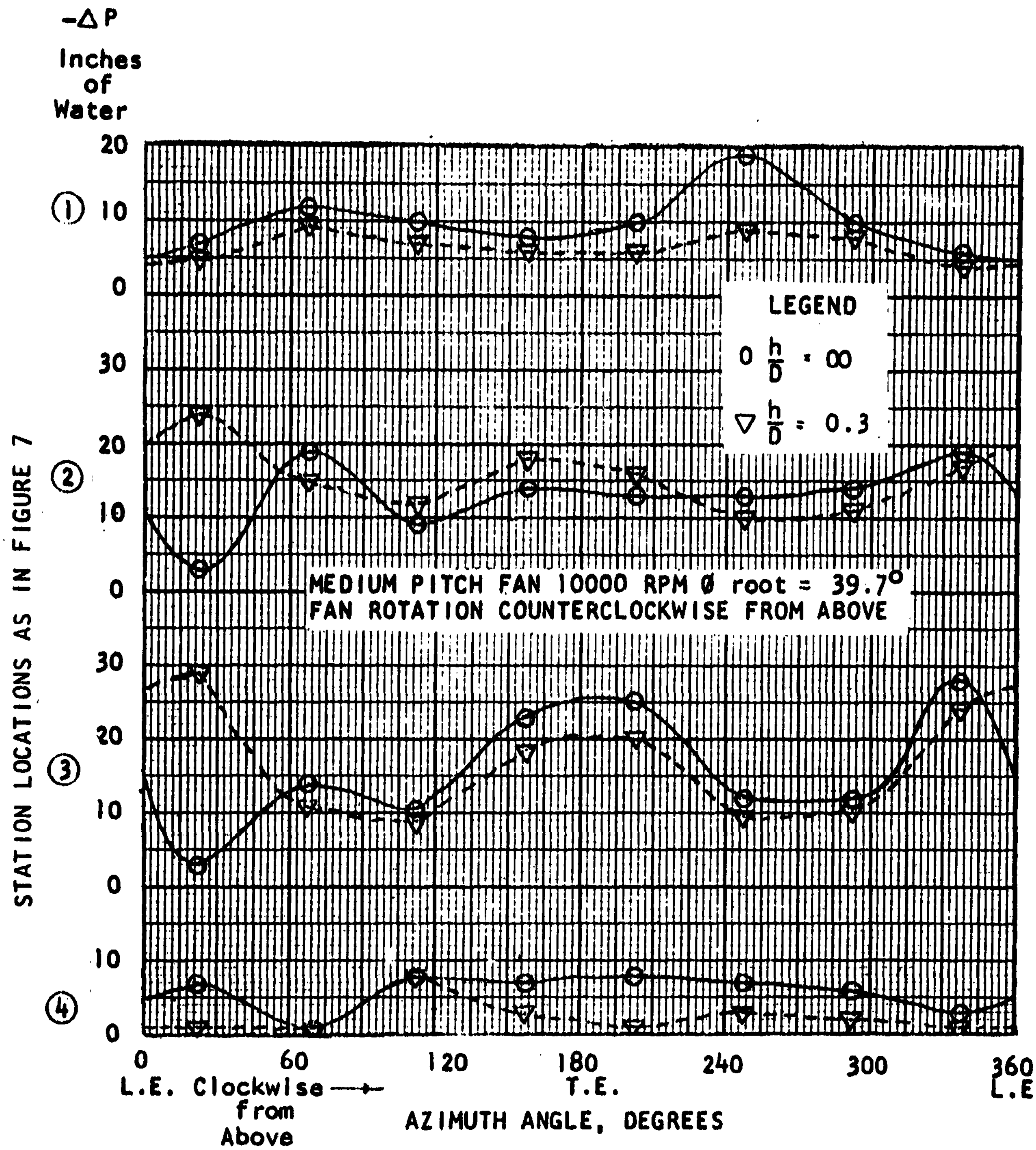

FIGURE 26

SHROUD PRESSURES, MEDIUM PITCH FAN, MODEL STATIC WITH GROUND EFFECT

HIGH PITCH FAN 9060 RPM Ø root = 55.9°

PRESSURES NOT INDICATED ARE ZERO

PRESSURES ARE IN RELATION TO AMBIENT STATIC PRESSURE

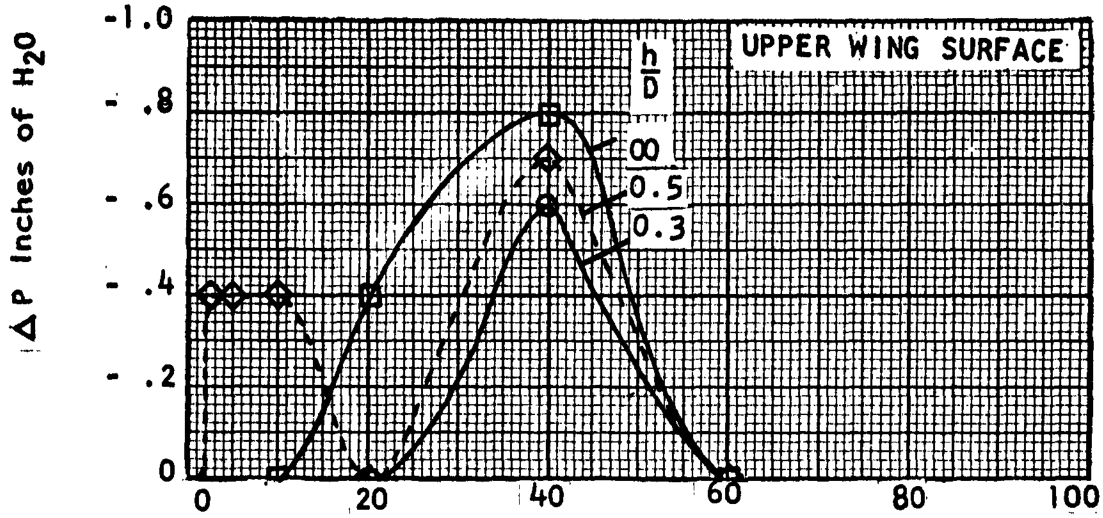

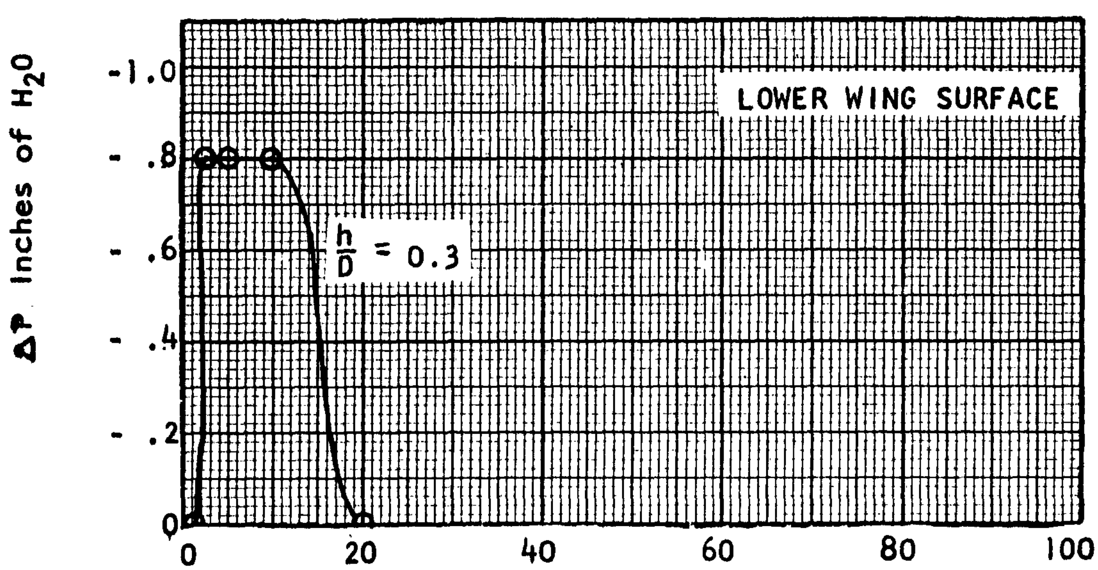

FIGURE 27

HIGH PITCH FAN, INBOARD PRESSURE STATION

HIGH PITCH FAN   9060 RPM   Ø root = 55.9°

PRESSURES NOT INDICATED ARE ZERO
PRESSURES ARE IN RELATION TO AMBIENT STATIC PRESSURE

UPPER WING SURFACE
ALL LOWER SURFACE PRESSURES ARE ZERO

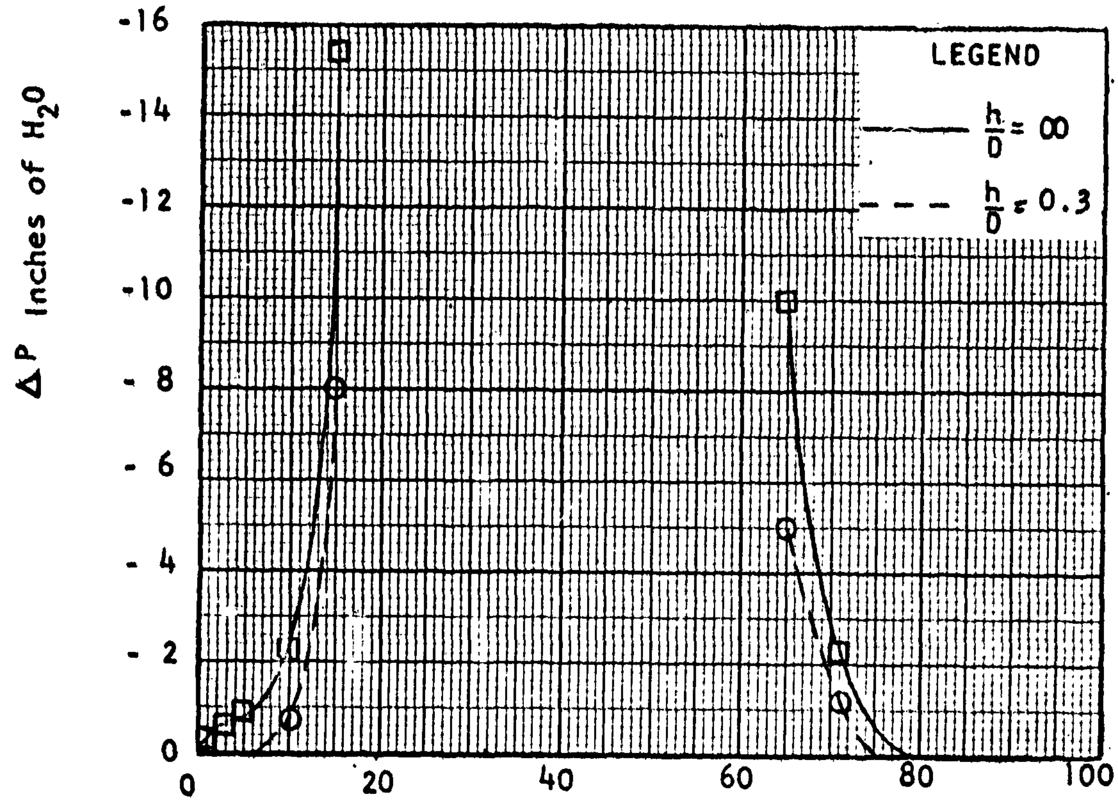

FIGURE 28

HIGH PITCH FAN, CENTER PRESSURE STATION

HIGH PITCH FAN 9060 RPM Ø root = 55.9°
PRESSURES NOT INDICATED ARE ZERO
PRESSURES ARE IN RELATION TO AMBIENT STATIC PRESSURE

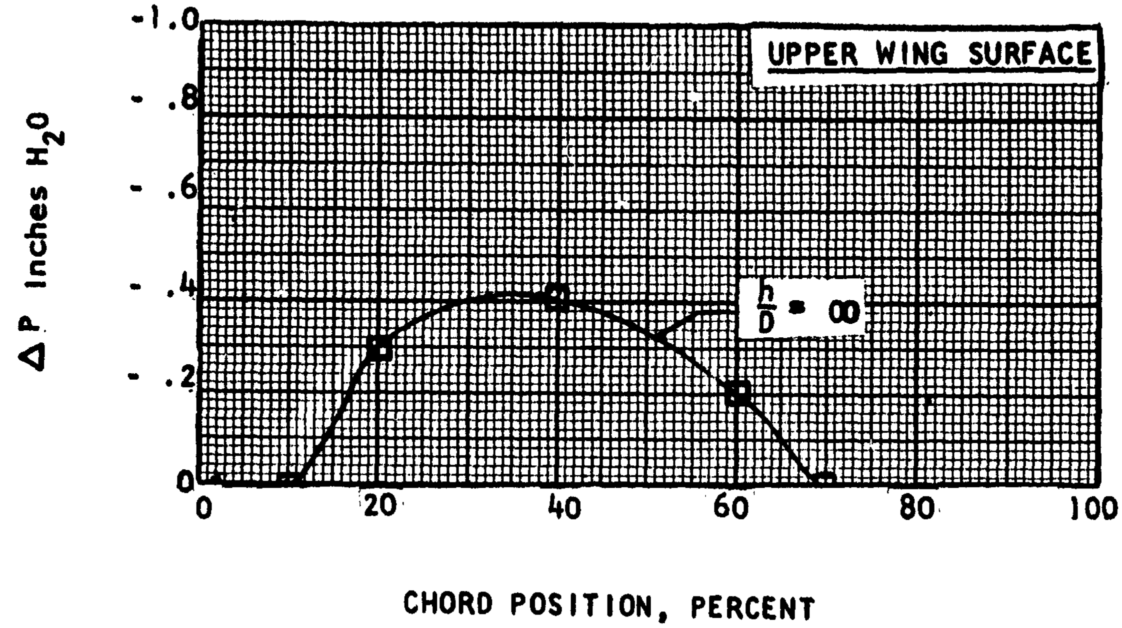

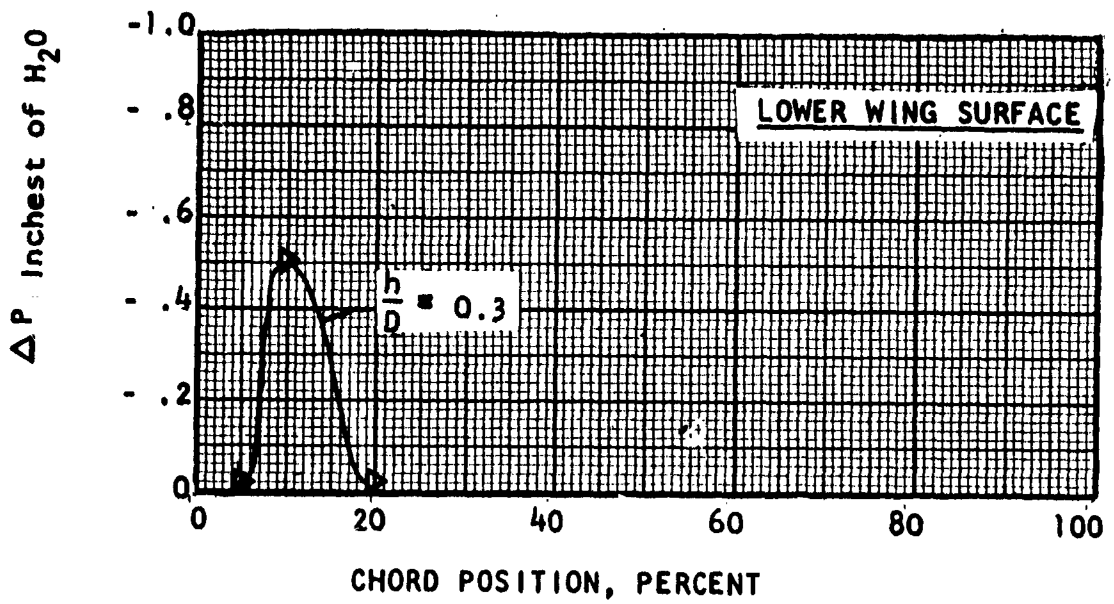

FIGURE 29

HIGH PITCH FAN, OUTBOARD PRESSURE STATION

For all static operating conditions, both in and out of ground effect, the fan shroud inlet pressures varied with the non-constant inlet radius. Also significant is the less negative pressure at the station (4) downstream of the fan with increased proximity to the ground, reflecting the previously mentioned back pressure on the fan hub and the previously mentioned back pressure on the fan hub and high solidity fan which might be expected from the studies on Reference 7.

With the high pitch fan in ground effect, all wing upper surface stations exhibited decreased negative pressures with decreasing ground height and both the inboard and outboard stations on the lower surface showed more negative pressures with decreasing ground height. This may be expected, because of the higher quantity air flow rates with the high pitch fan, at 9060 RPM, than with the medium pitch fan at 10,000 RPM. The fan shroud surface pressures downstream of the fan became less negative as the model was brought to the ground.

4. Performance of Fan

a. Static Fan Performance (Out of Ground Effect)

The design point of 200 pounds per square foot disc loading was for the high pitch fan (Ø root = 55.9°, RPM = 10,000). Because the same airfoil sections and blade twist distribution was used for the other two fans (Ø root = 39.7° and 25.0°), they did not operate at the same efficiency. A higher efficiency for the two lower pitch fans could have been obtained by designing blading specifically for those cases.

The thrust of the high pitch fan was 63 pounds at 10,000 RPM, compared to a design value of 100 pounds. Three effects account for this indicated performance discrepancy. First, the induced lift resulting from the inlet surface negative pressure was not all measurable on the fan lift system. A portion of this lift acted on the upper wing surface and was measured as total model lift. Secondly, the fan lift flexures measured net lift which was equal to fan thrust less the down load on the fan support struts which were located downstream of the fan, as shown in Figure 2. Although these struts were faired, they experienced a sub-critical Reynolds number with a resultant drag value of 8.5 lbs., for the high pitch fan at 10,000 RPM. The third effect to be considered is that the inlet shroud did not have a uniform adequate inlet radius around the whole periphery. It was determined in Reference 8 that the inlet radius to fan diameter ratio for a ducted fan should be at least 0.06 to preclude substantial inlet losses. This factor was taken into account in the Vertodyne model design. However, it was not possible to maintain this radius at all azimuth positions, as may be seen in Table V. The minimum value was 0.015 at the trailing edge. Incorporation of the desirable value of 0.06 would result, for the high pitch fan,

in blading operating partially within the lip of the inlet. Since, on the other hand, it was undesirable to make the wing thicker because of drag considerations, the compromised values of the inlet radius were retained. Another possibility of constructing a shallower transmission assembly to permit the fan to be moved away from the wing upper surface and still prevent the transmission from extending below the wing lower surface, would have involved a transmission of unwarrantedly high cost for the purpose of this test.

TABLE V - FAN SHROUD INLET RADIUS DATA

AZIMUTH POSITION	INLET RADIUS (INCHES)	R/D (PER CENT)
0° (Leading Edge)	0.37	3.1
30°	0.54	4.5
60°	0.72	6.0
90°	0.72	6.0
120°	0.72	6.0
150°	0.32	2.7
180° (Trailing Edge)	0.18	1.5
Fan Rotor Hub	0.50	4.2

NOTE: Reference 8 shows a minimum 6% R/D to maintain shrouded propeller static thrust efficiency.

It is noted that the high pitch fan could not be operated above 9060 RPM without the motor overheating. However, satisfactory extrapolation of thrust and power to 10,000 RPM was achieved by the use of conventional fan laws. The extrapolated point fell on the smooth extension of the curve through the test points, thus providing additional proof (see Figure 32).

An indication of power measurement inaccuracy was gained by running the transmission without a fan installed (see Figure 33). Accuracy appears to be ± 0.5 HP at low powers.

Fan longitudinal center of pressure data were obtained by dividing the fan pitching moment by the fan thrust. The center of pressure of the fan assembly was forward of the fan axial centerline for all static operating conditions, thus indicating that more suction lift was developed over the forward portion of the inlet lip. See Figures 30 to 36 for summary of data obtained by these tests.

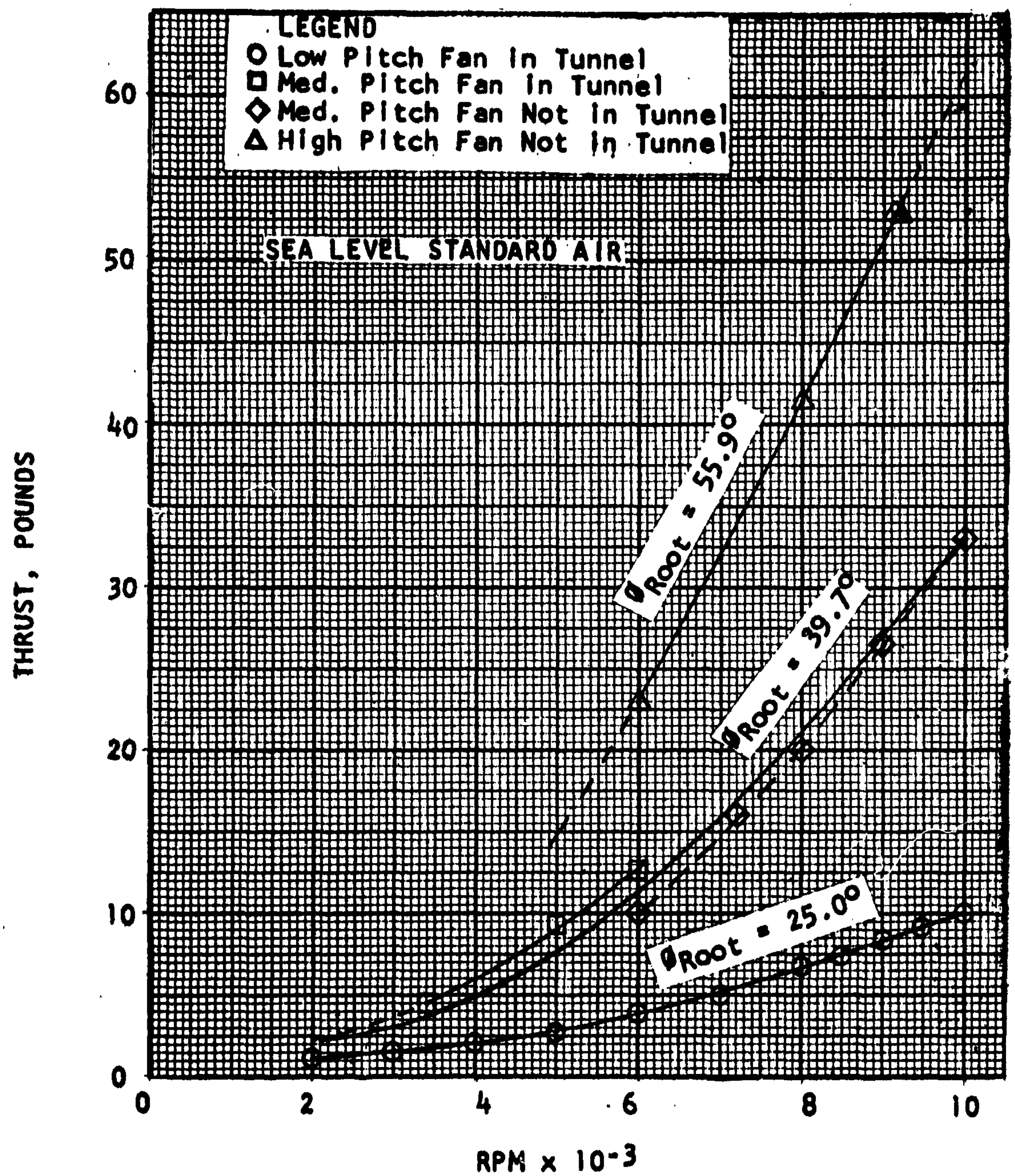

FIGURE 30

FAN STATIC THRUST VS. FAN RPM

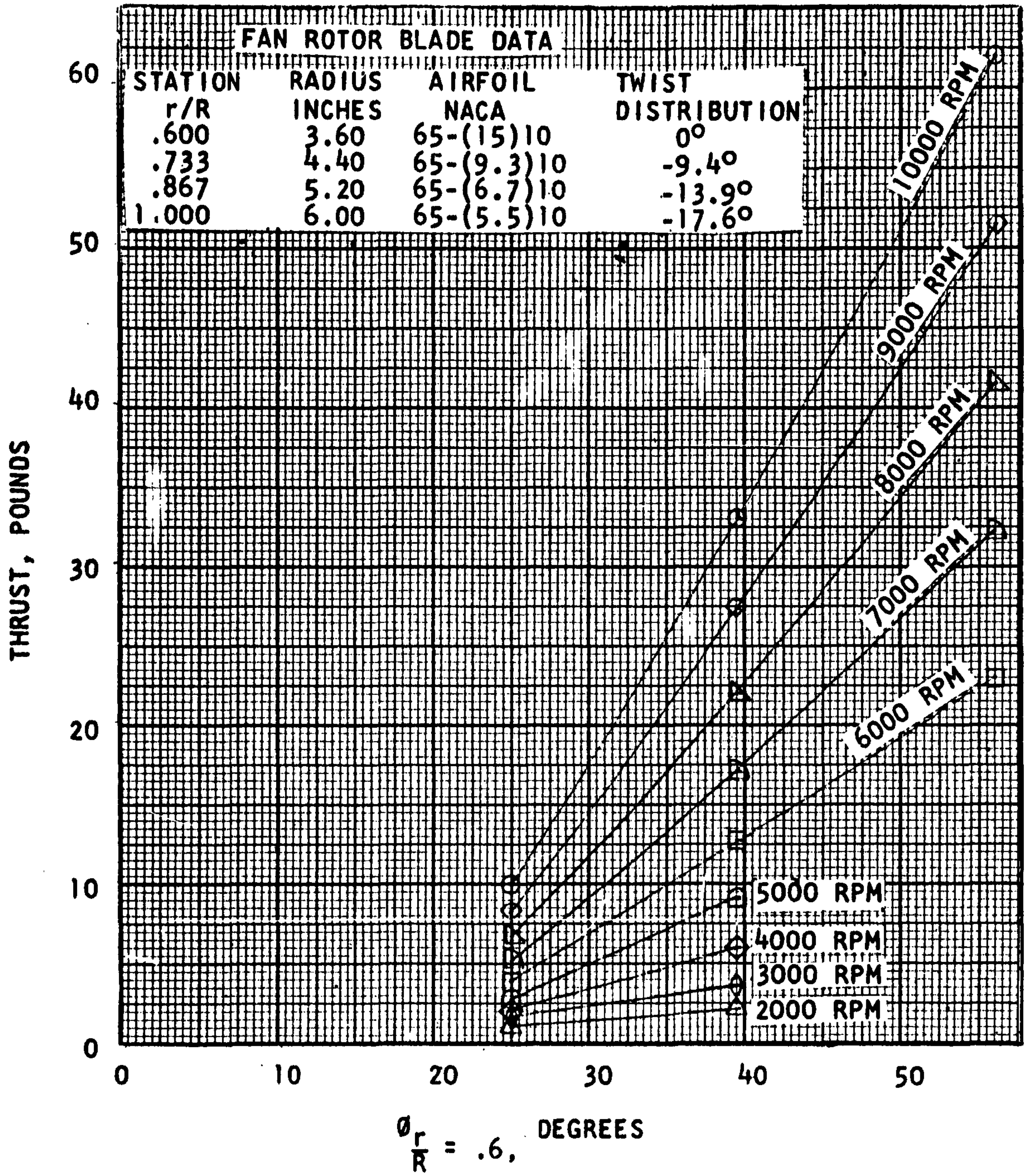

FIGURE 31

FAN STATIC THRUST VS. INCIDENCE ANGLE

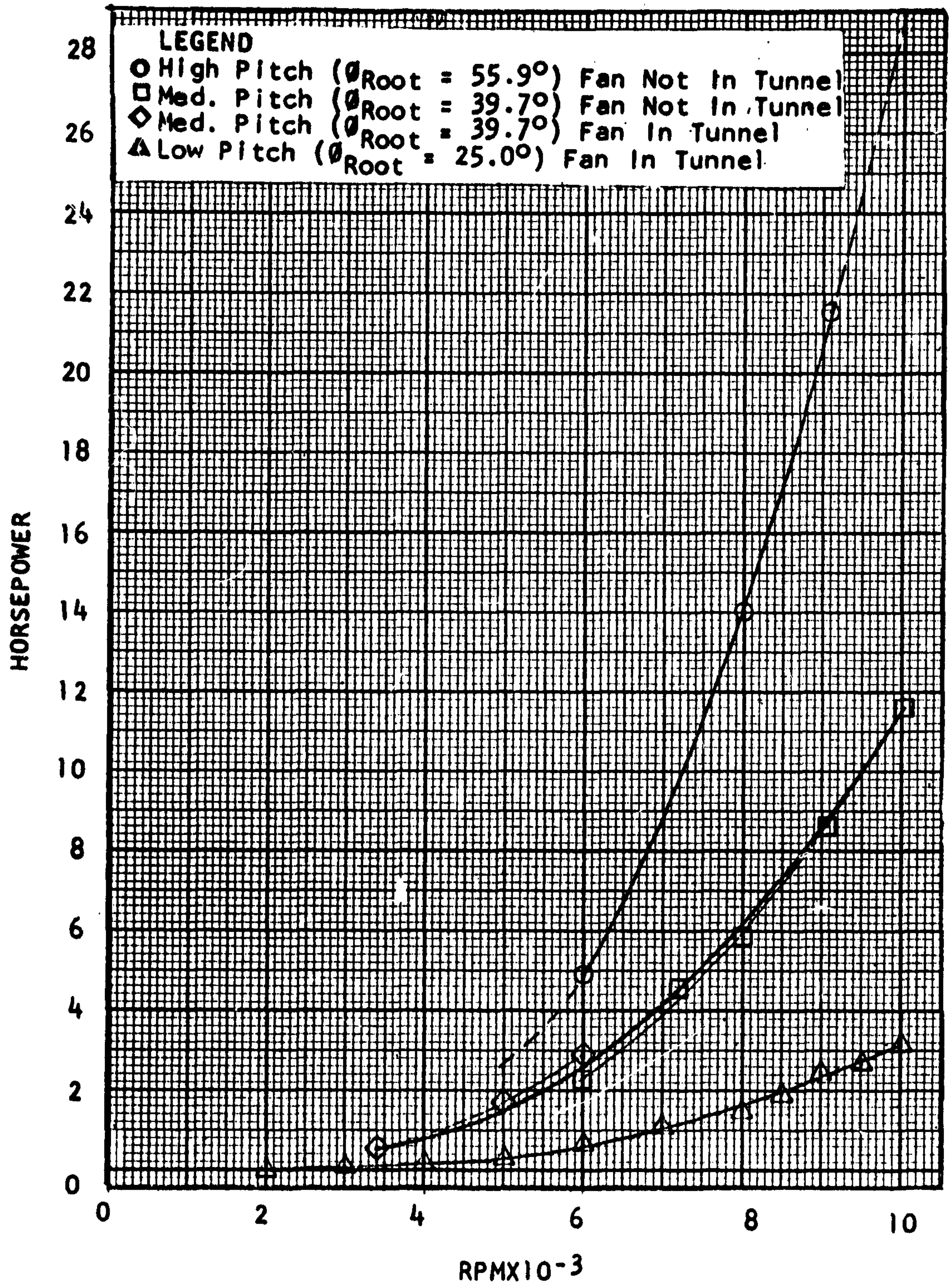

FIGURE 32

FAN POWER FROM TORQUE FLEXURES VS. FAN RPM

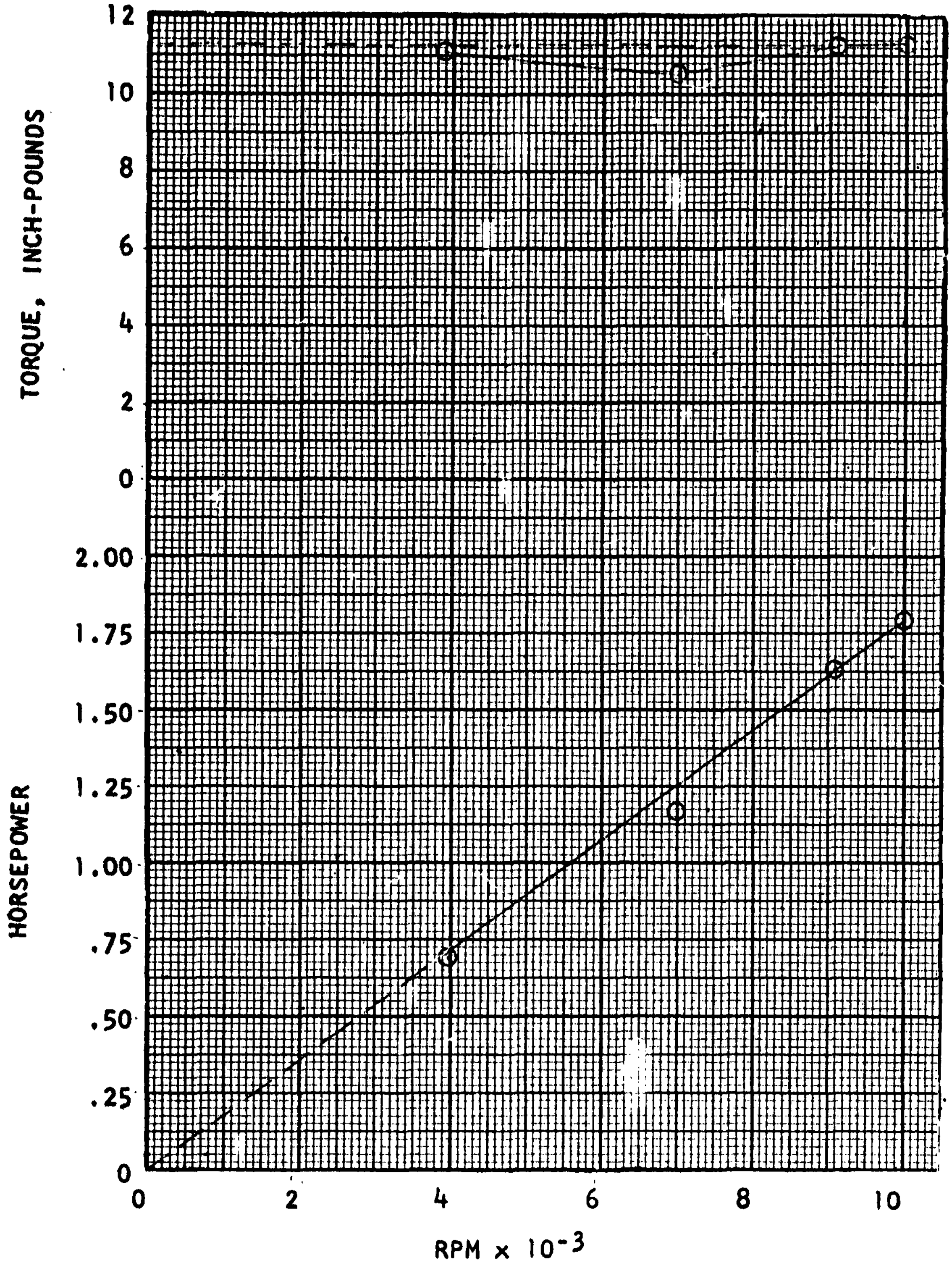

FIGURE 33

TORQUE AND HORSEPOWER VS. RPM (NO FAN)

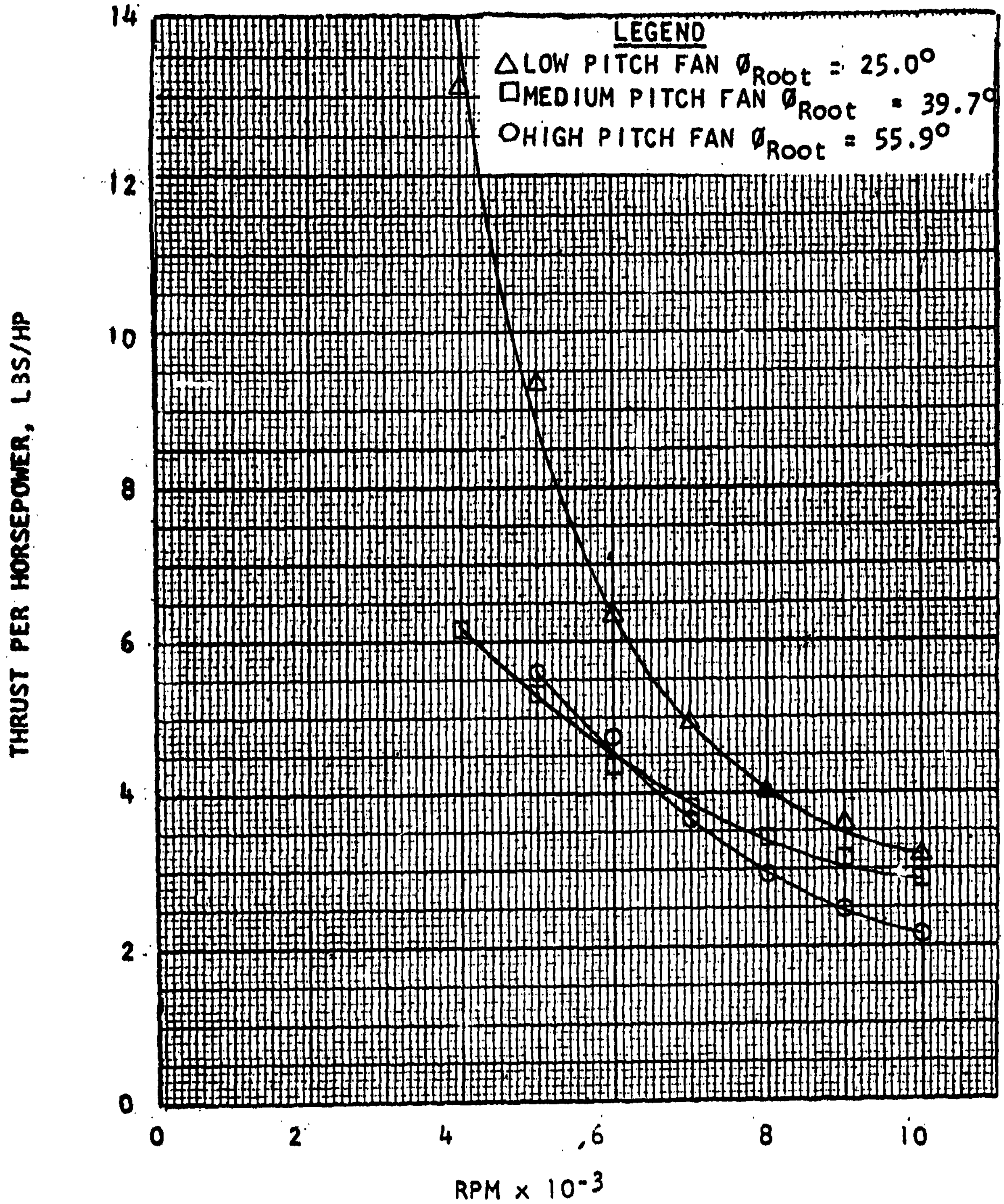

FIGURE 34

THRUST PER HORSEPOWER VS. RPM

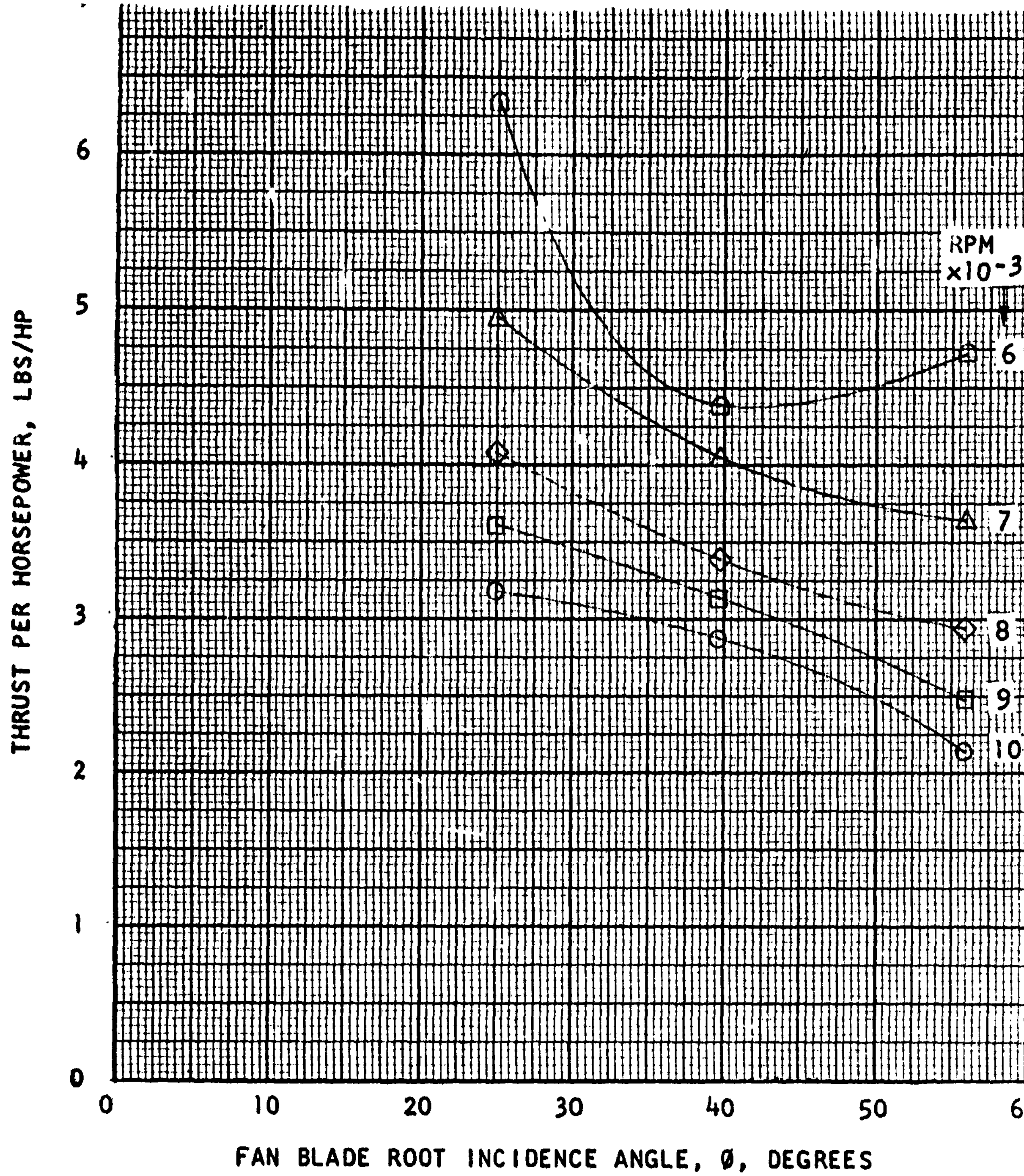

FIGURE 35

THRUST PER HORSEPOWER VS. INCIDENCE ANGLE

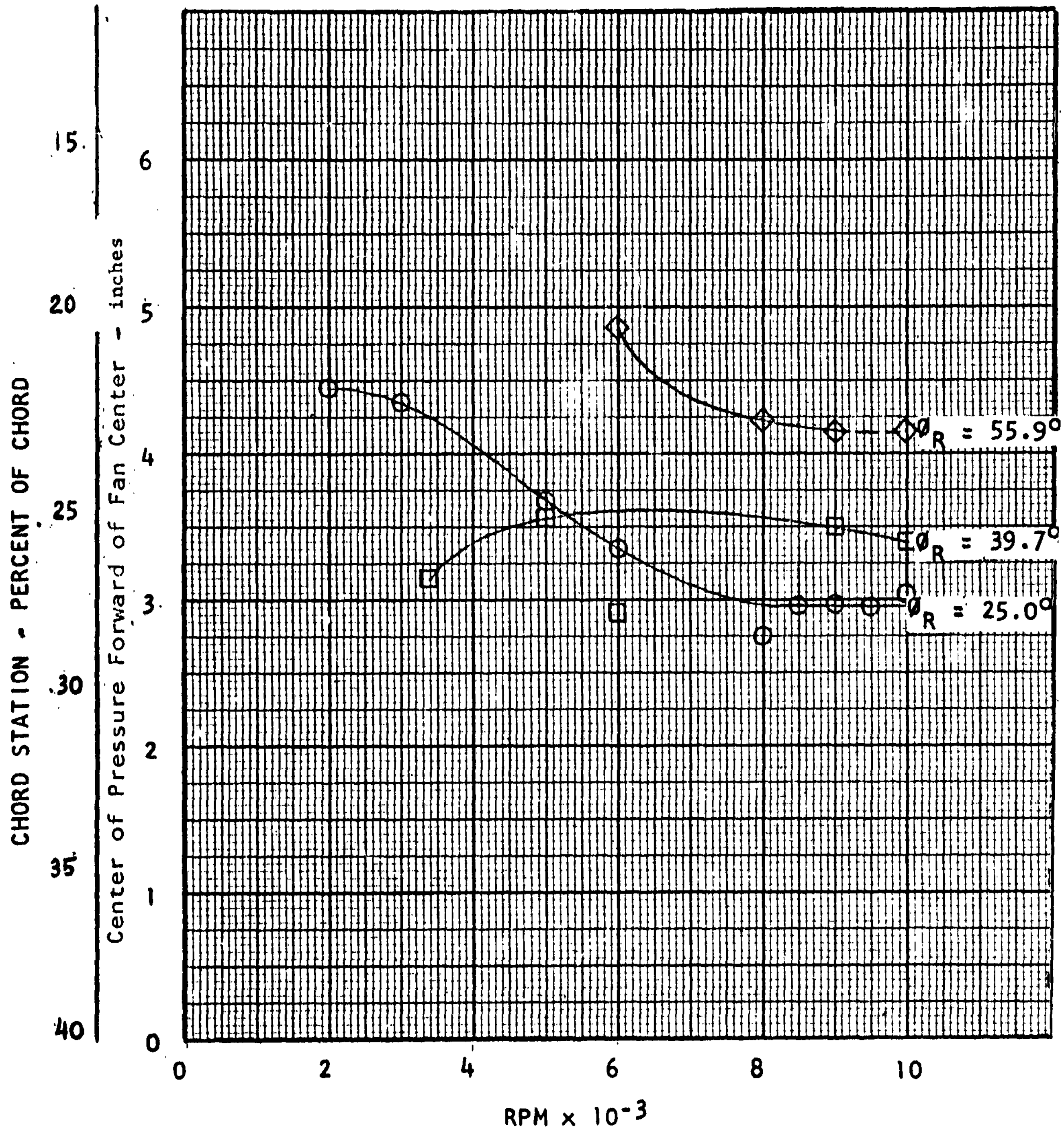

FIGURE 36

CENTER OF PRESSURE VS. FAN RPM

b. Static Fan Performance (In Ground Effect)

Important information was obtained in the ground proximity tests (see Figures 37 and 40).

At a given fan rotational speed, thrust increased with increasing ground proximity. In addition, pressure data showed that wing lower surface pressures, except for local deviations, remained at ambient static values in spite of the increasing ground proximity. Furthermore, fan static pressures in the shroud downstream of the fan (Station 4) became less negative with increasing ground proximity. These results are in agreement with Reference 7, but are in complete disagreement with References 3 and 8, which showed a negative thrust for a wing-fan arrangement below a height to diameter ratio of 0.4. The increased thrust with ground effect is attributed to the increased back pressure on the Vertodyne high solidity fan blading and on the fan hub, and to the absence of significantly large negative pressures on the lower wing surface.

Because the low pitch fan was destroyed in the wind tunnel test, prior to the static test, and because the replacement low pitch fan was destroyed during acceptance tests conducted by the fan manufacturer, no low pitch fan was available for the static tests. Instead, the medium pitch fan was operated at 6000 RPM to achieve the same disc loading as the low pitch fan at 10,000 RPM. It is believed that, in this way, conditions corresponding to the operation of the low pitch fan were sufficiently approximated for a study of ground effect at lower disc loadings.

For the three test conditions (high pitch fan at 9060 RPM and medium pitch fan at 10,000 and 6,000 RPM) the power increased with ground proximity at the same rate as the thrust, so that the thrust per horsepower remained constant, for a given fan RPM, from $h/D = \infty$ to $h/D = 0.3$. A summary of the ground effect data is given in Table VI, at $h/D = 0.5$. This value was chosen because of data consistency down to this ground height. Some inconsistency was experienced at the extreme test point ($h/D = 0.3$).

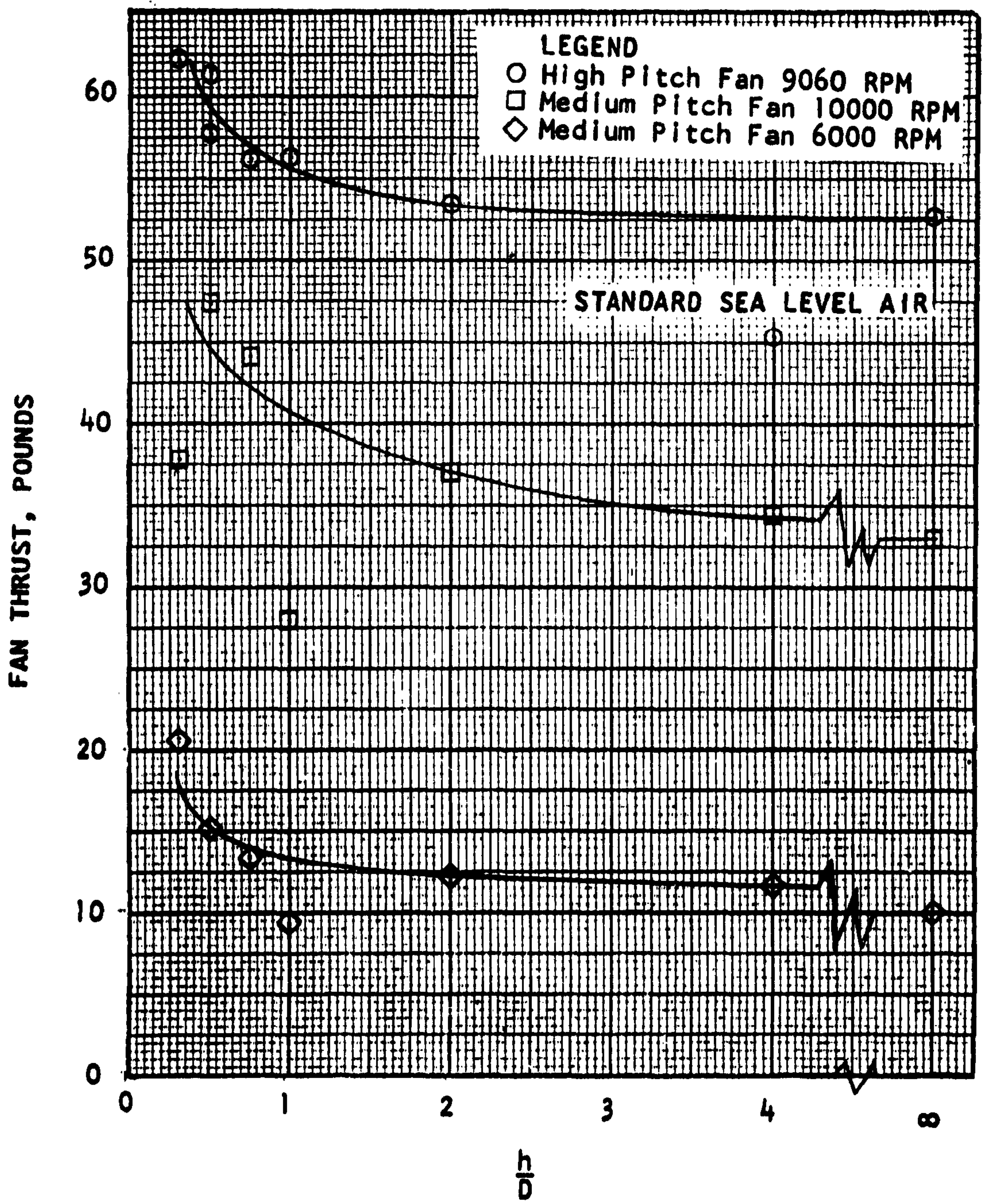

FIGURE 37

FAN STATIC THRUST VS. h/D

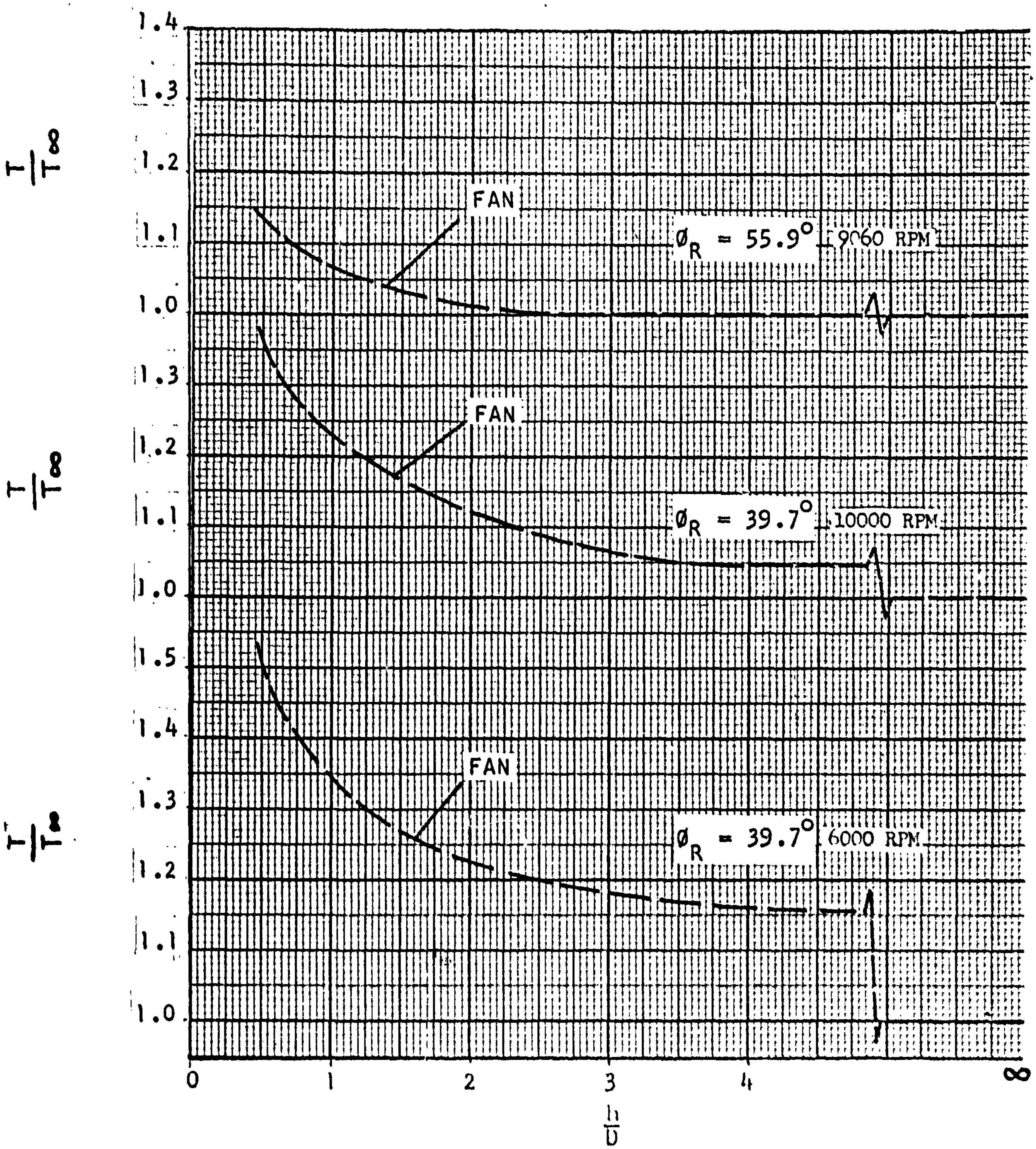

FIGURE 38

FAN STATIC THRUST (T/T_∞) VS. HEIGHT (h/D)

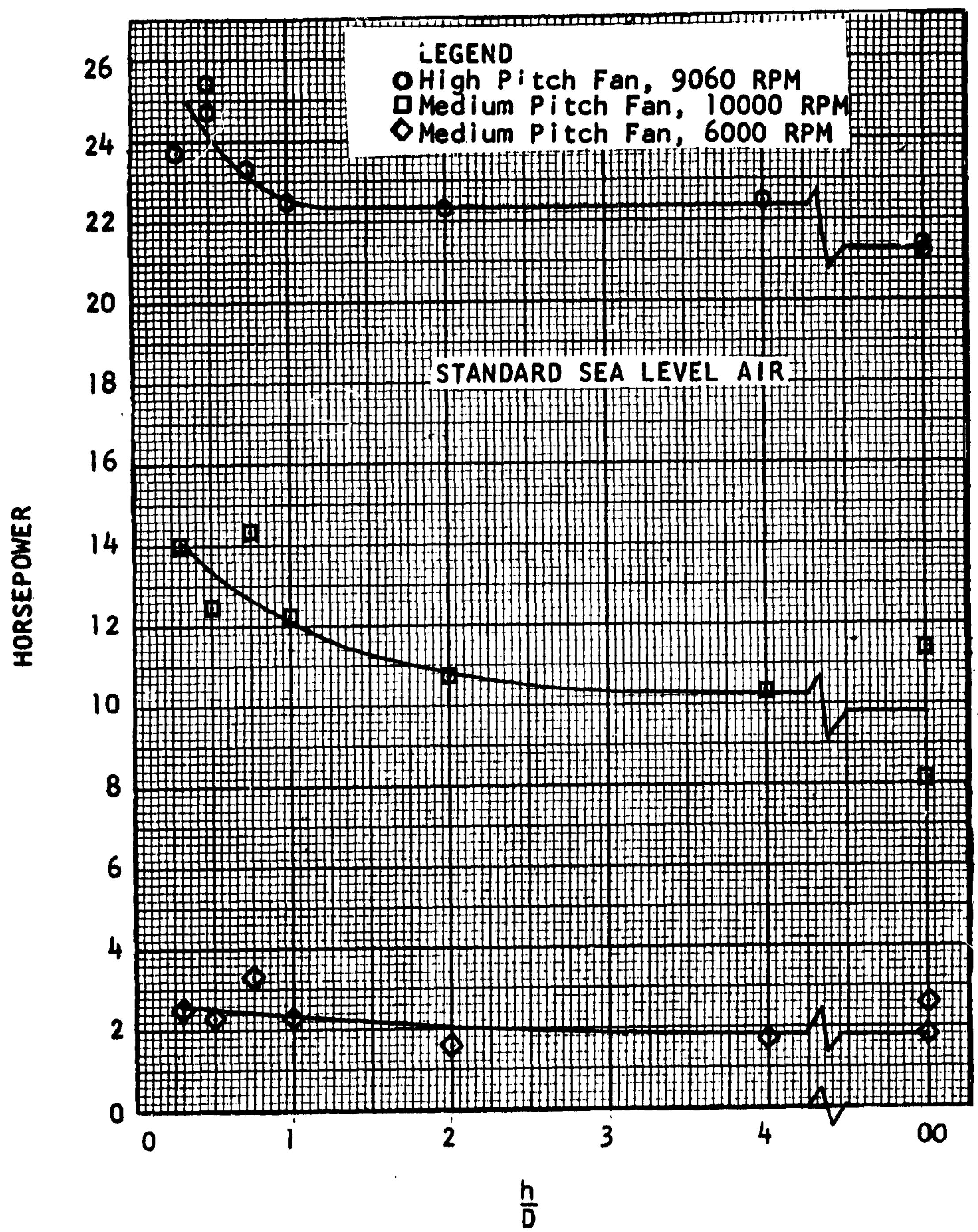

FIGURE 39

HORSEPOWER VS. h/D

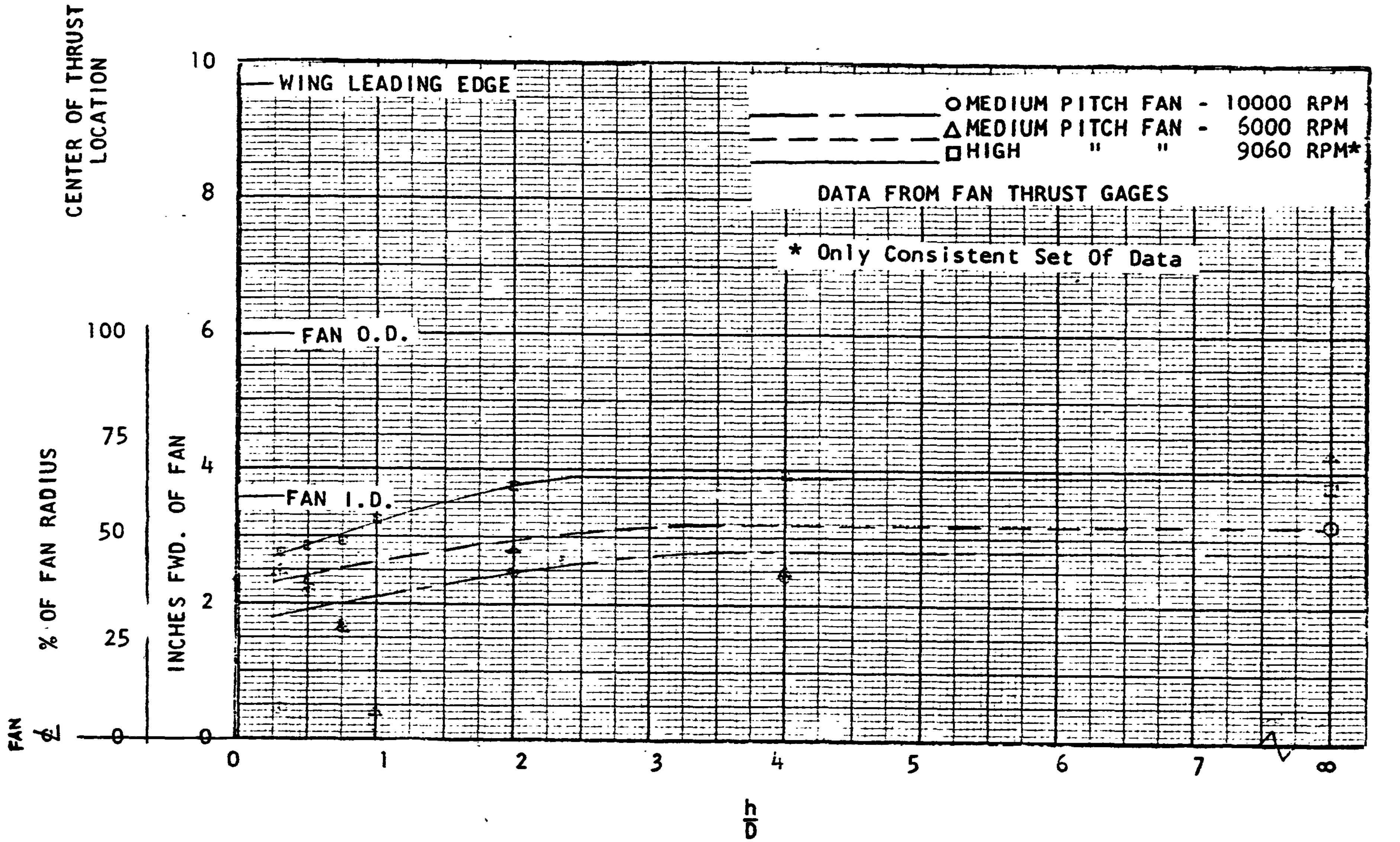

FIGURE 40

CENTER OF PRESSURE VS. h/D

TABLE VI. - SUMMARY OF GROUND EFFECT DATA

Nomenclature	T/T_∞	$(T/HP)/(T/HP)_\infty$
High Pitch	1.13	1.00
Ø root = 55.9° RPM = 9060		
Med. Pitch Fan	1.36	1.00
Ø root = 39.7° RPM = 10,000		
Med. Pitch Fan	1.52	1.00
Ø root = 39.7° RPM = 6,000		

The fan center of pressure moved aft towards the fan axial center with increasing ground proximity. The fan center of pressure would be expected to remain at the fan physical center for all static operating conditions, except for possible effects of inlet asymmetry and of fan exit flow variation between the wing lower surface and the ground in close ground proximity. The fact that the center of pressure is forward of the fan axial center is attributed to the non-symmetrical shroud inlet radius.

C. PHASE II - FORWARD FLIGHT PHASE

1. Total Model in Forward Flight (Out of Ground Effect)

The plotted data showing the performance of the total model in forward flight are presented in Figures 41 to 44. This group of data is one of the most important in this report. It depicts total model performance and longitudinal trim data for the model as a whole over the regime of transition from hovering to forward flight.

Regarding the effect of forward speed on the thrust to horsepower ratio, for the medium pitch fan, at $\alpha = 0^\circ$ and at $+10^\circ$, the thrust to horsepower ratio increased with forward speed. As expected, at $\alpha = -10^\circ$, the wing negative lift contributed to the decrease of the thrust to horsepower ratio with increasing speed.

Lift data show that at angles of attack of 0° and $+10^\circ$, the model lift increased with increasing tunnel speed. Further lift increases were achieved with wing flap deflections.

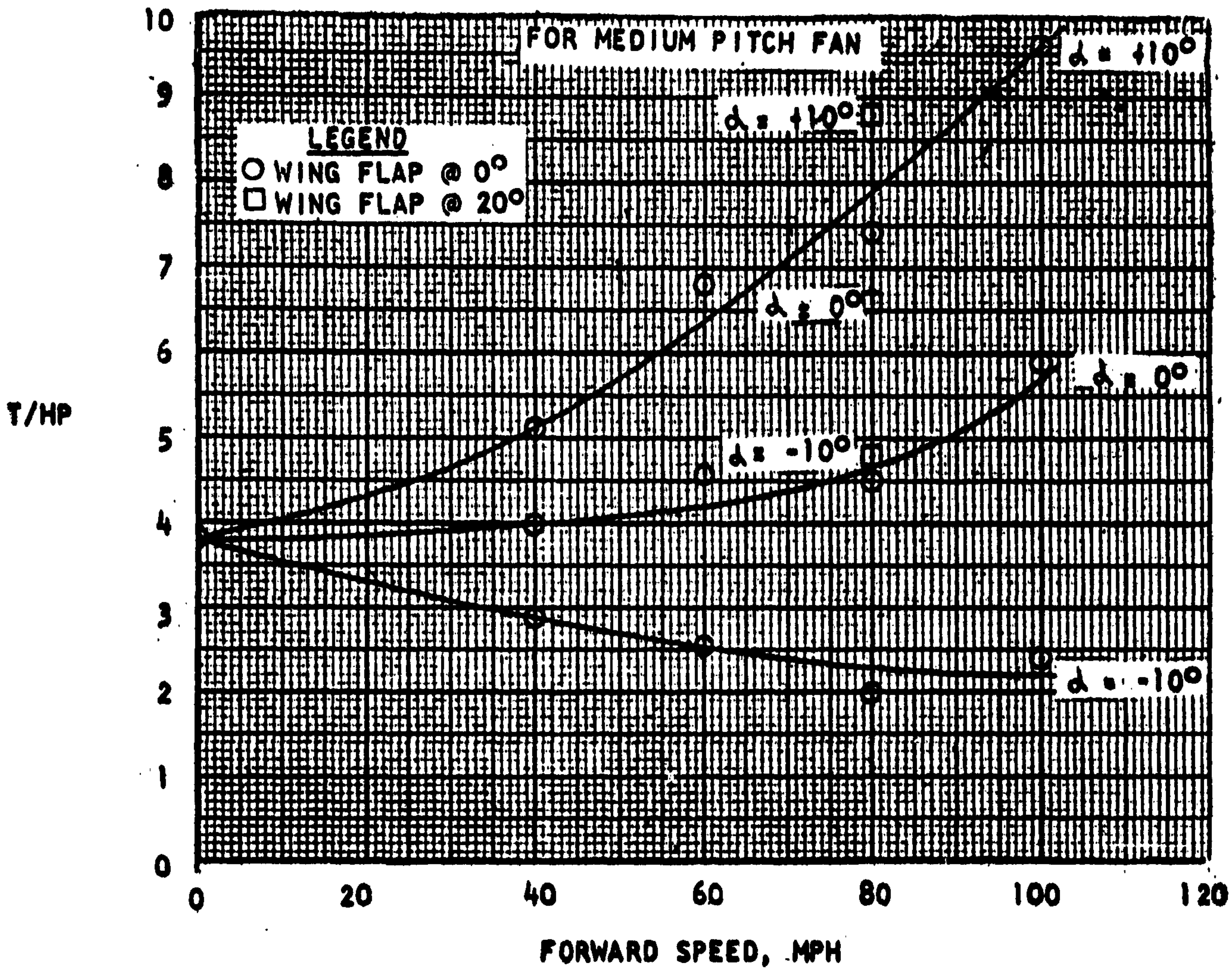

FIGURE 41

TOTAL MODEL THRUST PER HORSEPOWER
VS. FORWARD SPEED

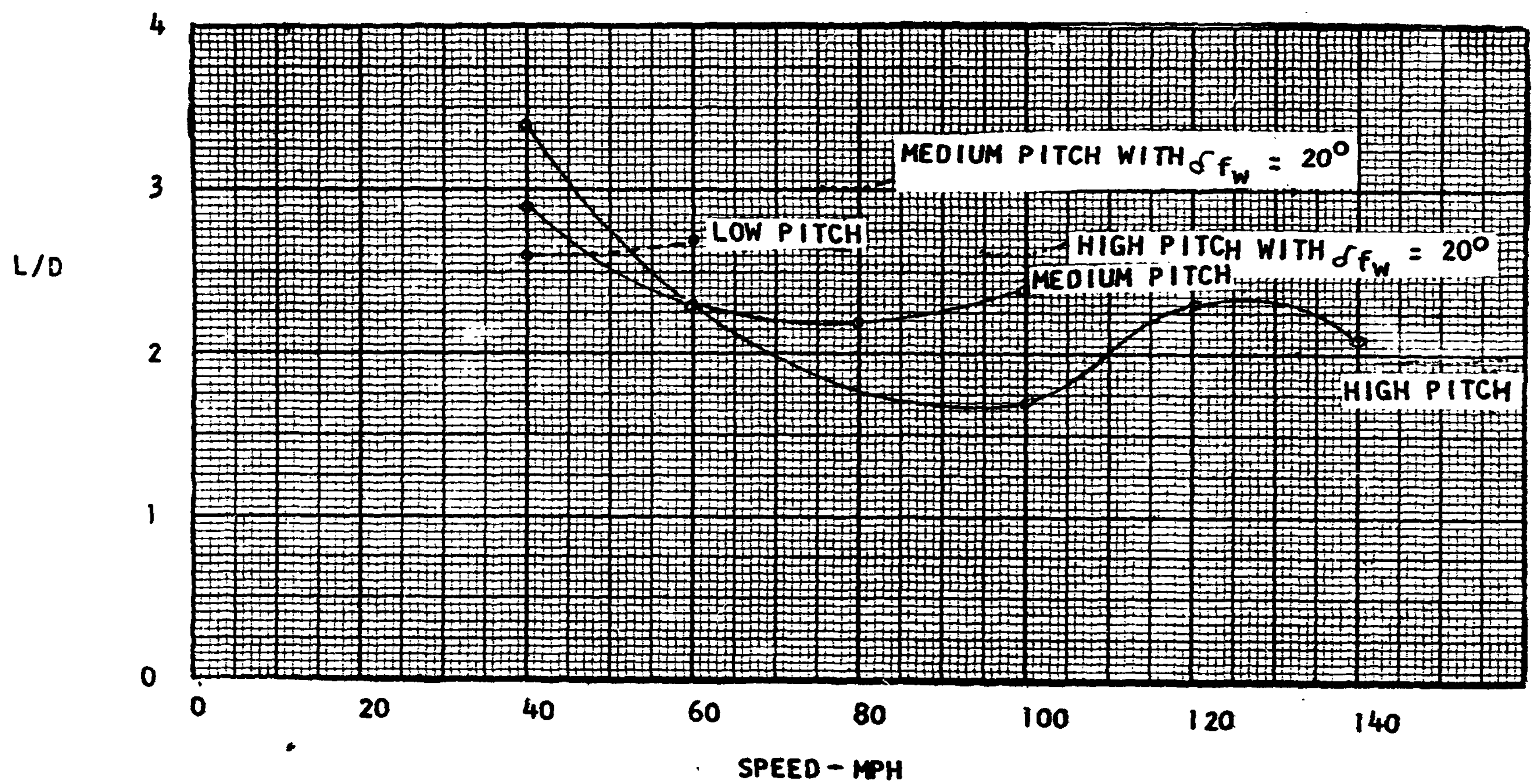

FIGURE 42

TOTAL MODEL L/D VS. FORWARD SPEED.
3 FANS, α WING = 0°

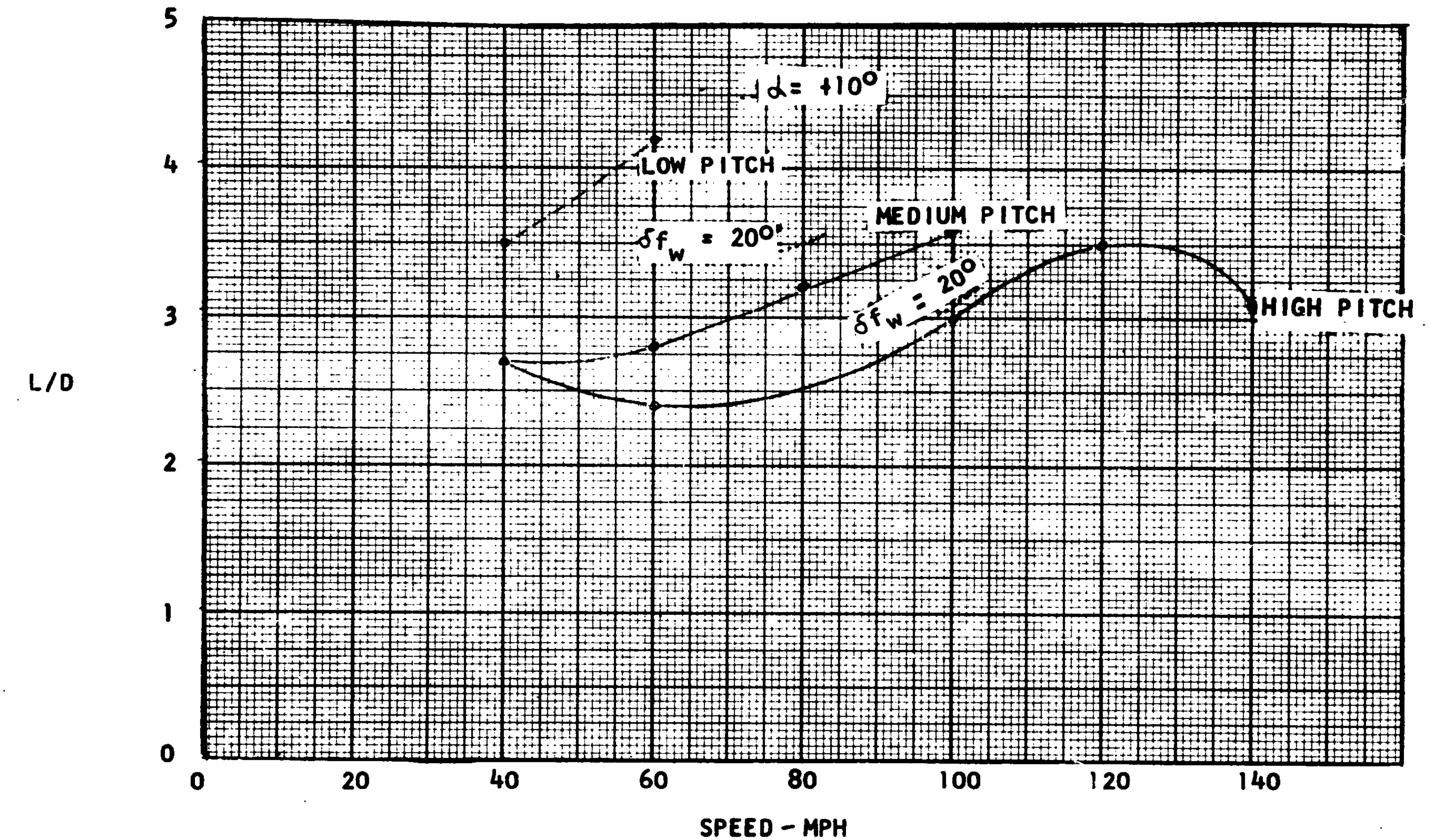

FIGURE 43

TOTAL MODEL L/D VS. FORWARD SPEED,
3 FANS, α WING = +10°

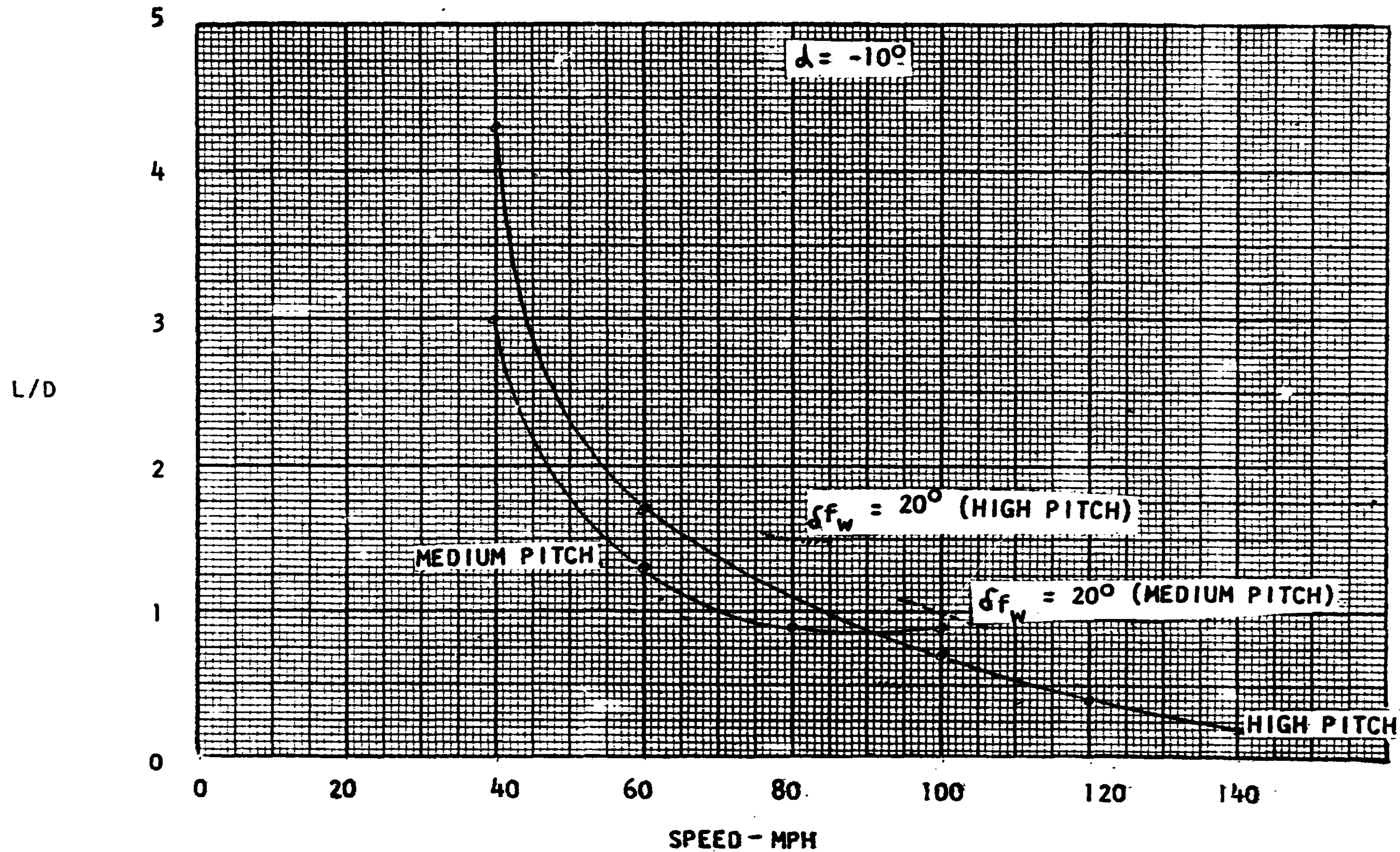

FIGURE 44

TOTAL MODEL L/D VS. FORWARD SPEED,
2 FANS, αWING = -10°

Plots of L/D versus forward speed for $\alpha = 0^\circ$ and $+10^\circ$ show the results with all three fans and, at $\alpha = -10^\circ$, the results with the medium and high pitch fans only. The low pitch fan was destroyed before it could be operated with the α at -10°. At $\alpha = 0^\circ$, with the medium pitch fan, the L/D values decreased with increasing forward speed, to a minimum value of 2.2 at 75 MPH and to 1.7 for the high pitch fan at 95 miles per hour. At higher speeds, L/D increased and a peak value of 2.3 is shown for the high pitch fan at 125 MPH. These results as well as the whole effect at the L/D versus speed curves must be attributed to the contribution of the fan induced drag whose effect is partially counterbalanced by the increasing wing lift and fan thrust. At $\alpha = +10^\circ$, the same phenomenon occurred for the high pitch fan, but the curves are rotated towards improved L/D because of the wing lift effect. The negative wing lift associated with increasing forward speed is shown at $\alpha = -10^\circ$.

A study of the variation of the pitching moment of the total model with forward speed, compared to the pitching moment of the medium pitch fan assembly, shows that both pitching moments increased with increasing forward speed. The effective center of pressure of the total model, studied for the medium pitch fan installation, moved forward at all wing angles of attack. The most severe movement is for $\alpha = -10^\circ$ and 80 MPH, where the apparent center of pressure moved to a point located 0.3 chord length forward of the wing leading edge. However, at $\alpha = 0^\circ$ and $+10^\circ$, and over the speed range from 40 MPH to 100 MPH, the apparent center of pressure was within 0.1 chord length of the leading edge.

2. Wing and Fan Shroud Surface Pressures (Model in Forward Flight)

All of the plotted data showing the effects of forward flight on wing and fan shroud surface pressures are presented in Figures 45 to 62. The effects of the deflection of the wing flap and of the fan exit elbows are included in these plots.

The surface pressures shown on all of the forward flight data plots are in relation to tunnel static pressure because of the failure of a tunnel vent line. The data may be used for comparative purposes but not as absolute values.

Prior to a detailed discussion of the results shown in the individual plots, a general observation can be made that the surface pressures with the fan operating reflect the nose up pitching moment measured by the tunnel balance system.

In fact, the surface pressure plots explain the reason for the nose up pitching moment. The first two forward flight pressure plots, Figures 45 and 46, illustrate this point. Figure 45, although showing the chordwise pressure distribution at the outboard pressure station, may be assumed to approximate the fan center station when the fan hole is closed. Because of the absence of wing surface pressure pickups across the fan opening, it was necessary to use the outboard station for comparison.

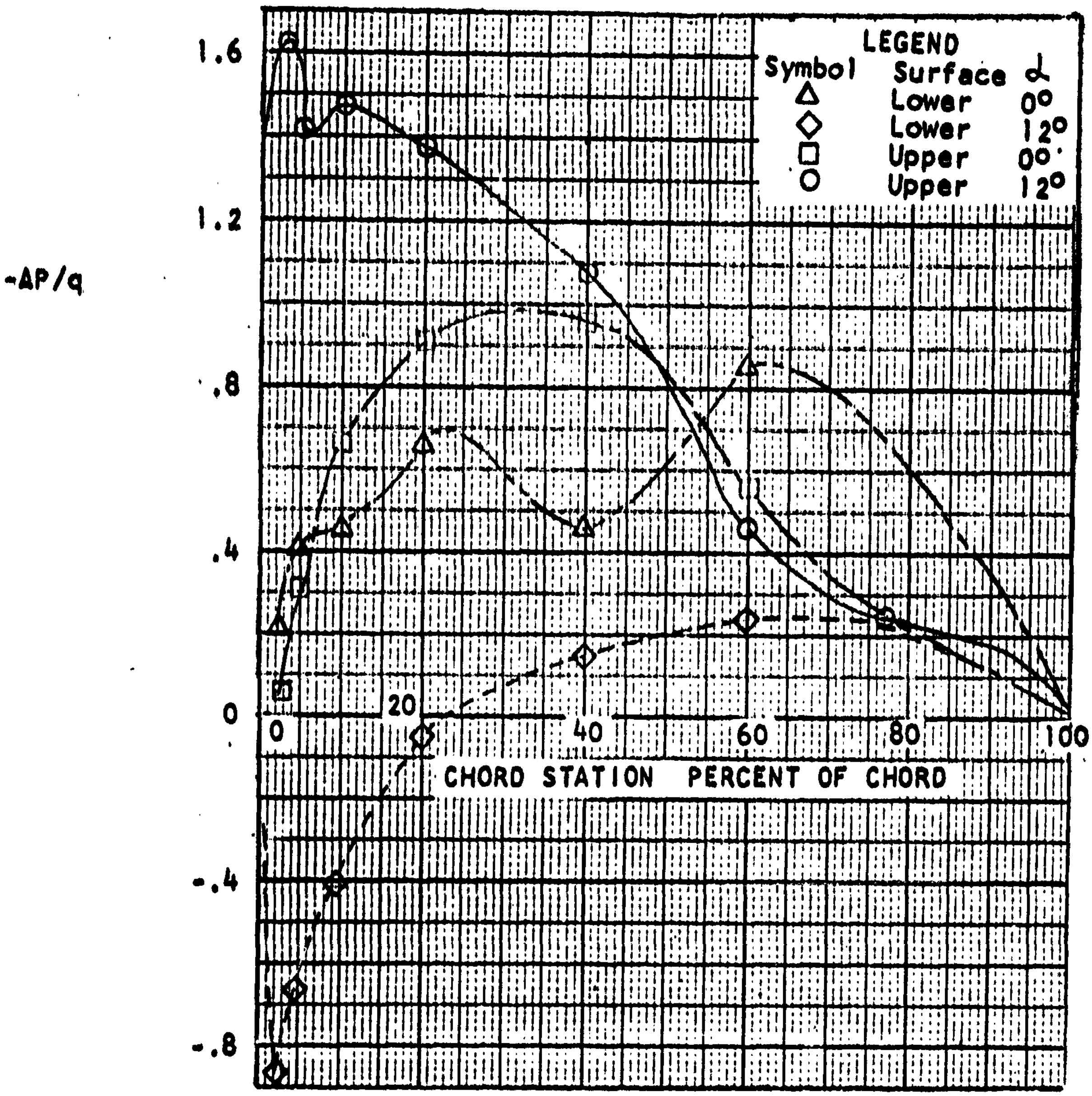

FIGURE 45

OUTBOARD WING PRESSURES, HOLE COVERED 100 MPH

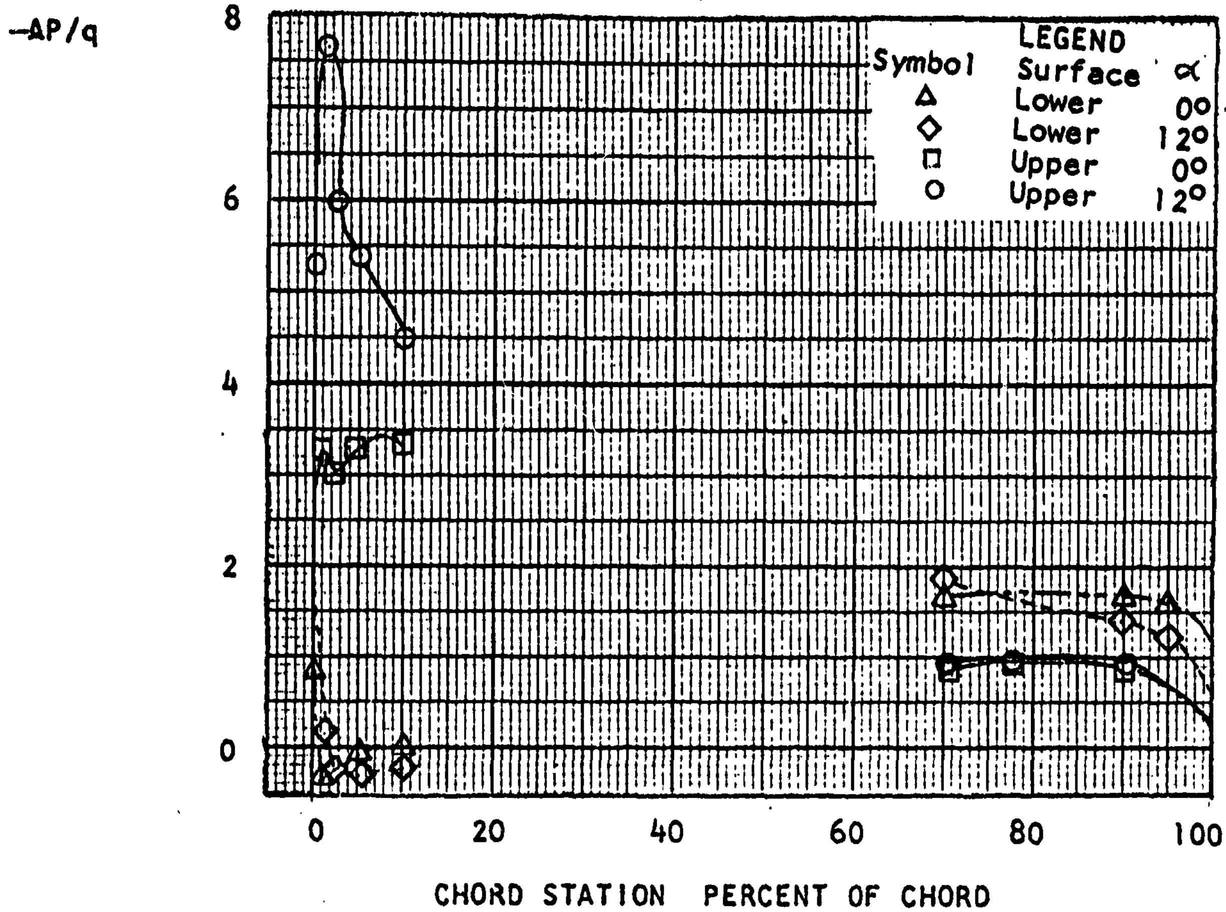

FIGURE 46

FAN CENTER WING PRESSURES, MEDIUM PITCH FAN, 10,000 RPM, 100 MPH

With the medium pitch fan operating at 10,000 RPM and at the tunnel airspeed of 100 miles per hour, it may be seen that the leading edge upper surface exhibited a negative pressure peak, while on the lower surface, the ambient pressure prevailed. This was especially noticeable at $+12^{\circ}\alpha$. Also, the trailing edge lower surface pressures aft of the fan were more negative than the upper surface pressures at α's of 0° and $+12^{\circ}$. With the hole covered, a normal airfoil pressure distribution is shown on both surfaces. In Figure 47, the pressure distribution through the fan center is shown for a locked rotor configuration at 100 MPH at $\alpha = +12^{\circ}$. These data may be compared to that in Figures 45 and 46. Here, the nose-up pitching moment is not present, indicating little lift across the fan section. Figure 48 shows the fan center surface pressures with the high pitch fan operating at 9060 RPM at 100 MPH. Here, at $\alpha = +14^{\circ}$, a slightly higher upper surface leading edge negative pressure peak occurred than with the medium pitch fan, as shown in Figure 46.

Figures 49 and 50 compare, at 60 MPH, the wing with the hole covered against that with the medium pitch fan operating at 10,000 RPM. Again, the wing operated normally with the hole covered, but showed a definite nose-up pitching tendency with the fan operating. The upper surface leading edge negative pressure peak occurred, while at the trailing edge, a differential pressure contributing to the nose-up pitching moment was also present.

Figure 51 shows the medium pitch fan at 40 MPH and Figure 52 the high pitch fan at 100 MPH. The same general tendencies are apparent.

Figures 53 and 54 are plots of the pressure distributions at four axial stations in the fan shroud. These stations are shown in Figure 33. Figure 53 shows the shroud pressure data with the medium pitch fan at 10,000 RPM, $\alpha = 0^{\circ}$ and tunnel speed of 60 MPH. Figure 54 shows the same data with the high pitch fan at 9060 RPM, $\alpha = 0^{\circ}$ and 100 MPH. It may be noted in each case that the high leading edge negative pressure disappears after the flow has passed through the fan. A pressure tap was not located at the 180° azimuth (leading edge) station, so the leading edge pressure peak was extrapolated.

Figure 55 shows the fan center wing surface pressure data with the medium pitch fan at 10,000 RPM, 100 MPH, and with the 40° fan air exit elbow installed. Comparing this figure to Figure 46 for the same operating conditions without the elbow, the significant differences are that the lower surface ahead of the elbow indicated possible flow separation and the lower surface immediately aft of the elbow showed a slightly positive pressure, which became more negative at about 90% chord, than without the elbow.

Figure 56 shows the pressure data for the same configuration as Figure 55, but at 60 MPH. The data appear to be consistent.

Figure 57 shows the fan center wing surface pressures with the medium pitch fan at 10,000 RPM at 80 MPH with the wing flap deflected 20°. Figure 58 shows the same condition with the wing flap at 0°. The expected decreased nose-up pitching tendency is reflected in the data. Increased lift and drag forces also resulted from the flap deflection.

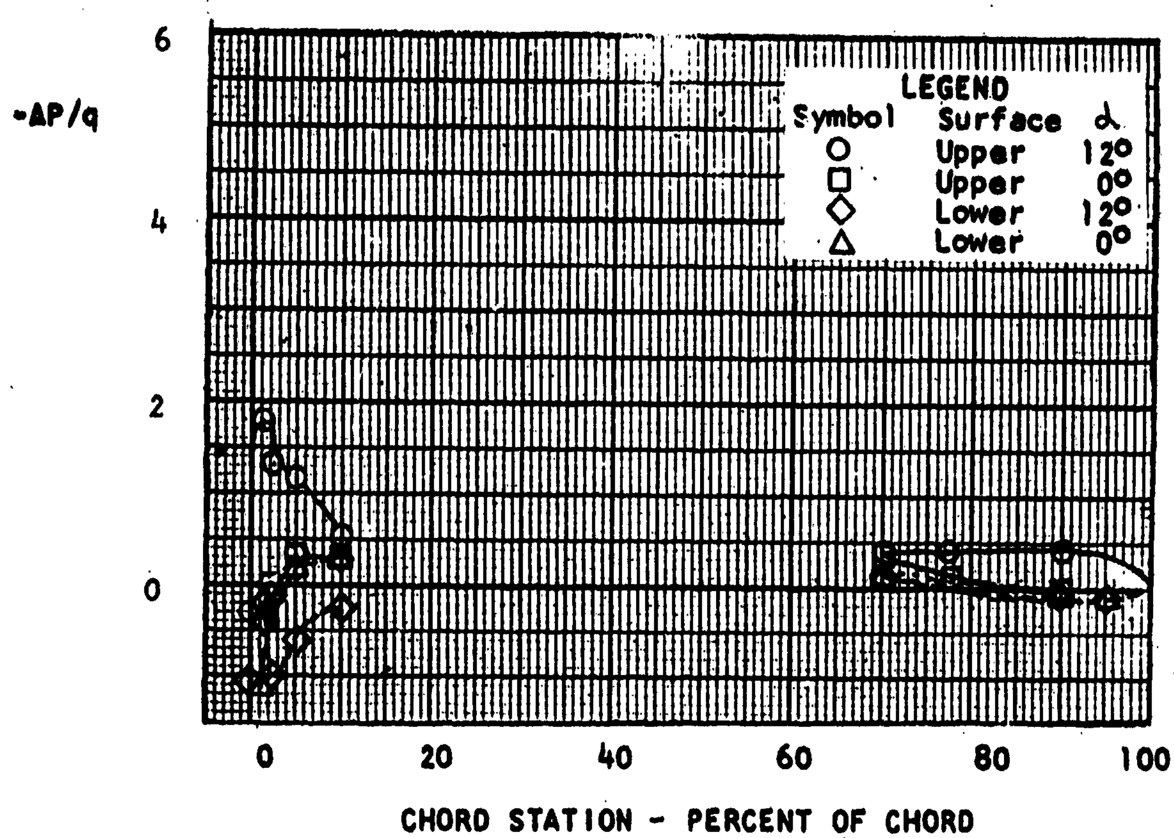

FIGURE 47

FAN CENTER WING PRESSURES, LOCKED ROTOR, 100 MPH

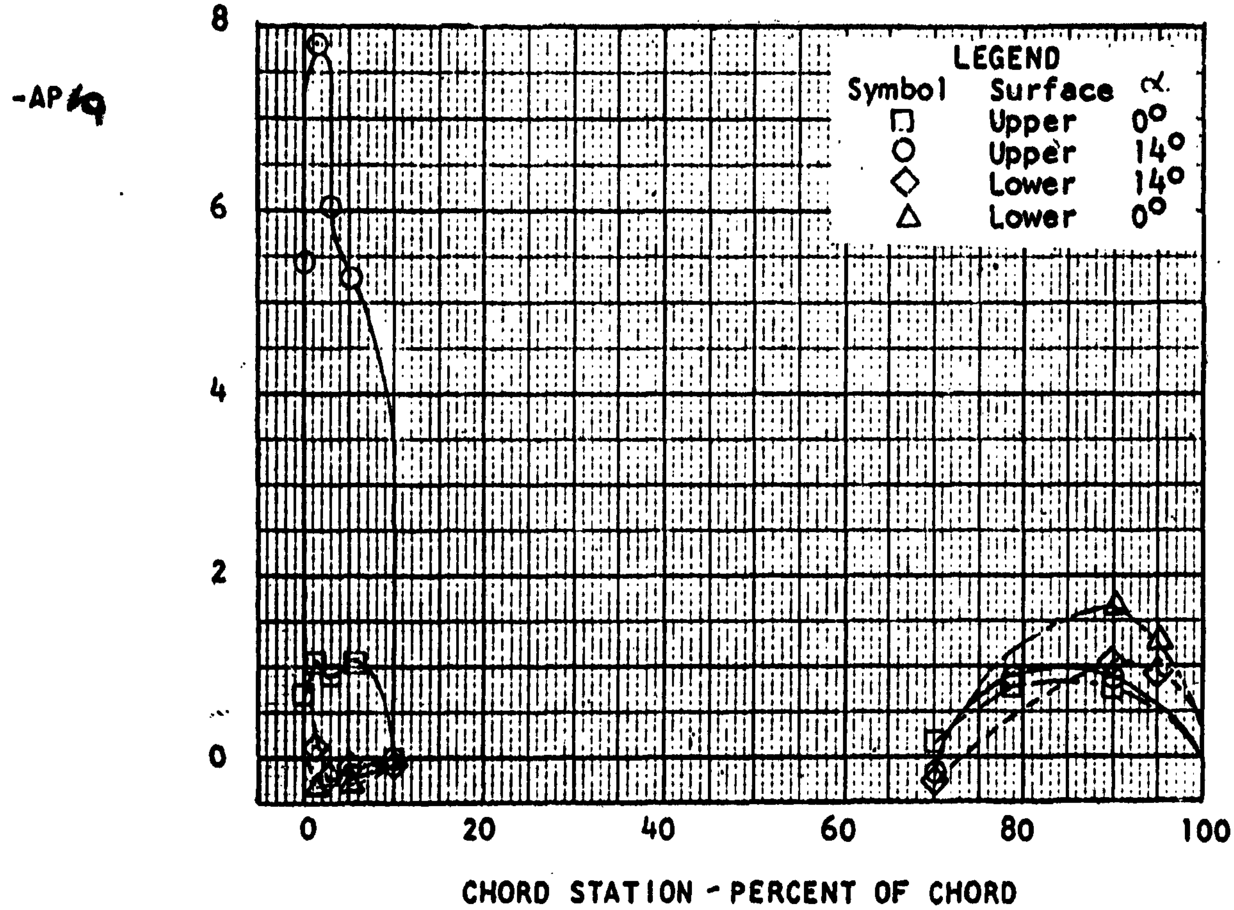

FIGURE 48

FAN CENTER WING PRESSURE, HIGH PITCH FAN,
9,060 RPM, 100 MPH

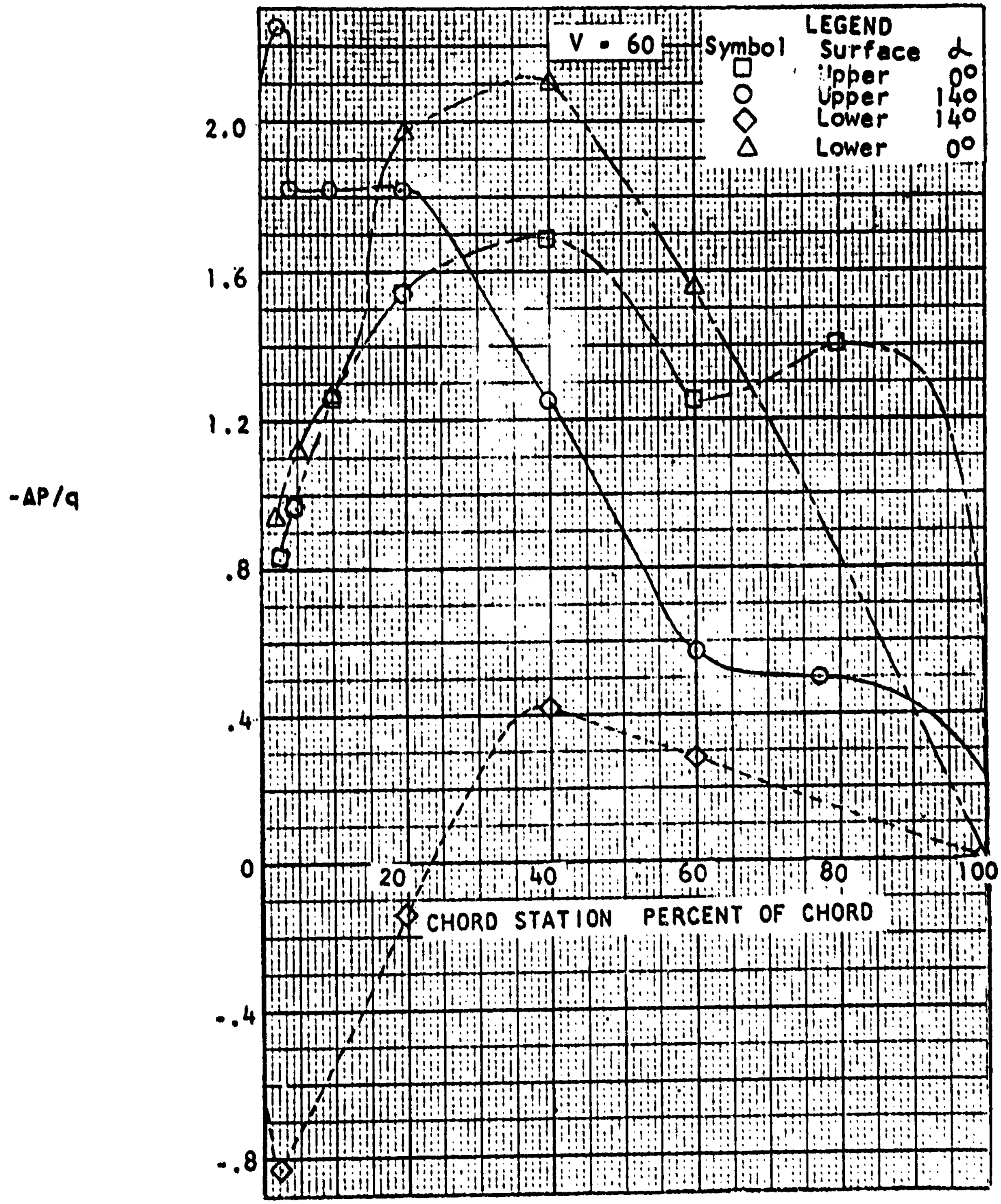

FIGURE 49

OUTBOARD WING PRESSURE, HOLE COVERED, 60 MPH

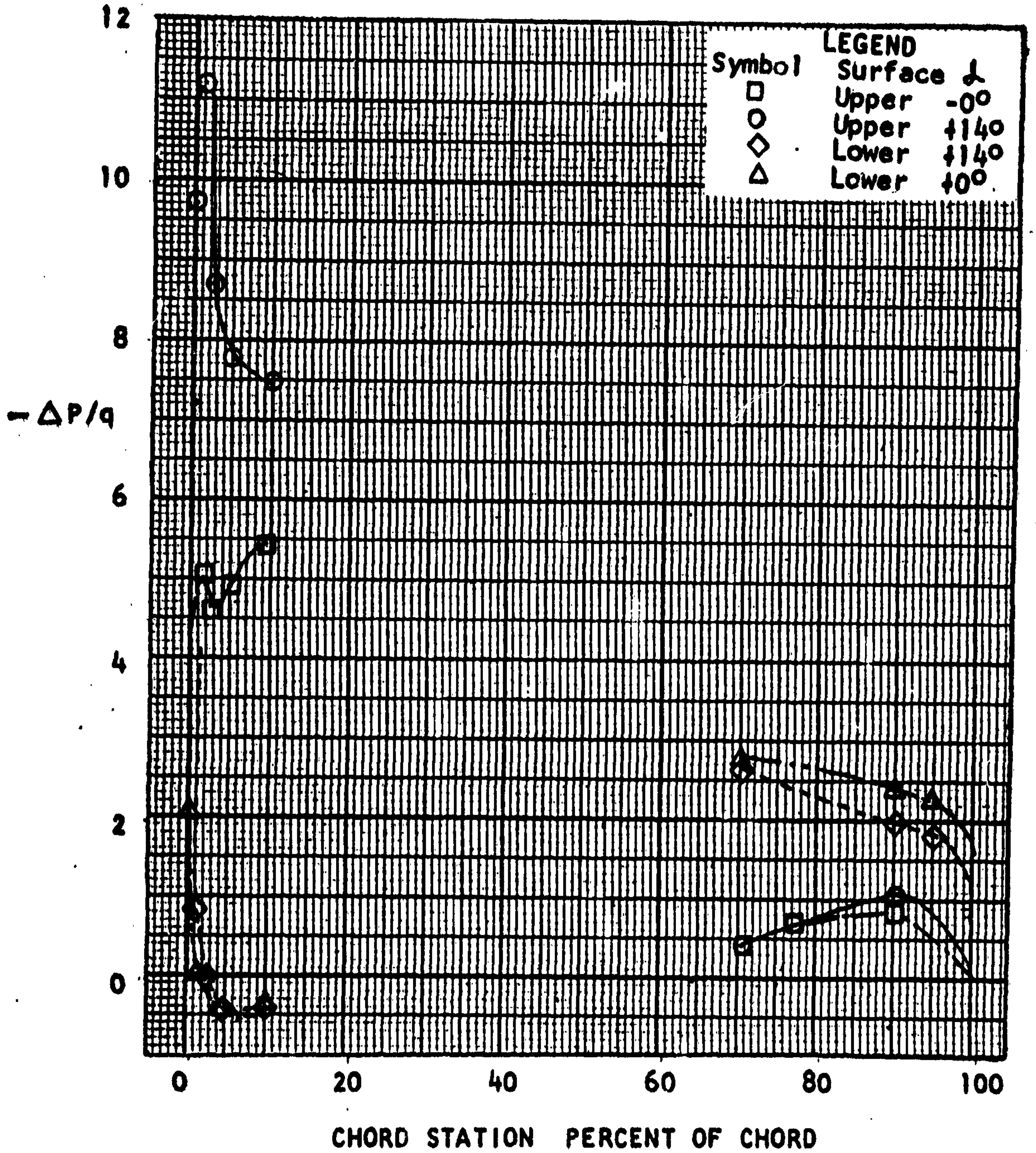

FIGURE 50

FAN CENTER WING PRESSURE, MEDIUM PITCH FAN, 10,000 RPM, 60 MPH

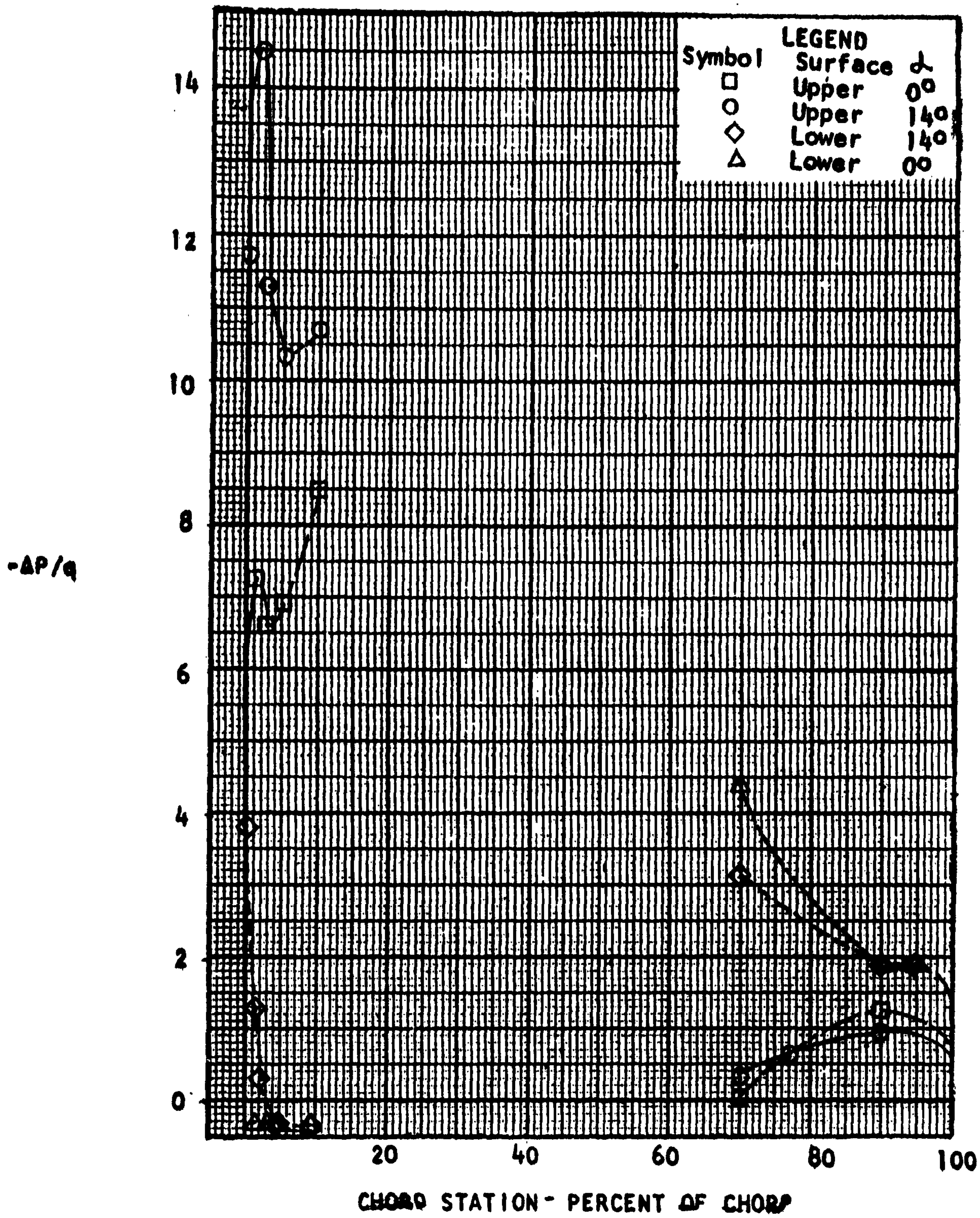

FIGURE 51

FAN CENTER WING PRESSURE, MEDIUM PITCH FAN
10,000 RPM, 40 MPH

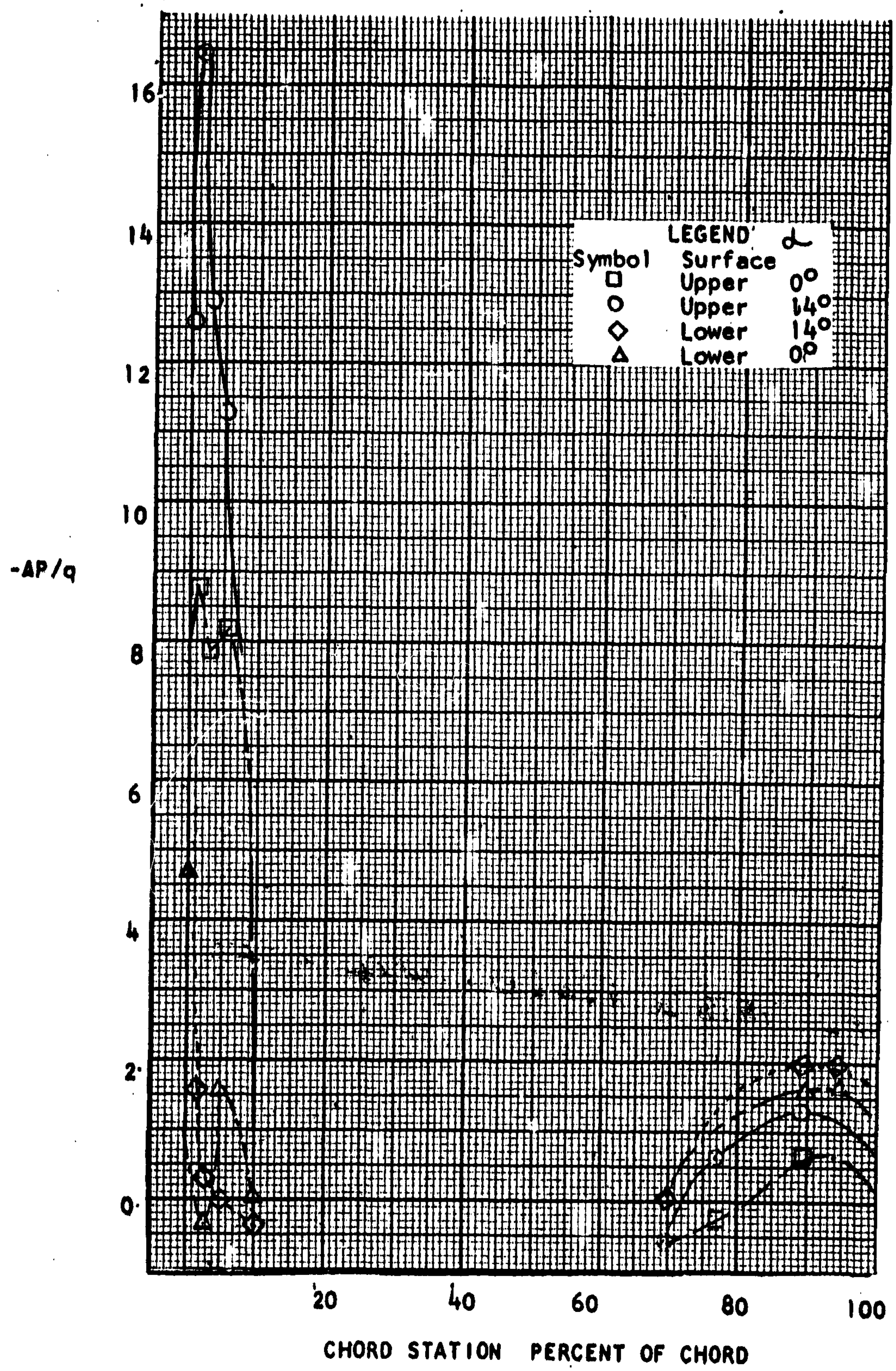

FIGURE 52

FAN CENTER WING PRESSURE, HIGH PITCH FAN, 9,060 RPM, 100 MPH

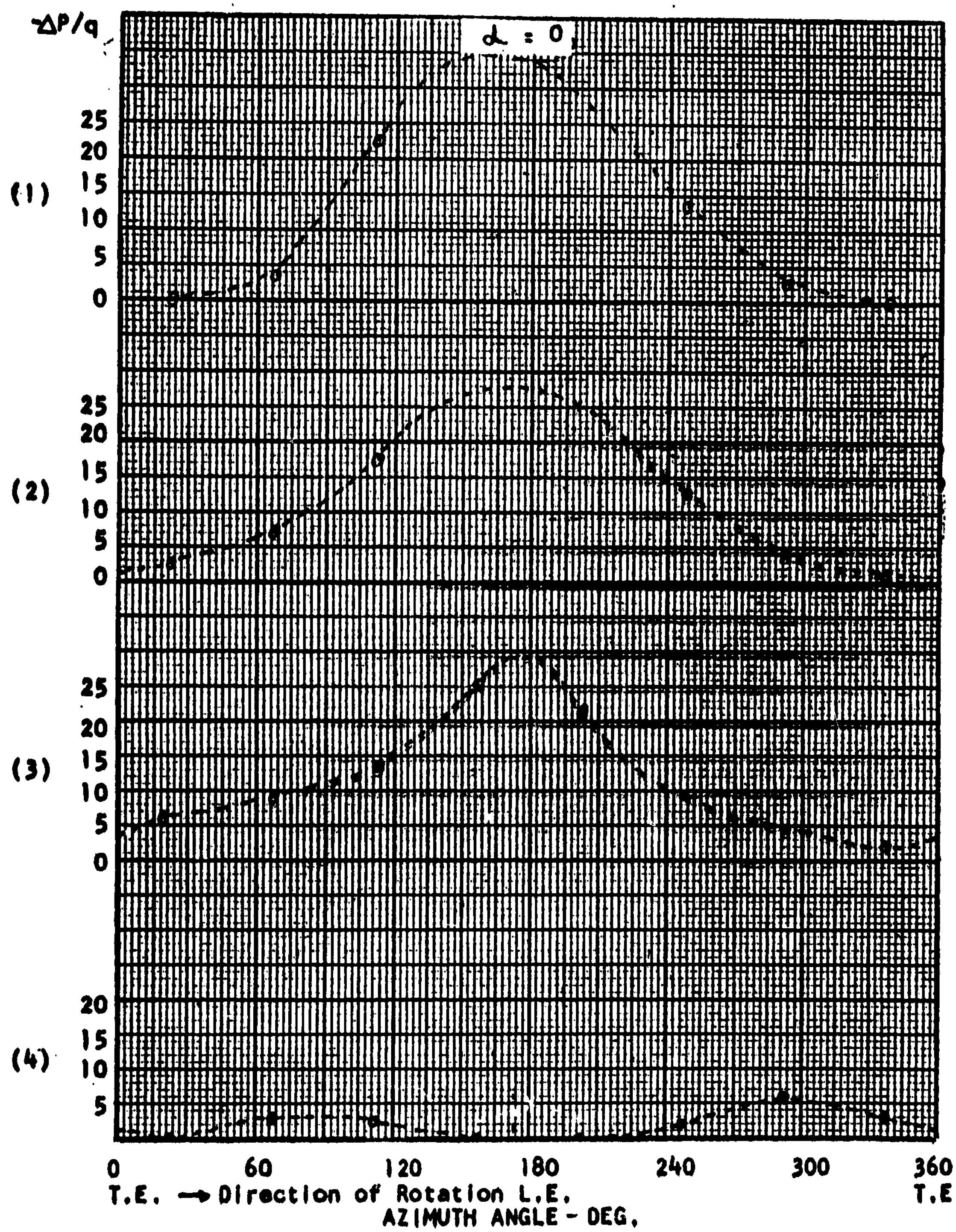

FIGURE 53

FAN SHROUD PRESSURE, MEDIUM PITCH FAN, 10,000 RPM, 60 MPH

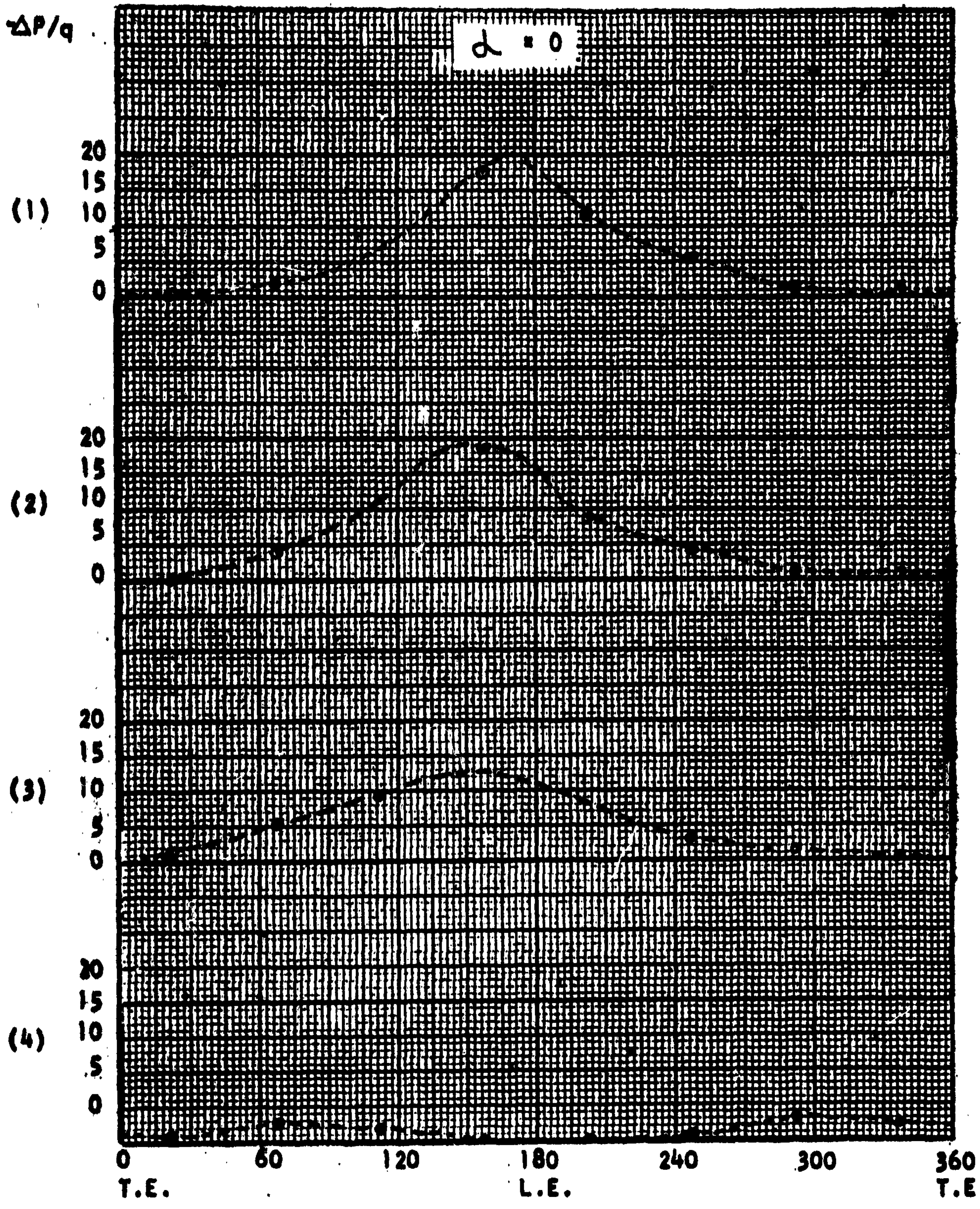

FIGURE 54

FAN SHROUD PRESSURE, HIGH PITCH FAN, 9,060 RPM, 100 MPH

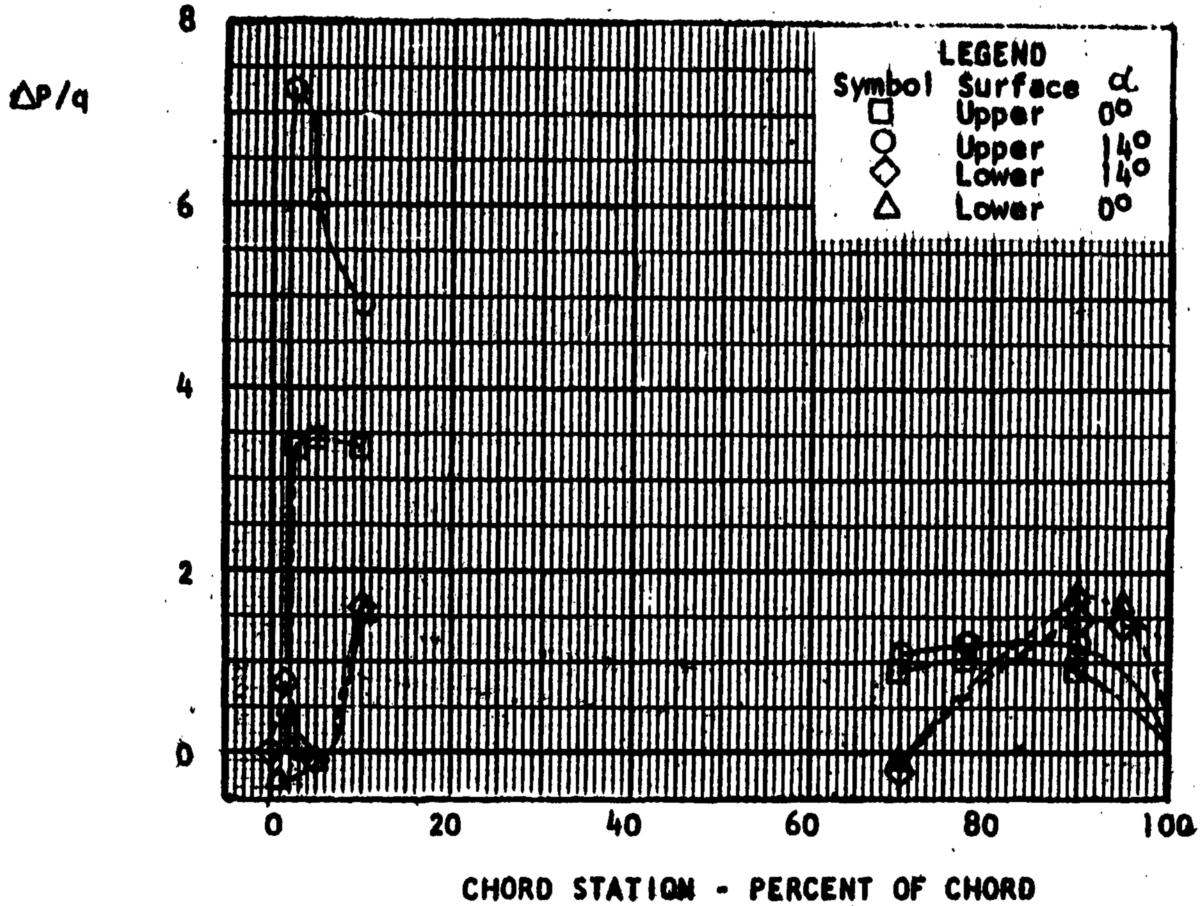

FIGURE 55

FAN CENTER WING PRESSURE, MEDIUM PITCH FAN, 10,000 RPM, 100 MPH, 40° FAN EXIT ELBOW

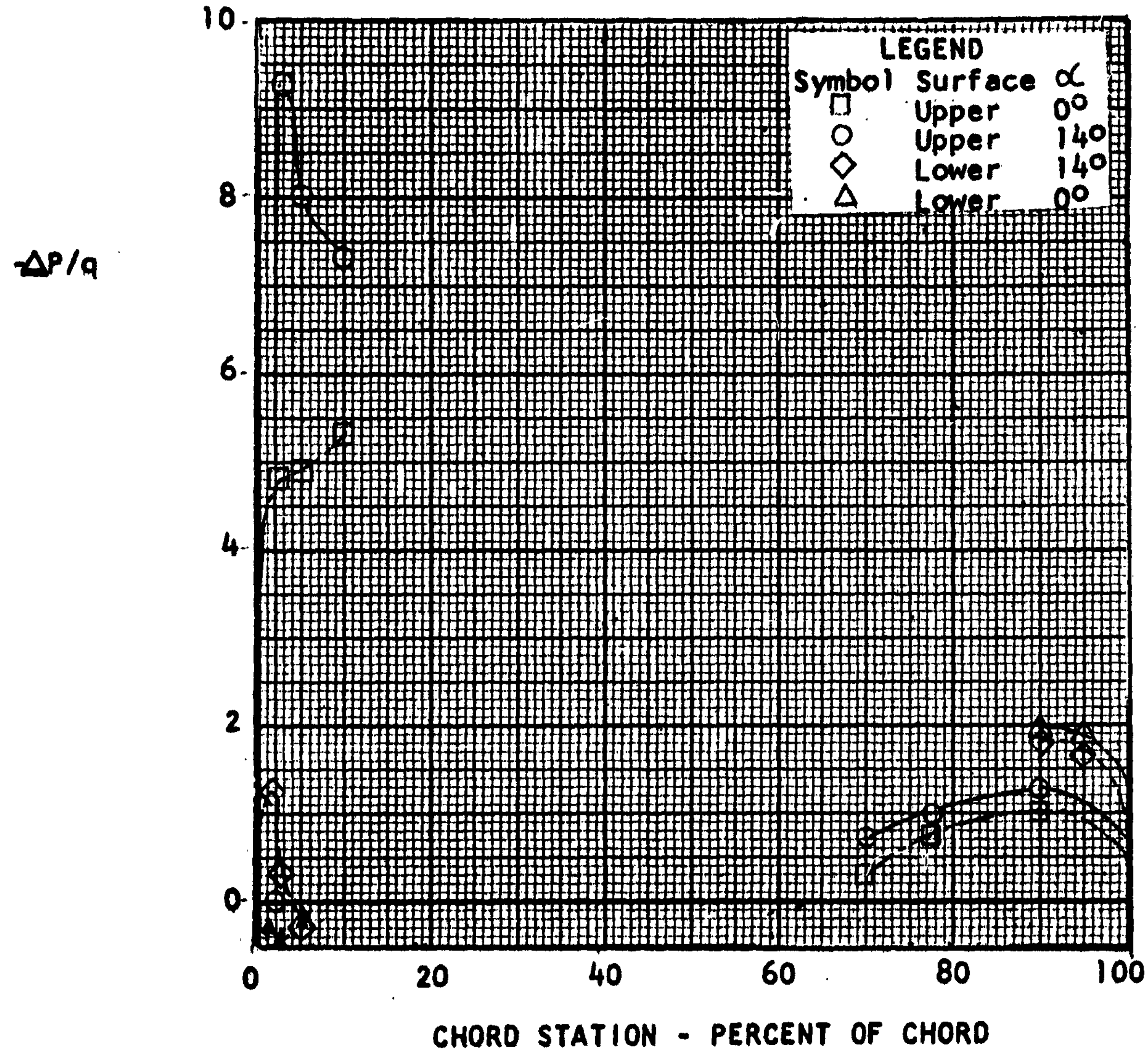

FIGURE 56

FAN CENTER WING PRESSURE, MEDIUM PITCH FAN,
10,000 RPM, 60 MPH, 40° FAN EXIT ELBOW

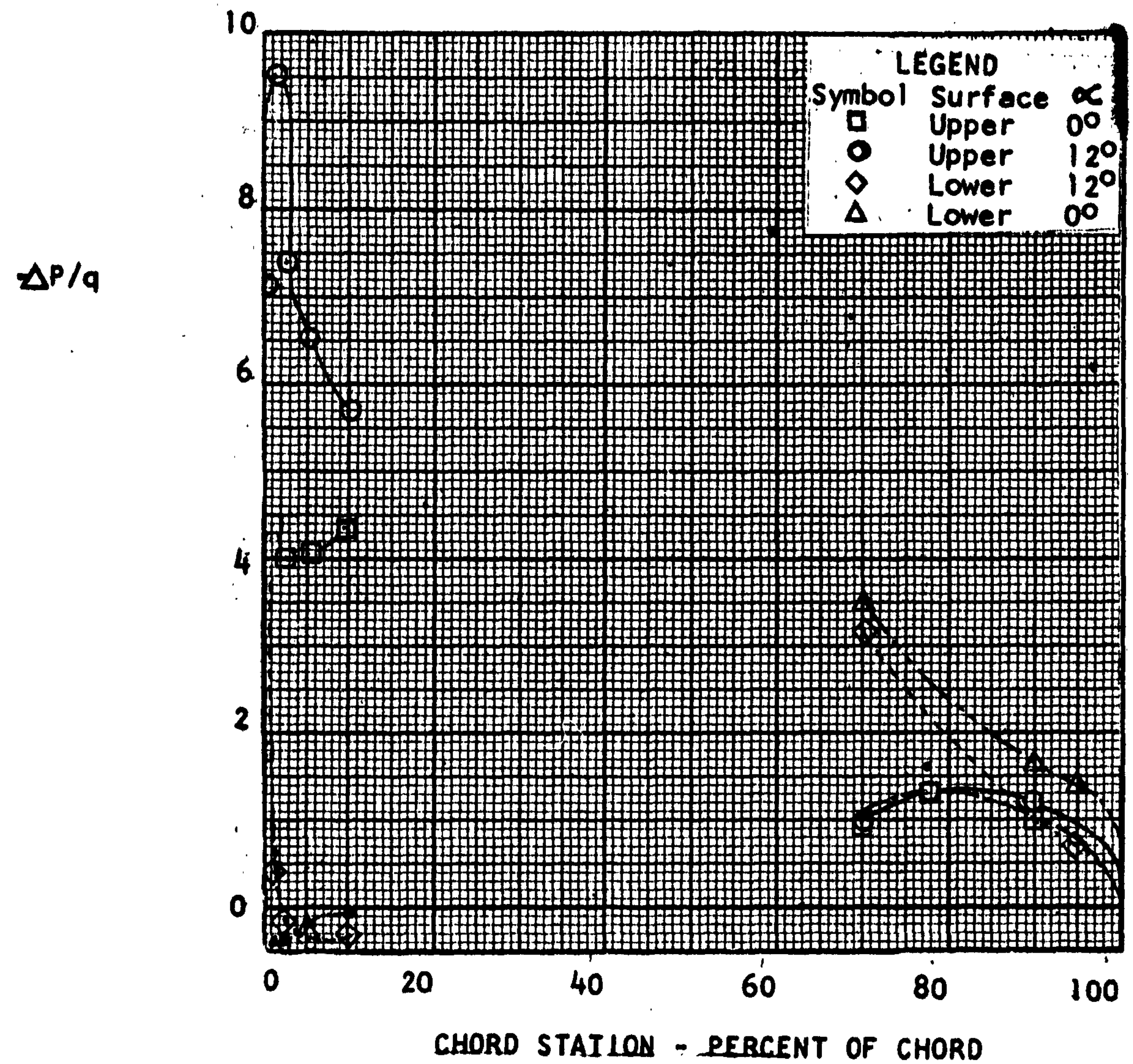

FIGURE 57

FAN CENTER WING PRESSURE, MEDIUM PITCH FAN, 10,000 RPM, 80 MPH, 20° WING FLAP

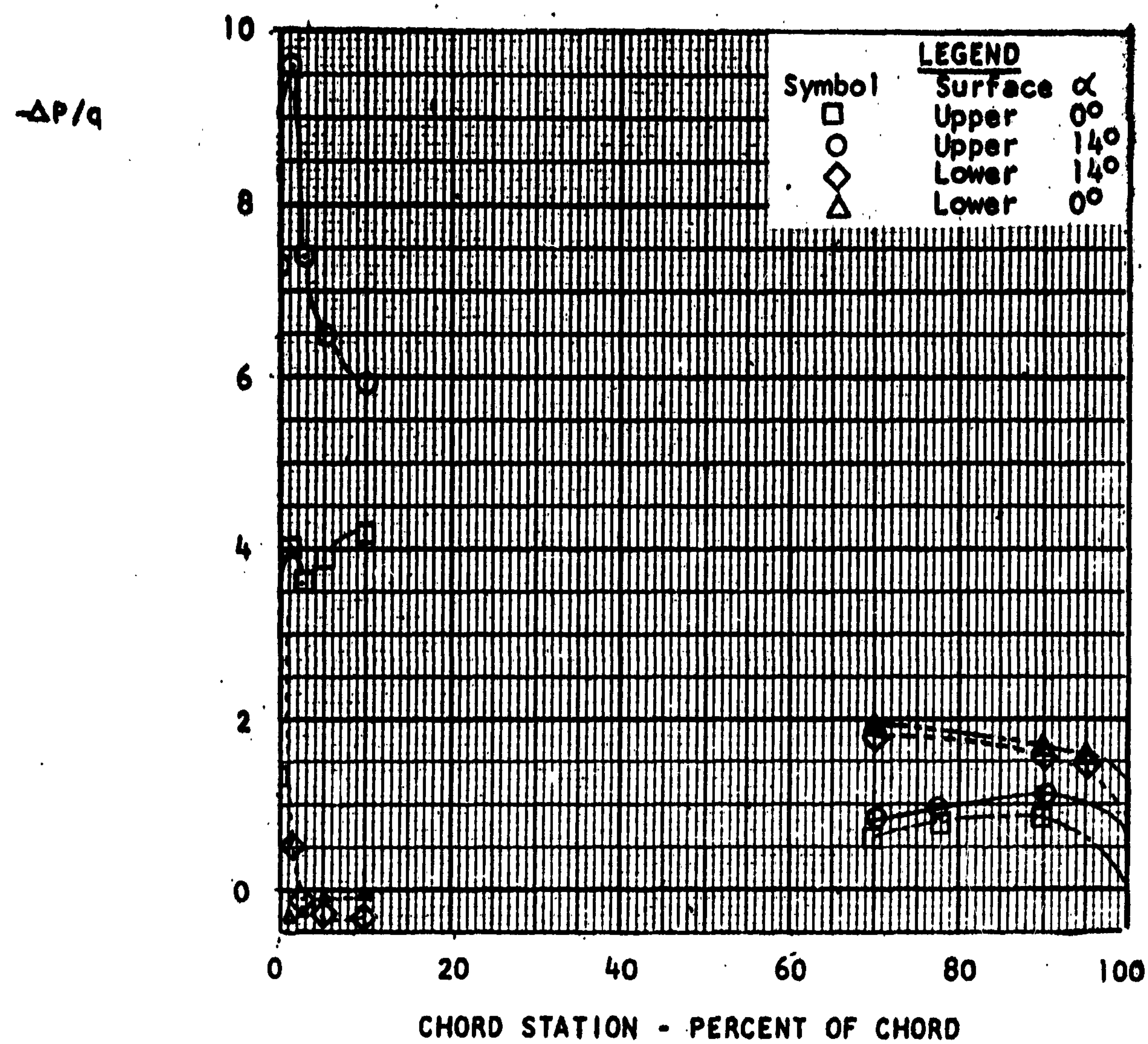

FIGURE 58

FAN CENTER WING PRESSURE, MEDIUM PITCH FAN,
10,000 RPM, 80 MPH

Figure 59 shows the fan center wing surface pressures with the high pitch fan at 9060 RPM and 60 MPH. It may be compared to Figure 60 for the hole covered and Figure 50 for the medium pitch fan at 10,000 RPM at the same airspeed. The significant difference is that the lower surface trailing edge pressures have the appearance of the wing operating with the wing flap deflected.

Figure 60 shows the high pitch fan at 9060 RPM with the wing flap deflected 20° at 100 MPH. Comparing this plot to Figure 48 for the same conditions without a flap deflection, it can be seen that the deflected flap caused an increase of negative pressure on the flap upper surface.

Figure 61 shows the high pitch fan at 9060 RPM and 120 MPH without a flap deflection. In comparison, Figures 52, 59, and 48 present data for the same configuration of 40, 60, and 100 MPH, respectively.

Figure 62 shows the high pitch fan at 9060 RPM and 100 MPH with the 40° fan exit duct installed. It may be compared to Figure 55 for the medium pitch fan at 10,000 RPM at the same airspeed and exit duct deflection angle and to Figure 48 for the high pitch fan at the same airspeed without a deflection of the fan exit flow.

3. Forward Flight Fan Performance

Fan thrust, for each of the three fans tested, increased with increasing forward speed at positive wing angles of attack (see Figures 63 to 71). The thrust of the high pitch fan at 9060 RPM and $\emptyset$ root = 55.9°, for example, was 55 pounds at 0 MPH, 60 pounds at 80 MPH and 80 pounds at 140 MPH, with a wing angle of attack of plus ten degrees. Fan power required increased, as well as thrust, with increasing forward speed. The fan center of pressure moved forward with increasing forward speed, to a maximum value, and after that the center of pressure indicated a slight reversal towards the fan center with further increases in forward speed. It should be noted that, although the low pitch fan was tested only at 40 and at 60 MPH before its destruction, the most forward position of the center of pressure was determined for the low pitch fan configuration. The rate of forward movement of the center of pressure is less pronounced with increasingly positive wing angles of attack.

D. NONDIMENSIONAL PRESENTATION OF PHASE I AND PHASE II DATA

In order to facilitate its applications to future studies and designs and to permit its comparison with other investigations, the results of the Vertodyne test are presented in Appendix C in nondimensional coefficient form.

An investigation of the presentations used in published reports was conducted to find the most desirable form consistent with these requirements. Static data is presented in terms of C_T (thrust coefficient) and C_P (power coefficient) which are related to fan tip speed. These factors are plotted versus fan blade pitch angle.

Model performance in forward flight is presented in conventional wing coefficients C_L (lift), C_D (drag), and C_M (pitching moment) which are related to forward speed. These factors are plotted versus $\mu^2 = (V_T/V_0)^2$.

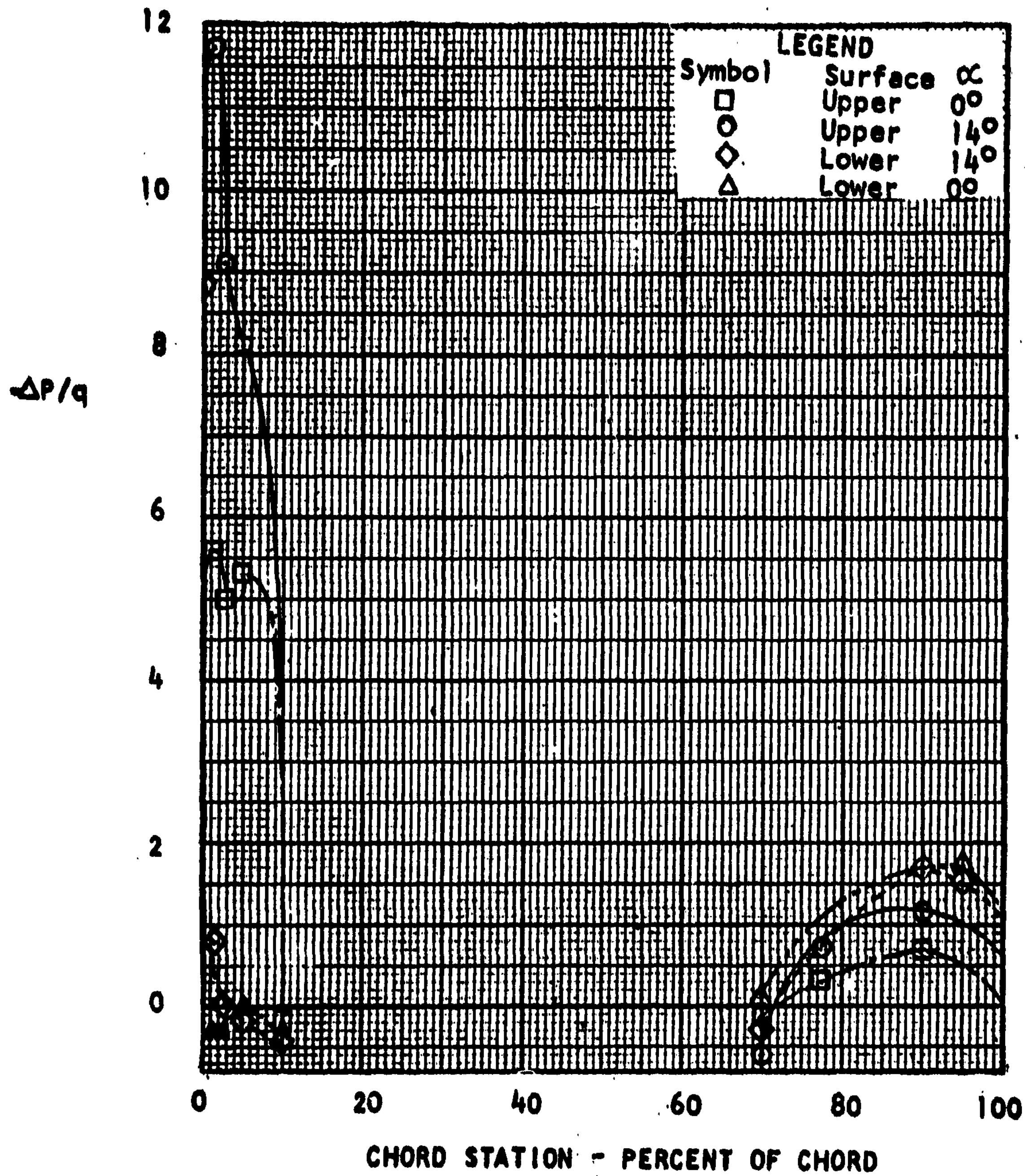

FIGURE 59

FAN CENTER WING PRESSURE, HIGH PITCH FAN,
9,060 RPM, 60 MPH

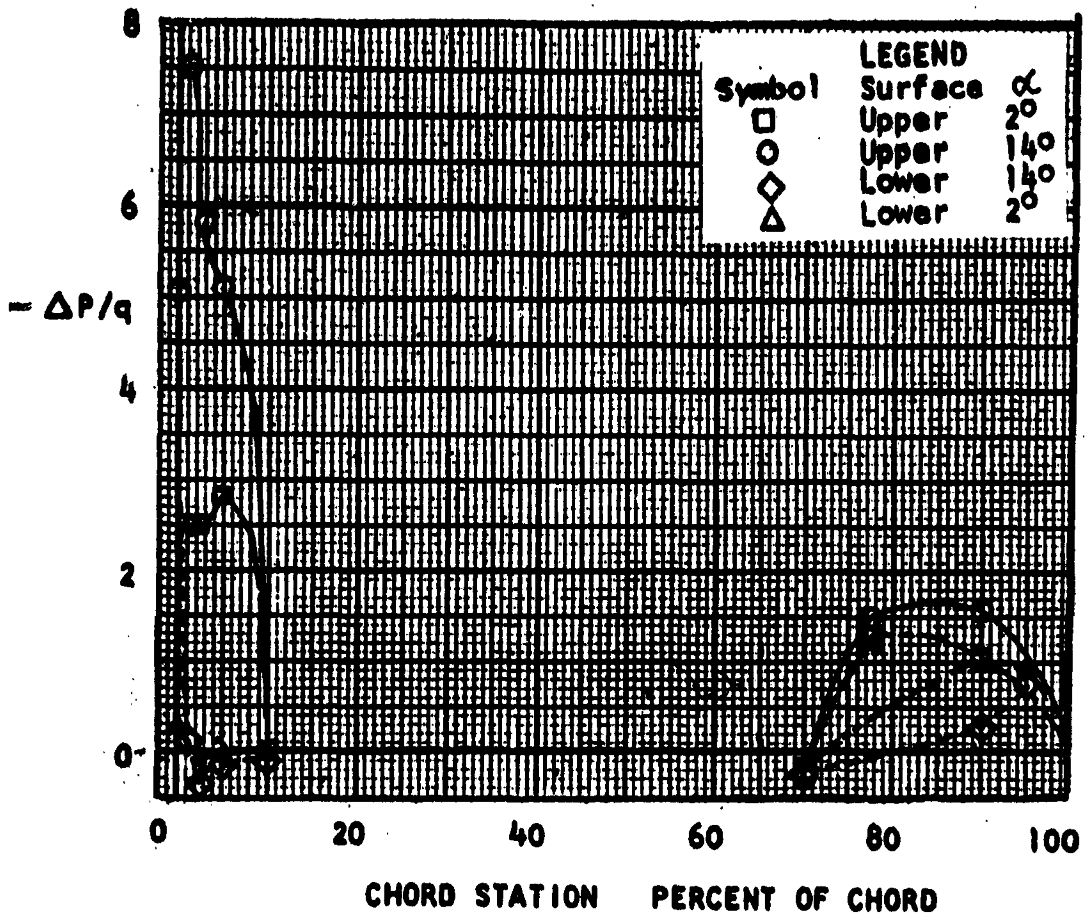

FIGURE 60

FAN CENTER WING PRESSURE, HIGH PITCH FAN,
9,060 RPM, 100 MPH, 20° WING FLAP

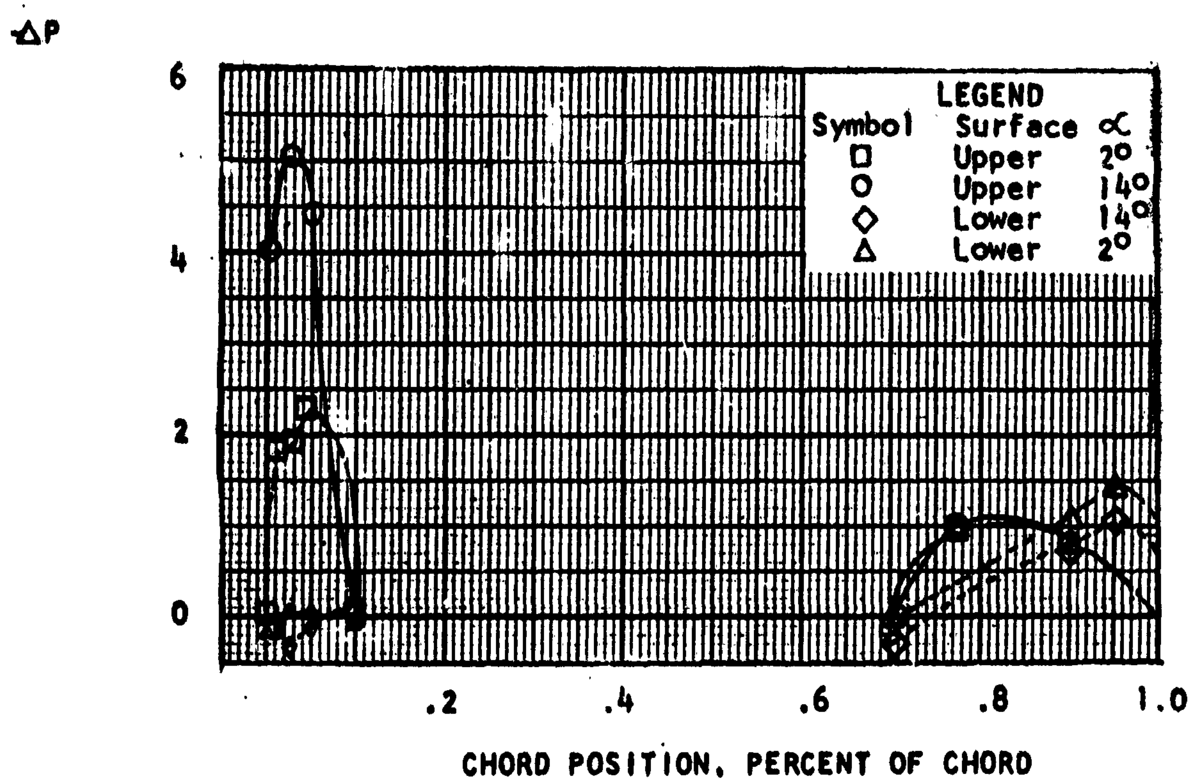

FIGURE 61

FAN CENTER WING PRESSURE, HIGH PITCH FAN,
9.060 RPM, 120 MPH

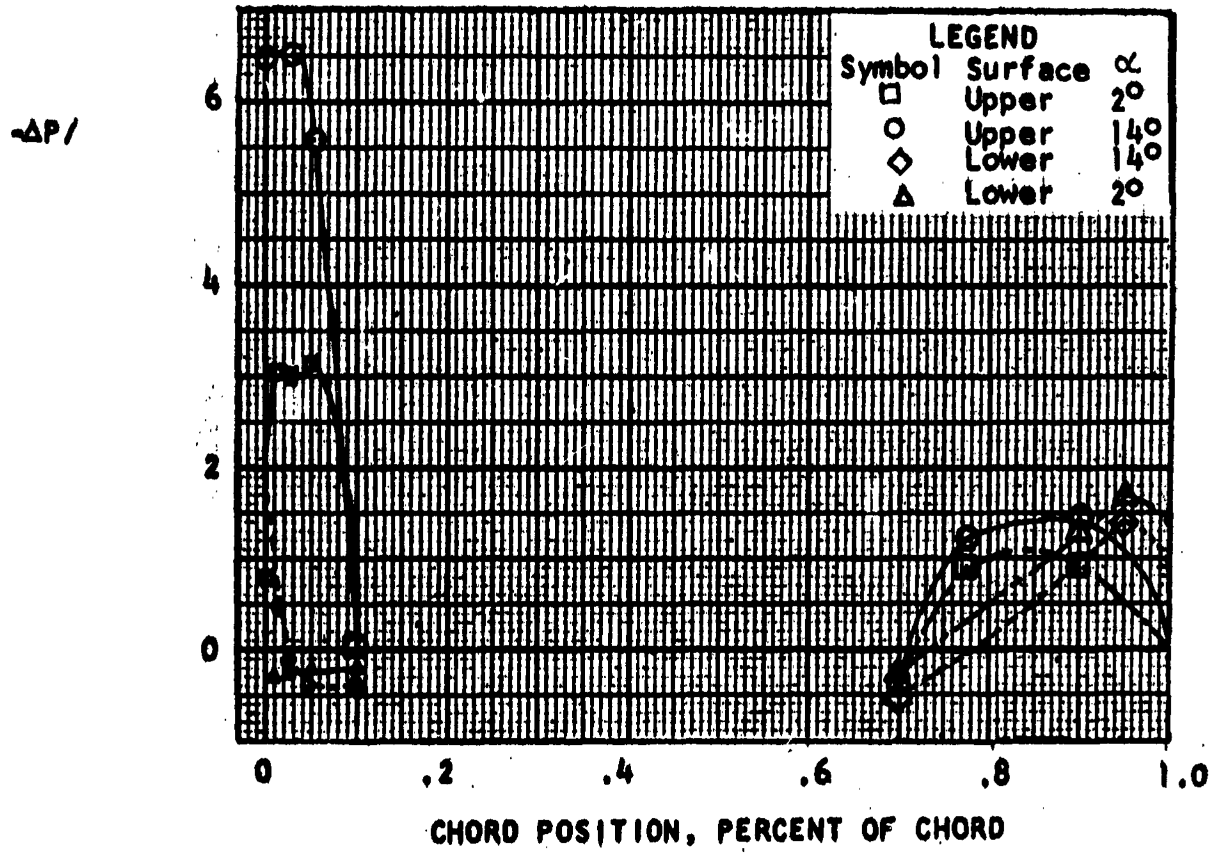

FIGURE 62

FAN CENTER WING PRESSURE, HIGH PITCH FAN, 9,060 RPM, 100 MPH, 40° FAN EXIT ELBOW

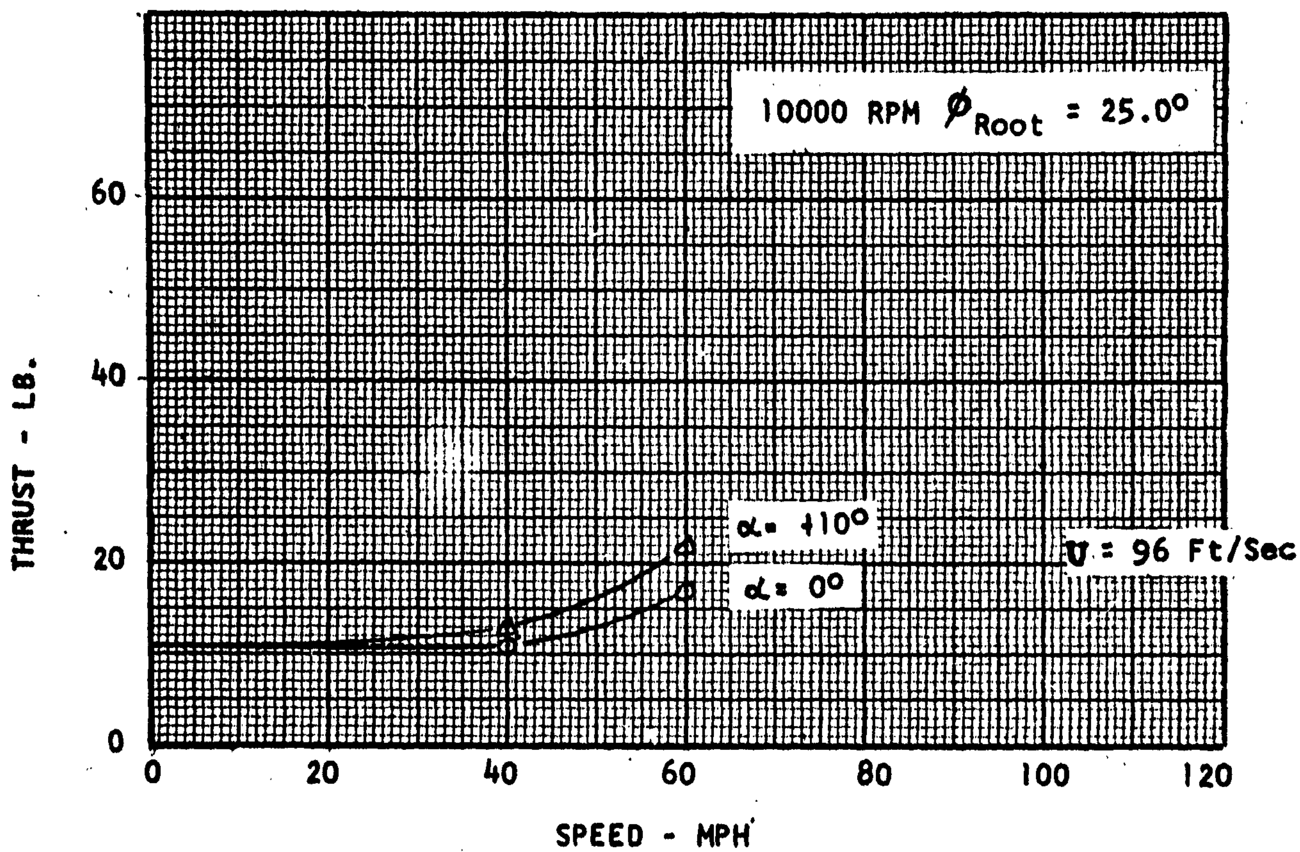

FIGURE 63

FAN THRUST VS. FORWARD SPEED, LOW PITCH FAN

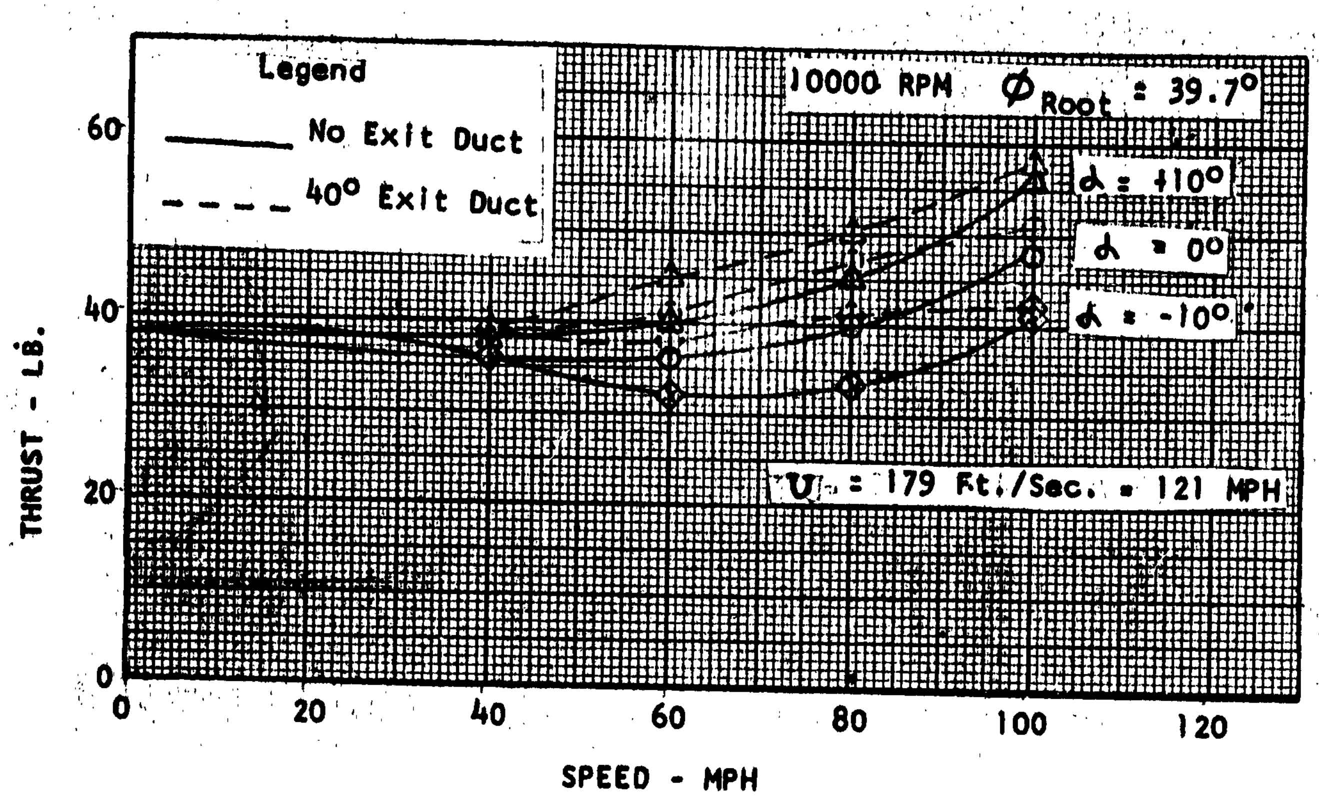

FIGURE 64

FAN THRUST VS. FORWARD SPEED, MEDIUM PITCH FAN

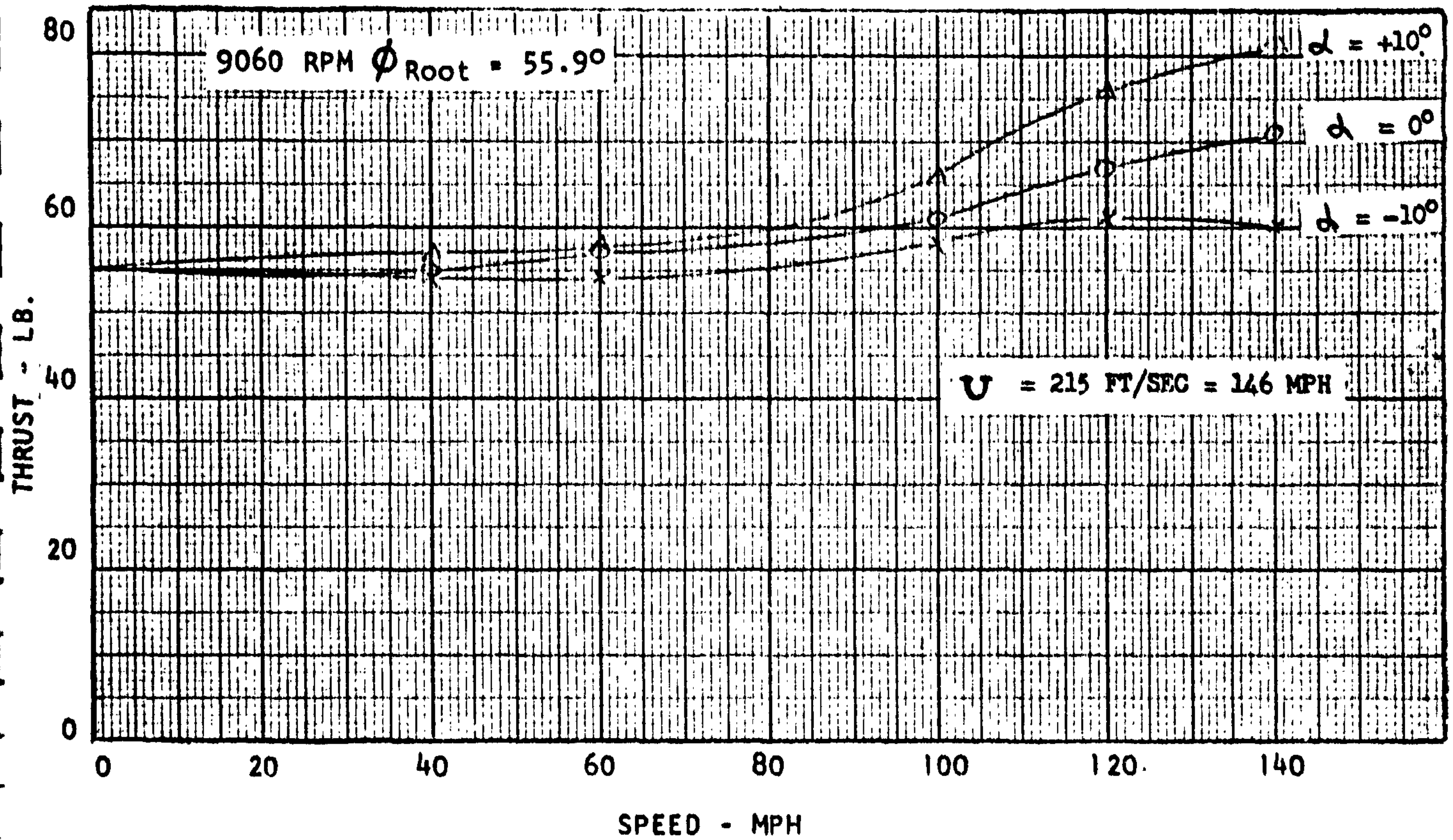

FIGURE 65

FAN THRUST VS. FORWARD SPEED, HIGH PITCH FAN

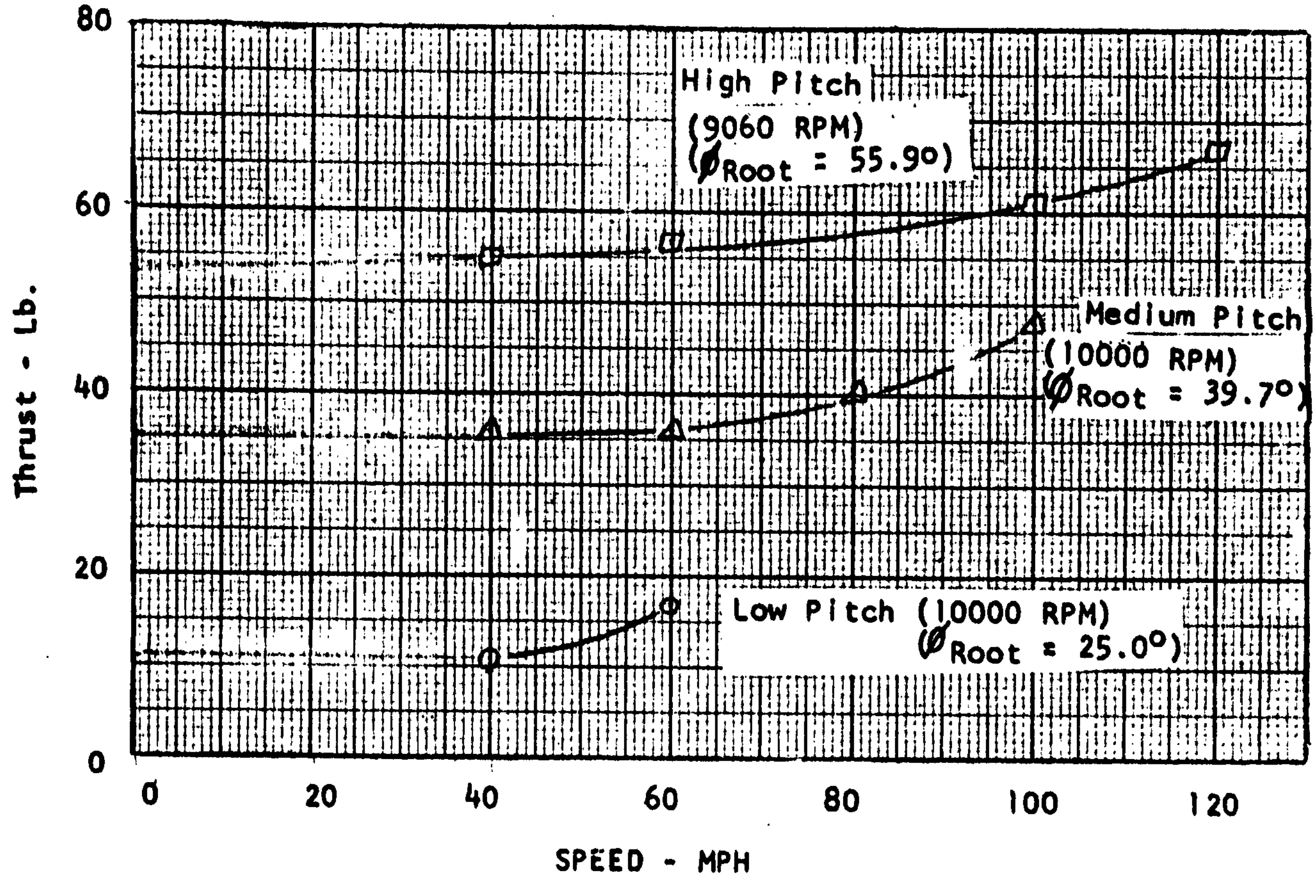

FIGURE 66

SUMMARY FAN THRUST
VS. FORWARD SPEED, α WING = 0°

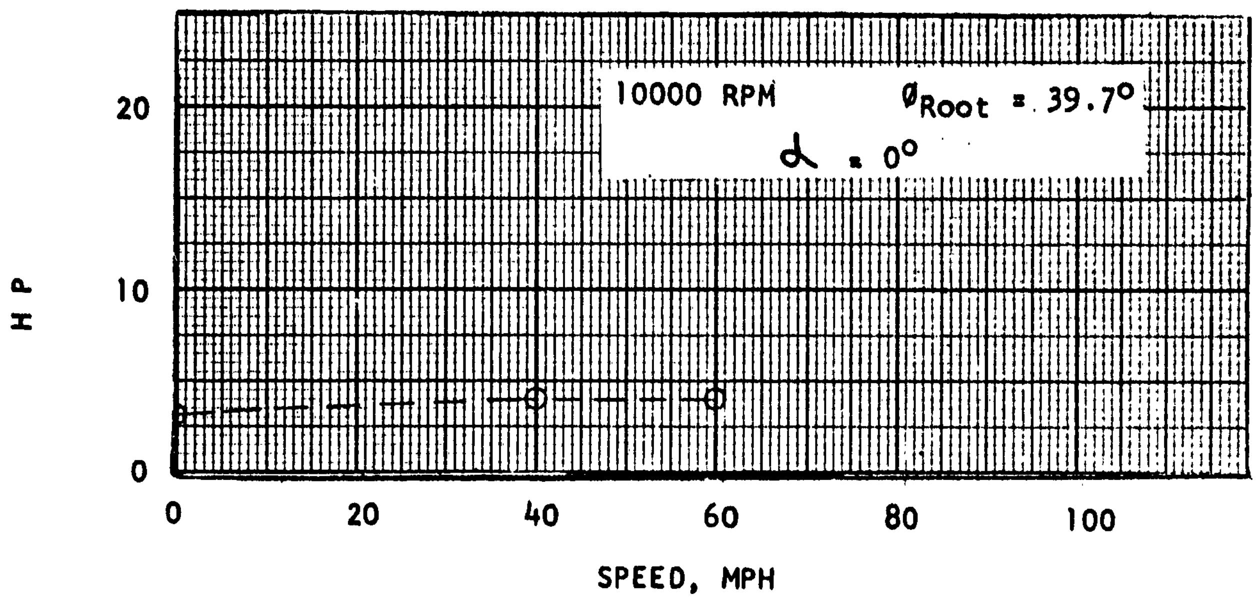

FIGURE 67

FAN HORSEPOWER VS. FORWARD SPEED, LOW PITCH FAN

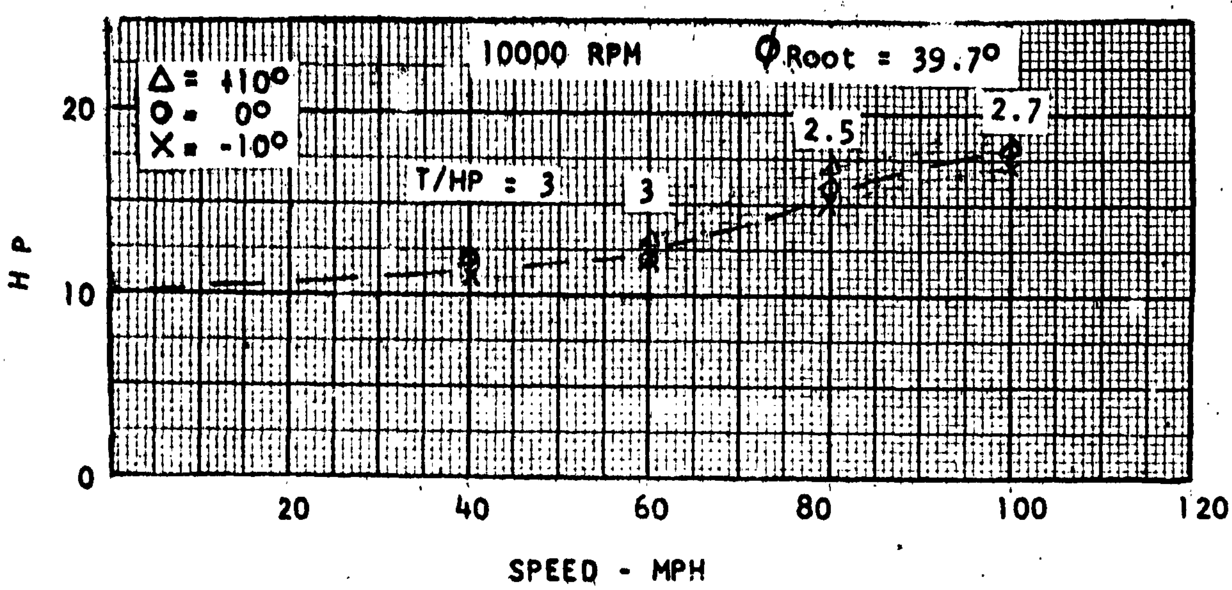

FIGURE 68

FAN HORSEPOWER VS. FORWARD SPEED, MEDIUM PITCH FAN

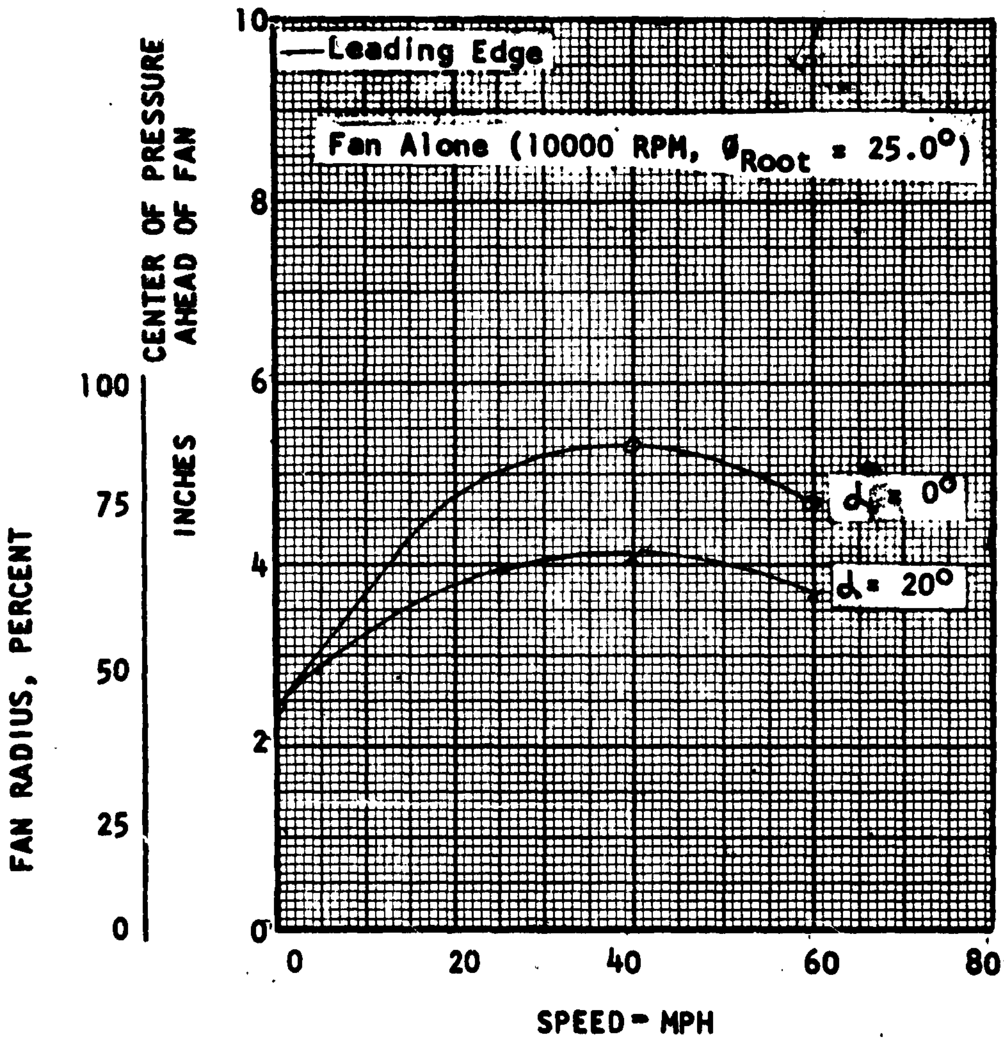

FIGURE 69

CENTER OF PRESSURE VS. FORWARD SPEED, LOW PITCH FAN

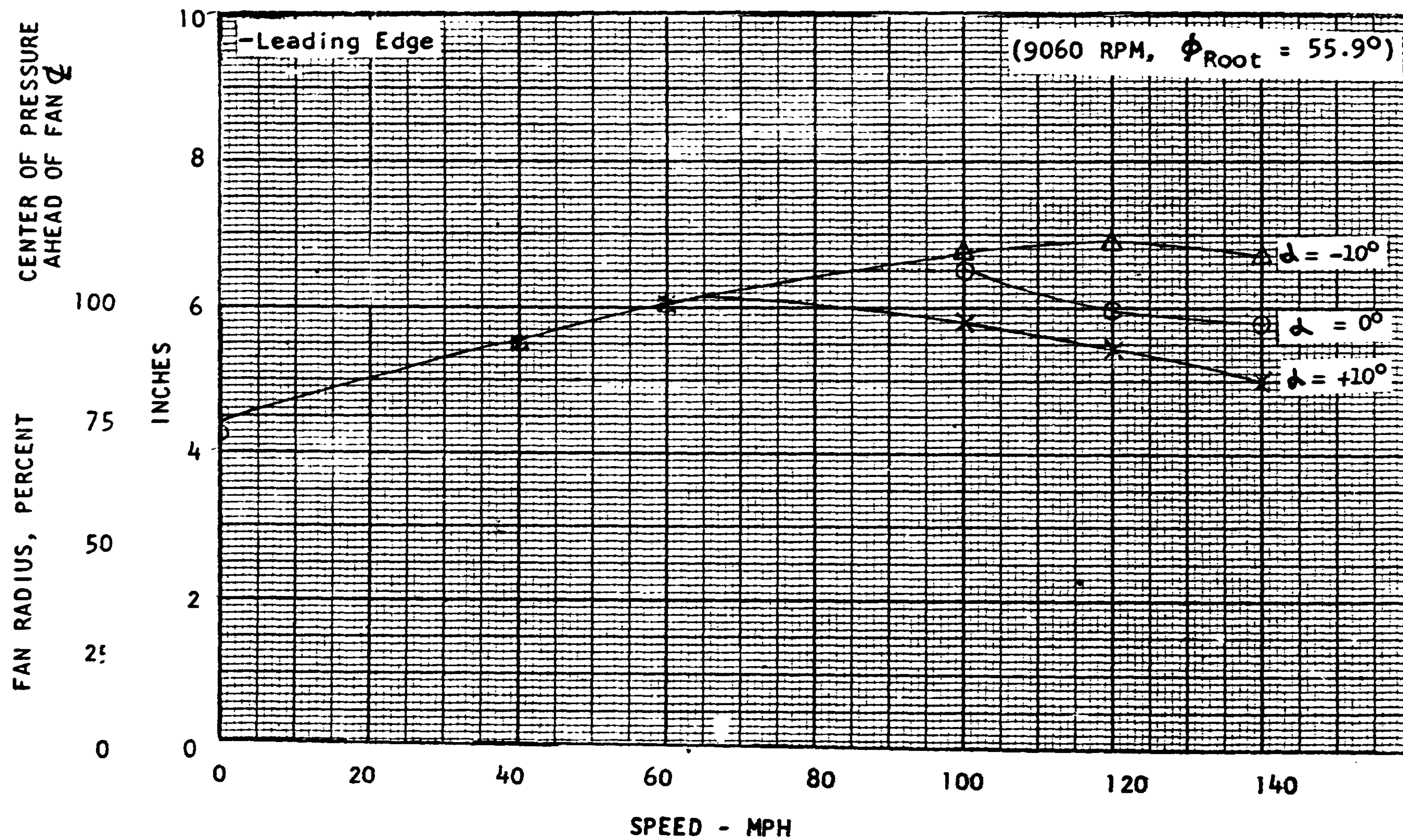

FIGURE 70

CENTER OF PRESSURE VS. FORWARD SPEED, MEDIUM PITCH FAN

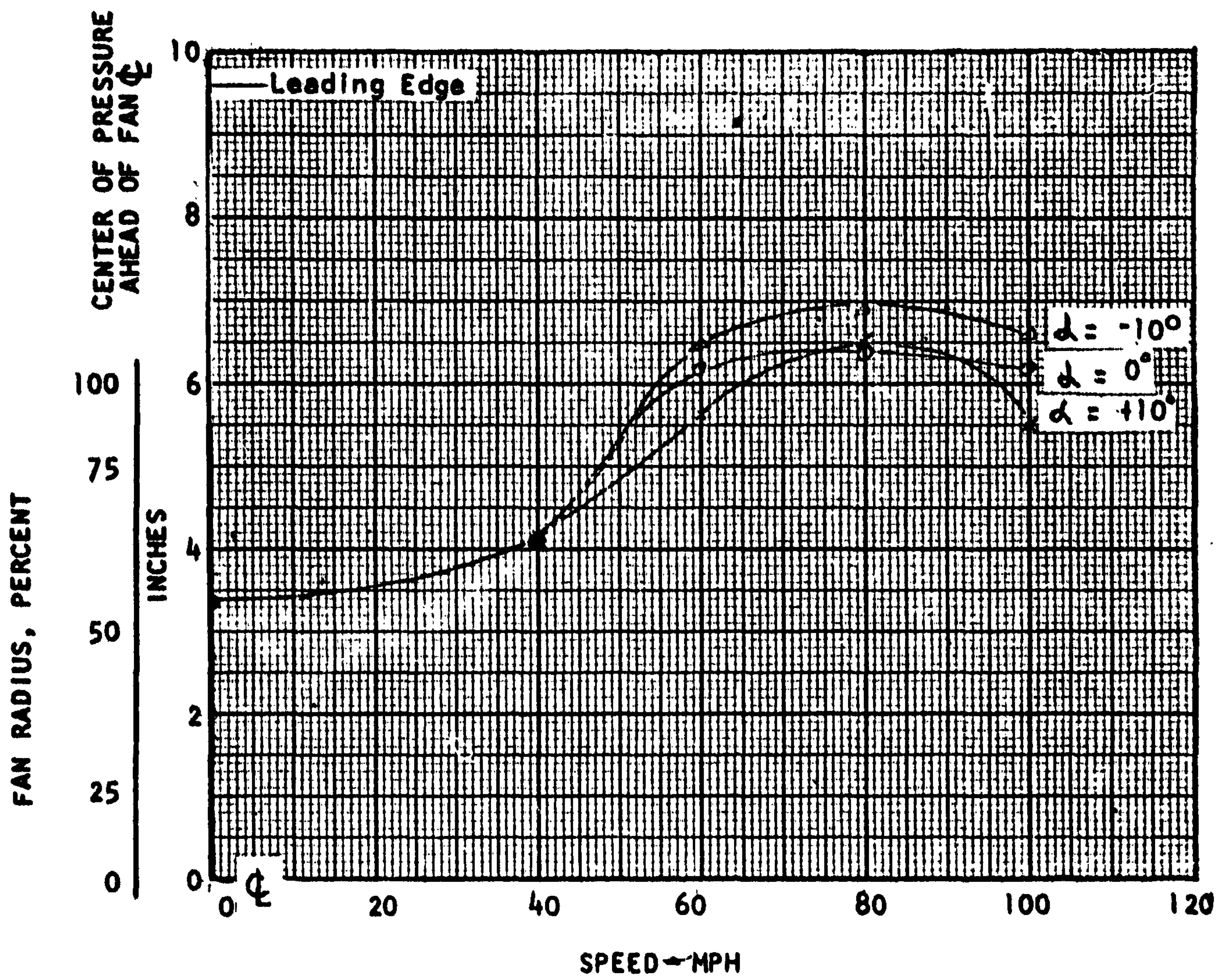

FIGURE 71

CENTER OF PRESSURE VS. FORWARD SPEED, HIGH PITCH FAN

PART V

THEORY AND DATA CORRELATION FOR WING SUBMERGED FAN CONFIGURATIONS

V. THEORY AND DATA CORRELATION FOR WING SUBMERGED FAN CONFIGURATIONS

A. GENERAL

Tests from different sources have been compared and correlated in this section. Also, a theory for separating fan lift from the shroud lift is presented. This theory develops the velocity, pressure, and lift distribution on the upper surface of the shroud which encloses a ducted fan.

B. STATIC PERFORMANCE (OUT OF GROUND EFFECT)

1. Thrust Per Horsepower Vs. Disc Loading

Figures 72 to 78 indicate that all the data falls below the ideal ducted fan theory (M=1). These figures also show that all of the data, except General Electric data, are between M=.70 and M=.75. It is probable that the General Electric data would be in the same area provided it had been corrected for the drive motor and strut interference with the airstream. The selection of M=.72 (together with a compatible L_o, HP and A_{Fan}) should be compatible with the state-of-the-art for an initial approximation to a design.

2. Figure of Merit Vs. Total Lift Coefficient Per Solidity

Figures 79 to 84 show the Figure of Merit (M) is constant through a range of total lift coefficients. As indicated by these figures, the majority of the data forms a general pattern which provides a useful range of C_T/σ from .10 to .35. The correlated data in Figure 84 could be used in preliminary design of wing submerged fans.

C. FORWARD FLIGHT PERFORMANCE

1. Lift Rotor Vs. Dynamic Pressure

Curves showing the values obtained under this category are shown in Figures 85 to 90. All values of lift (L) have been related to static lift (L_o) so that $\frac{L}{L_o} = 1$ when q = 0. By this method all lift curves (runs) have the same common denominator. Each run is defined by a particular fan RPM or pitch setting (see Table 7) which has been held constant over a range of tunnel dynamic pressures. Wind tunnel effects are included in all of the data except the static runs by Vertol and M.I.T. which were performed outside the wind tunnel.

When all of the data is plotted on the same scale (see Figure 90), the configurations with poor static lift have a greater $\frac{L}{L_o}$ in forward flight than those with good static lift, for the same q. This is best demonstrated by the data shown in Table 7 and Figure 96 and itemized as follows:

	Vertol	Canadian
Run	2	13
$\frac{L_O}{A^*}$	80.5	38.3
C_{T_o}	.151	.0670
$\frac{A^*}{S}$	.143	.0269
M	.590	.425
$\frac{L}{L_o}$ @ q=10	1.03	2.7

Considering the listed values as being a measure of the static lift and efficiency ($\frac{L_O}{A^*}$, C_{T_O}, $\frac{A^*}{S}$ and M), the Canadian values are lower than the Vertol values. However, the Canadian data shows a marked increase in lift when compared with Vertol data at q=10.

The data in Table 7 follows the same trend as the above example; therefore, this trend is used in the correlation.

2. Lift Ratio Vs. Dynamic Pressure Static Factor

Since the trend of data are known, (see Figures 91 to 98) a more rigorous method of showing this trend is needed. The performance of a ducted fan in wing must be a function of the items tabulated below. A term, herein called the Static Factor (SF) was developed to include all pertinent functions.

Item No.	Parameters
1	Fan Lift
2	Total Lift
3	Power
4	Fan* Area
5	Fan Annulus Cross-Sectional Area, (Hub to Tip Radii)
6	Bellmouth Radius and Airflow Guides
7	RPM
8	Wing Area
9	Aspect Ratio
10	Wing Angle of Attack
11	Fan Angle of Attack
12	Fan Blade Section and Twist
13	Fan Tip Clearance
14	Fan Blade Uniformity and Solidity
15	Duct Expansion
16	Fan Location Relative to the Wing Chord and Span
17	Free Air Dynamic Pressure

TABLE VII - SUMMARY OF STATIC PARAMETERS

* Estimated Values

TYPE	RUN	AIR FOIL	FAN* AREA	WING AREA	FAN ANNULAR AREA	FAN RPM	FAN TIP SPEED	COEFFICIENT OF THRUST	LIFT	FIGURE OF MERIT	STATIC FACTOR	POWER
			A*	S	A_P		V_T	C_{TO}	L_o	M	SF	HP
			Ft^2	Ft^2	Ft^2	RPM	Ft/Sec		Pounds		$Pounds/ft^2$	HP
Vertol	1	NACA 694-221	.785	5.50	.503	10,000	523	.0850	43.5	.676	.306	11.15
(Reference 14)	2					9,060	473	.151	63.2	.590	.604	22.40
GE-NASA	3	NACA 16-015	2.18	12.50	2.18	7,200	629	.0680	140	.426	.1370	49.0
(Reference 10 and 11)	4					6,600	576	.0692	118.5	.434	.1240	37.5
	5					6,000	524	.0705	101	.428	.1028	30.0
	6					5,200	454	.0705	75	.444	.0832	18.5
	7					4,500	392	.0705	56	.408	.0577	13.0
MIT Moser	8		1.76	11.75	1.76	6,500	510	.00846	9.25	.604	.00243	.65
(Reference 12)	9	NACA 0012				6,500	510	.0230	25.10	.727	.0261	2.40
	10					6,500	510	.0350	38.3	.747	.0634	4.38
MIT Duvivier	11		1.76	18.77	1.76	5,000	393	.0300	19.3	.485	.00776	2.47
(Reference 23)	12	NACA 0018				7,000	550	.0310	39.3	.647	.0272	5.40
Canadian	13		.306	11.39	.195	15,000	490	.0670	11.7	.425	.0124	2.94
(Reference 13)	14	NACA 0018				10,000	326	.0516*	4.05	.425*	.00322*	-
	15					5,000	163	.0388	.755	.425*	.000456*	-

When the Figure of Merit (M) is equal to one (M=1) then the flow conditions at infinity are equal to the flow conditions at the fan. The slipstream area is constant ($A_{Fan} = A_{\infty}$) and the slipstream velocity is constant ($U = U_{\infty}$). Also, all energy input to the fan is in the slipstream.

Therefore, M includes the effects of many of the important static parameters (Item Numbers 1, 2, 3, 5, 6, 7, 11, 12, 13, 14 and 15):

$$M = \frac{L_o}{HP} 53.66 \sqrt{\frac{L_o}{A_{Fan}}}$$

C_{t_o} also includes the effects of many of the important static parameters (Item Numbers 2, 4, 6, 7, 11, 12, 13, 14 and 15):

$$C_{t_o} = \frac{L_o}{A^* \, V_T 2}$$

The only parameters not mentioned are Item Numbers 8, 9, 10, 16 and 17.

Item No. 8: Wing area is used together with the Fan* area as a nondimensional parameters $\frac{A^*}{S}$

Item Nos. 9 and 10: The effects of aspect ratio and wing angle of attack are minimized at $\alpha = 0$. All test data have been correlated at this angle.

Item No. 16: The effect of fan location relative to the wing chord and span has not been taken into account; however, the cordwise location of all tested fans is between .3c and .5c.

Item No. 17: All of the correlation plots are essentially $\frac{L}{L_o}$ vs $\frac{q}{\text{Constant}}$, so that the effect of q is primary.

For a good static configuration, the parameters $\frac{L_o}{A^*}$, $\frac{A^*}{S}$, C_{t_o}, and M should be maximized. In addition, it also follows that the product of these terms $\frac{(L_o \, C_{t_o} \, M)}{S}$ should be maximized.

For correlation purposes the parameter $\frac{L_o \, C_{t_o} \, M^2}{S}$ has been used as the static factor (SF).

The Vertol data (see Figure 91) does correlate by using the Static Factor method. Total model data plots as one curve and fan data plots as two curves with the same trend. By integrating shroud pressures, fan data are changed to Fan* data. Then two curves become one curve similar to the G-E Fan* data.

After correlating, all of the G-E data are presented on two curves as shown in Figure 92. Assuming this correlation method is correct, the accuracy of data can be determined immediately. Thus, of the last two total model points for 7200 RPM, the lower point is probably the most accurate because it is on the correlation curve. In addition, the lift produced at different RPM's and different fan angle of attacks should be predictable through different calculated static factors. Figure 93 depicts a general trend of data; however, the correlation does not define one curve as did the two previous graphs.

Figure 94 shows a correlation for two different runs. The curve levels off at a low value of $\frac{L}{L_o}$ compared to other data. This could be because L_o was measured out of the tunnel while L was measured in the tunnel. However, if tunnel effects caused a reduced lift in the tunnel, the shape of the curve would be different. Figure 95 also indicates a general trend of data; however, the correlation does not define an exact curve. The general trend is interesting since it is the same as the other data in which the static factor is very low (.000456) and the lift ratio is very high (19.2 to 1).

Figure 96 provides a composite correlation of all the data. The general trend is for those configurations with high static factors to be at the left and those with low static factor to be to the right of the graph. Observe that Figure 96 indicates similarity of GE-NASA and the Vertol data by the closeness of their values.

Figure 97, on the other hand, shows the GE-NASA and Vertol data on a magnified scale. Although the two curves are entirely different on the magnified scale, they are very similar when compared to the other data.

Figure 98 illustrates that $\frac{L}{L_o}$, SF, and q are definitely related for both the GE-NASA and Vertol data. Other data also show the same trend; however, the scatter is too great for an acceptable curve. If in preliminary design a calculated static factor is in the range of .06 to .6, it could be assumed that Figure 98 predicts the forward flight performance.

D. STATIC THEORY

In hovering with a wing submerged ducted fan, part of the total lift is developed by the fan and part by the shroud. The following theory is mainly concerned with separating these two lifts. In the development of this theory, only the two dimensional case is considered. The three dimensional case was attempted, but it was discontinued upon discovering that the complexity of this approach goes beyond the possibilities of handling the theory within the present contract.

It is assumed that the lift of the shroud is due to the flow over the surface of the shroud. It is also assumed that the bellmouth radius is small compared to the shroud radius so that the shroud velocity is always perpendicular to the fan axis. A diagram of the streamline flow pattern is shown in Figure 99.

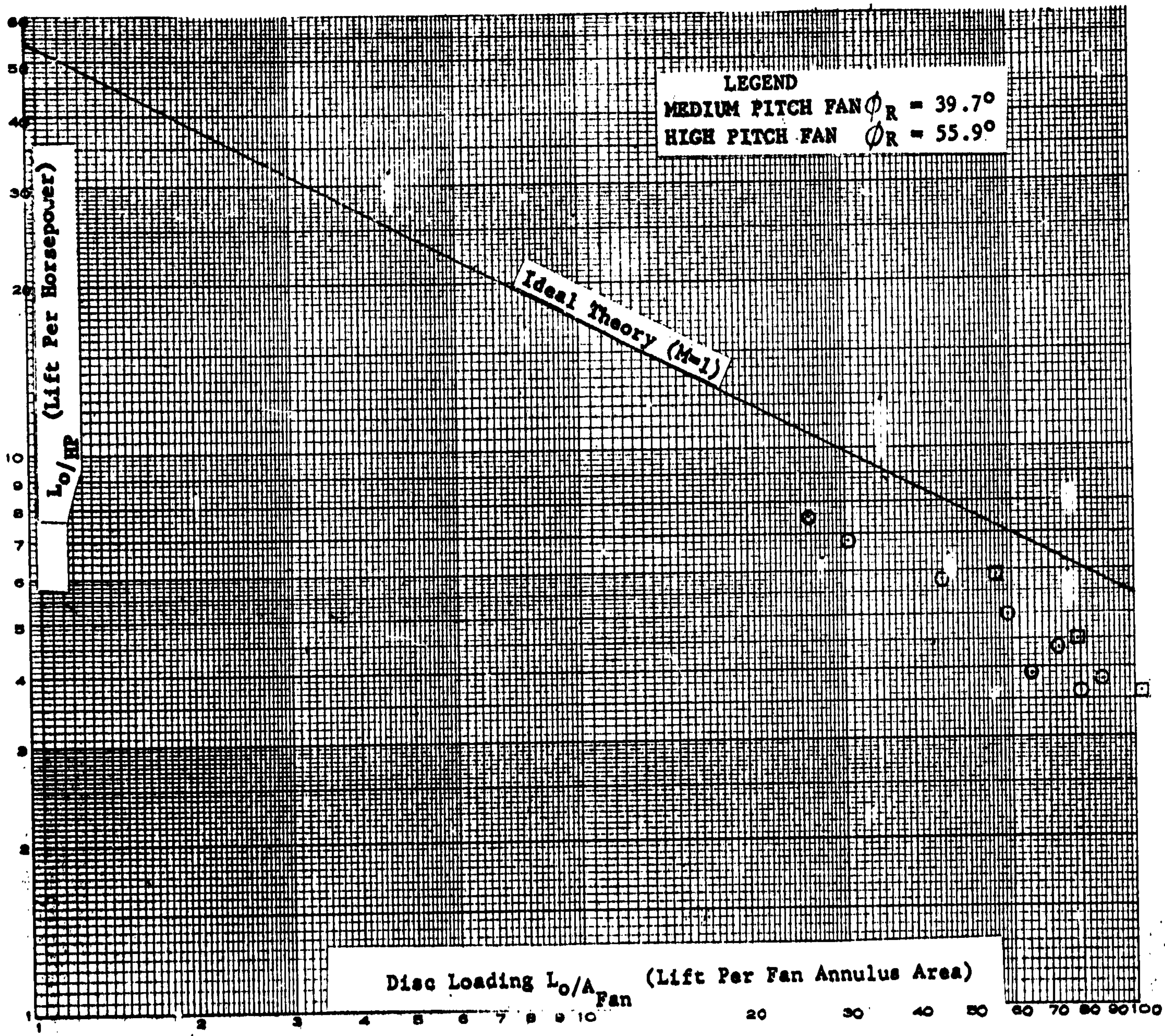

FIGURE 72

LIFT PER HORSEPOWER VS. DISC LOADING (VERTOL)

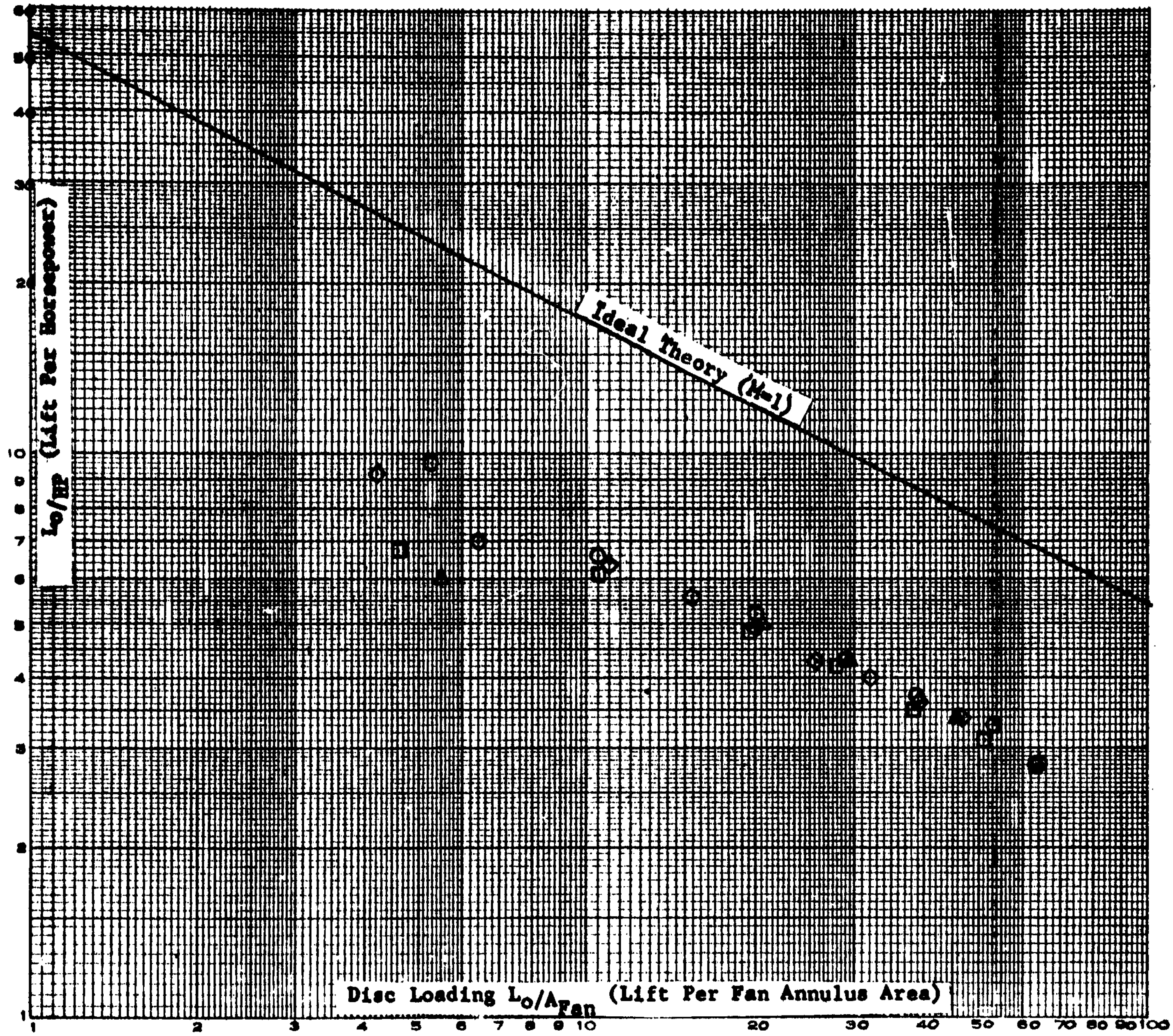

FIGURE 73

LIFT PER HORSEPOWER VS. DISC LOADING (G-E)

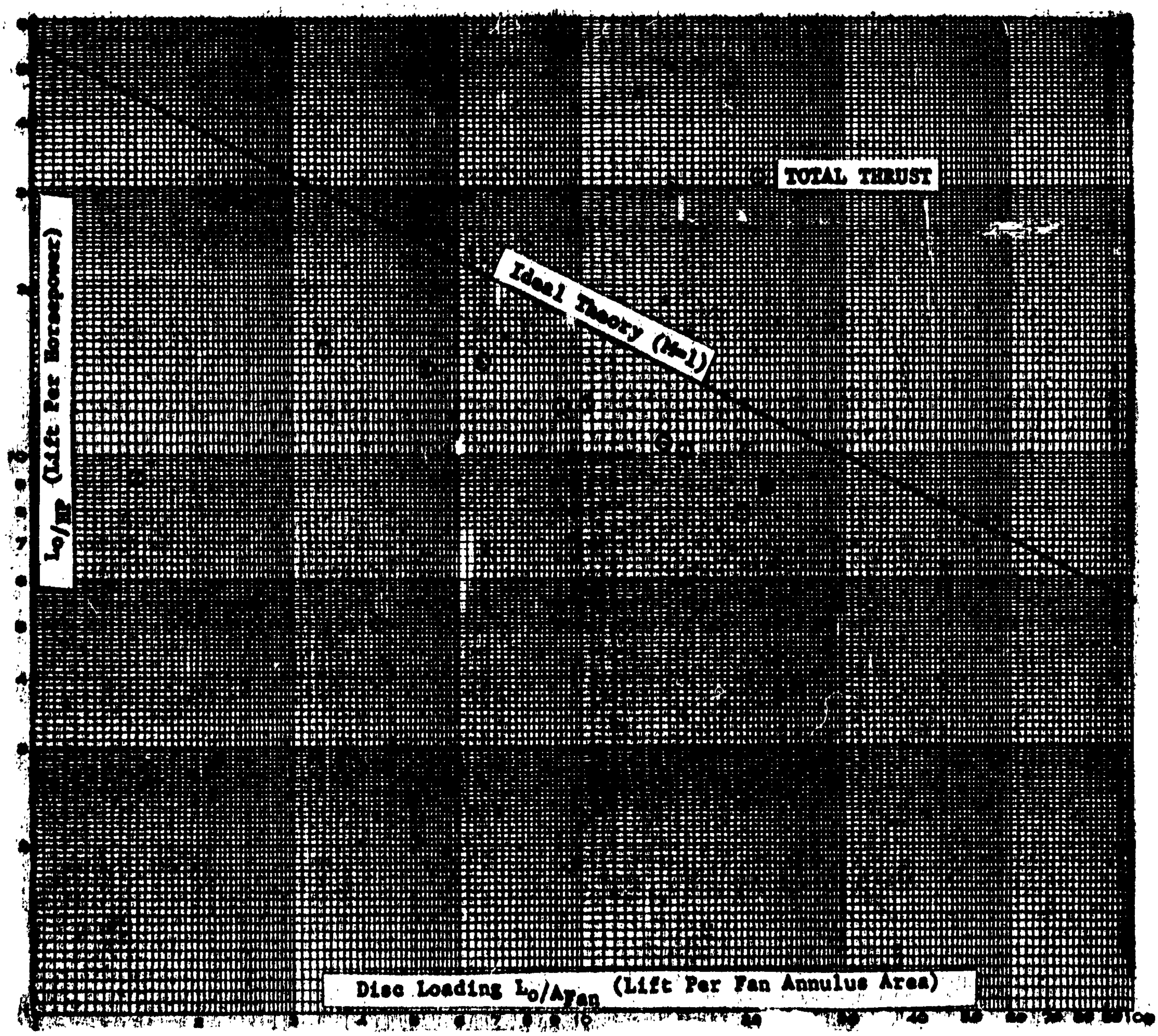

FIGURE 74

LIFT PER HORSEPOWER VS. DISC LOADING (M.I.T./MOSER)

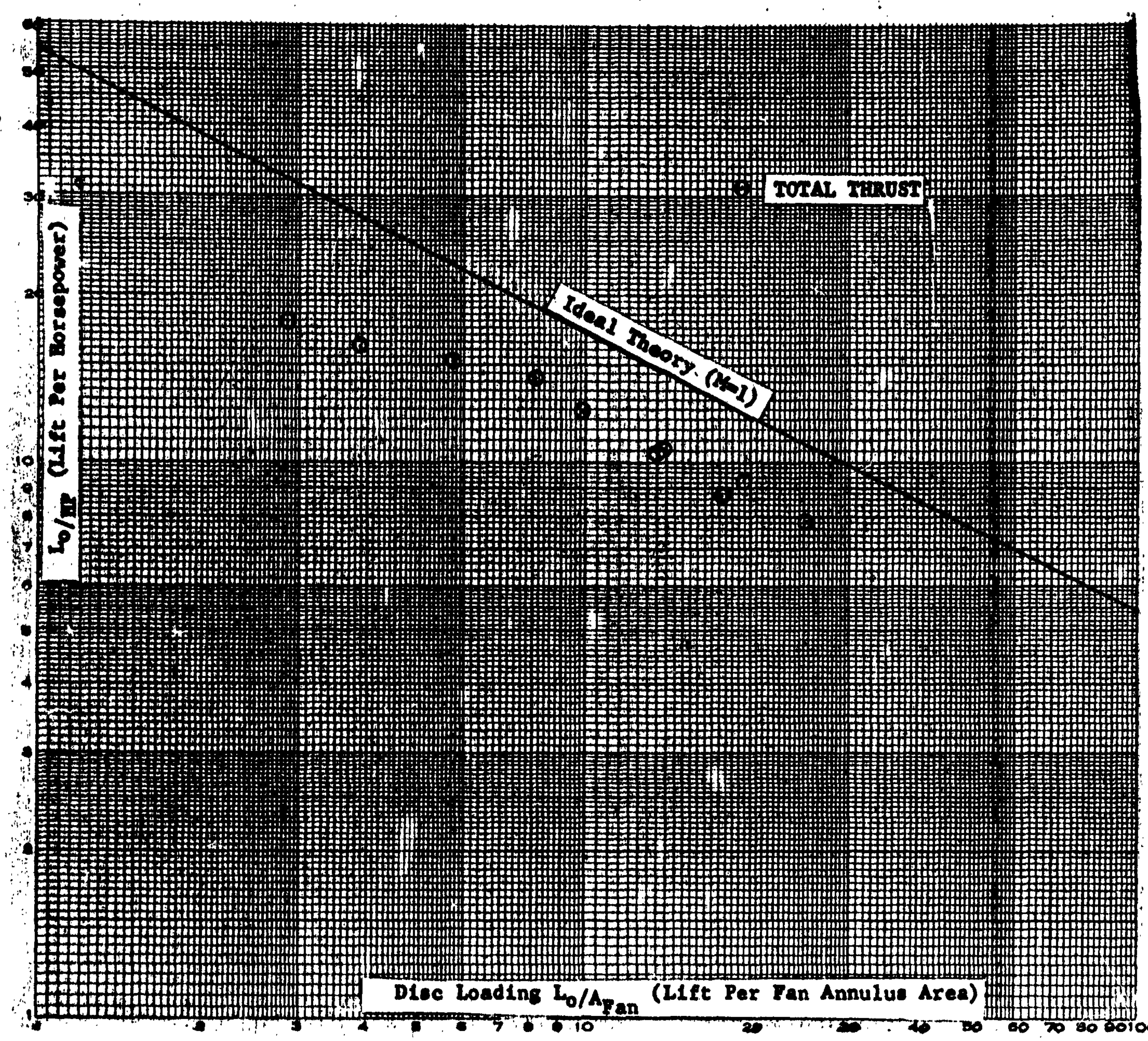

FIGURE 75

LIFT PER HORSEPOWER VS. DISC LOADING (M.I.T./MOSER-DUCTED FAN)

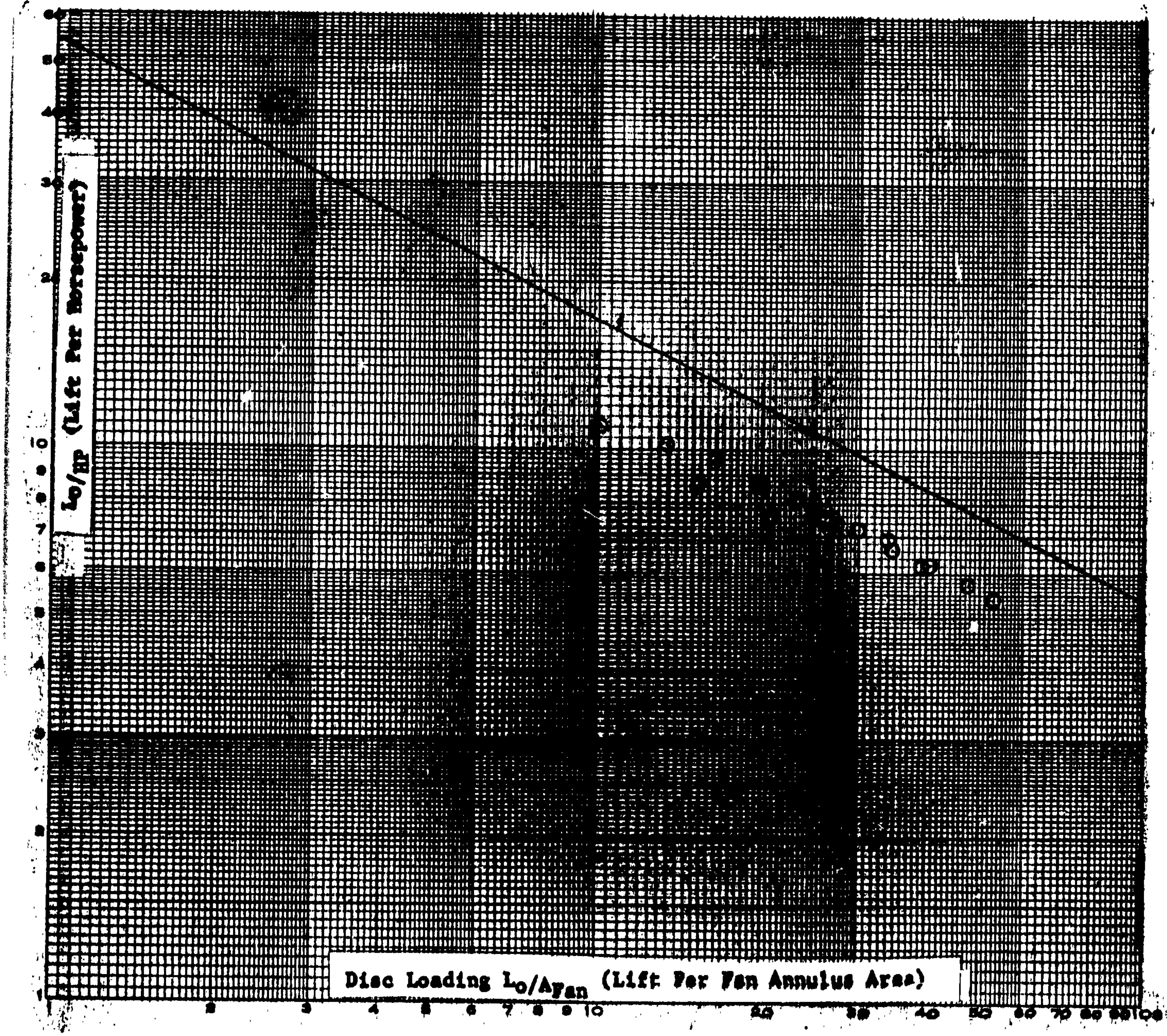

FIGURE 76

LIFT PER HORSEPOWER VS. DISC LOADING (HILLER-DUCTED FAN)

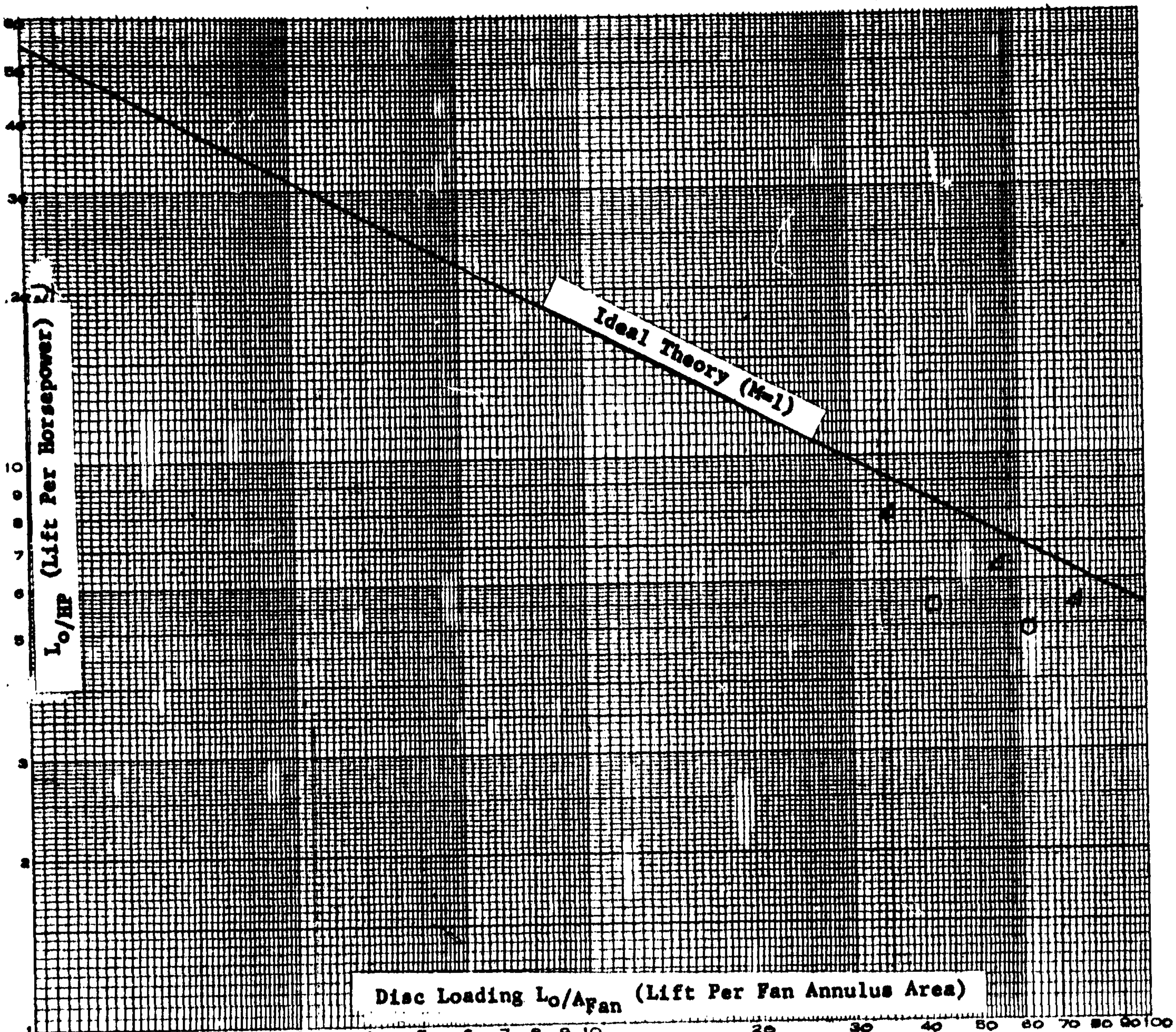

FIGURE 77

LIFT PER HORSEPOWER VS. DISC LOADING (GRUMMAN-DUCTED FAN)

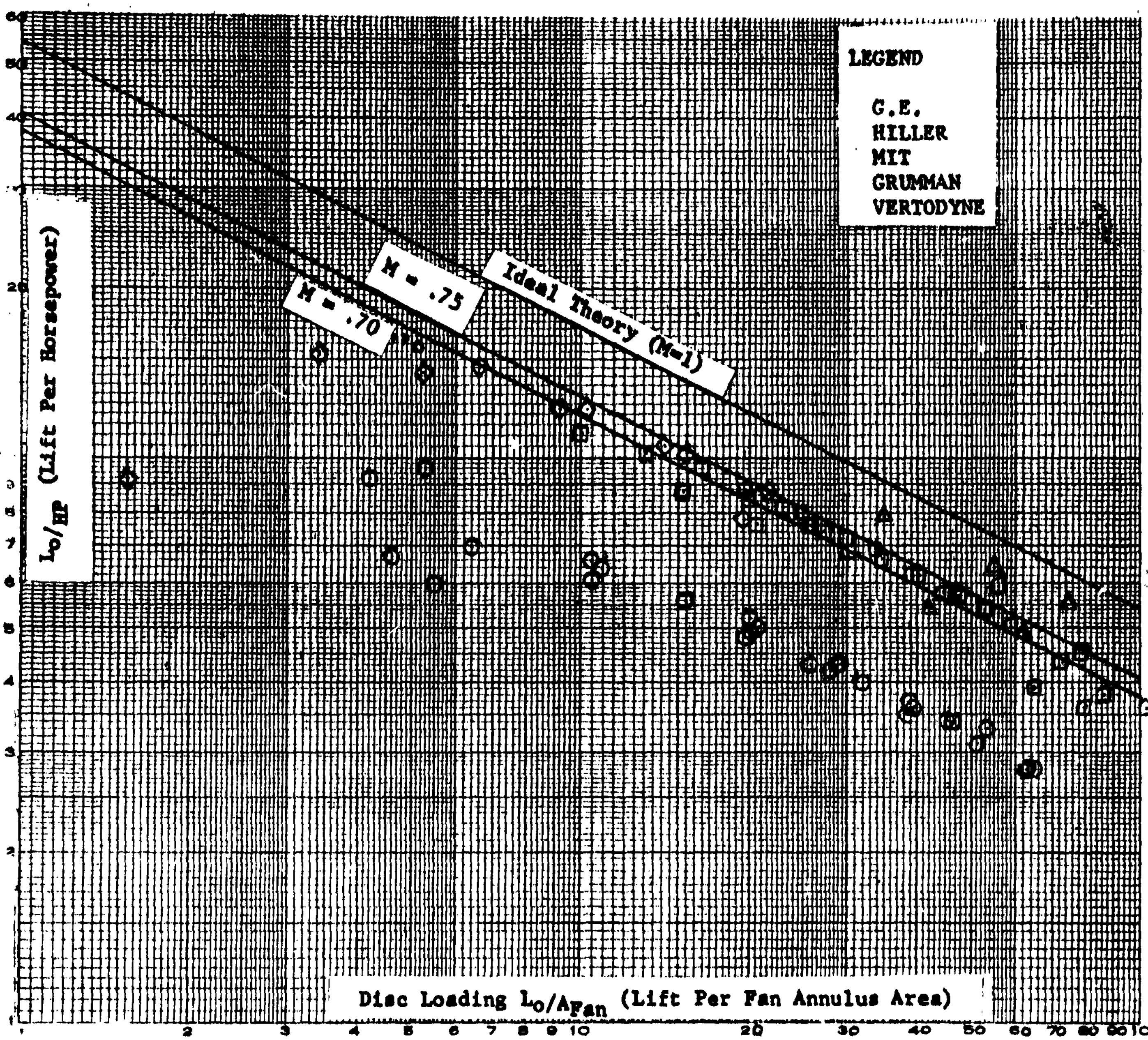

FIGURE 78

LIFT PER HORSEPOWER DISC LOADING (CORRELATED DATA)

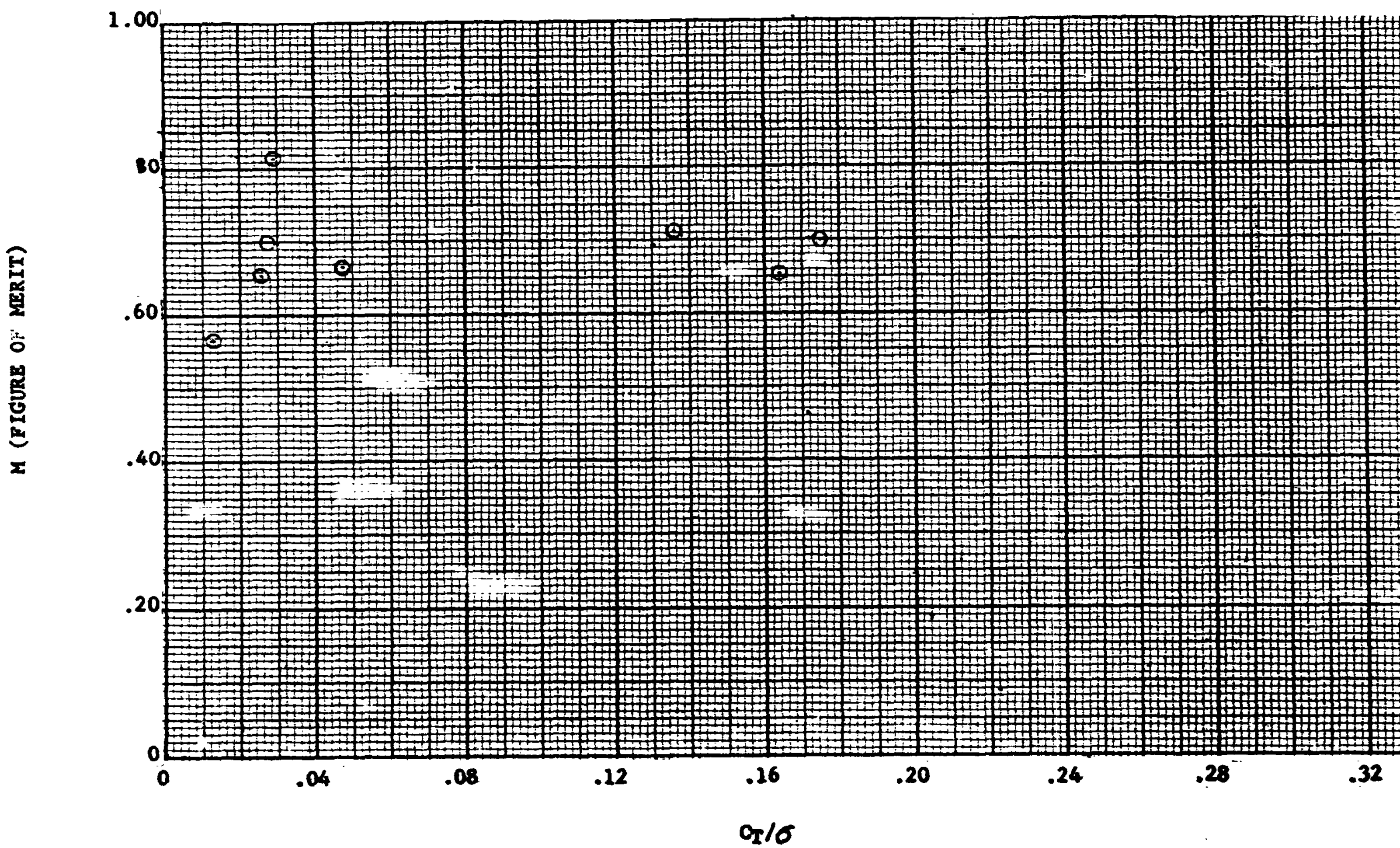

FIGURE 79

FIGURE OF MERIT VS. C_T/σ (VERTOL)

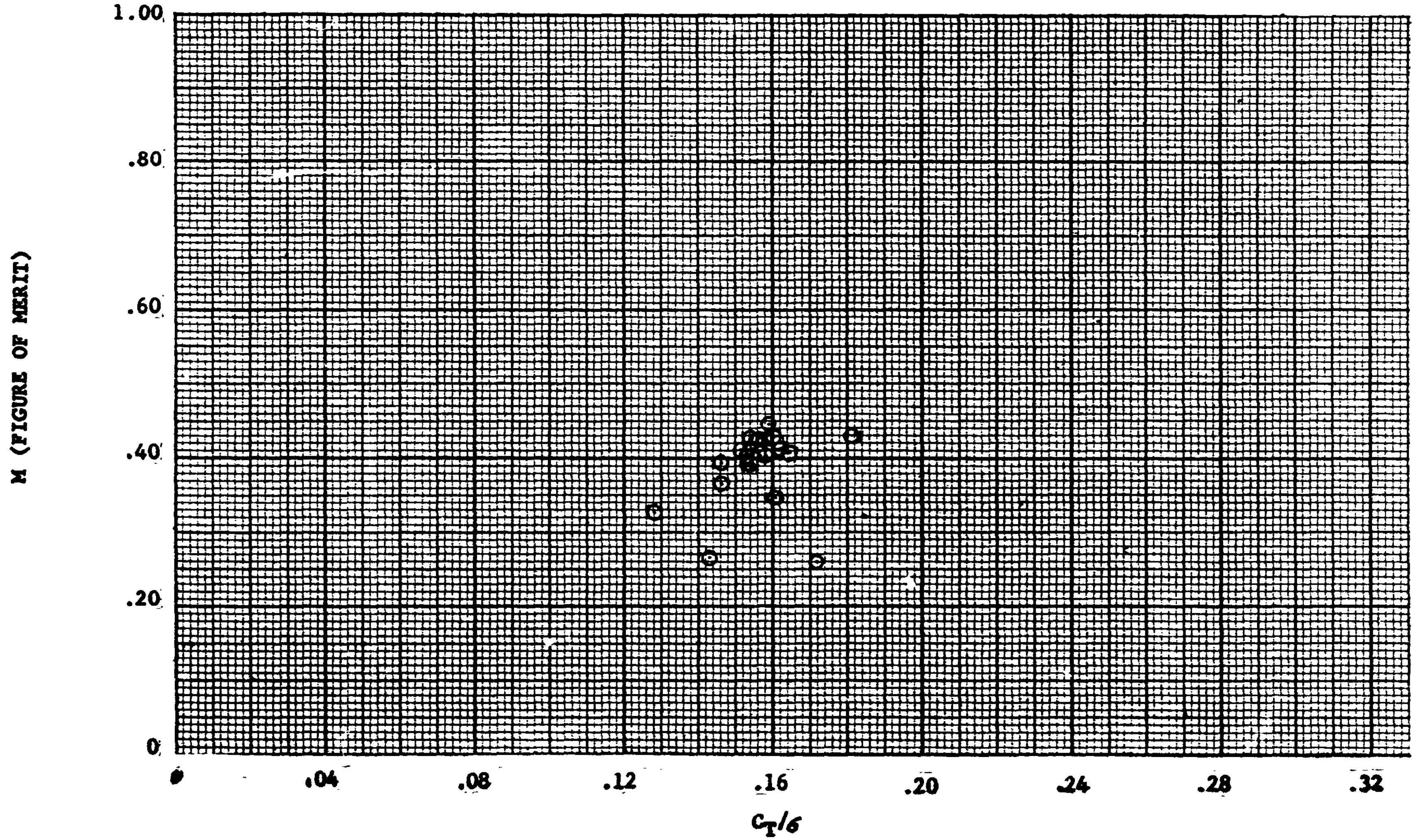

FIGURE 80

FIGURE OF MERIT VS. C_T/σ (b-2)

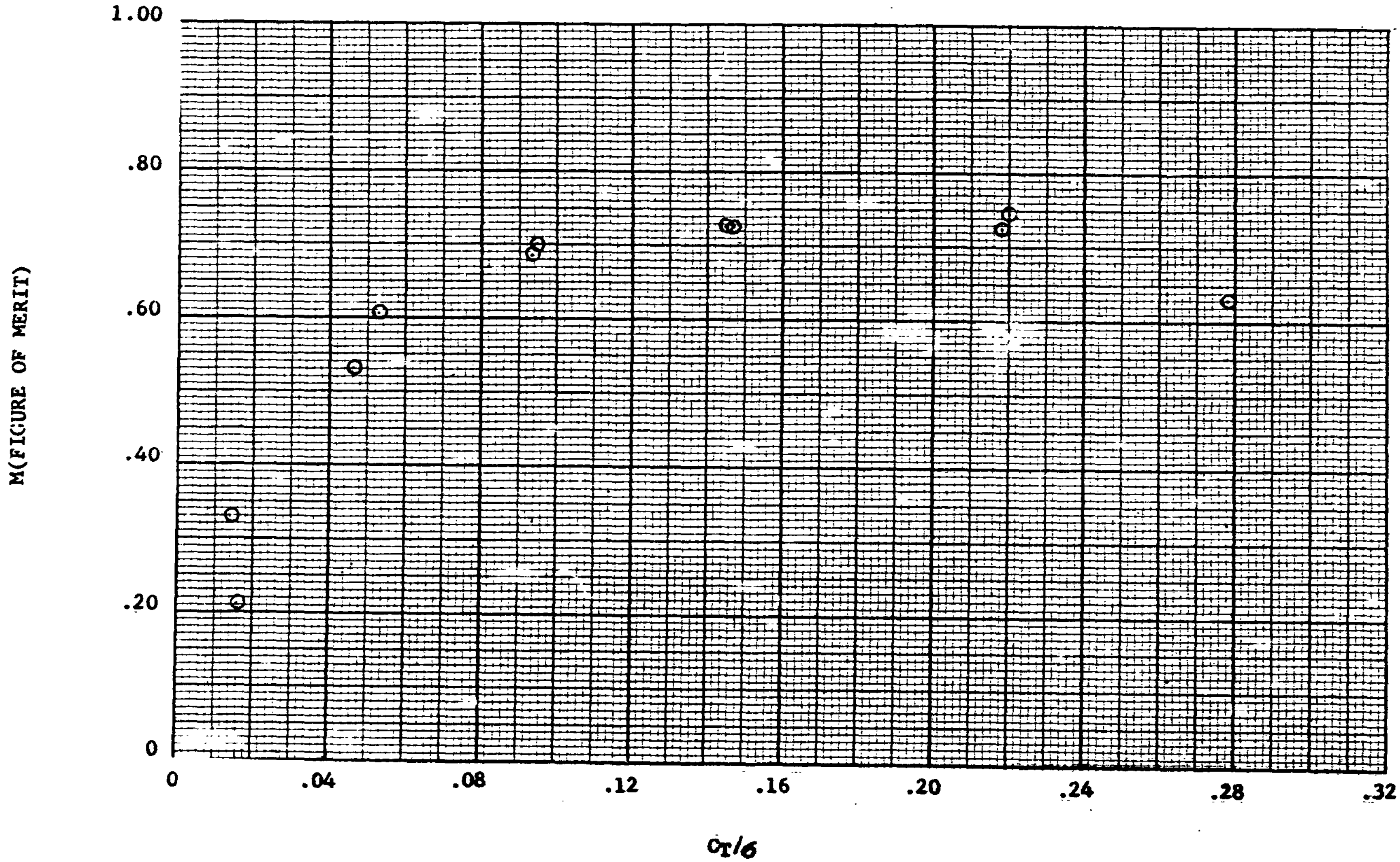

FIGURE 81

FIGURE OF MERIT VS. C_T/σ (M.I.T./MOSER)

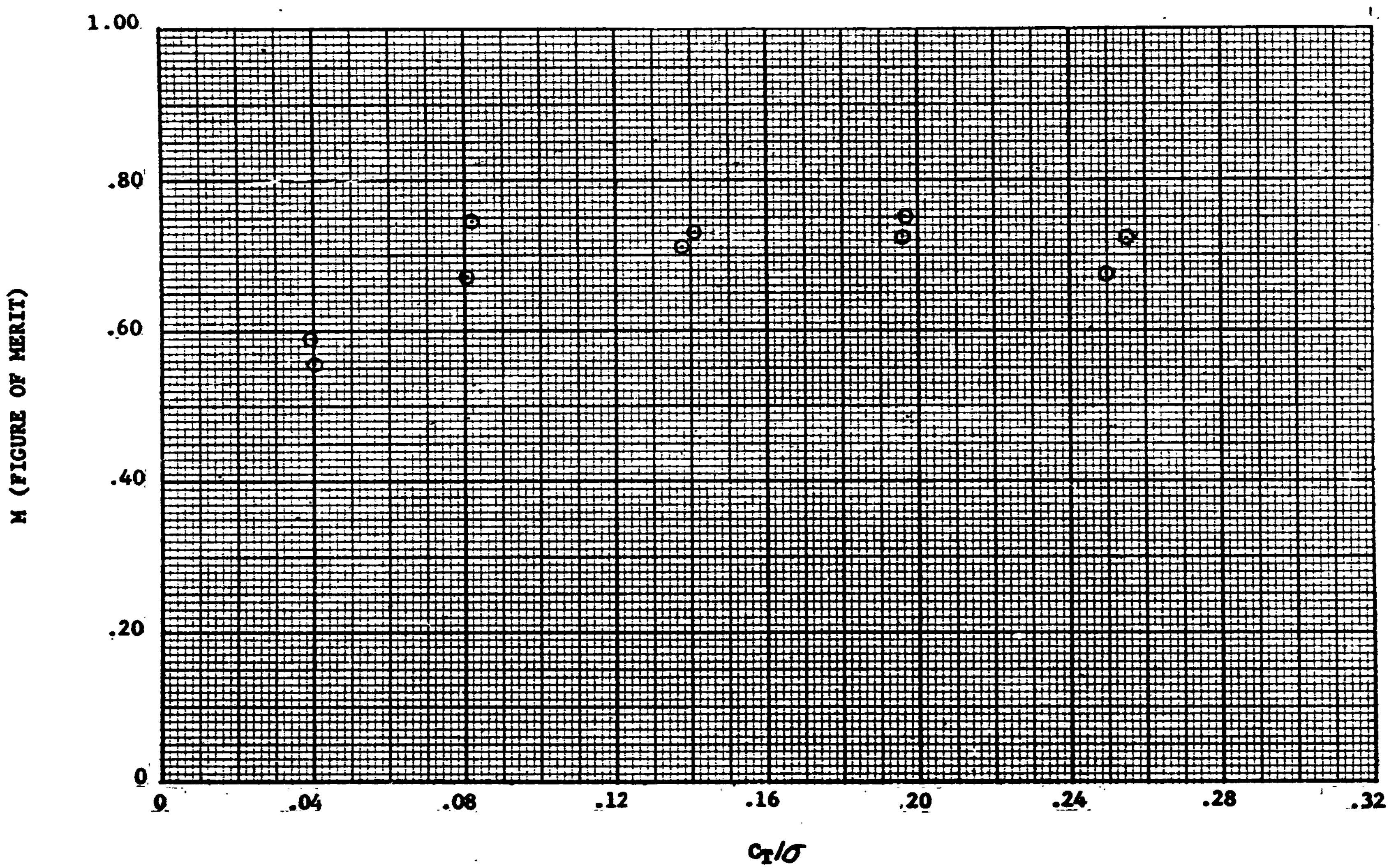

FIGURE 82

FIGURE OF MERIT VS. C_T/σ (M.I.T./MOSER-DUCTED FAN)

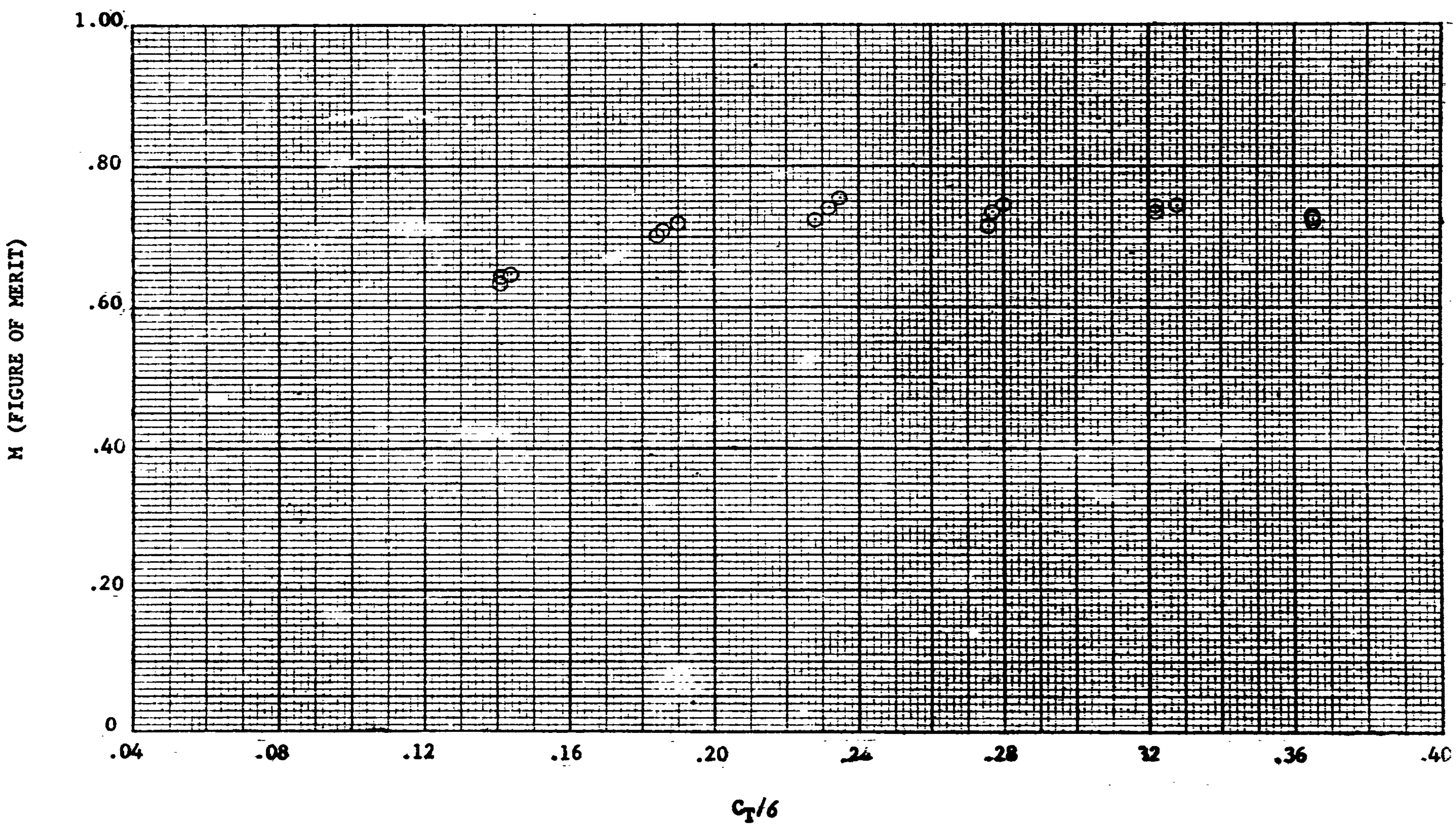

FIGURE 83

FIGURE OF MERIT VS. C_T/σ (HILLER-DUCTED FAN)

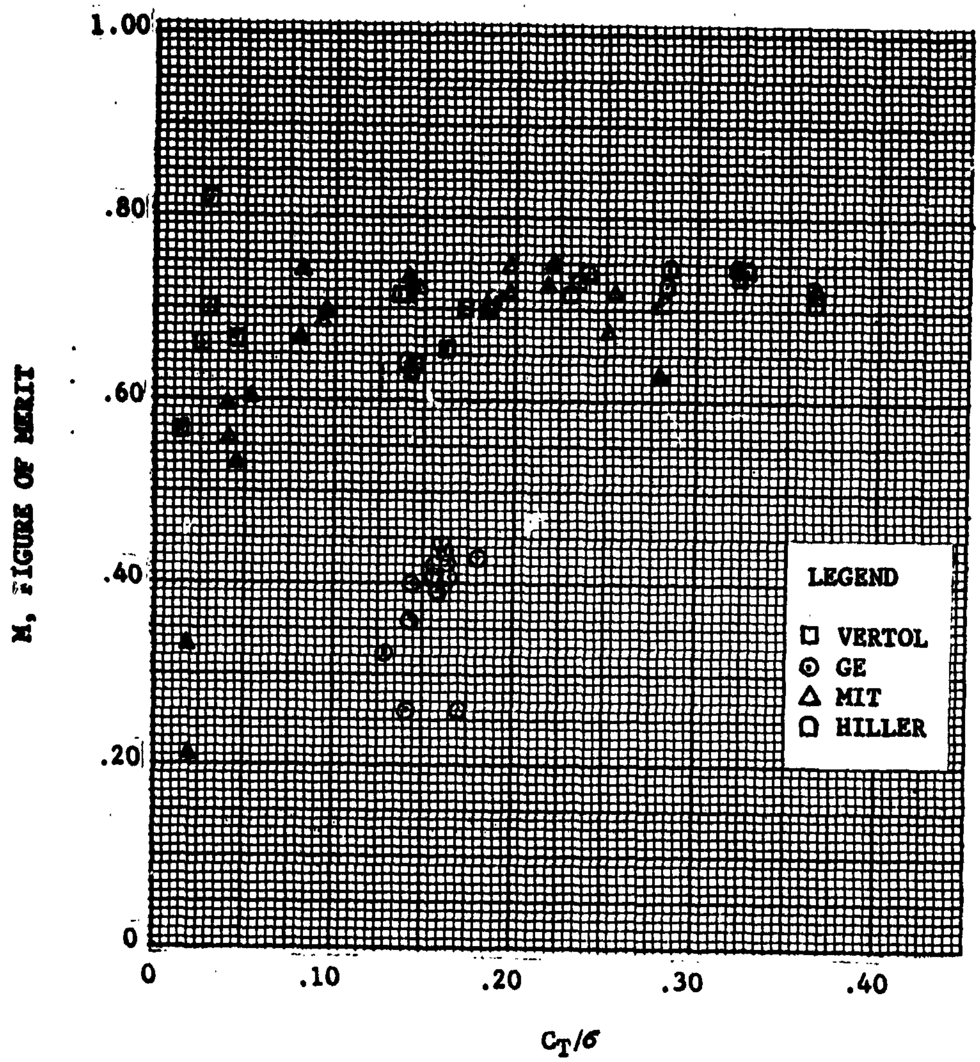

FIGURE 84

FIGURE OF MERIT VS. C_T/σ (CORRELATED DATA)

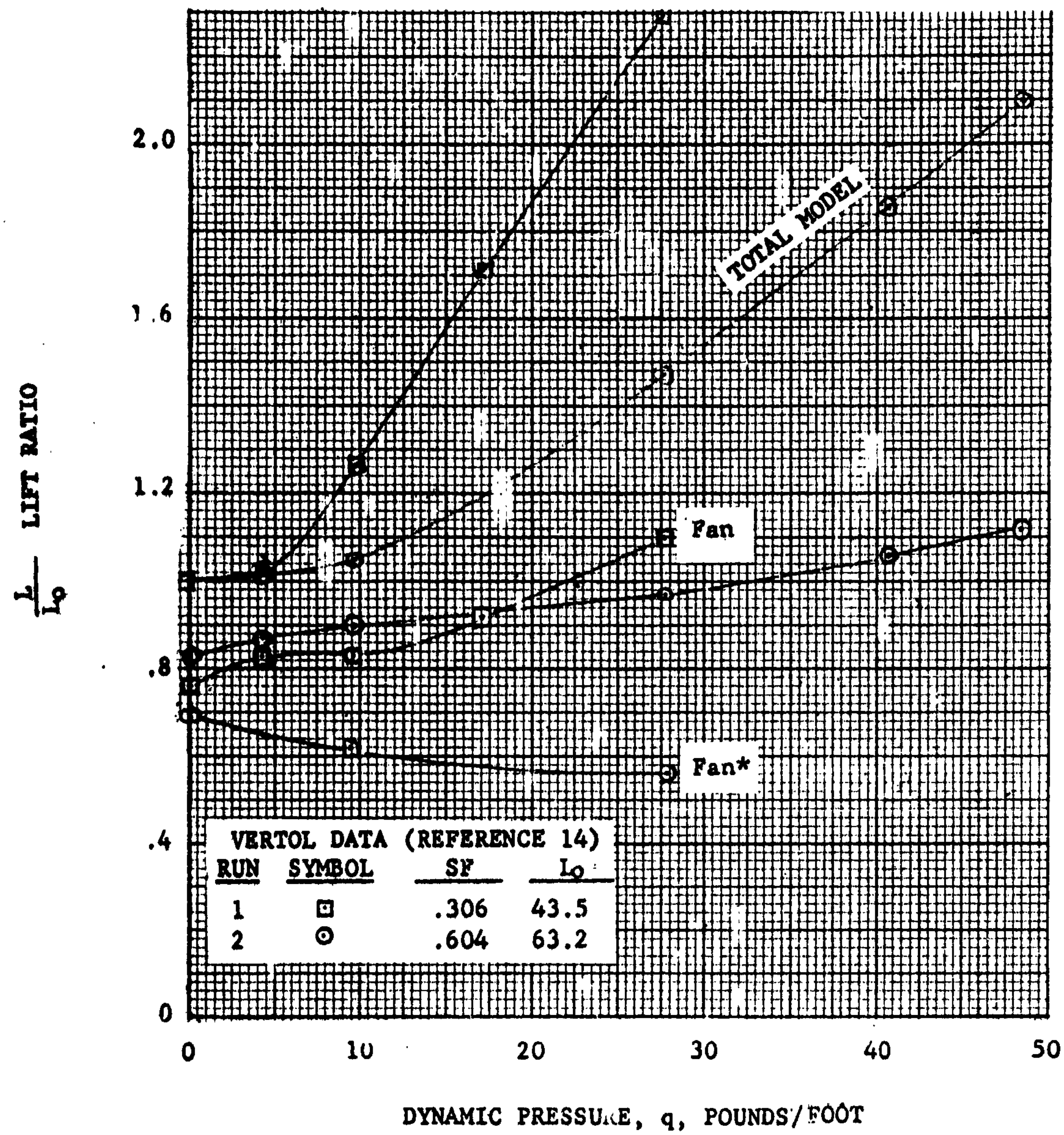

FIGURE 85

LIFT RATIO VS. DYNAMIC PRESSURE (VERTOL)

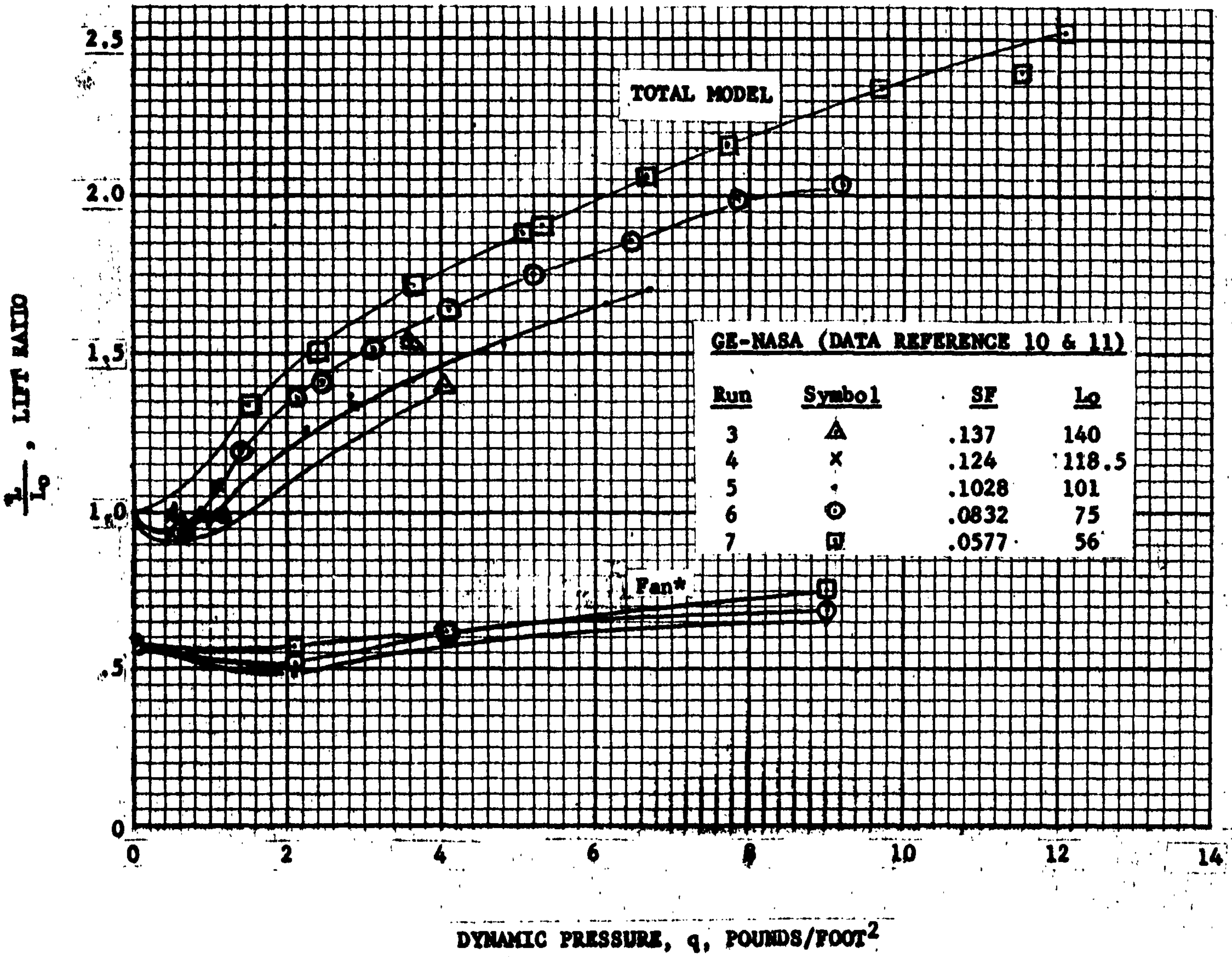

FIGURE 86

LIFT RATIO VS. DYNAMIC PRESSURE (GE-NASA)

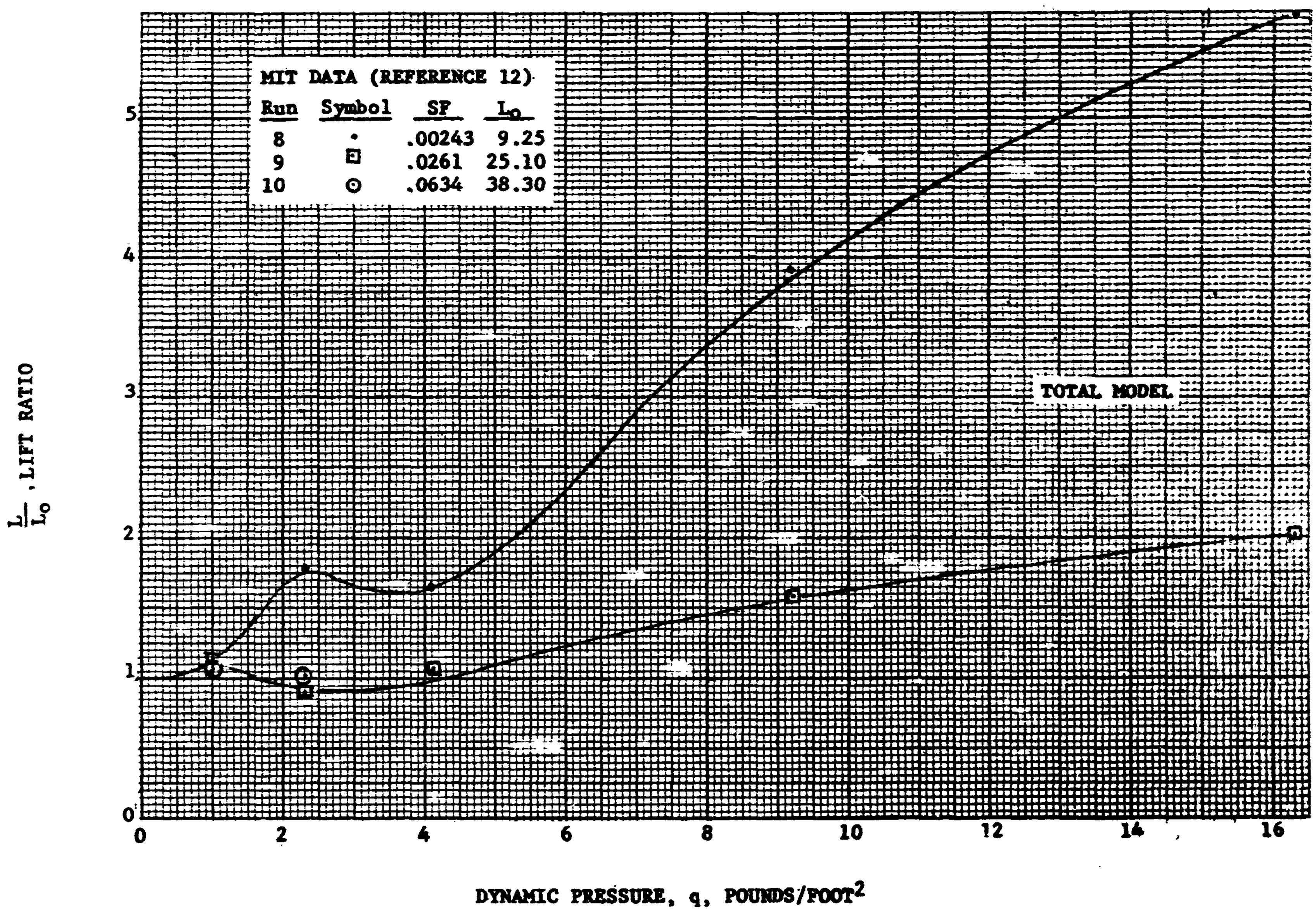

FIGURE 87

LIFT RATIO VS. DYNAMIC PRESSURE (M.I.T./MOSER)

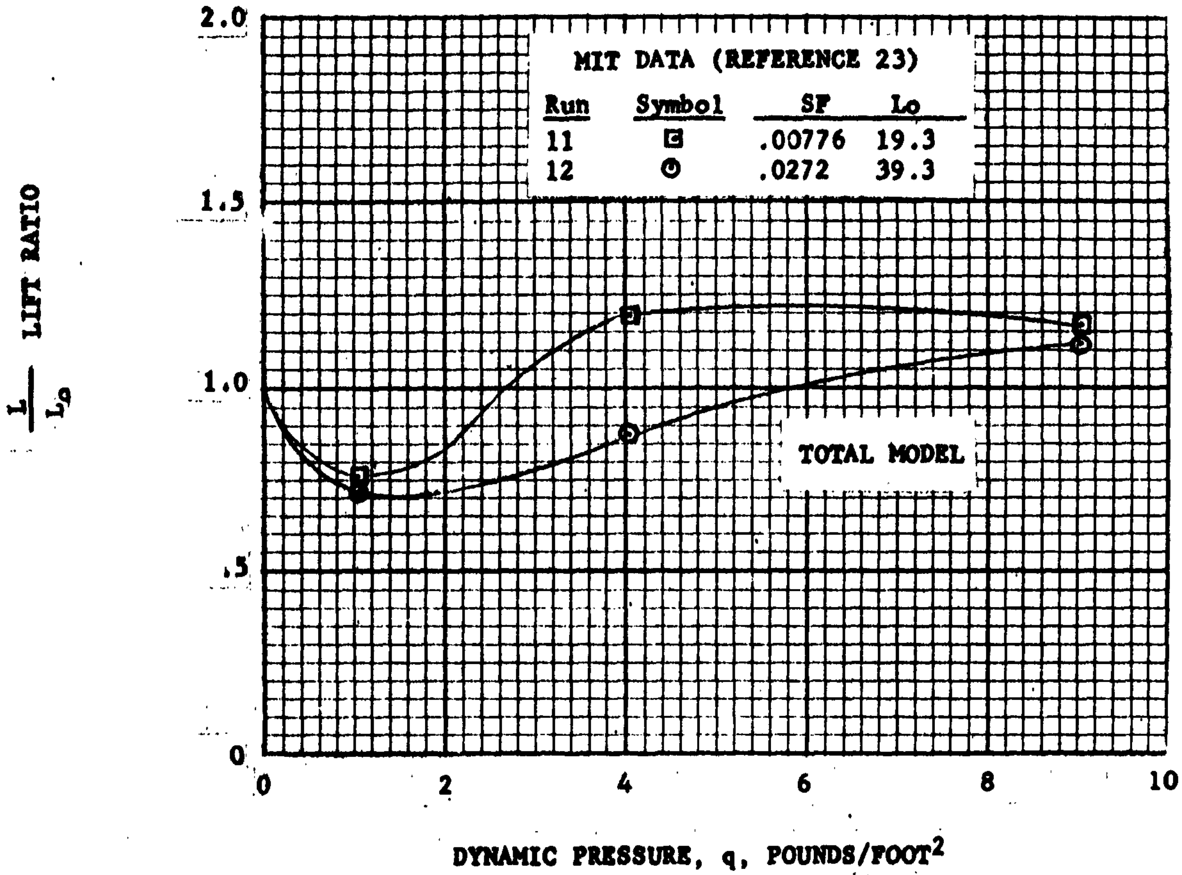

FIGURE 88

LIFT RATIO VS. DYNAMIC PRESSURE (M.I.T./DUVIVIER)

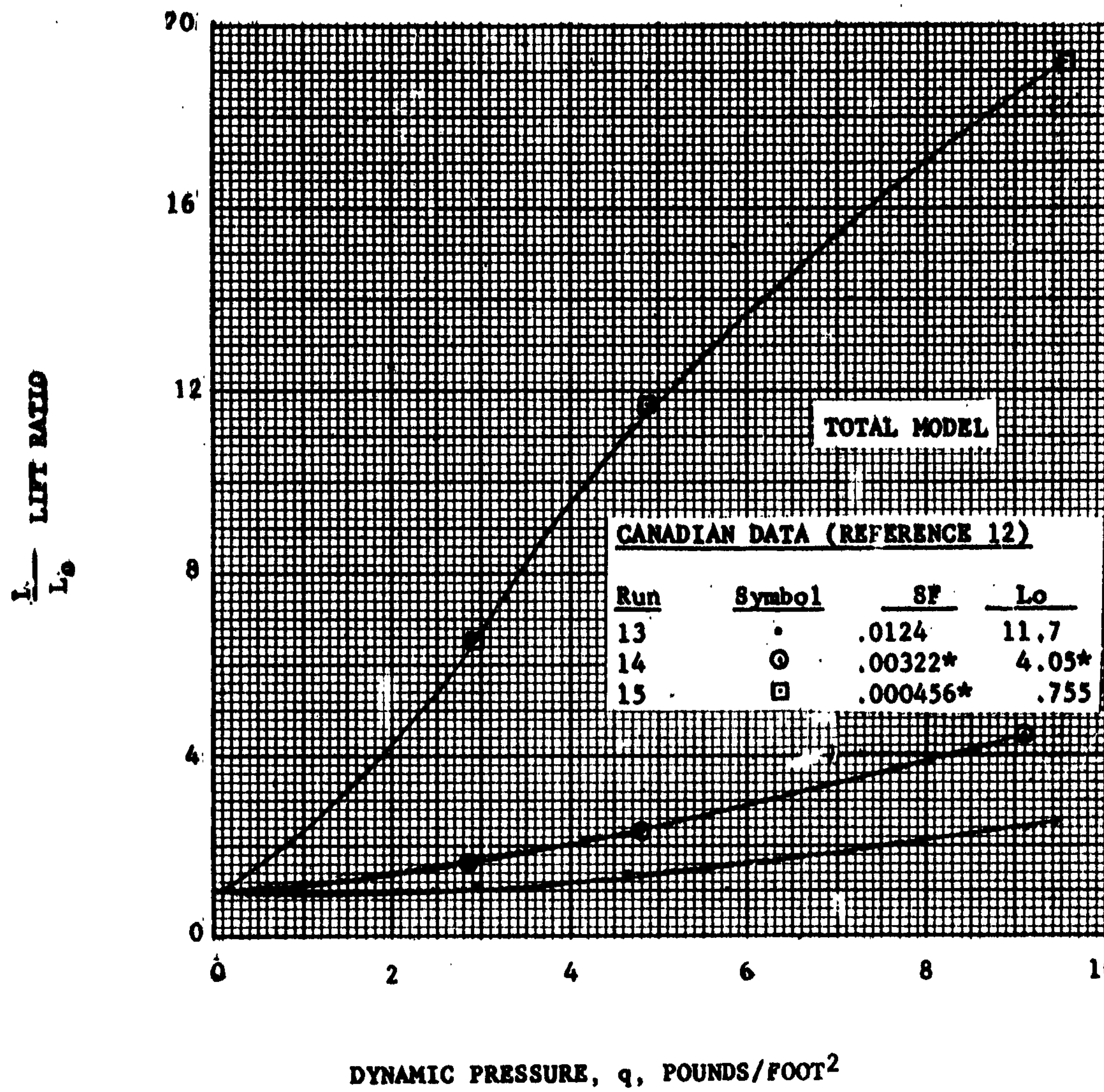

FIGURE 89

LIFT RATIO VS. DYNAMIC PRESSURE (CANADIAN)

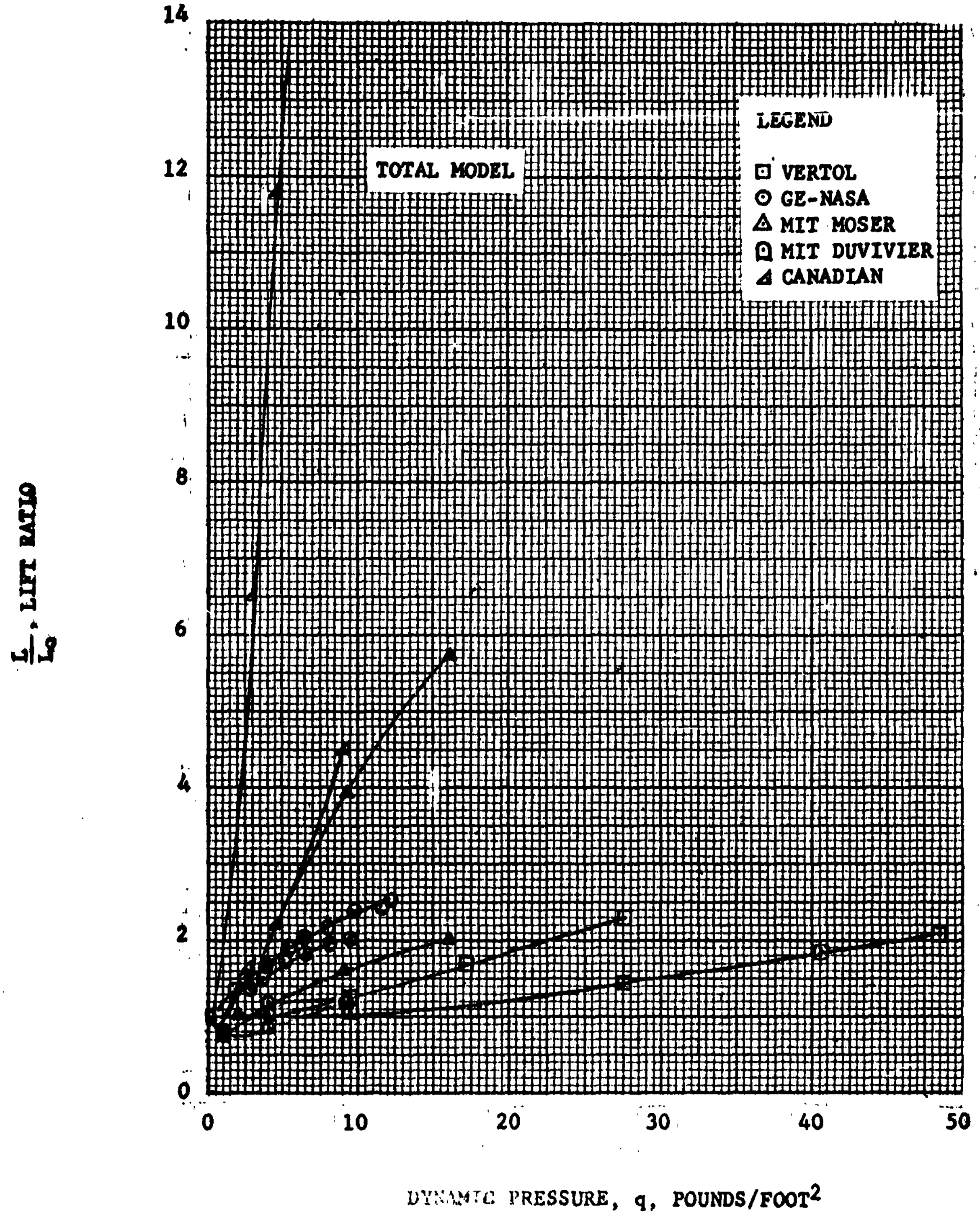

FIGURE 90

LIFT RATIO VS. DYNAMIC PRESSURE (CORRELATED DATA)

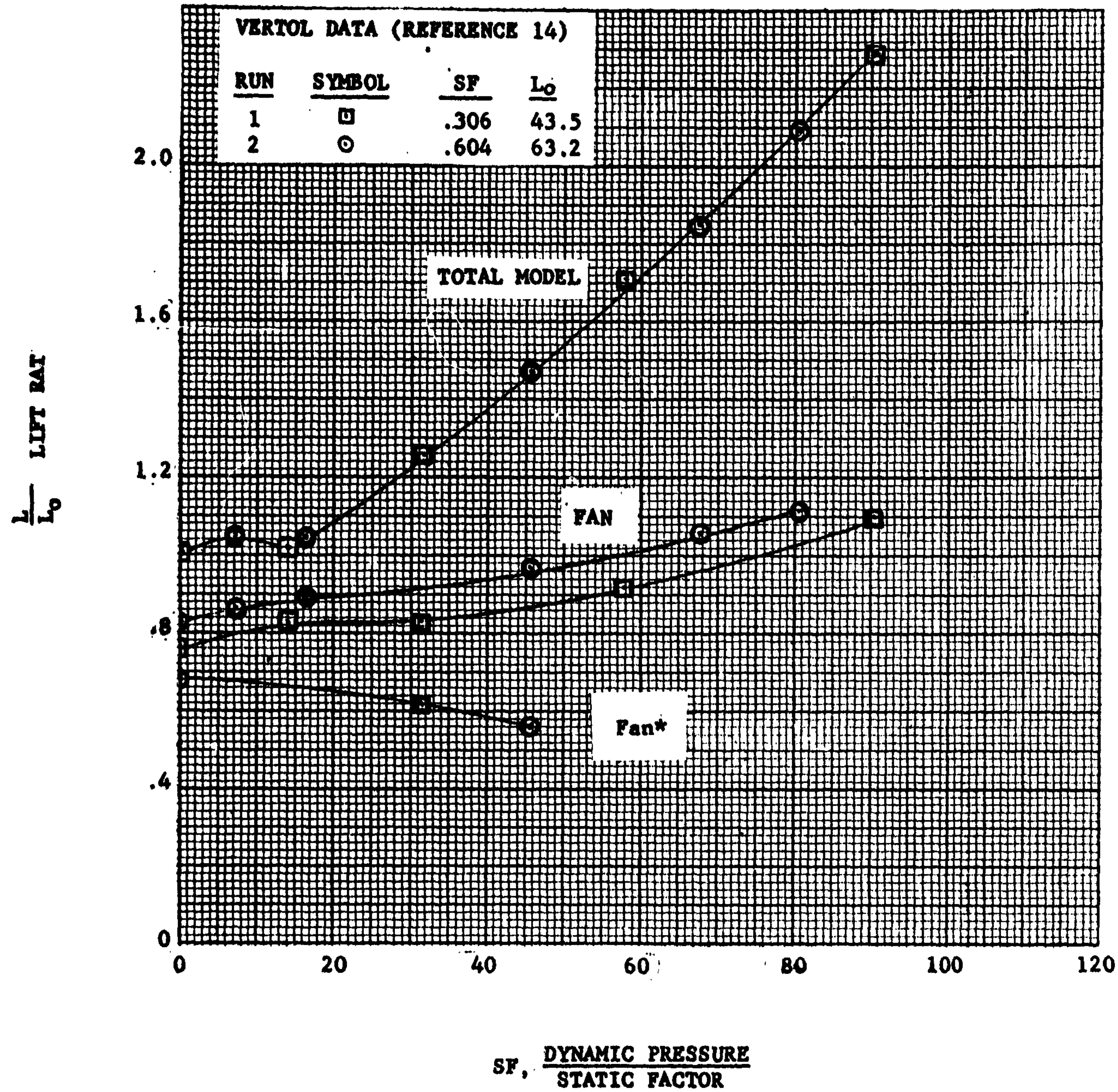

FIGURE 91

LIFT RATIO VS. DYNAMIC PRESSURE/STATIC FACTOR (VERTOL)

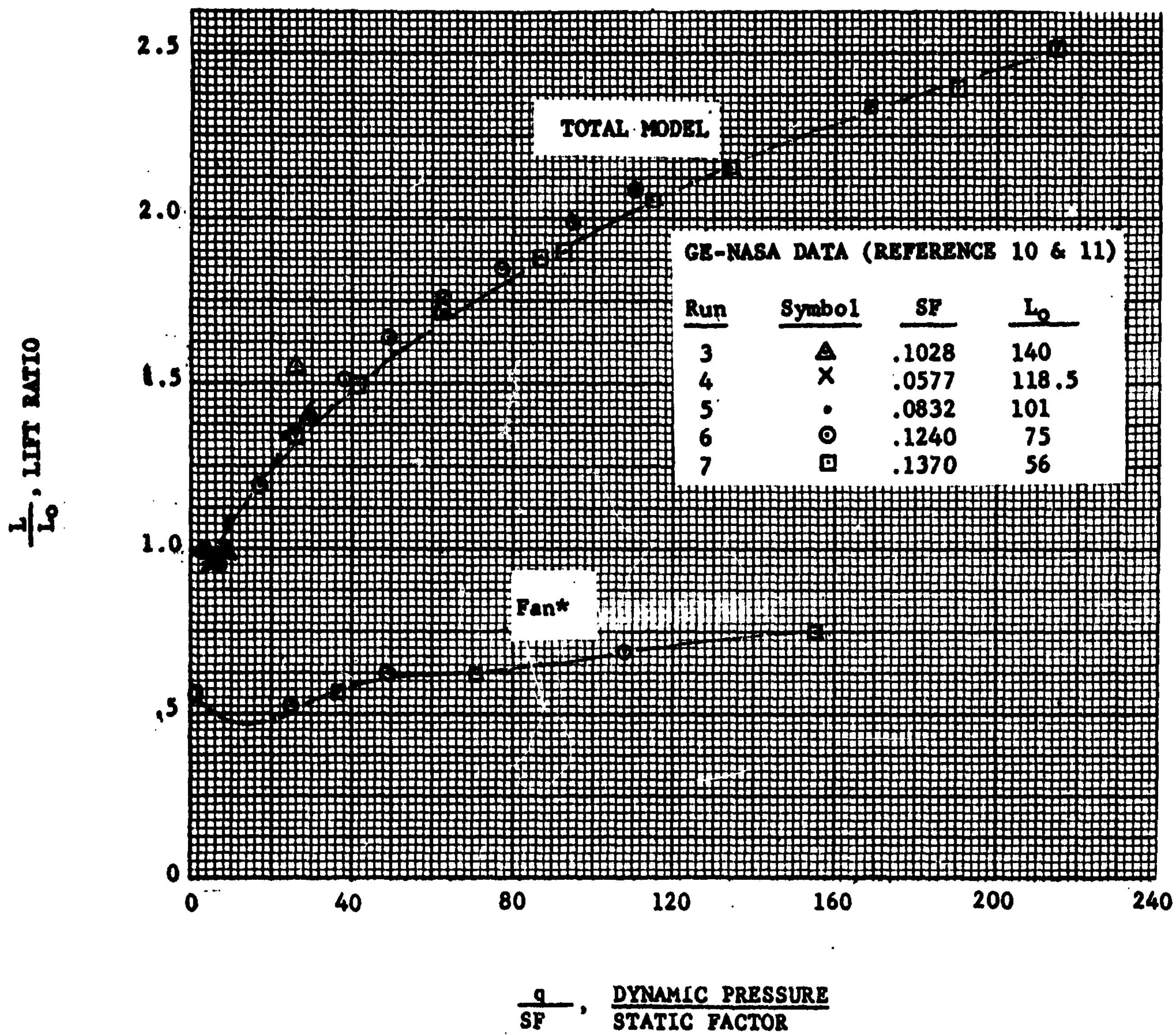

FIGURE 92

LIFT RATIO VS. DYNAMIC PRESSURE/STATIC FACTOR (GE-NASA)

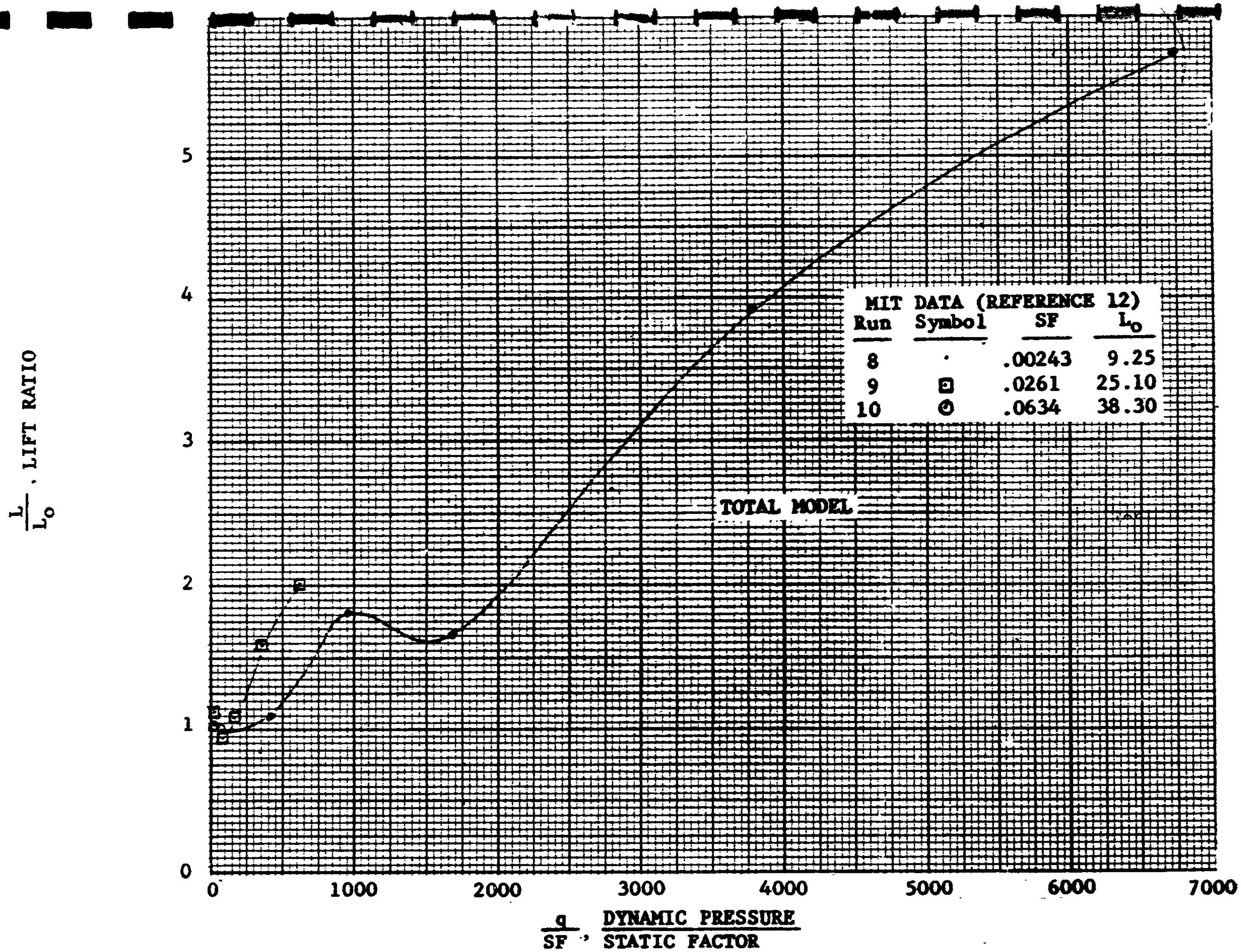

FIGURE 93

LIFT RATIO VS. DYNAMIC PRESSURE/STATIC FACTOR (M.I.T./MOSER)

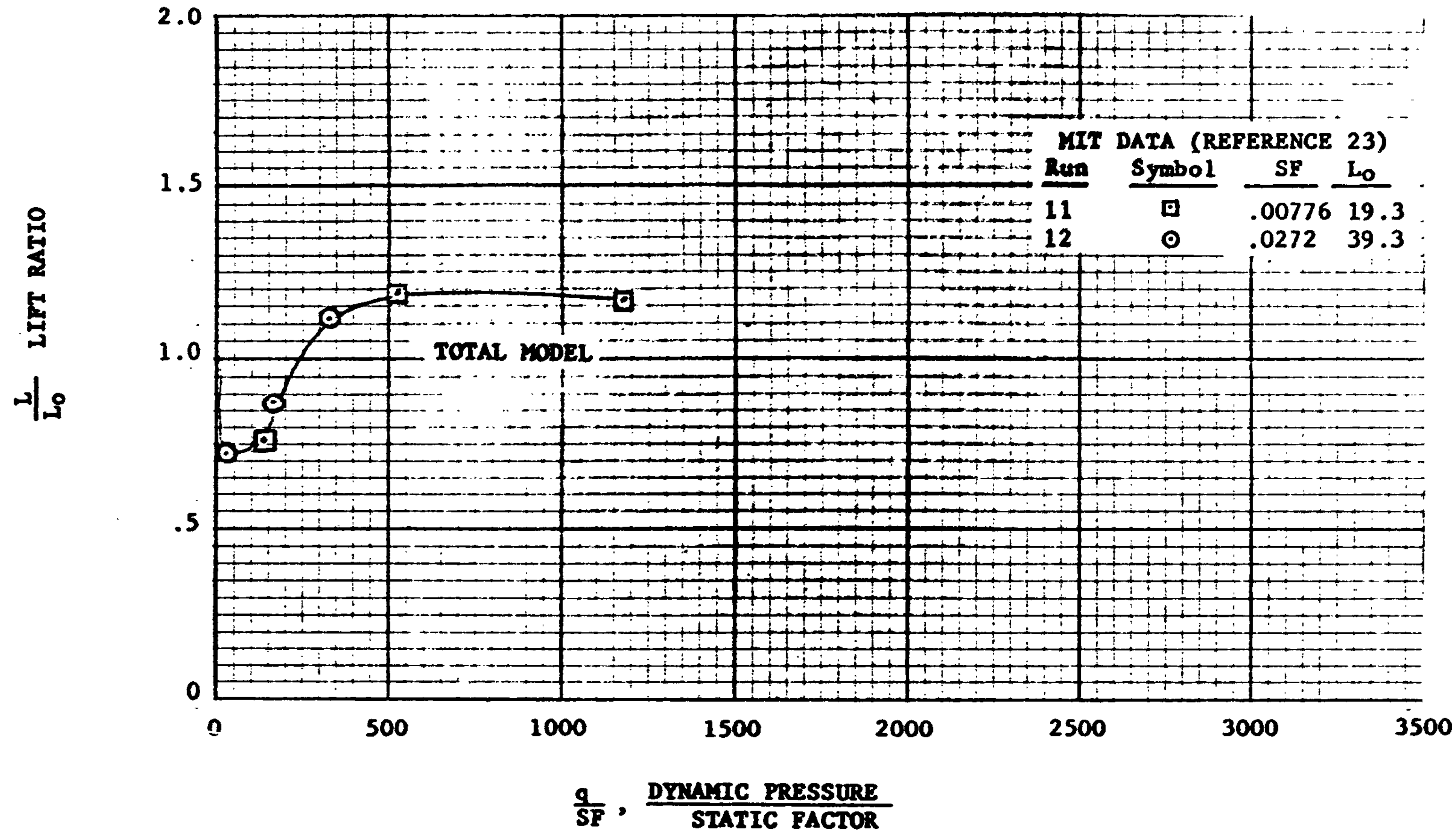

FIGURE 94

LIFT RATIO VS. DYNAMIC PRESSURE/STATIC FACTOR (M.I.T./DUVIVIER)

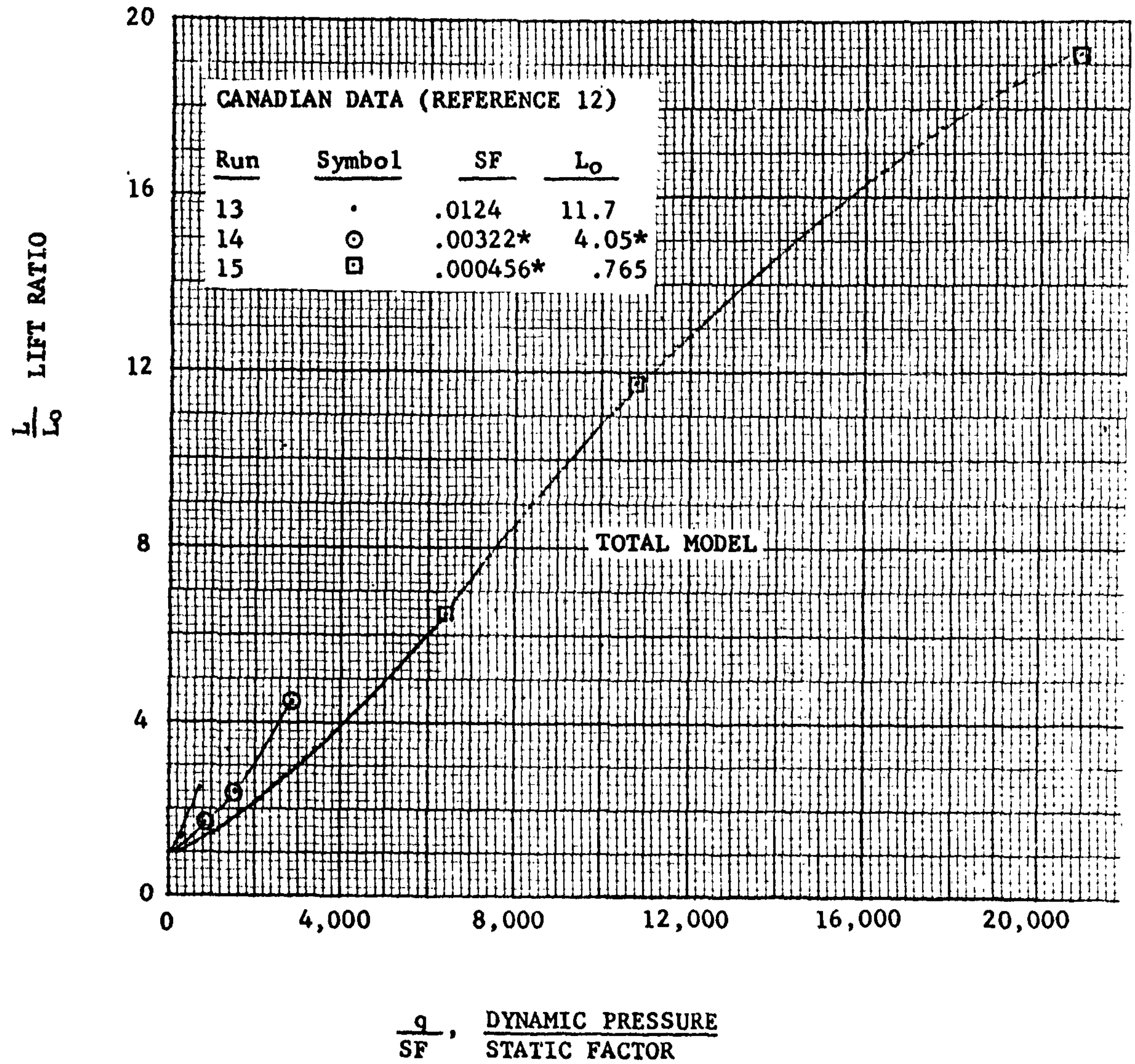

FIGURE 95

LIFT RATIO VS. DYNAMIC PRESSURE/STATIC FACTOR (CANADIAN)

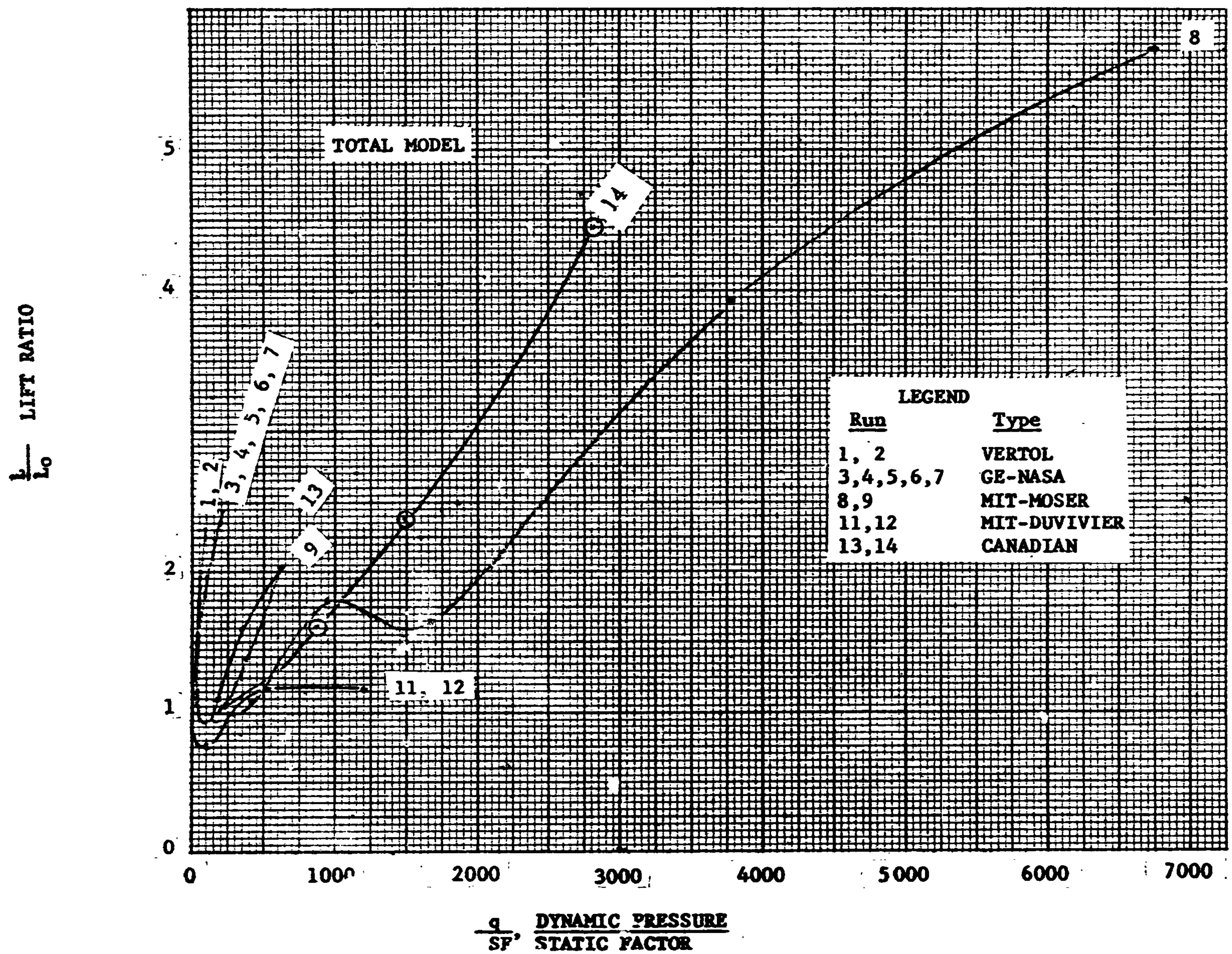

FIGURE 96

LIFT RATIO VS. DYNAMIC PRESSURE/STATIC FACTOR (CORRELATED DATA)

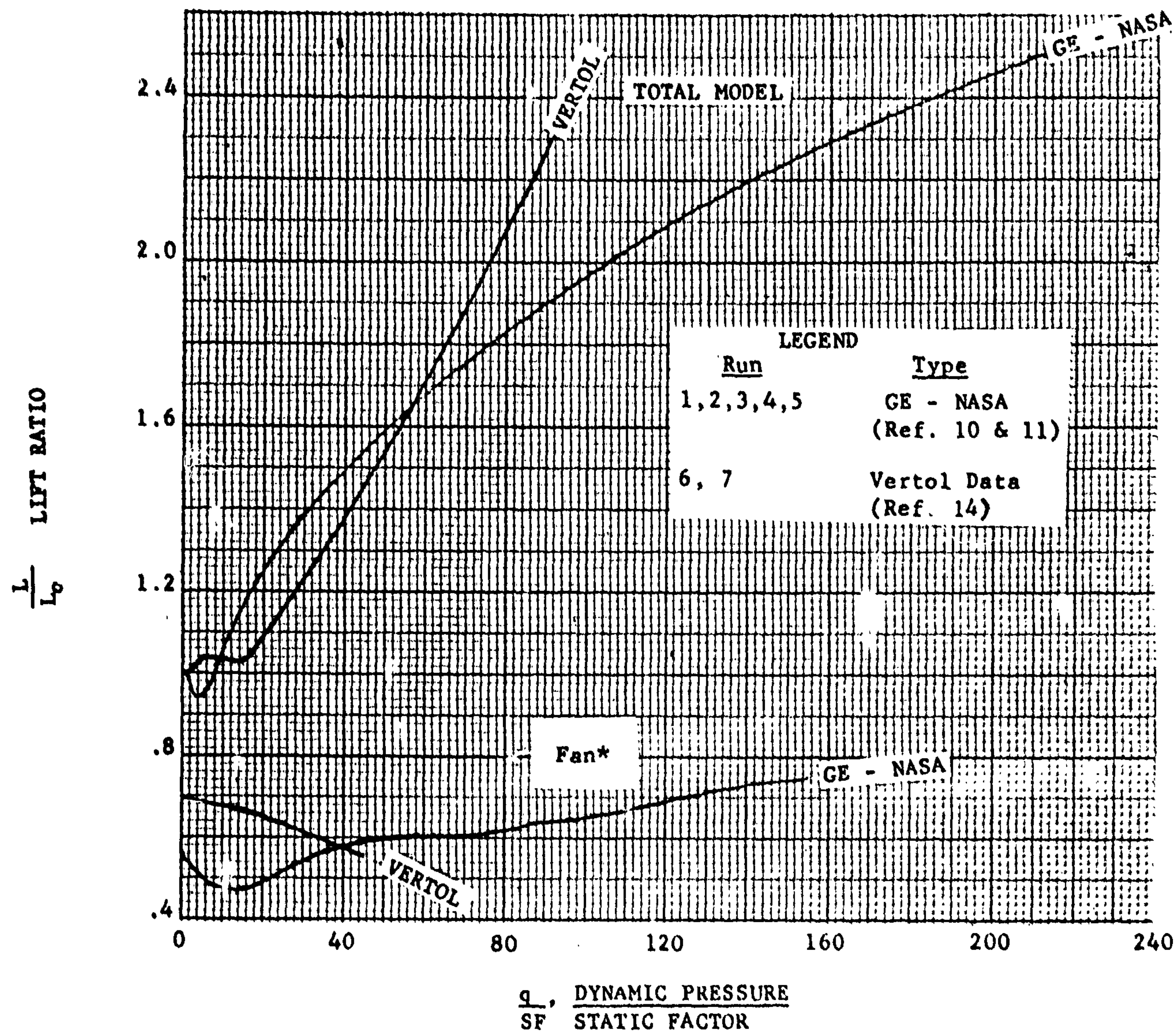

FIGURE 97

LIFT RATIO VS. DYNAMIC PRESSURE/STATIC FACTOR (CORRELATED DATA)

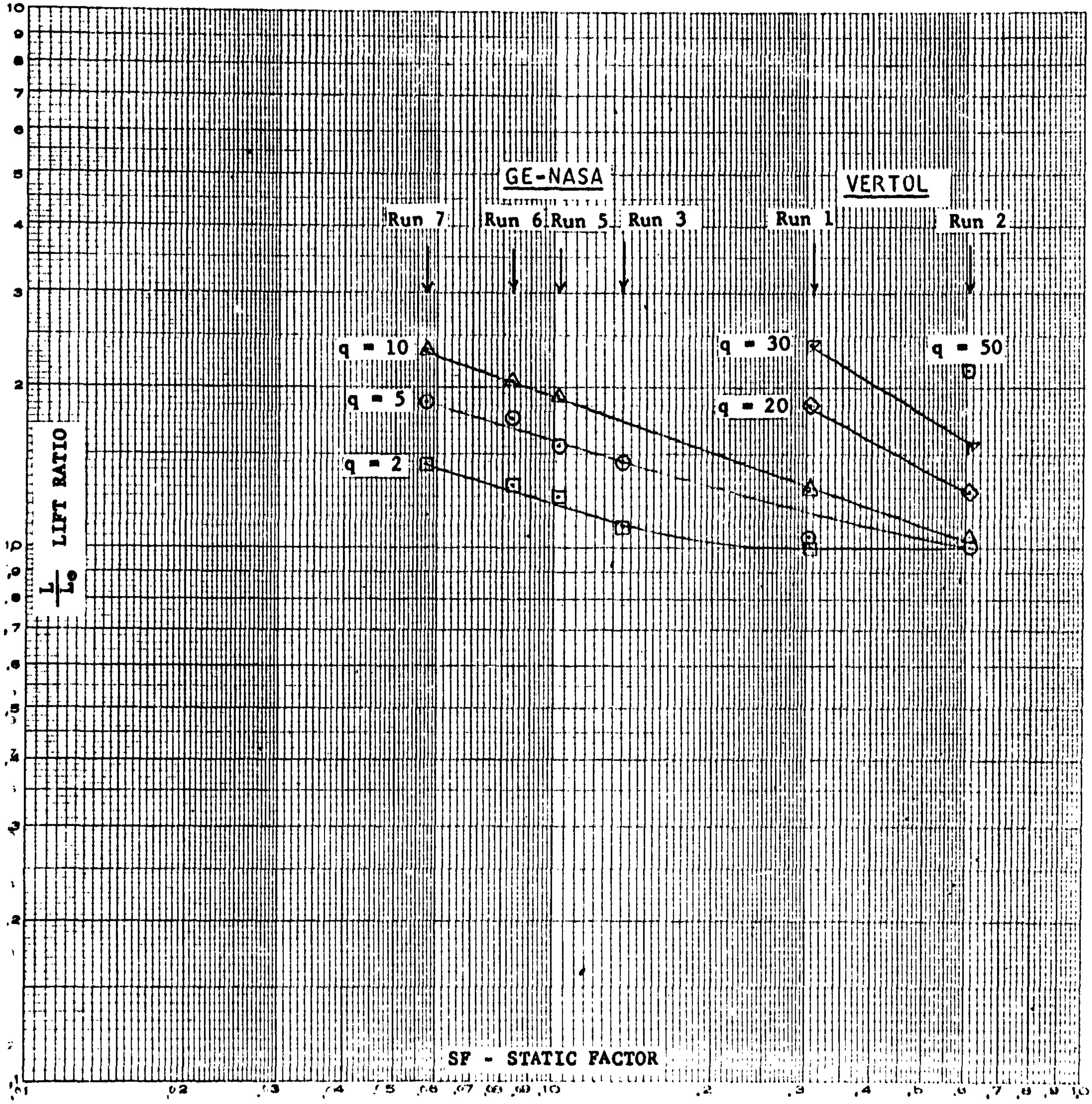

FIGURE 98

LIFT RATIO VS. DYNAMIC PRESSURE/STATIC FACTOR (CORRELATED DATA)

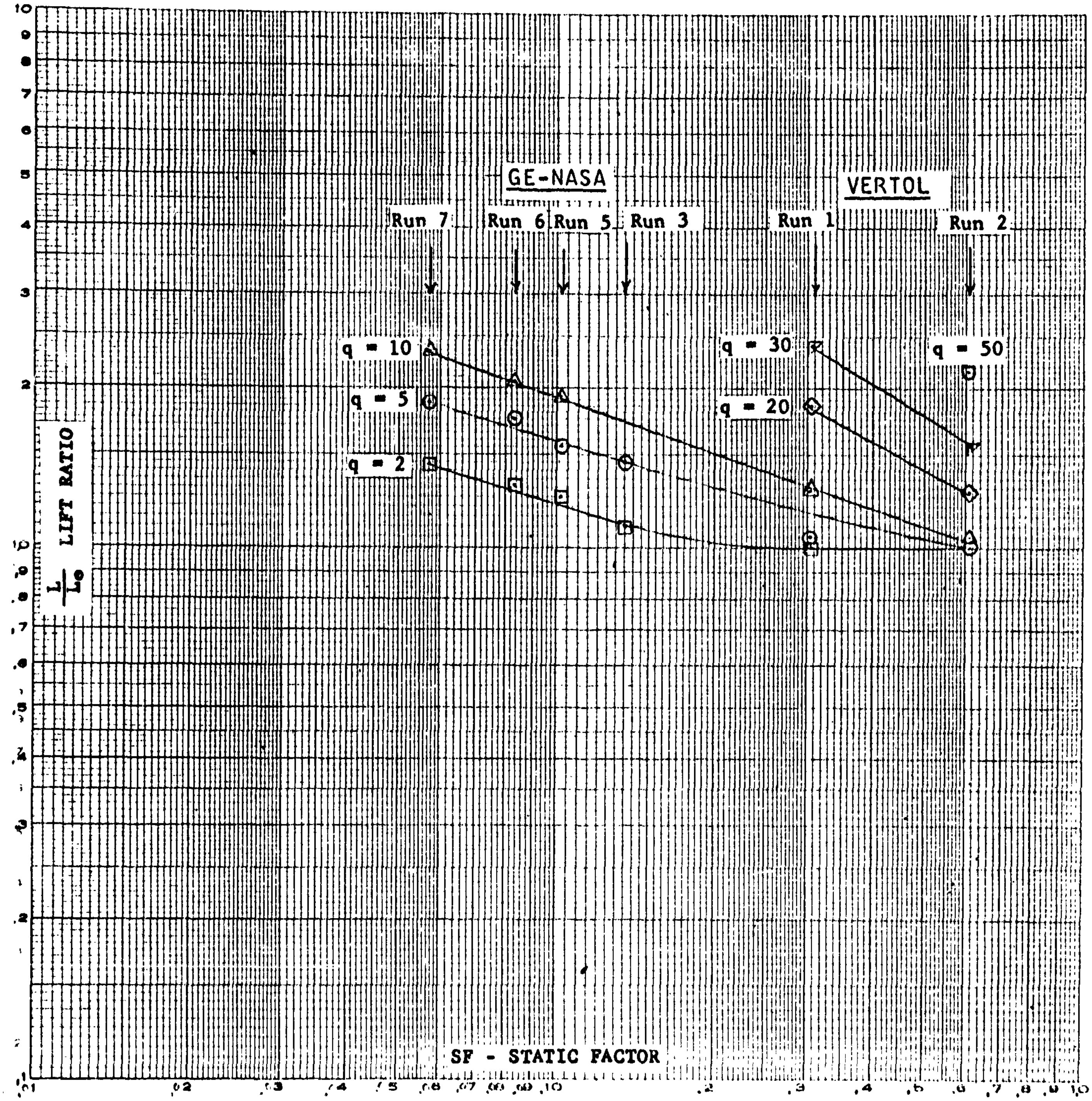

FIGURE 98

LIFT RATIO VS. DYNAMIC PRESSURE/STATIC FACTOR (CORRELATED DATA)

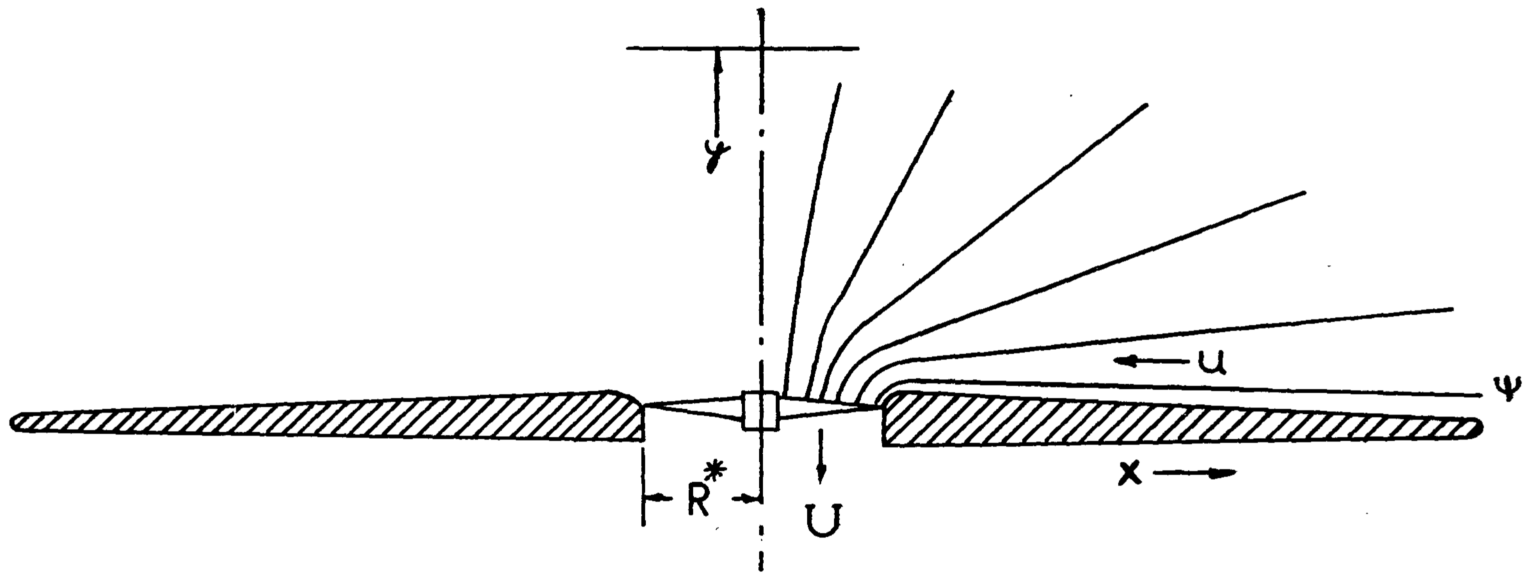

FIGURE 99

STREAMLINE FLOW PATTERN

In order to develop the shroud pressure distribution and thus the shroud lift, a simple model is assumed. This model is a flat plate ring, with the outer section of the ring representing the shroud and the inner section of the ring representing the fan (Example No. 1)

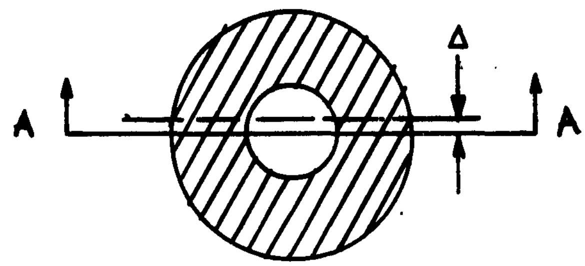

Example 1

Considering Section A-A (Example No. 1) and an incremental width (Δ), it is possible to approximate the flow pattern in this sectional area by a two dimensional hyperbolic flow through a rectangular slot (Example No. 2, References 20 and 21).

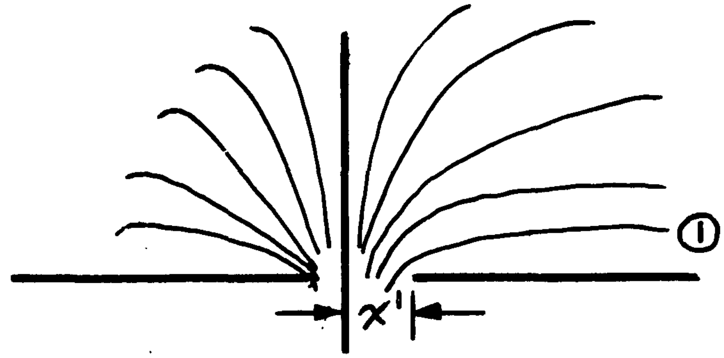

Example 2

Streamline 1 is along the shroud surface, so that the velocity along this streamline is equal to infinity at the slot entrance (x') (Example No. 3). However, in the real case, u attains a maximum velocity of u_c at the fan* radius (R^*).

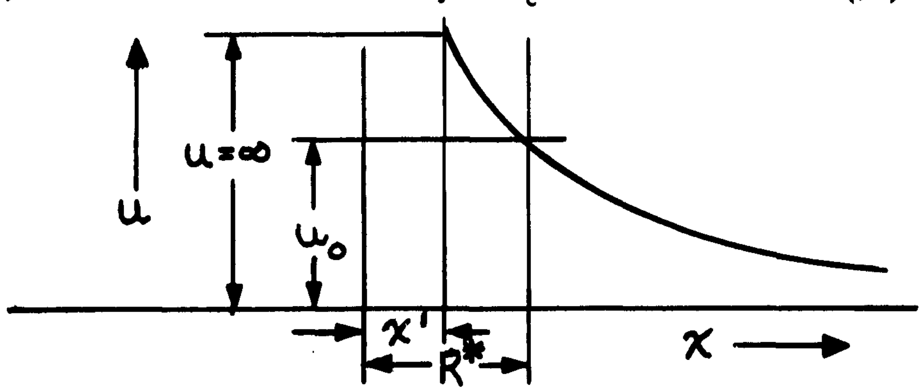

Example 3

On the basis of test data (see Figure 101), it was determined that two dimensional, hyperbolic flow through a rectangular slot can be accepted as a satisfactory approximation to the real case. This flow (see References 20 and 21) has been developed as follows:

$$\frac{x^2}{(x')^2 \cos^2 \psi} - \frac{y^2}{(x')^2 \sin^2 \psi} = 1 \qquad (1)$$

$$\frac{x^2}{(x')^2 \cos h^2 \phi} + \frac{y^2}{(x')^2 \sin h^2 \phi} = 1 \qquad (2)$$

Consider the case where the streamline (1) is along the shroud (x) so that y = o.

Equation Number 2 now becomes:

$$x = x' \cos h \ \phi \qquad (3)$$

differentiating Equation Number 3 with respect to x

$$1 = x' \sin h \ \phi \frac{\partial \phi}{\partial x} \qquad (4)$$

since $\frac{\partial \phi}{\partial x} \equiv -u$ (5)

From Equation Number 4,

$$u = \frac{1}{-x' \sin h \ \phi} \qquad (6)$$

since Equation Number 7

$$\cos h^2 \phi = 1 + \sin h^2 \phi \qquad (7)$$

and from Equation Number 3

$$\cos h^2 \phi = \left(\frac{x}{x'}\right)^2 \qquad (8)$$

Then Equation Number 9

$$\sin h \ \phi = \sqrt{\frac{x^2}{(x')^2} - 1} \qquad (9)$$

$$u = -\left[x\sqrt{\left(\frac{x}{x'}\right)^2 - 1}\right]^{-1} \qquad (10)$$

$$u = \left[x^2 - (x')^2\right]^{-\frac{1}{2}} \qquad (11)$$

Equation Number 11 is desired in terms of the fan area (A^*) and the shroud area (A_s). Let A_{s_x} = the shroud area enclosed at any radius x.

$$A_{s_x} = \pi x^2 - A^* \tag{12}$$

$$x^2 = \frac{A_{s_x} + A^*}{\pi} \tag{13}$$

Defining the effective area as the area where $u = \infty$, or $\pi (x')^2$, then the ratio of the effective area to the fan* area $\left(\frac{\pi (x')^2}{A^*}\right)$ is defined as a shroud shape factor (K).

A similar factor (C_f) has been used by General Electric (Reference 10) Figure 100.

$$K = \frac{\pi (x')^2}{A^*} < 1 \tag{14}$$

or

$$(x')^2 = \frac{K A^*}{\pi} \tag{15}$$

Substituting Equation Numbers 15 and 13 in Equation Number 11 the following is attributed:

$$u = \left[\frac{A_{s_x} + A^*}{\pi} - \frac{KA^*}{\pi} \right]^{\frac{1}{2}} \tag{16}$$

or

$$u = \left[\frac{\pi}{A_{s_x} + (1-K)\, A^*} \right]^{\frac{1}{2}} \tag{17}$$

where u is the velocity at any radius x.

In order to determine the shroud lift, the pressure ditribution has been assumed uniform across the fan* area (A^*). Pressure values have been plotted on Figure 101.

Let P_s be the static pressure along the shroud and P_a be the ambient pressure.

$$P_a = P_s + \frac{1}{2}\rho u^2 \qquad (18)$$

(See Figure 101)

$$P_a - P_s = \frac{1}{2}\rho u^2 = P \qquad (19)$$

At station 0:

$$P_o = \frac{1}{2}\rho u_o^2 \qquad (20)$$

also at station 0:

$$L_p = \rho A^* U^2 \qquad (21)$$

or

$$P_o = \rho U^2 \qquad (22)$$

Equating Equation Number 20 to Equation Number 22:

$$U^2 = \frac{1}{2} u_o^2 \qquad (23)$$

$$U = \frac{1}{1.414} u_o \qquad (24)$$

Substituting Equation Number 17 for u_o when $A_s = 0$:

$$U = \frac{1}{1.414} \left(\frac{\pi}{(1-K)A^*}\right)^{\frac{1}{2}} \qquad (25)$$

Multiplying Equation Number 17 by $\frac{U}{U}$

$$u = \frac{U}{U} \left(\frac{\pi}{A_{s_x} + (1-K) A^*}\right)^{\frac{1}{2}} \qquad (26)$$

Substituting Equation Number 25 in Equation Number 26:

$$u = \frac{U}{\frac{1}{1.414}\left(\frac{\pi}{(1-K) A^*}\right)^{\frac{1}{2}}} \left(\frac{\pi}{A_{s_x} + (1-K) A^*}\right)^{\frac{1}{2}} \qquad (27)$$

$$u = 1.414 U \left[\frac{1}{1 + \frac{A_{s_x}}{(1-K) A^*}}\right]^{\frac{1}{2}} \qquad (28)$$

Substituting Equation Number 28 in Equation Number 19 and simplifying:

$$P_a - P_s = \rho U^2 \left(\frac{1}{1 + \frac{A_{s_x}}{(1-K)\ A^*}} \right) \tag{29}$$

With Equation Numbers 28 and 29 the velocity and pressure may be predicted with a knowledge of U and K. U is the fan velocity and is readily obtained from a knowledge of the fan characteristics. K is a characteristic of each shroud shape.

Total Thrust of the Shroud

$$L_s = \int_o^{A_s} (P_a - P_s)\ dA_{s_x} \tag{30}$$

From Equation Number 19:

$$L_s = \tfrac{1}{2}\rho \int_o^{A_s} u^2\ dA_{s_x} \tag{31}$$

From Equation Numbers 31 and 29:

$$L_s = \rho\ U^2\ (1-K)\ A^* \int_o^{A_s} \frac{dA_{s_x}}{A_{s_x} + (1-K)\ A^*} \tag{32}$$

Since A and U are constants:

$$L_p = \rho U^2\ A^* \tag{33}$$

then

$$\frac{L_s}{L_p} = (1-K) \int_o^{A_s} \frac{dA_{s_x}}{A_{s_x} + (1-K)\ A^*} \tag{34}$$

now

$$\frac{L_s}{L_p} = (1-K) \left|_o^{A_s} \ln \left[A_{s_x} + (1-K)\ A^* \right] \right. \tag{35}$$

$$\frac{L_s}{(1-K)\ L_p} = \ln \left[A_s + (1-K)\ A^* \right] - \ln \left[(1-K)\ A^* \right] \tag{36}$$

Defining:

$$L_p = L_o - L_s \tag{37}$$

$$\frac{L_s}{(1-K) L_o - L_s} = \ln \left[\frac{A_s + (1-K)\ A^*}{(1-K)\ A^*} \right] = \ln \left[1 + \frac{A_s}{(1-K)\ A} \right] \tag{38}$$

$$e^{\frac{\frac{L_s}{L_o}}{(1-K)\left(1-\frac{L_s}{L_o}\right)}} = 1 + \frac{A_s}{(1-K)\,A^*} \tag{39}$$

Equation Number 39 is plotted on Figure 102 for different values of K and test data points are plotted on the same graph. For the same shroud area and fan area, test data shows that as the Figure of Merit increases the shroud lift increases. In addition, most of the test data indicates a relationship between the Shroud Shape Factor (K) and the Figure of Merit (M).

The theory by the Russian mathematician Shaidakov indicates that the shroud lift may be predicted by a method similar to the one presented. As an example, the line, "long shroud", Figure 102, can be defined by Equation Number 39 with a K between 0 and .40. This theory was derived for an inlet radius proportional to the shroud area (A_s).

Figure 103 shows four different types of shrouds. The type of shroud will determine the value of K which in turn can be used in Equation Numbers 28, 29, and 39 to determine the shroud velocity, pressure, and lift, respectively.

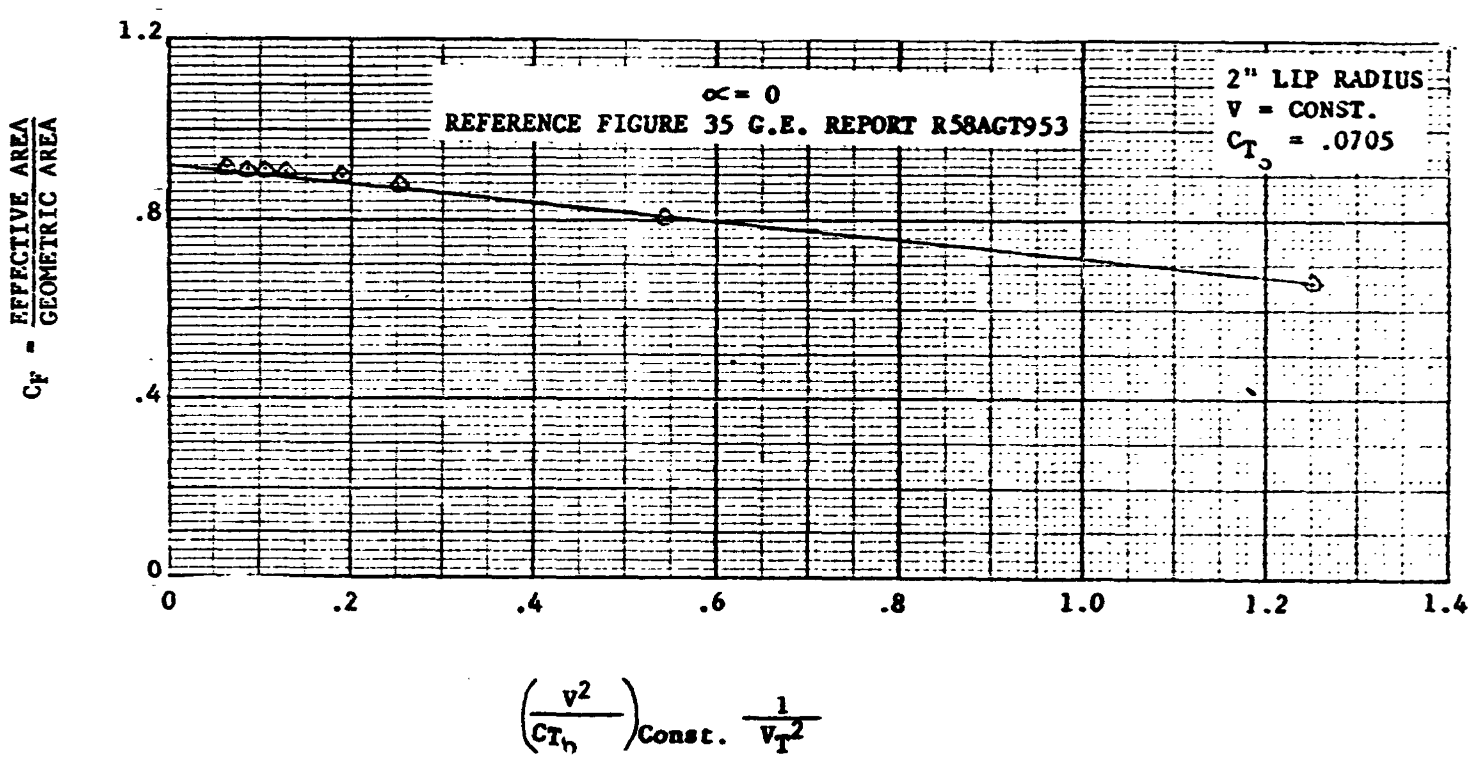

FIGURE 100

G-E FAN EFFECTIVE AREA COEFFICIENT

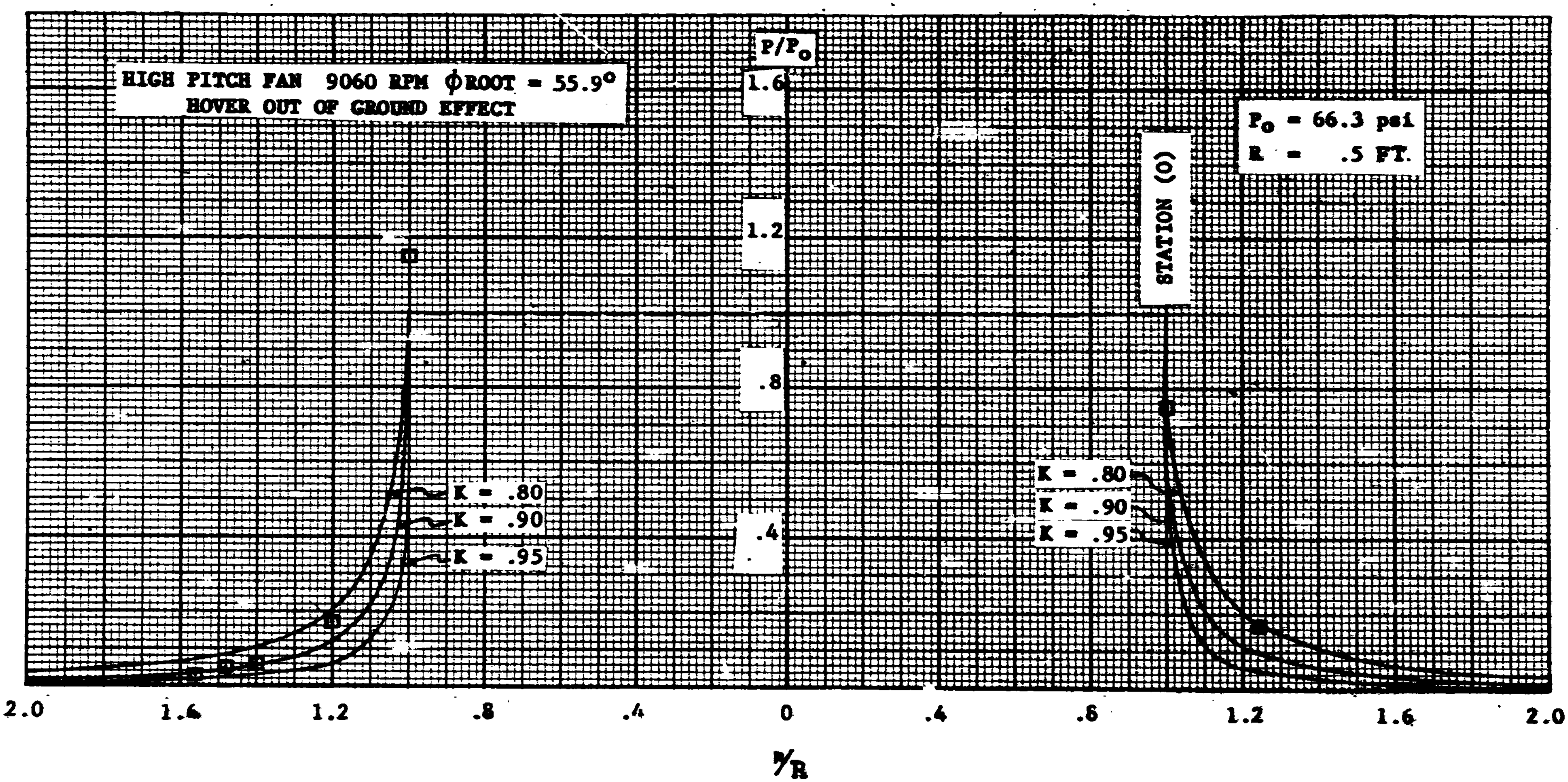

FIGURE 101

PRESSURE DISTRIBUTION NEAR FAN

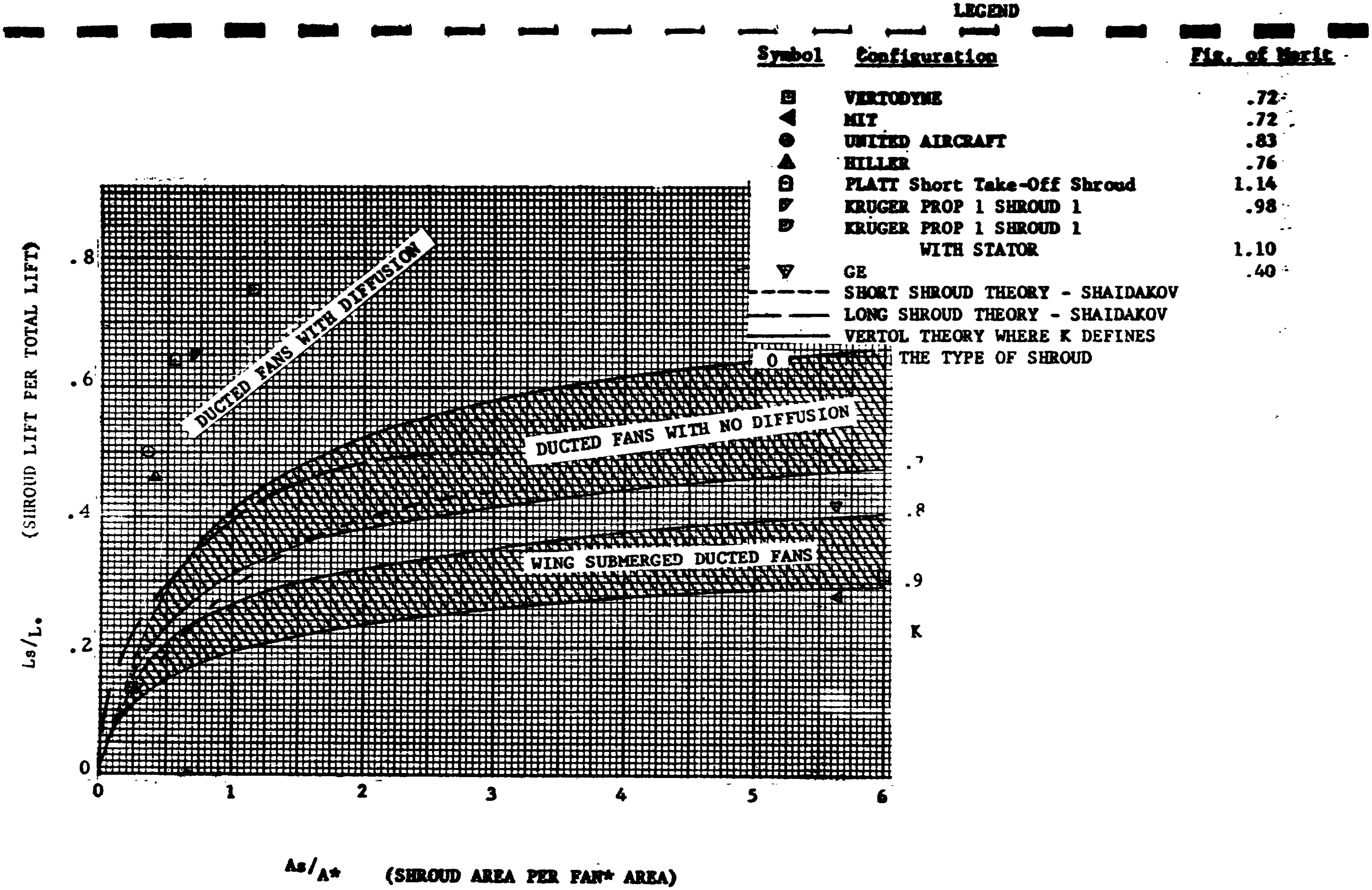

FIGURE 102

STATIC THRUST DISTRIBUTION

TYPE OF SHROUD		K
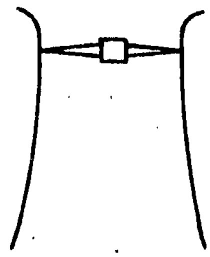	Ducted Fan With Diffusion	Not Applicable
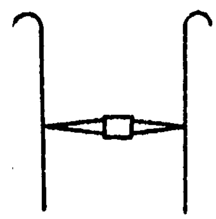	Ducted Fan With No Diffusion Long Shroud	0 - .40
	Ducted Fan With No Diffusion Short Shroud	.40 - .75
	* Wing Submerged Ducted Fan	.75 - .95

FIGURE 103

REPRESENTATIVE VALUES OF K

* GE WILL PROBABLY BE IN THIS RANGE WITHOUT MOTOR INTERFERENCE

PART VI

CONCLUSIONS

VI. CONCLUSIONS

The conclusions obtained from the Vertodyne Test Program, as well as their correlation with accomplishments by others in this field, are as follows:

1. Forward flight characteristics indicate a significant increase in lift due to the fan at negative as well as positive angles of attack (See Page 55).

2. Large magnitude nose up pitching moments were recorded for the model in forward flight. These were caused by high induced lift on the wing leading edge relative to that on the trailing edge (See Page 28).

3. Total model static thrust is greater than the thrust of the fan due to induced lift on the wing upper surface and bell mouth (See Page 28).

4. Model static thrust obtained for a constant fan rotational speed increases in ground effect (See Page 28).

5. Model static thrust per horsepower decreases in ground effect (See Table IV).

6. Model lift per horsepower increases with increasing forward speed (See Figures 41 to 44).

7. The exit ducts which were used were ineffective in turning the fan exit air aft, and did not produce a significant reduction in drag (See Page 60 and Figures 45 to 62).

8. Static shroud and propeller lifts may be predicted by determining a shroud shape factor (K) (See Figure 103).

9. The majority of static data has a Figure of Merit (M) between .70 and .75 together with a C_{T_O}/σ between .10 and .35 (See Page 91).

10. Vertol and GE-NASA lift data, at zero angle of attack, may be predicted from static data by determining a Static Factor (SF). See Page 92.

11. The important correlation parameters are q [illegible], J_p, L_o, M, C_{T_O}, σ, A, Ap, and S (See Pages 92 and [illegible]

PART VII

RECOMMENDATIONS

VII. RECOMMENDATIONS

The recommendations, itemized below, represent the observations of Boeing-Vertol based upon analytical studies performed under the Vertodyne Test Program in addition to data correlated by a survey of other non-company investigations into wing-submerged ducted fan configurations.

1. The GE-NASA and Vertol data correlate very well, but this is considered to be a limited scope correlation and futher correlation would be profitable. The most important correlation factors are discussed in Section VI of this report.

2. In future tests, the propeller lift should be measured in and out of the wind tunnel. This would minimize limitations on correlated data.

3. More wing-submerged fan tests should be conducted using a flexible model designed with a variable fan area. These tests would expand the scope of correlation studies and predict general performance.

4. Parametric studies should be undertaken using the parameters determined by an expanded scope correlation.

This study could then be directed toward design and fabrication of a full scale wing-submerged fan vehicle.

VIII. REFERENCES

1. Vertol Aircraft Corporation, Final Summary Report Comparative Study VTOL Aircraft, Report No. R-85.

2. General Electric Company Flight Propulsion Laboratory Department, Preliminary Study Data, Convertible Propulsion Systems for VTOL Aircraft, June 1958.

3. Hickey, D. H.,Preliminary Investigation of the Characteristics of a Two-Dimensional Wing and Propeller with the Propeller Plane of Rotation in the Wing-Chord Plane. NACA RM A S7F03, August 1957.

4. Fay, C. B.,Characteristics of a Shrouded Rotor in a Cross Flow, Massachusetts Institute of Technology, M. S. Thesis, June 1957.

5. Wardlow, R. L. and Templin, R. J., Preliminary Wind Tunnel Tests of a Lifting Fan in a Two-Dimensional Aerofoil, National Aeronautical Establishment (Canada) Report LR-207, September 1957.

6. Ham, N. D. and Moser, H. H., Preliminary Investigation of a Ducted Fan in Lifting Forward Flight, Massachusetts Institute of Technology, June 1958.

7. von Glahn, U., Exploratory Study of Ground Proximity Effects on Thrust of Annular and Circular Nozzles, NACA TN 3982, April 1957.

8. Taylor, R. T., Experimental Investigation of the Effects of Some Shroud Design Variables on the Static Thrust Characteristics of a Small Scale Shrouded Propeller Submerged in a Wing, January 1958.

9. Vertol Aircraft Corporation, Proposal for Vertodyne Wind Tunnel Program Extension, Report No. PR-240, March 1958.

10. Switzer, J. R., VTOL Wing-Fan Model Tests, General Electric Company, Flight Propulsion Laboratory, Report No. R58AGT953, 1959.

11. Hickey, D. H. and Ellis, D. R., Wind Tunnel Tests of a Semi-Span Wing with a Fan Rotating in the Plane of the Wing, NASA TN-D-?8, October 1959.

12. Moser, H. H. and Livingston, C. L., Experimental and Analytic Study of the Ducted Fan and Fan-In-Wing in Hovering and Forward Flight, Massachusetts Institute of Technology, ASTIA Document No. 213316, January 1959.

13. Wardlaw, R. L. and McEachern, N. V., A Wing-Submerged Lifting Fan: Wind Tunnel Investigations and Analysis of Transition Performance, National Aeronautical Establishment (Canada) Report LR-243 April 1959.

14. Vertol Division, The Boeing Company, The Vertodyne VTOL Aircraft Study Semi-Span Model Tests in Hovering and Forward Flight, Report No. R-158, March 1960.

15. Gill, W. J., Wind Tunnel Tests of Several Ducted Propellers in Non-Axial Flow, Advanced Research Division of Hiller Aircraft Corporation, Report No. ARD-224, April 1959.

16. Sacks, A. H. and Burnell, J. A., Ducted Propellers - A Critical Review of the State of the Art, Advanced Research Division of Hiller Aircraft Corporation, Report No. ARD-232, June 1959.

17. Grose, R. M., Wind Tunnel Tests of Shrouded Propellers at Mach Numbers from 0 to .6, United Aircraft Corporation, ASTIA Document No. AD-205464, WADC Technical Report 58-604.

18. Platt, Jr., R. J. Static Tests of a Shrouded and an Unshrouded Propeller, NACA RM No. L7H25, February 1948.

19. Kruger, W., On Wind Tunnel Tests and Computations Concerning the Problem of Shrouded Propellers, NACA TM No. 1202, February 1949.

20. Streeter, V. L., Fluid Mechanics, 3rd Edition.

21. Eshbach, Handbook of Engineering Fundamentals, 2nd Edition.

22. Shaidakov, V. I., Influence of the Position of the Fan in the Shroud on Aerodynamic Characteristics of the Assembly in Hovering, Aviationnaya Technuika, February 1960.

PART VIII

REFERENCES

VIII. REFERENCES (Continued)

23. Duvivier, J. F., and McCallum R. B., Investigation of Tilting Duct and Fan-Wing in Transition Flight, Massachusetts Institute of Technology TRECOM Technical Report 61-19, December 1960.

PART IX

APPENDICES

APPENDIX A

WIND TUNNEL PROGRAM AND LOG OF TEST RUNS

1. Wind Tunnel Program
2. Wind Tunnel Test Log
3. Static Test Log

APPENDIX A

Test log data are presented in this Appendix. Section 1, Vertodyne Tunnel Program, was the proposed test schedule. Section 2, Wind Tunnel Test Log, covers the actual series of tests run in the University of Detroit Wind Tunnel. Reference is made to Section 1 when discussing specific runs. It was necessary to modify the test schedule following the failure of the low pitch fan, and the subsequent appearance of discrepancies in the medium and high pitch fans. Section 3 covers the later series of static tests conducted in the test laboratory of the University of Detroit.

1. <u>VERTODYNE TUNNEL PROGRAM</u>
University of Detroit

Run No. 1 Duct covered
$V_o = 60$ mph
whence: V_o = Tunnel velocity
Vary α from $\alpha_{\text{negative stall}}$ to $\alpha_{\text{positive stall}}$

Record: <u>Model</u>

Lift
Drag
Pitching Moment
Pressure Distribution

Run No. 2 Repeat No. 1 at $V_o = 100$ mph ($q = 25.6$ lbs/ft^2)

Run No. 3 Repeat No. 1 at $V_o = 140$ mph

Run No. 4 Duct covered, flap deflected 20°
$V_o = 100$ mph

Run No. 5 Fan unpowered
$V_o = 100$ mph
Vary α from $\alpha_{\text{negative stall}}$ to $\alpha_{\text{positive stall}}$

Record: <u>Model</u>

Lift
Drag
Pitching Moment
Pressure Distribution

Run No. 6 Fan unpowered, flap deflected 20°
Same as Run No. 5

Run No. 7 Fan powered ($\phi_R = 25.0°$), low pitch
ϕ_R = Fan blade root angle setting
V_o = 30, 20, 50, 60 @ (8000 RPM)
Vary α from $\alpha_{\text{zero lift}}$ to α_{stall}, $\alpha = 2°$

Record:

<u>Model</u>	<u>Fan</u>
Lift	Thrust
Drag	Torque
Pitching Moment	Pitching Moment
Pressure Distribution	RPM

Run No. 8 Fan powered, fan exit flap 20°
Procedure same as Run No. 7

1. VERTODYNE TUNNEL PROGRAM (Continued)

Run No. 9 Fan powered, fan exit flap 40°
Procedure same as Run No. 7

Run No. 10 Fan powered, ($\phi_R = 39.7°$), medium pitch
V_o = 30, 50, 75, 100 mph
Vary α from α zero lift to α stall, $\Delta\alpha$ = 2°

Record:

Model	Fan
Lift	Thrust
Drag	Torque
Pitching Moment	Pitching Moment
Pressure Distribution	RPM

Run No. 11 Fan powered, fan exit flap 20°
Procedure same as Run No. 10

Run No. 12 Fan powered, fan exit flap 40°
Procedure same as Run No. 10

Run No. 13 Fan powered, ($\phi_R = 55.9°$), high pitch
V_o = 40, 60, 100, 140 mph
Vary α from α zero lift to α stall, $\Delta\alpha$ = 2°

Record:

Model	Fan
Lift	Thrust
Drag	Torque
Pitching Moment	Pitching Moment
Pressure Distribution	RPM

Run No. 14 Fan powered, fan exit flap 20°
Procedure same as Run No. 13

Run No. 15 Fan powered, fan exit flap 40°
Procedure same as Run No. 13

Run No. 16 Fan powered, low pitch fan, outer panel removed
V_o = 40, 60, 80 mph
Vary α from α zero lift to α stall, $\Delta\alpha$ = 2°

Record:

Model	Fan
Lift	Thrust
Drag	Torque
Pitching Moment	Pitching Moment
Pressure Distribution	RPM

Run No. 17 Fan Powered, low pitch, outer panel removed
Fan exit flap 20°
Procedure same as Run #16

Run No. 18 Fan powered, low pitch, outer panel removed
Fan exit flap 40°
Procedure same as Run #16

1. VERTODYNE TUNNEL PROGRAM (Continued)

Run No. 19 Fan powered, medium pitch, outer panel removed
V_o = 40, 60, 80, 100 mph
Vary α from $\alpha_{\text{zero lift}}$ to α_{stall}, $\Delta\alpha = 2^\circ$

Record:

Model	Fan
Lift	Thrust
Drag	Torque
Pitching Moment	Pitching Moment
Pressure Distribution	RPM

Run No. 20 Fan powered, medium pitch, outer panel removed
Fan exit flap 20°
Procedure same as Run No. 19

Run No. 21 Fan powered, medium pitch, outer panel removed
Fan exit flap 40°
Procedure same as Run No. 19

Run No. 22 Fan powered, high pitch, outer panel removed
V_o = 40, 60, 100, 140 mph
Vary α from $\alpha_{\text{zero lift}}$ to α_{stall}, $\Delta\alpha = 2^\circ$

Record:

Model	Fan
Lift	Thrust
Drag	Torque
Pitching Moment	Pitching Moment
Pressure Distribution	RPM

Run No. 23 Fan powered, high pitch, outer panel removed
Fan exit flap 20°
Procedure same as Run No. 22

Run No. 24 Fan powered, high pitch, outer panel removed
Fan exit flap 40°
Procedure same as Run No. 22

2. WIND TUNNEL TEST LOG

A. March 4 - March 19, 1958

March 4-10:

Finished installation of the Vertodyne model in the wind tunnel test section. The work involved installing the "ground plane", building and installing a fairing around the model motor enclosure to minimize tare drag reading into the balance system, connecting the 92 pressure pickups to the 100 tube monometer bank and calibrating the angle of attack indicator.

March 11:

Made first wind tunnel runs. Run No. 1 and No. 2 were made as defined in the Vertodyne Wing Tunnel Program. Metal duct covers were used in place of cardboard covers in Run Nos. 2, 3, and 4.

March 12:

Run Nos. 3, 4, 5, and 6 were completed. Run Nos. 3 and 4 were with the duct covered; Nos. 5 and 6 were with the medium pitch fan installed and unpowered.

March 13:

Model was partially dismantled in order to free the fan shaft. Also, a fairing was made to eliminate the gap between the model and the ground plane.

March 14-17:

Run Nos. 5 and 6 were repeated in order to substantiate the nonlinearity of the lift curve at small angles of attack found in the earlier runs. These repeats, Run Nos. 5a and 6a, gave data at two degree increments, and checked very well with the earlier runs.

March 18-19:

The generator supplying power for the Vertodyne model was dismantled and sent to Spaulding Corporation of Detroit to be balanced and checked in preparation for the "powered" phase of the Vertodyne program.

B. March 25 - April 3

March 25:

Started Run No. 7, V = 40 mph. Pronounced shaking in the strain gage recorders prevented testing angles of attack above 28°.

Run No. 7, V = 60 mph was stopped at 26° angle of attack, due to loss of low pitch fan. No damage to model, hub badly damaged - all blades destroyed. One blade among 13 could not be located.

2. WIND TUNNEL TEST LOG (Continued)

March 26:

Repaired tunnel and had special washers made to prevent a recurrence of fan leaving the model. Checked tunnel and model, using medium pitch fan. Took "zero readings" for Run No. 10, V = 40 mph, but during the run-up of fan, No. 2 strain gage recorder went erratic. No. 2 thrust gage in model was replaced.

March 27:

Calibrated new thrust gage. Proceeded with Run No. 10, V = 40 mph. Encountered loud "screech" noise at 14° angle of attack. The same noise could be reproduced at all positive angles of attack at very low tunnel speeds. The noise was seemingly aerodynamic rather than mechanical.

March 28:

Proceeded with Run No. 10, V = 60, 80 and 100 mph, limiting the angles of attack to 16° in order to avoid conditions which apparently cause the "screech" noise. An additional run was added to the program, testing the Vertodyne model at 80 mph with wing flap deflected 20°.

March 29:

Run Nos. 11 and 12 were started and completed with no difficulties occurring.

March 31:

The high pitch fan was installed and run up to 9500 rpm. The model motor, however, could not be cooled enough to continue; therefore, the fan was shut down and the model was disassembled in order to check water leaks.

April 1:

After reassembling the model and running the fan at 9060 RPM, the model motor temperatures were checked and found to be within the motor limits. Thus, the high pitch fan runs were conducted at 9060 RPM rather than the design speed of 10,000 RPM. Run No. 13, V = 40 mph was started and completed.

April 2:

Run No. 13, V = 60, 100, 140 and 120 mph were completed. Run No. 13, V = 100 mph, flap angle at 20°, was completed. Run No. 15, V = 40, 60, 100 and 120 mph were completed.

While inspecting the fan, some small cracks were found in the fan blades. The medium and high pitch fans were then packed and prepared for a "Zyglo" inspection process.

2. WIND TUNNEL TEST LOG (Continued)

April 3:

The Zyglo process indicated that cracks had developed in both fans, thus the wind tunnel program was terminated. These indications later proved to be erroneous.

3. **LOG OF STATIC TEST RUNS - VERTODYNE STATIC TEST PROGRAM**
University of Detroit, August 26-28, 1958

DATE	RUN NO.	FAN ØRoot°	RPM	h/D
August 26	1a	39.7	6,000	∞
	1a	39.7	7,200	
	1a	39.7	8,000	
	1a	39.7	9,000	
	2a	39.7	10,030	
	3a	55.9	6,000	
	3a	55.9	8,000	
	3a	55.9	9,060	
	3a	55.9	8,490	
	3a	55.9	8,280	
	3a	55.9	8,760	
	3a	55.9	8,960	
August 27	3b	55.9	9,030	4.0
	1b	39.7	6,060	4.0
	2b	39.7	10,000	4.0
	1c	39.7	6,000	2.0
	2c	39.7	10,000	2.0
	3c	55.9	9,060	2.0
	3c'	55.9	9,120	2.0
	3d	55.9	9,060	1.0
	1d	39.7	6,000	1.0
	2d	39.7	10,030	1.0
	1e	39.7	6,030	0.75
	2e	39.7	10,000	0.75
	3e	55.9	9,030	0.75
	3f	55.9	9,060	0.5
	1f	39.7	6,030	0.5
	2f	39.7	10,000	0.5
	1a'	39.7	6,060	∞
	2a'	39.7	10,000	
	3a'	55.9	9,000	
	1a''	39.7	6,000	
	2a''	39.7	10,000	
	3a''	55.9	9,000	
	3f'	55.9	9,000	0.5
	3g	55.9	9,060	0.3
	1g	39.7	6,060	0.3
	2g	39.7	9,930	0.3
August 28	2f'	39.7	60,000	0.5
	1c'	39.7	60,000	2.0
	2c'	39.7	9,960	2.0
	3c'	55.9	9,090	2.0
	3a'''	55.9	9,600	
	3a'''	55.9	9,450	
	3a'''	55.9	9,180	
	3a'''	55.9	9,000	

APPENDIX B

WIND TUNNEL BALANCE SYSTEM

DATA PLOTS

Forward flight test data plots obtained from the University of Detroit are presented in this appendix. The symbols used differ slightly from those used in the main body of the report. A list of symbols for Appendix B has been included.

APPENDIX B

LIST OF FIGURES

(All are plots of lift, drag, and pitching moment coefficients vs. wing angle of attack)

FIGURE NO.	TITLE
B-1	Basic Wing Data, Fan Hole Covered
B-2	Basic Wing with Duct Open
B-3	Low Pitch Fan Data
B-4	Medium Pitch Fan Data
B-5	Medium Pitch Fan Data with 20° Exit Duct
B-6	Medium Pitch Fan Data with 40° Exit Duct
B-7	High Pitch Fan Data
B-8	High Pitch Fan Data with 40° Exit Duct

SYMBOLS USED IN APPENDIX B

1. Basic Wing Data - Fan Not Rotating

Coefficient of Lift, $C'_L = \frac{\text{Lift Force}}{qs}$

Coefficient of Drag, $C'_D = \frac{\text{Drag Force}}{qs}$

Coefficient of Pitching Moment, $C'_{mt} = \frac{\text{Pitching Moment}}{qsc}$, with the center of moment the fan axis

2. Fan Powered

Coefficient of Lift, $C'_L = \frac{\text{Lift Force}}{\frac{1}{2}\rho S(wr^2)}$

Coefficient of Drag, $C_D = C'_D + \Delta C_{D_L}$

$$= \frac{\text{Net Drag Force}}{\frac{\rho}{2} S(wr)^2} + 0.01599 \, (C'_{LW})^2 \times \frac{q^2}{\frac{\rho}{2} (wr^2)^{\ 2}}$$

Coefficient of Pitching Moment,

$$C'_{mt} = \frac{\text{Pitching Moment}}{\frac{\rho}{2} Sc(wr)^2}$$

3. General

q	Forward speed velocity pressure
s	Wing area, square feet
C	Wing chord length, feet
ρ	Air density, slugs per cubic foot
w	Fan rotational velocity, radius per second
r	Fan rotor radius, feet
δ_{f_w}	Wing flap deflection, degrees
δ_{f_f}	Fan exit turning angle, degrees

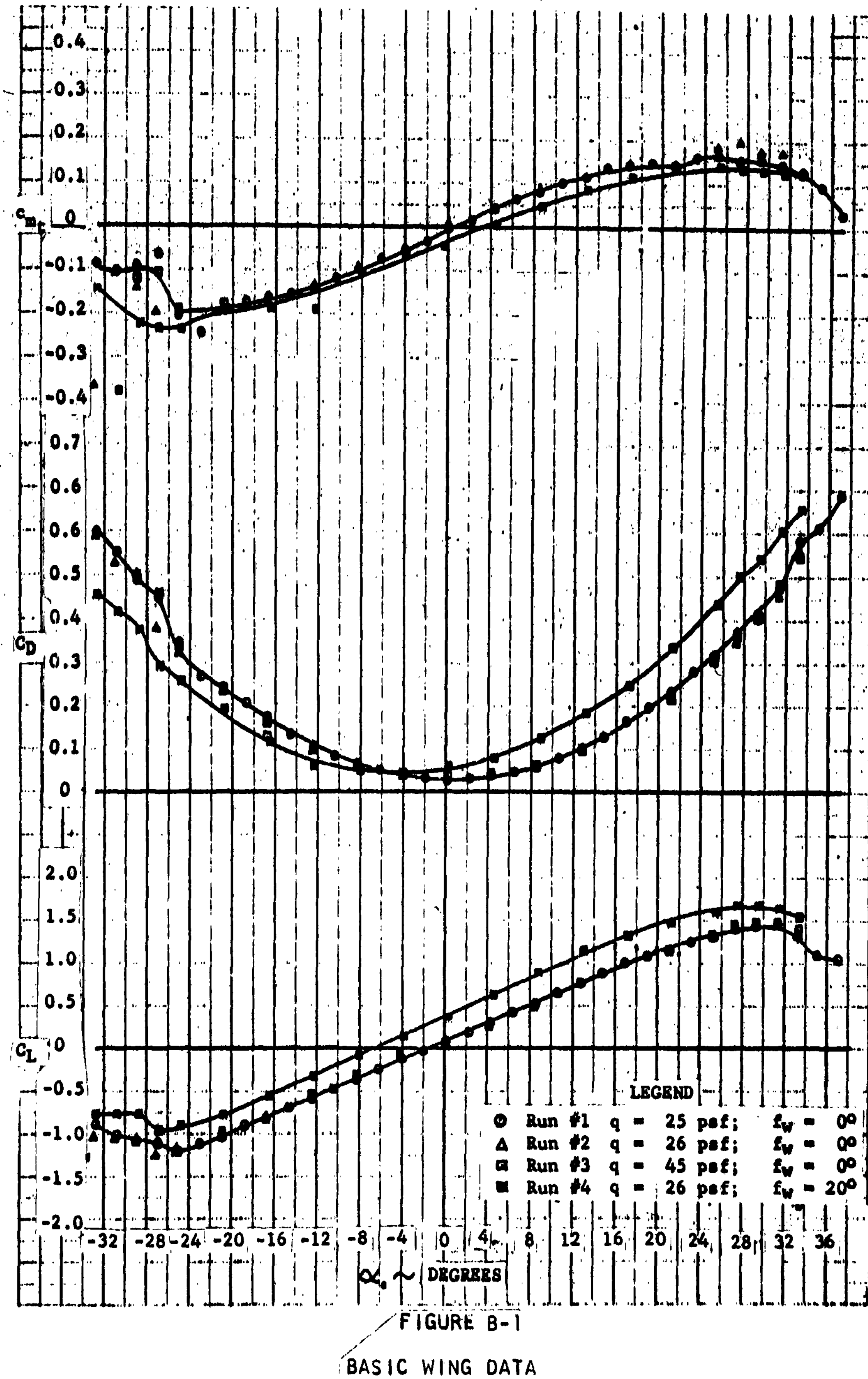

FIGURE B-1

BASIC WING DATA

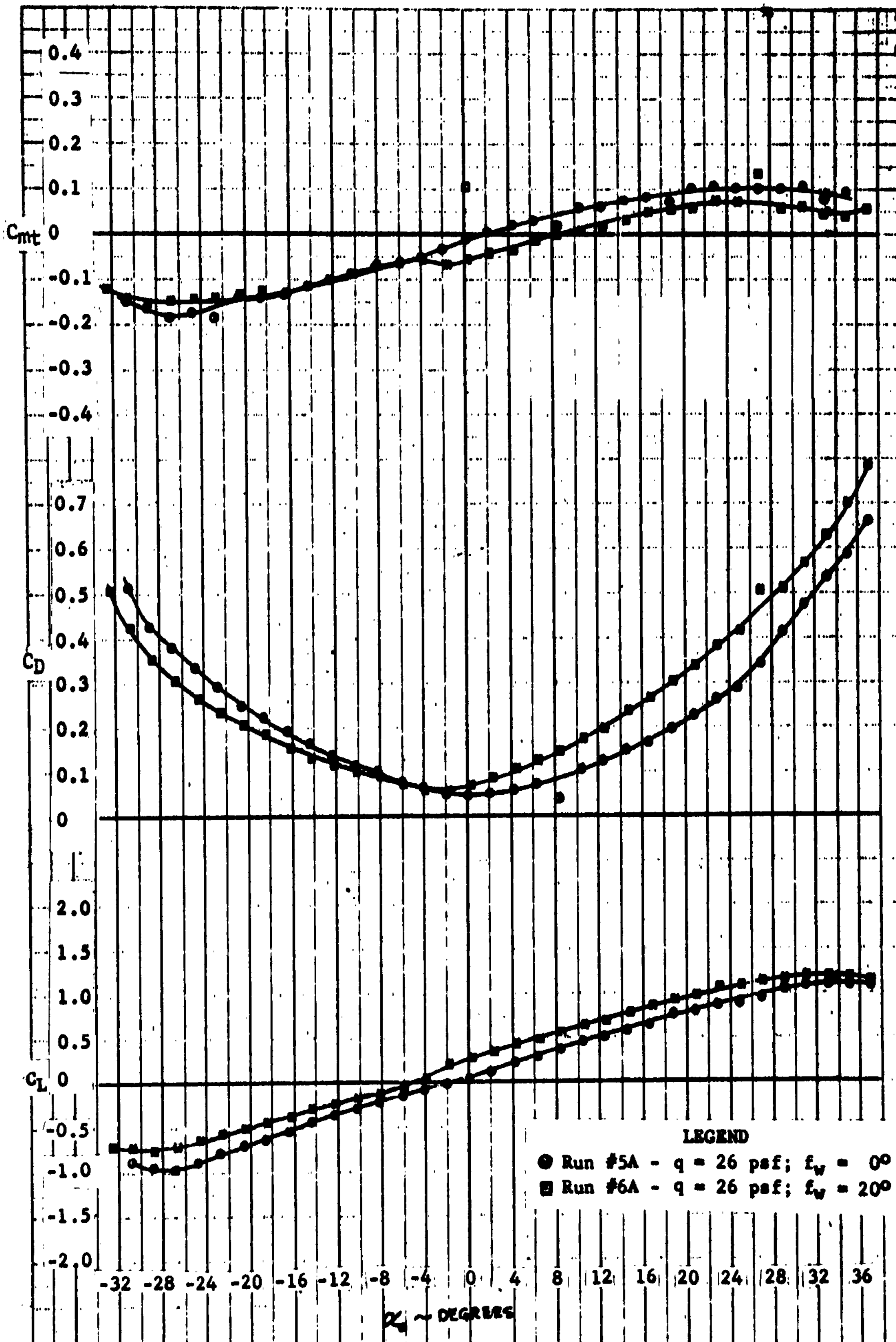

FIGURE B-2

BASIC WING WITH DUCT OPEN

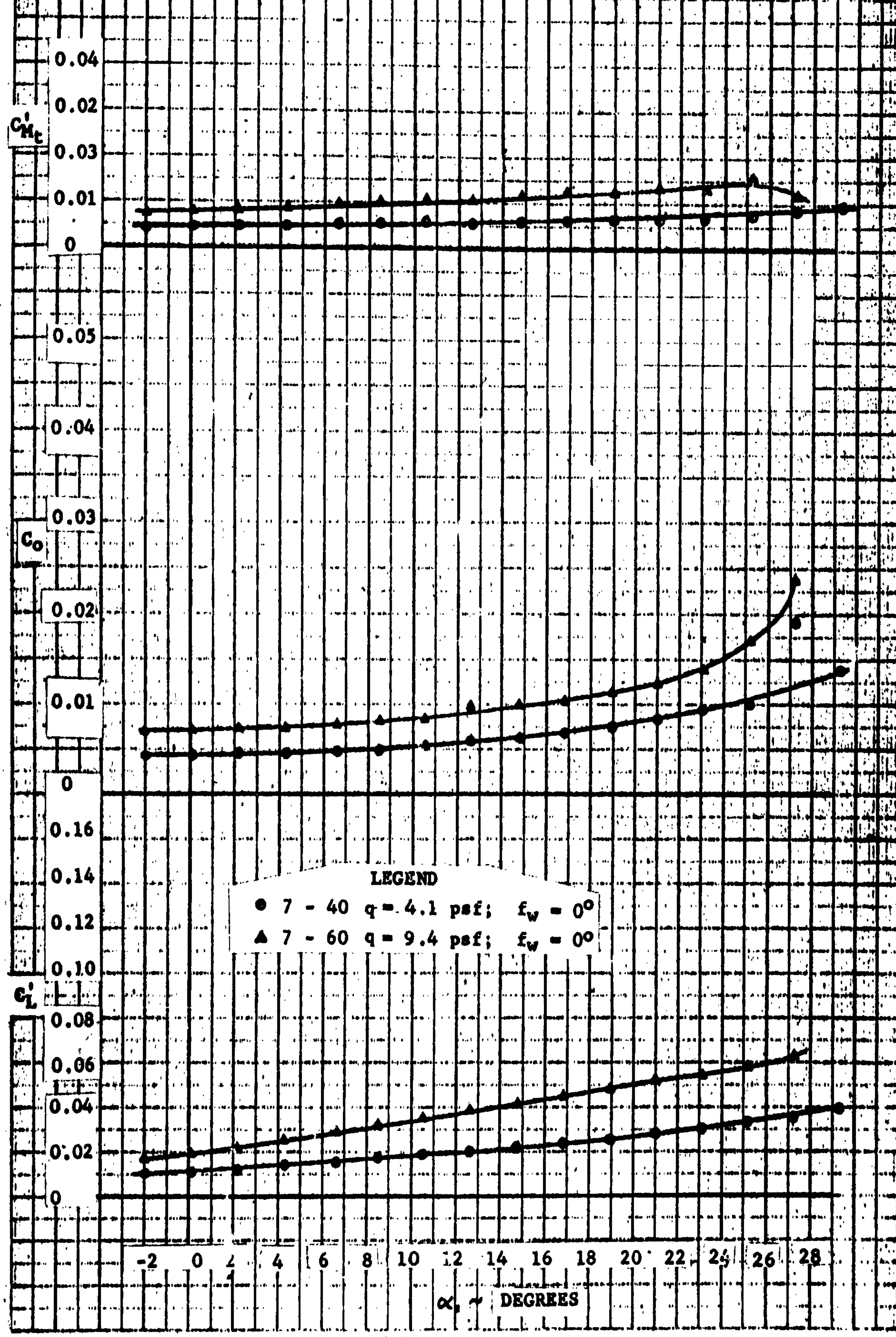

FIGURE B-3

LOW PITCH FAN DATA

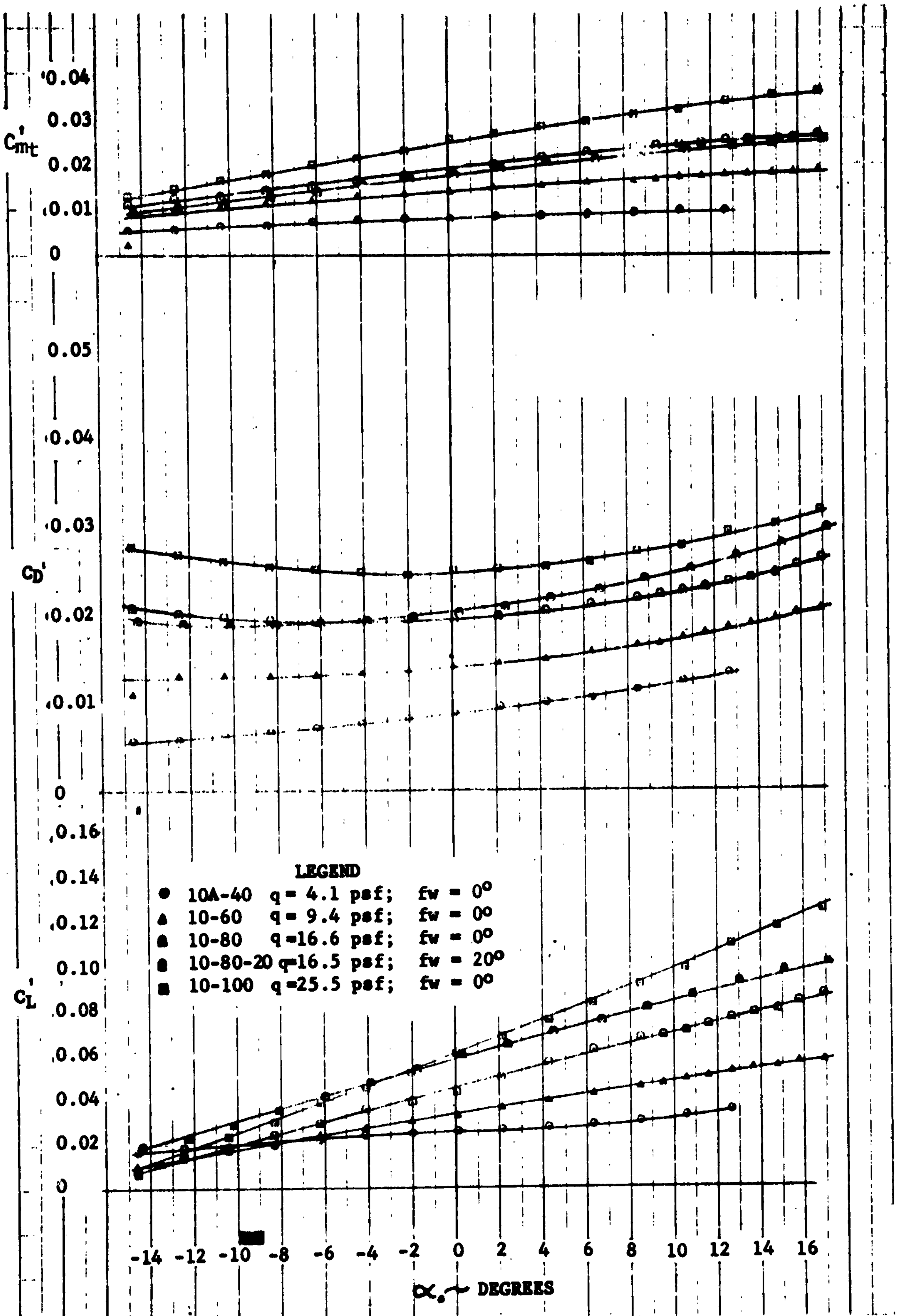

FIGURE B-4

MEDIUM PITCH FAN DATA

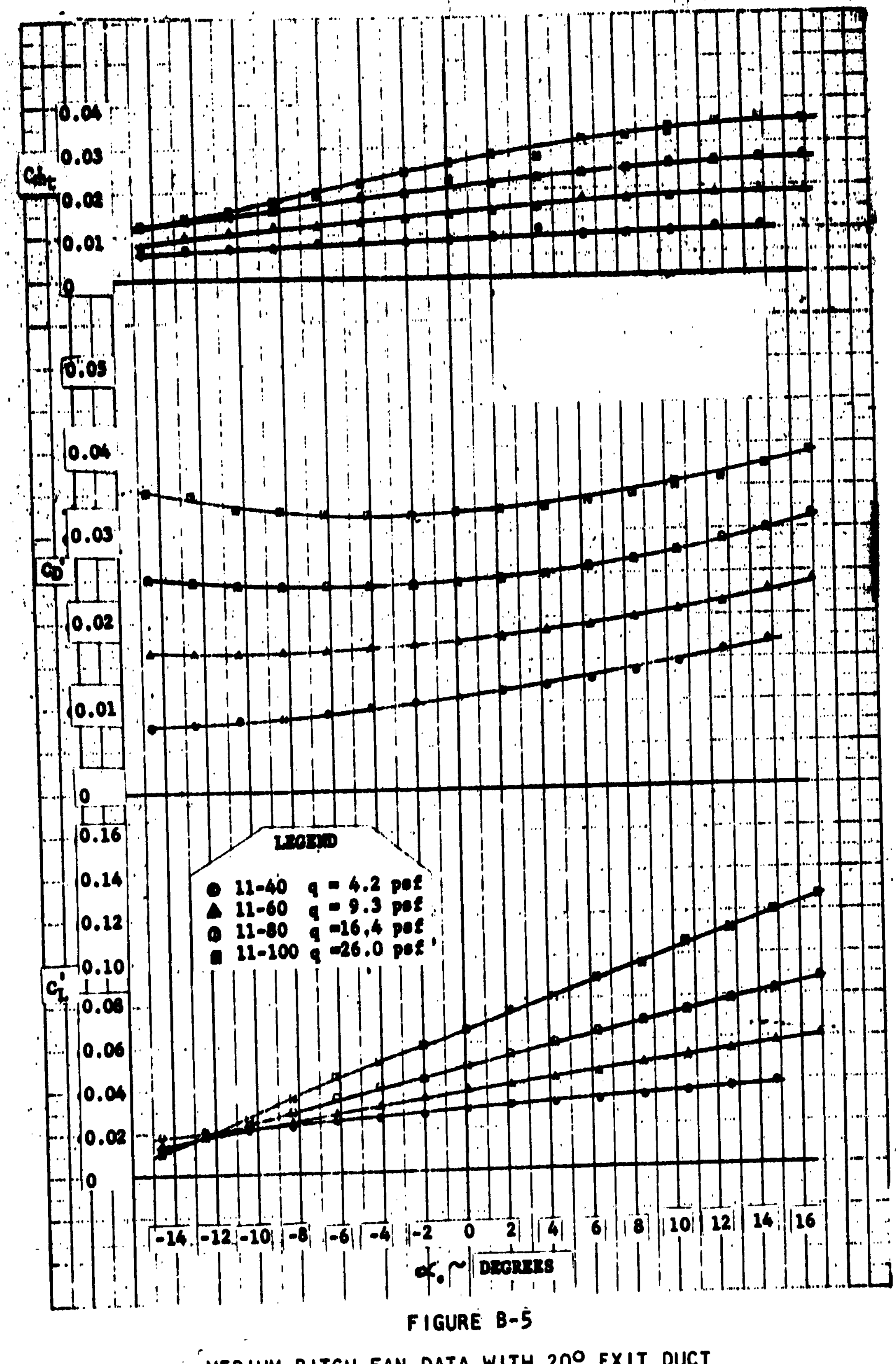

FIGURE B-5

MEDIUM PITCH FAN DATA WITH 20° EXIT DUCT

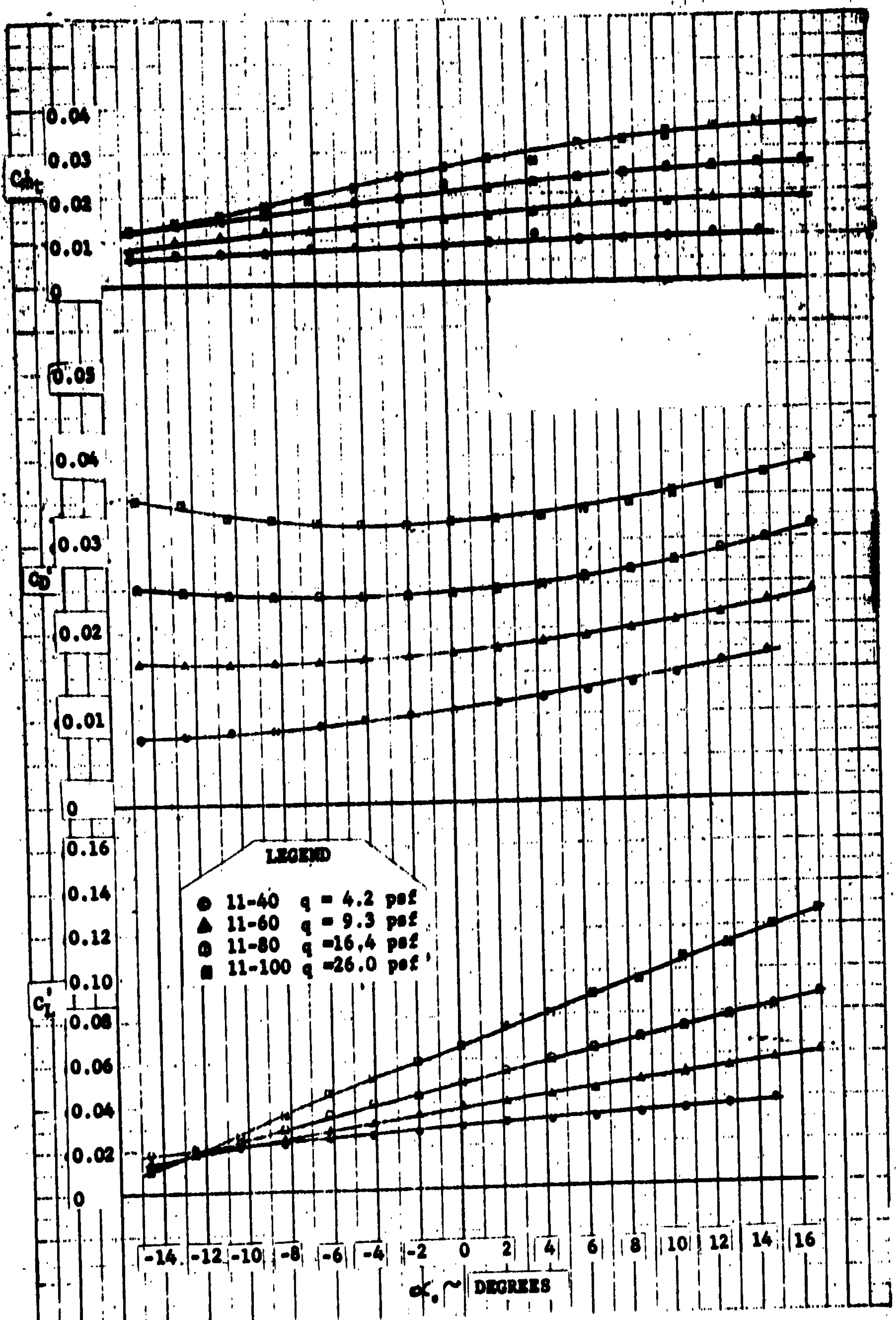

FIGURE B-5

MEDIUM PITCH FAN DATA WITH 20° EXIT DUCT

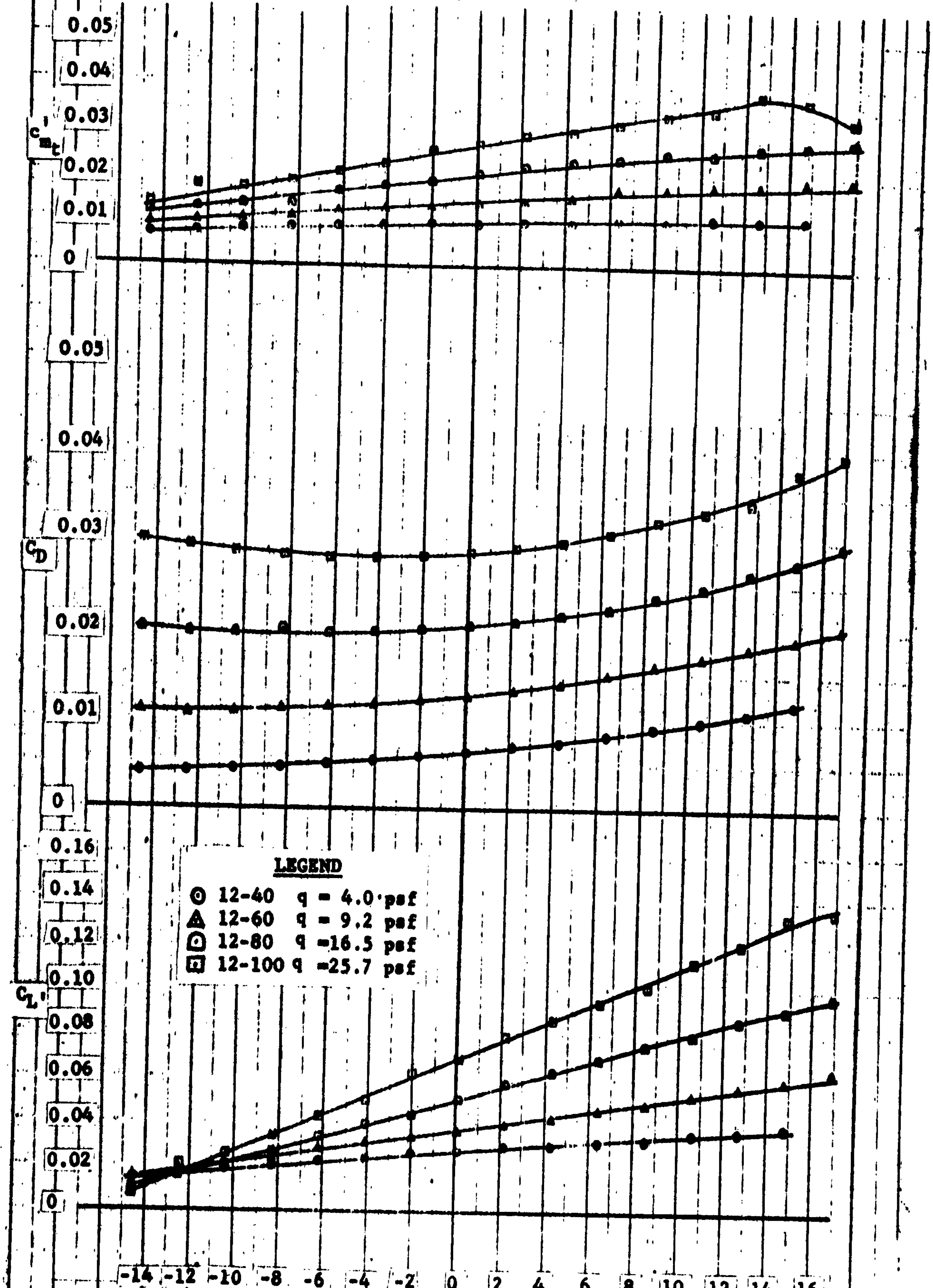

FIGURE B-6

MEDIUM PITCH FAN DATA WITH 40° EXIT DUCT

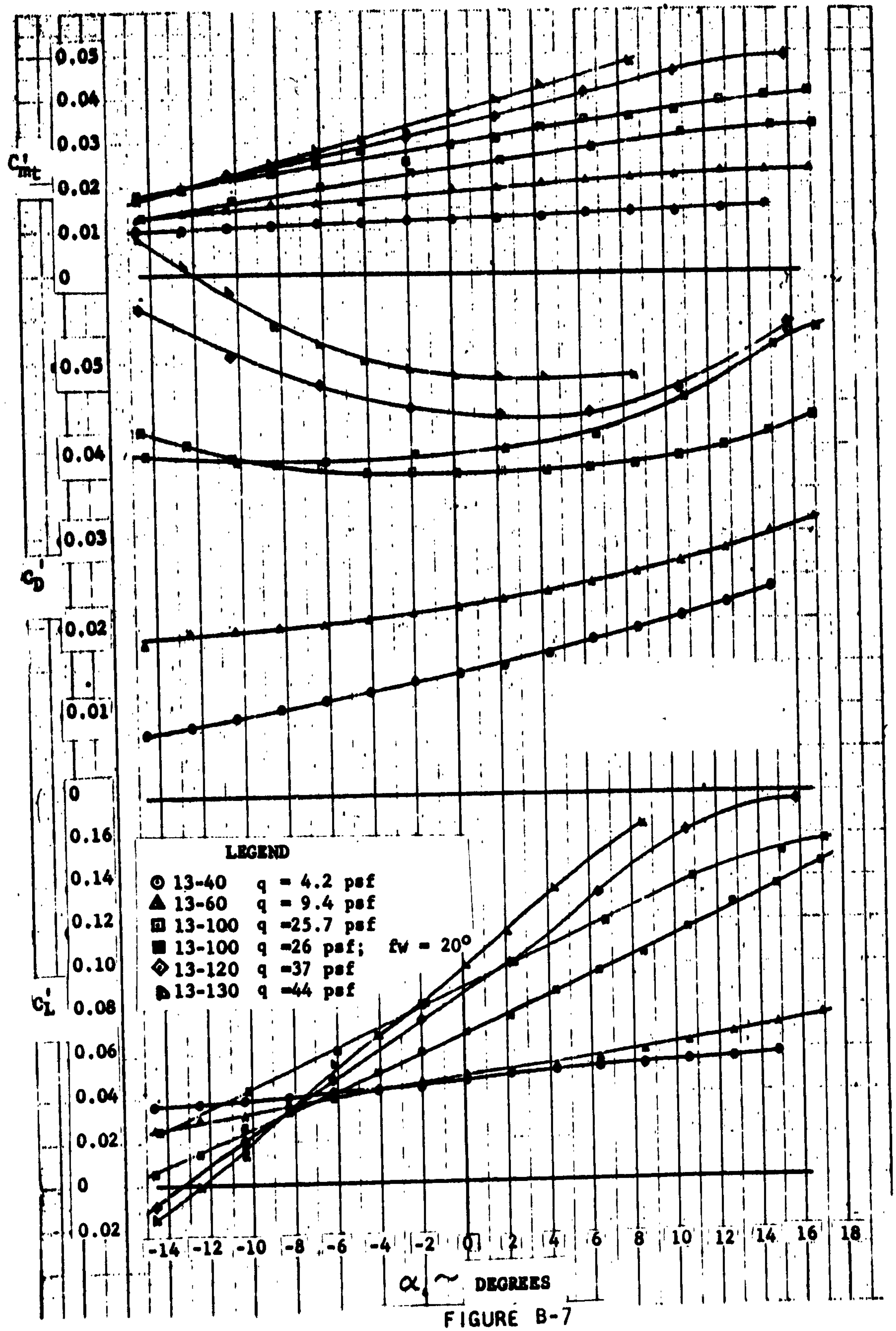

FIGURE B-7

HIGH PITCH FAN DATA

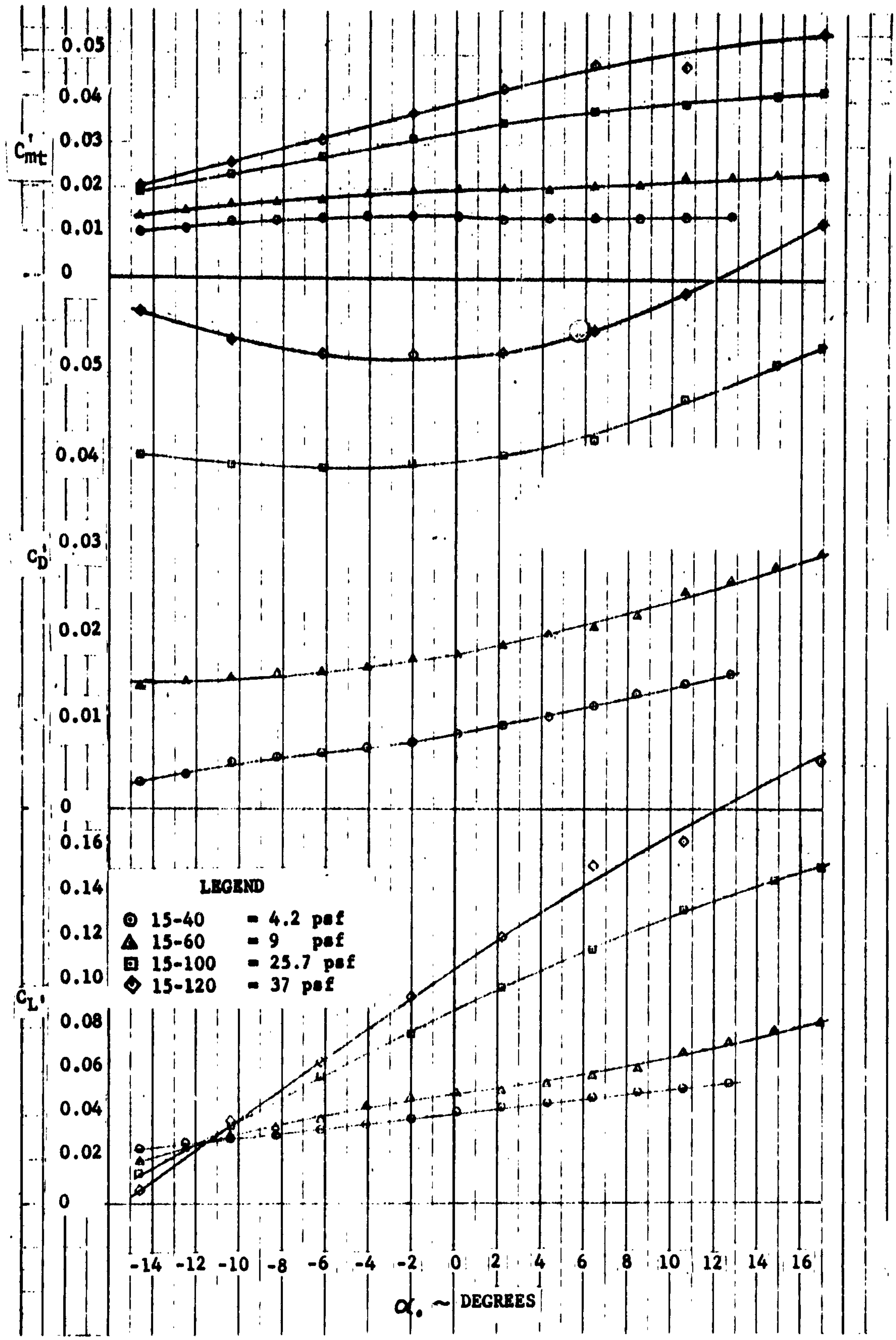

FIGURE B-8

HIGH PITCH FAN DATA WITH 40° EXIT DUCT

APPENDIX C

NONDIMENSIONAL PLOTS OF PHASE I AND PHASE II DATA

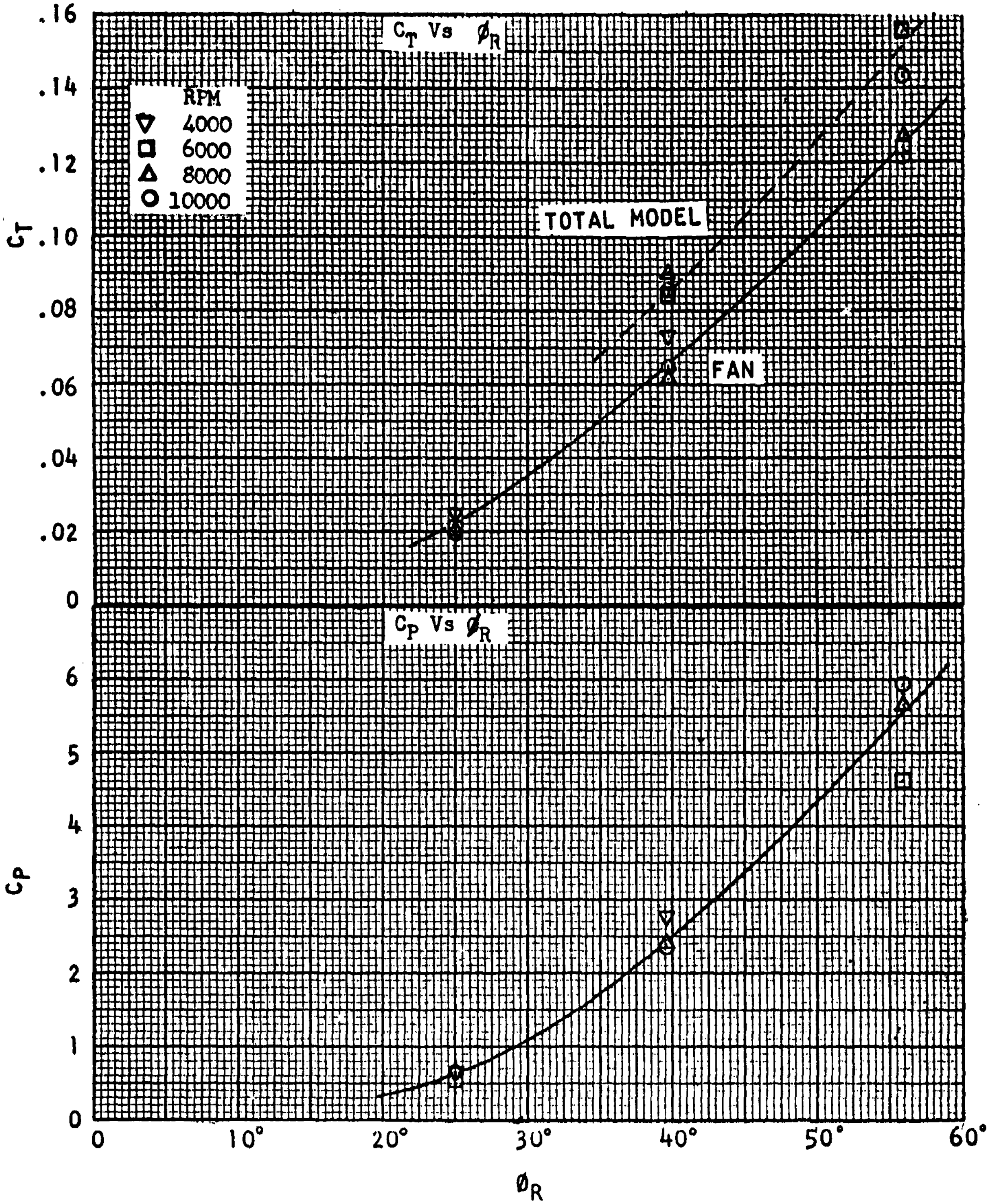

FIGURE C-1

MODEL STATIC C_T AND C_P VS $\emptyset_R$

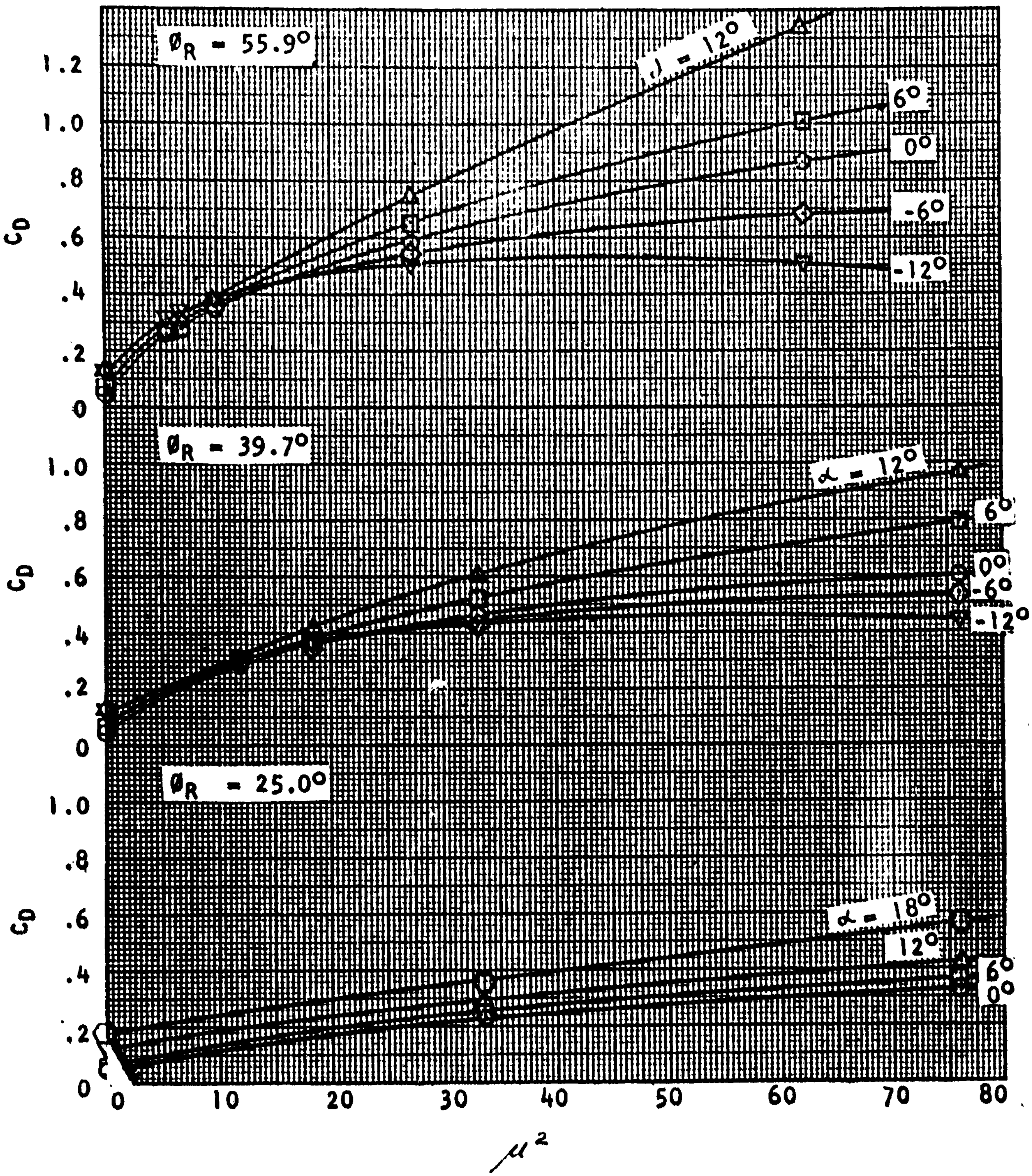

FIGURE C-3

MODEL C_D VS. μ^2

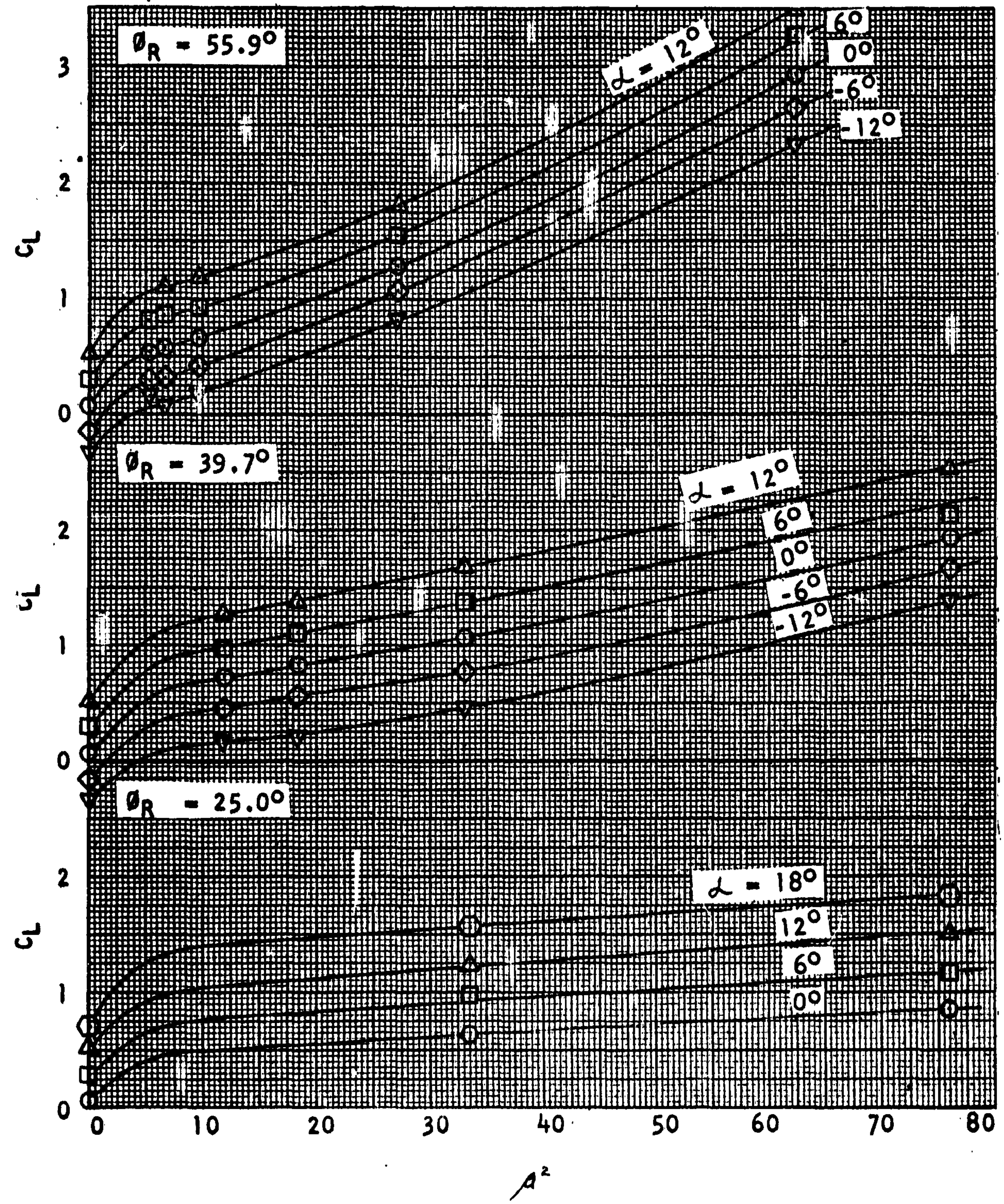

FIGURE C-2

MODEL C_L VS. μ^2

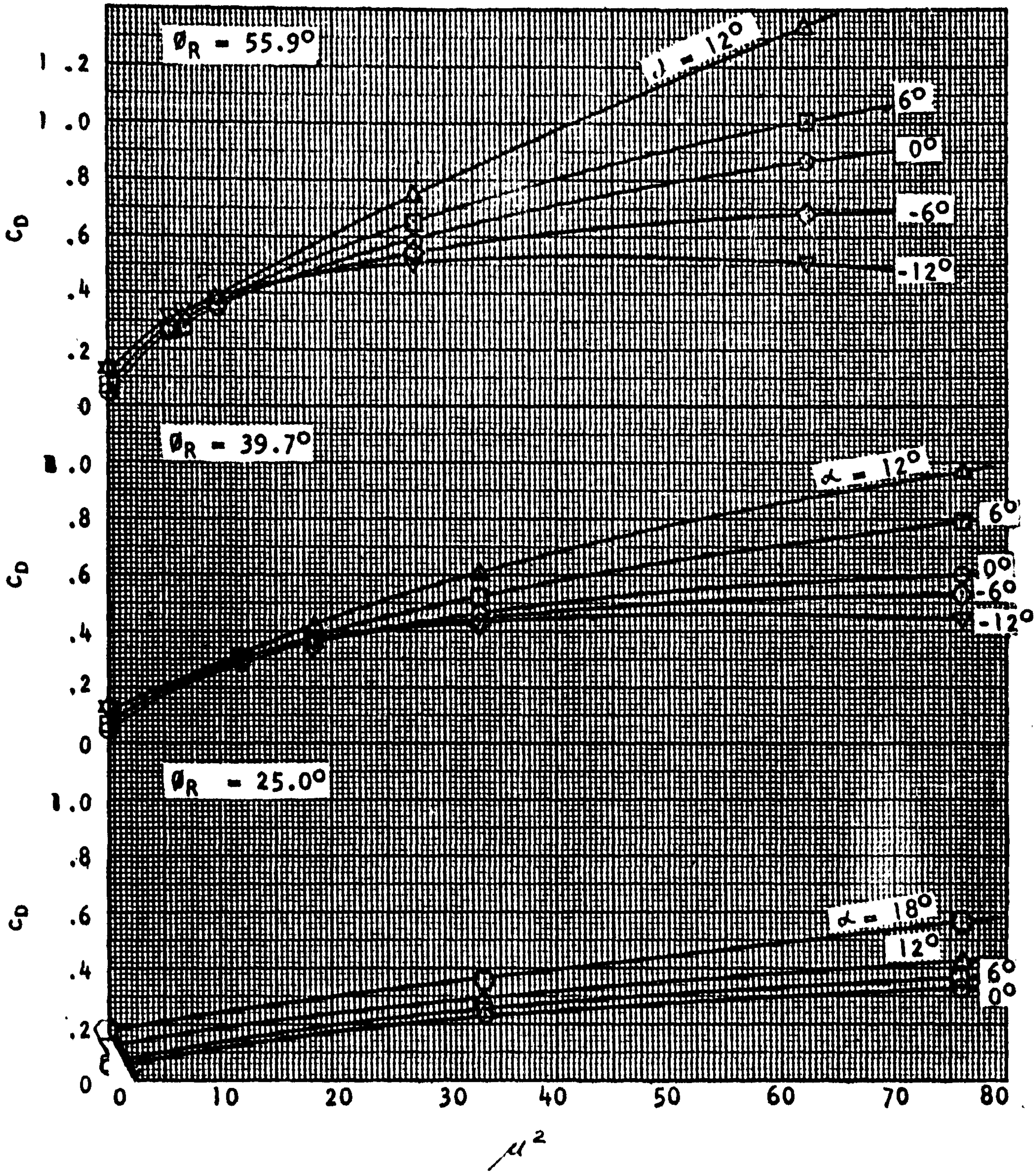

FIGURE C-3

MODEL C_D VS. μ^2

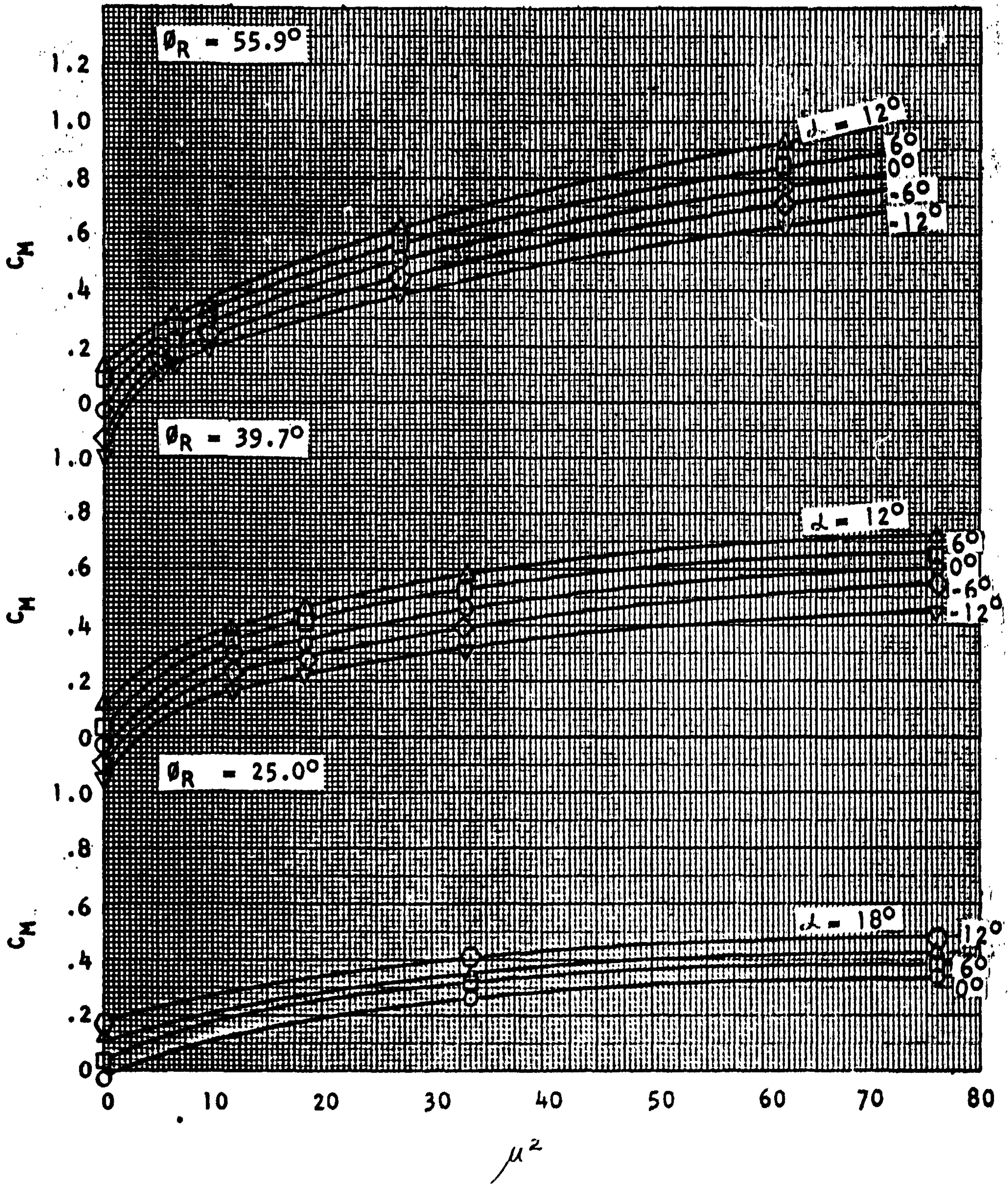

FIGURE C-4

MODEL C_M VS. μ^2

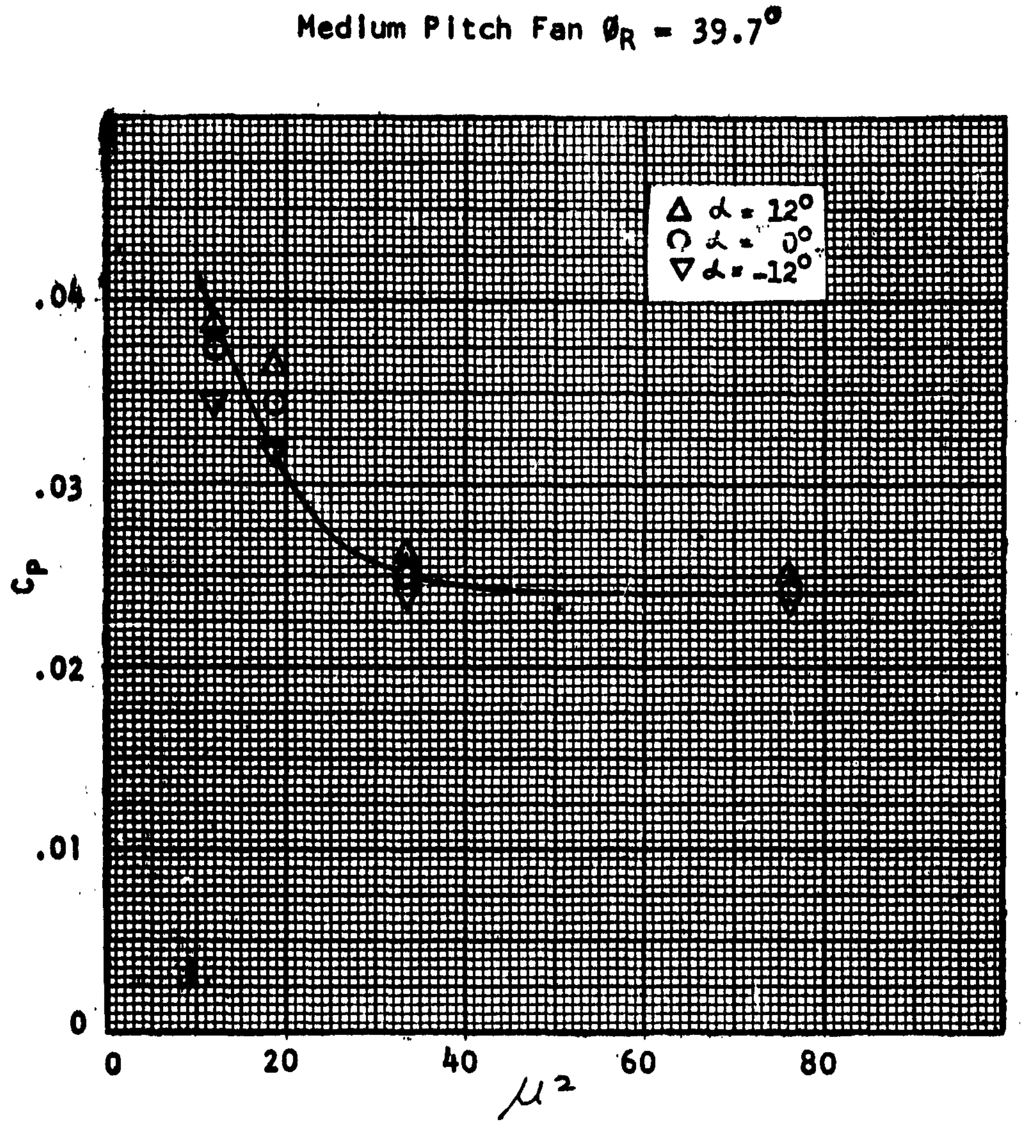

FIGURE C-5

MODEL C_P VS. μ^2

High Pitch Fan $\emptyset_R = 55.9^o$

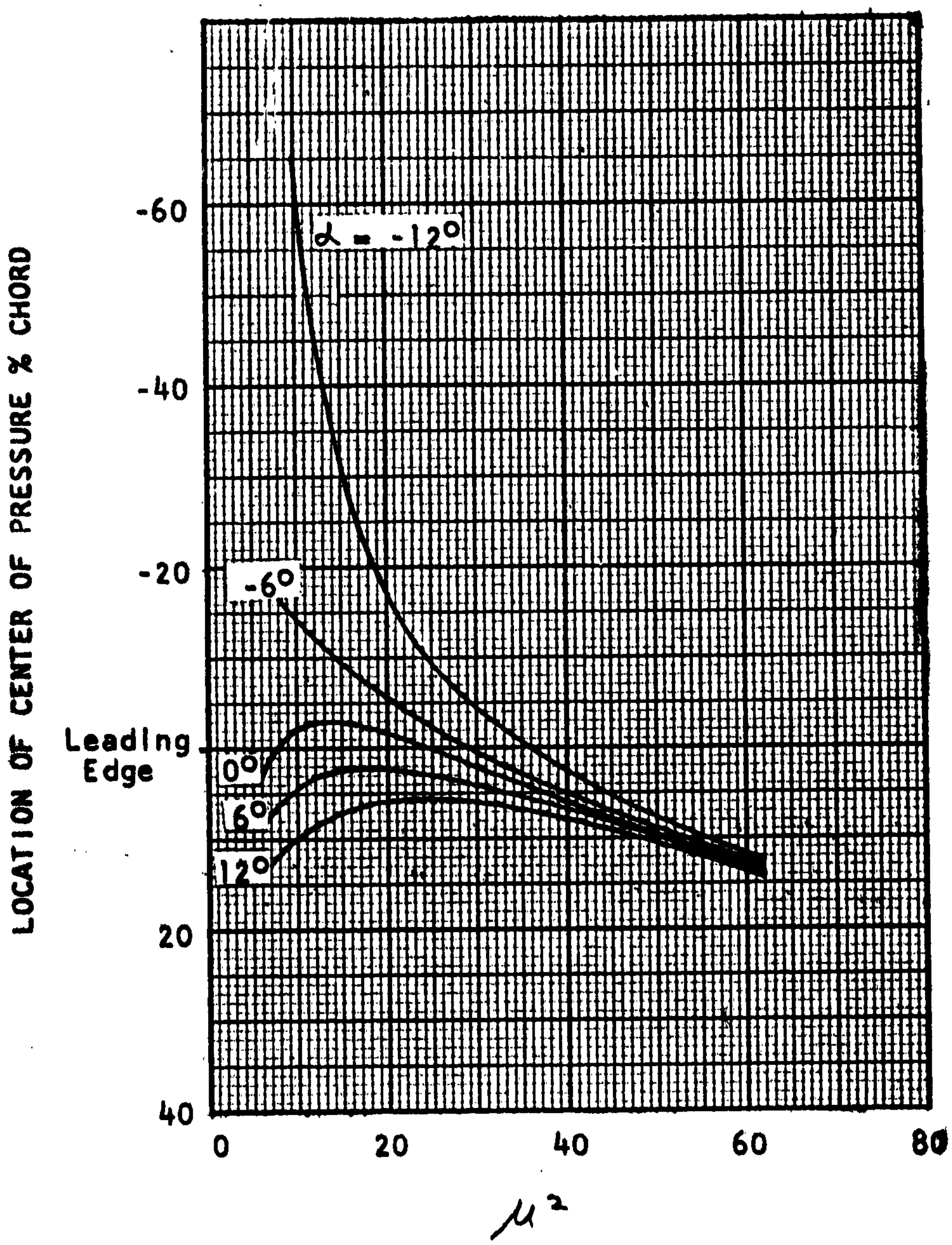

FIGURE C-6

LOCATION OF MODEL CENTER OF PRESSURE VS. μ^2 ; $\emptyset_R = 55.9$

Medium Pitch Fan $\phi_R = 39.7°$

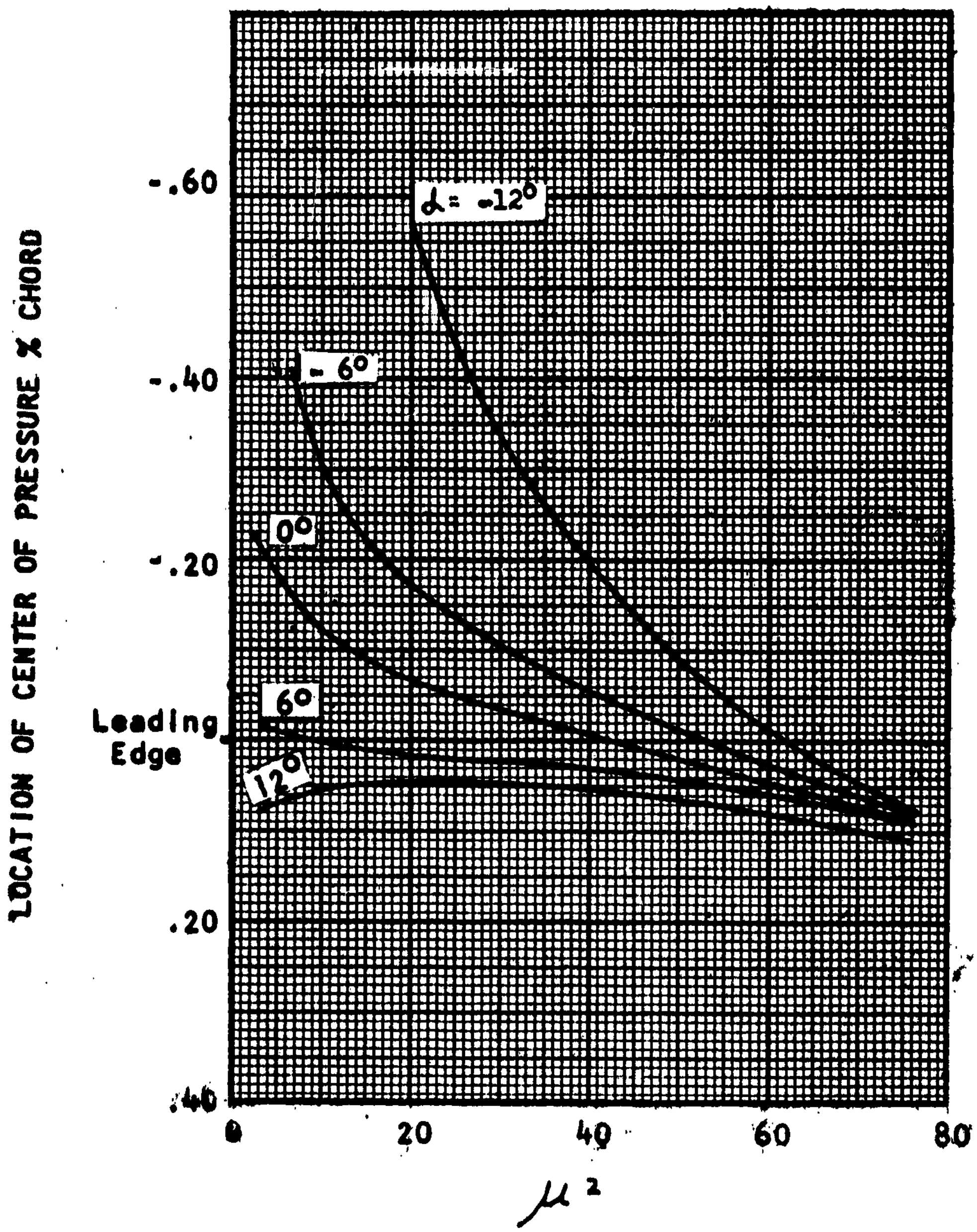

FIGURE C-7

LOCATION OF MODEL CENTER OF PRESSURE VS. μ^2 ; $\phi_R = 39.$

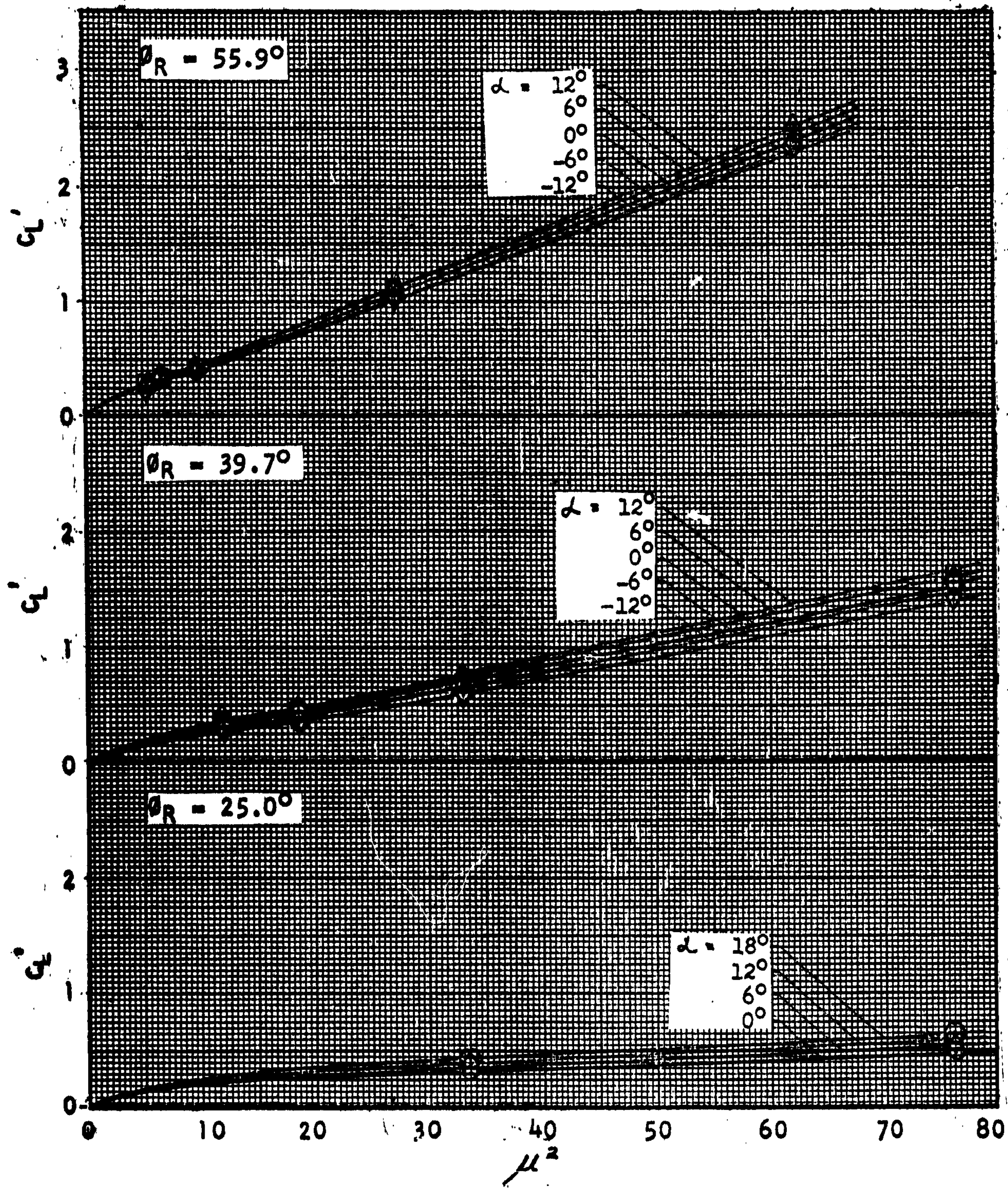

FIGURE C-8

FAN C_L VS. μ^2

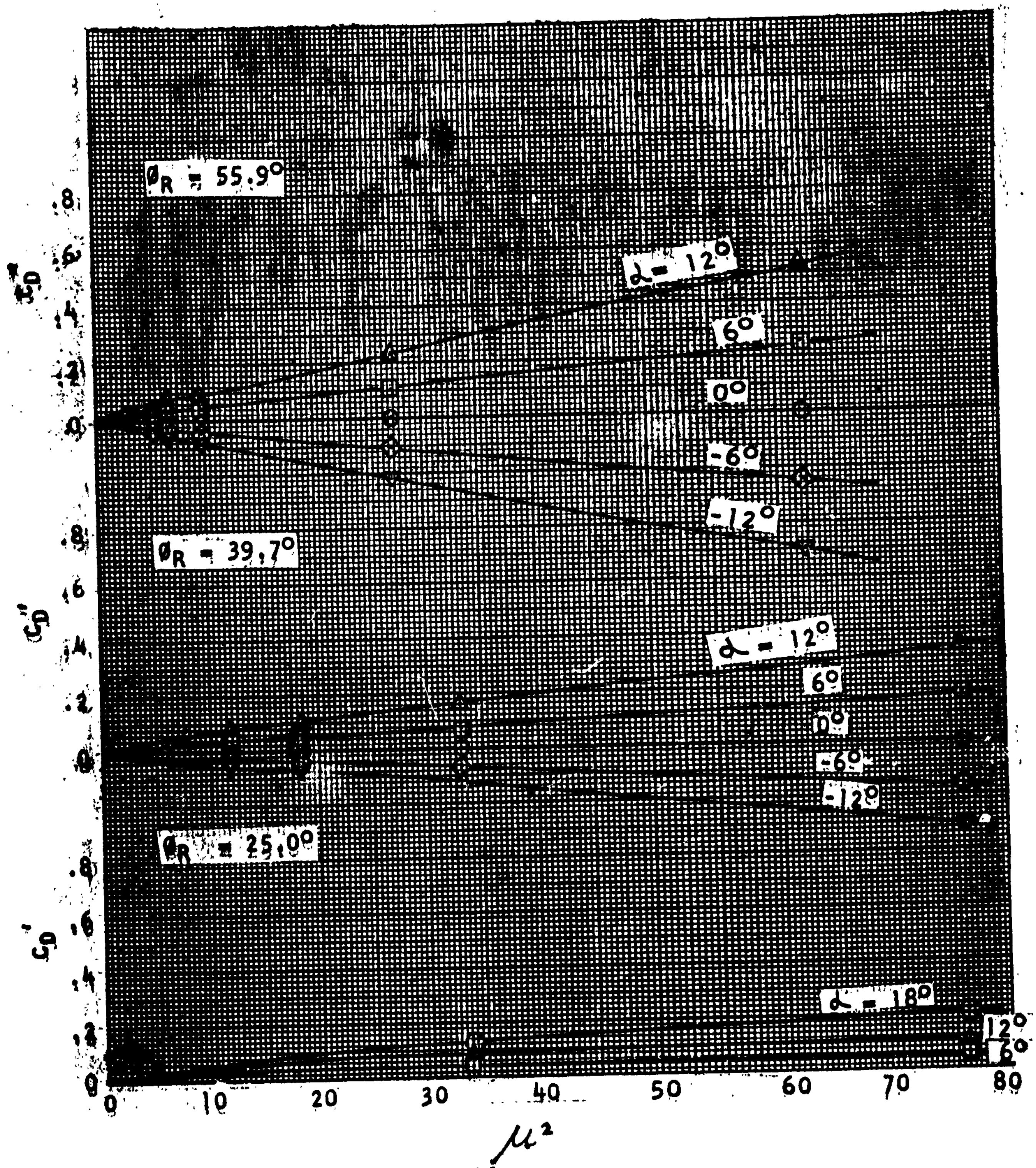

FIGURE C-9

FAN C_D VS. μ^2

MEDIUM PITCH FAN 10,000 RPM

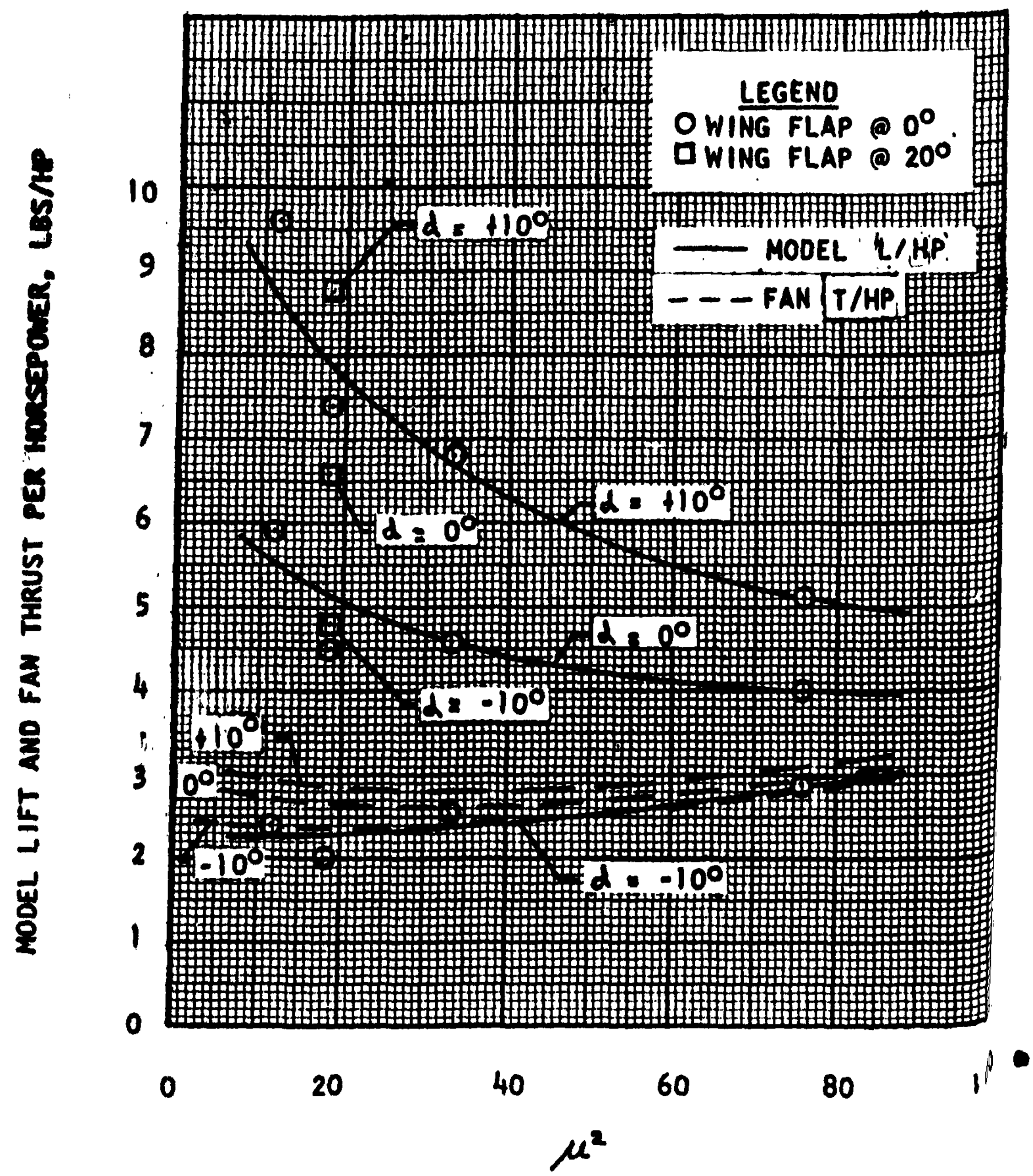

FIGURE C-10

MODEL LIFT AND FAN THRUST PER HORSEPOWER VS. μ^2 ; $\emptyset_R$ = 39.7